



## Durham E-Theses

---

*Automatic methods for the interpretation of gravity  
and magnetic field anomalies and their application to  
marine geophysical surveys*

Laving, Gerald John

### How to cite:

---

Laving, Gerald John (1971) *Automatic methods for the interpretation of gravity and magnetic field anomalies and their application to marine geophysical surveys*, Durham theses, Durham University. Available at Durham E-Theses Online: <http://etheses.dur.ac.uk/8704/>

### Use policy

---

The full-text may be used and/or reproduced, and given to third parties in any format or medium, without prior permission or charge, for personal research or study, educational, or not-for-profit purposes provided that:

- a full bibliographic reference is made to the original source
- a [link](#) is made to the metadata record in Durham E-Theses
- the full-text is not changed in any way

The full-text must not be sold in any format or medium without the formal permission of the copyright holders.

Please consult the [full Durham E-Theses policy](#) for further details.

AUTOMATIC METHODS FOR THE INTERPRETATION  
OF GRAVITY AND MAGNETIC FIELD ANOMALIES  
AND THEIR APPLICATION TO MARINE  
GEOPHYSICAL SURVEYS.

A Thesis submitted for the Degree of  
Doctor of Philosophy  
in the  
University of Durham.

by

Gerald John Laving

University College

September, 1971.



ACKNOWLEDGEMENTS

I wish to thank Professor G.M. Brown for providing departmental facilities and Professor M.H.P. Bott for his supervision.

I am deeply indebted to Dr. G.H. Keller of the United States National Oceanographic and Atmospheric Administration (N.O.A.A.) Laboratory, Miami, Florida for permitting me to take part in the N.O.A.A. trans-Atlantic and Caribbean cruises, for providing the data analysed in Chapter 5 of this work, and for the generous hospitality he showed to me during my period at the N.O.A.A. Laboratories.

I am also grateful to Messrs. R.K. Lattimore, G.A. Lapine, B.G. Bassinger, S.A. Bush, R.N. Harbison and Dr. L.W. Butler of the N.O.A.A. Laboratories for their many useful discussions and generous hospitality.

I wish to thank the officers and men of H.M.S. Hydra for providing the data analysed in Chapter 6, and in particular Sub. Lt. Sheather for his help and advice.

I am grateful to my colleagues A.D. Ingles, P.J. Gunn and A.K. Goodacre for their help and many useful discussions and I am deeply indebted to Dr. M. Al-Chalabi for his advice and encouragement during the development of the magnetic interpretation programs presented in Chapter 3.

ABSTRACT

Direct methods for the interpretation of gravity and magnetic field anomalies have been developed and applied to interpret marine geophysical surveys of the Caribbean eastern margin and the Sierra Leone continental shelf.

The gravity interpretation programs compute, under certain constraints to remove inherent ambiguity, the space form of the body producing a specified gravity anomaly. The computed body is built up from a set of two-dimensional trapezia thus producing a geologically realistic model. The programs can interpret interfering anomalies, caused by adjacent bodies and anomalies due to bodies with a known lateral variation in density. The method is based on an equivalent layer technique, the non-linear problem being solved by repeated solution of a linear integral equation, which is approximated by a finite set of linear algebraic equations. The technique has been extended to three dimensional analysis, the source body being built up from a set of rectangular prisms.

The magnetic interpretation method is basically similar to the gravity method, but it is necessary to compute the dip of the body magnetisation vector before a solution can be obtained for the body space form. The programs have been used to interpret a marine gravity survey of the south eastern Caribbean margin. The gravity data is used to determine the possible crustal structure, between points where the structure is known

from seismic refraction data. Conclusions are drawn on the generalised crustal structure of the region and on the southward extension of the Lesser Antilles Island arc and the Barbados Ridge.

A marine gravity survey of the Sierra Leone Continental Shelf has been interpreted using the programs developed. The space form of the Freetown Complex, a layered gabbroic intrusion, and its extension onto the continental shelf are determined.

## CONTENTS

	Page .	
CHAPTER 1	INTRODUCTION TO THE EQUIVALENT LAYER TECHNIQUE	1
1-1	Introduction	1
1-2	The Gravity Equivalent Layer	1
1-3	The Magnetic Equivalent Layer	5
CHAPTER 2	THE MATRIX METHOD APPLIED TO GRAVITY INTERPRETATION	8
2-1	Introduction	8
2-2	Previous Work	8
2-3	Application of the Matrix Technique	9
2-3-1	Computer Method for a Body with Inward Sloping Contacts	11
2-3-2	Computer Method for a Body with Outward Sloping Contacts	13
2-3-3	Method of Solution	15
2-3-4	Available Programs	15
2-4	Examples of the Application of the Programs	15
2-4-1	Test Data	15
2-4-1-1	Outward Sloping Contact Model	15
2-4-1-2	Inward Sloping Contact Model	16
2-4-2	Field Data	16
2-5	Limitations of the Method	17
2-5-1	Resolving Power	17
2-5-1-1	The Variable Block Coordinate Program	19
2-5-2	Infinite Structures	20
2-5-3	Interfering Anomalies	21
2-5-4	Steep Body Contacts	21
2-6	Conclusions	21
2-7	Extension of the Method to Three Dimensions	22
2-7-1	Calculation of the Gravity Anomaly due to a Rectangular Prism	22
2-7-2	Inward Sloping Contact Program	23
2-7-3	Outward Sloping Contact Program	24
2-7-4	Example of the Application of the Programs	24
2-7-5	Conclusions	25
CHAPTER 3	THE MATRIX METHOD APPLIED TO MAGNETIC INTERPRETATION	26
3-1	Introduction	26
3-1-1	Comparison Methods	26
3-1-2	Direct Methods	27
3-2	Non-Linear Optimisation	27
3-3	Notation	28
3-4	Application of the Matrix Technique	28
3-4-1	Determination of the Body Magnetisation Angle	29
3-4-1-1	Method	30
3-4-1-2	Results Using the Matrix Technique	32
3-4-1-3	Limitations of the Method	33
3-4-2	Determination of the Space Form	34
3-4-2-1	Method	34

	Page
3-4-3 Available Programs	36
3-5 Examples of the Application of the Programs	36
3-5-1 Test Data	36
3-5-1-1 Model 1 - Outward Sloping Contacts	36
3-5-1-2 Model 2 - Inward Sloping Contacts	37
3-5-1-3 General Remarks	37
3-5-2 Field Data	38
3-5-2-1 Lesser Antilles Arc Anomaly	38
3-5-2-2 The Carlisle Anomaly	39
3-5-2-3 The Solway Firth Anomaly	40
3-6 Limitations of the Method	41
3-6-1 Shallow Angle Magnetisation	41
3-7 Other Applications of the Magnetic Equivalent Layer	42
3-8 Conclusions	43
3-9 Extension of the Technique to Three Dimensional Analysis	44
 CHAPTER 4	
THE MEASUREMENT OF GRAVITY AT SEA	47
4-1 Introduction	47
4-2 Vertical Accelerations of the Ship	47
4-3 Horizontal Accelerations of the Ship	48
4-3-1 Off Leveling Errors	48
4-3-2 Cross Coupling Errors	49
4-4 The Eotvos Effect	50
4-5 Gravimeter Drift	51
4-6 Land Ties	51
 CHAPTER 5	
INTERPRETATION OF A MARINE GRAVITY SURVEY OF THE CARIBBEAN EASTERN MARGIN SOUTH OF ST.VINCENT	53
5-1 Introduction	53
5-1-1 Island Arcs General	53
5-1-2 Lesser Antillean Geology	55
5-1-3 Surrounding Framework	56
5-1-3-1 Northern South America, Trinidad and Tobago	56
5-1-3-2 Barbados	57
5-1-4 Previous Geophysical Work	58
5-2 Reduction of the Gravity Survey	58
5-2-1 Introduction	58
5-2-2 Gravity Base Station	59
5-2-3 Navigation	60
5-2-4 Analogue Records	60
5-2-5 Reduction to Free Air Anomaly	60
5-2-6 Reduction to Bouguer Anomaly	61
5-2-7 Errors	62
5-3 Description of the Bouguer Anomaly Map	62
5-4 Interpretation	63

5-4-1	Profiles R-R' and S-S' and the Extension of the Lesser Antilles Arc into the Venezuelan Shelf	63
5-4-1-1	Continuity of the Arc Trend	68
5-4-1-2	Profile S-S'	68
5-4-2	Profile T'-T' Trinidad Shelf to Grenada	69
5-4-3	Profiles U-U', V-V'-V'' and W-W' and the Barbados Ridge	73
5-4-3-1	Gravitational Effect of the Downgoing Lithosphere	73
5-4-3-2	Profile W-W' St. Vincent to Barbados	75
5-4-3-3	Profile U-U'	79
5-4-3-4	Profile V-V'-V''	80
5-4-3-5	Barbados Ridge - Discussion	82
5-5	General Conclusions	84
CHAPTER 6	INTERPRETATION OF A MARINE GRAVITY SURVEY OF THE SIERRA LEONE CONTINENTAL SHELF	87
6-1	Introduction	87
6-1-1	Structural Framework of the West African Continental Margin	87
6-1-2	The Senegal and Sierra Leone Embayments	89
6-1-2-1	Seismic Refraction Resnets from the Sierra Leone Continental Shelf	89
6-1-3	The Geology of Sierra Leone	90
6-2	Reduction and Interpretation	92
6-2-1	Introduction	92
6-2-2	Navigation	93
6-2-3	Base Station	93
6-2-4	Errors	94
6-2-5	The Bouguer Anomaly Map	94
6-2-6	Additional Data	95
6-2-7	Densities	96
6-2-8	Interpretation	96
6-2-8-1	Profile A-A'	96
6-2-8-2	Profile C-C'	100
6-2-8-3	Profile F-F'	103
6-2-8-4	Profile D-D'	105
6-2-8-5	Profile E-E'	107
6-3	Summary and Discussion	108
APPENDIX 1		114
APPENDIX 2		135
APPENDIX 3		137
REFERENCES		138





INTRODUCTION TO THE EQUIVALENT LAYER TECHNIQUE.

1-1 Introduction

Automatic computer techniques for the determination of the space form of the source body resulting in a given gravity or magnetic field anomaly are developed in the first section of this work. (Chapters 1-3)

Ambiguity in such interpretation has been widely documented in the geophysical literature (e.g. Skeels, 1947; Roy, 1962; Al-Chalabi, 1970)

It can be shown by an extension of Green's Theorem (Kellogg, 1929) that any observed anomaly can be produced by an infinite number of surface distributions either on or beneath the level of observation. However, additional geological or geophysical data often make it possible to impose constraints that result in the existence of a unique solution (e.g. knowledge of the depth and density or magnetisation of the source body). Alternatively, estimated limits on these parameters allows limiting models between which the true structure must lie, to be computed.

When determining the space form of a homogeneous body under a particular set of constraints, use can be made of this inherent ambiguity by initially removing the constraint that the source body is homogeneous and synthesizing the geophysical anomaly by an equivalent layer, either of surface density or surface magnetisation. From this equivalent layer the homogeneous body can be computed by successive approximation.

1-2 The Gravity Equivalent Layer

Let us consider a rectangular Cartesian co-ordinate system with the positive  $z$  - axis pointing downward. It is assumed that a source distribution of mass  $M$  causing

a scalar gravitational potential  $U$  is situated entirely below the plane  $z=0$  (Fig. 1-1). The potential  $U$  is a continuous function of  $x, y, z$  with first and second derivatives that are both continuous and integrable. If two horizontal planes are considered  $z=0$  and  $z=z_1$  ( $z_1 < 0$ ) (Fig. 1-1) it can be shown from a corollary of Green's Theorem (Kellogg, 1929) that the potentials at the two planes are related by the equation:

$$U(x_1, y_1, z_1) = \frac{1}{2\pi} \int_S \frac{1}{R} \frac{d}{dz} U(x, y, 0) \cdot dS. \quad (1-1)$$

where:

$$R = ((x_1 - x)^2 + (y_1 - y)^2 + z_1^2)^{\frac{1}{2}}$$

and the integration is carried out over the entire surface  $S$  of the plane  $z=0$ .

Thus if the vertical component of attraction (gravity) due to  $M$  at any point on  $z=0$  is  $g(x, y, 0)$  the value of the potential at any point on  $z=z_1$  is given by:

$$U(x_1, y_1, z_1) = \frac{1}{2\pi} \int_S \frac{1}{R} \cdot g(x, y, 0) \cdot dS. \quad (1-2)$$

If we now remove  $M$  and place a coating of surface density  $\sigma(x, y)$  over the plane  $z=0$  (Fig. 1-1) the potential at any point on  $z=z_1$  due to a small element  $dS$  of the coating will be:

$$U(x_1, y_1, z_1) = \frac{G \sigma dS}{R} \quad (1-3)$$

where  $G$  is the universal gravitational constant.

and the potential on  $z=z_1$  due to the entire coating of  $z=0$  will be:

$$U(x_1, y_1, z_1) = G \int_S \frac{1}{R} \sigma(x, y) \cdot dS. \quad (1-4)$$

By comparing equations (1-2) and (1-4) we can see that they are of the same form and will be identical if we put:

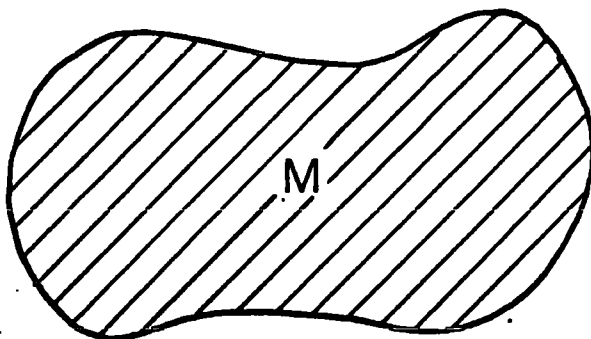
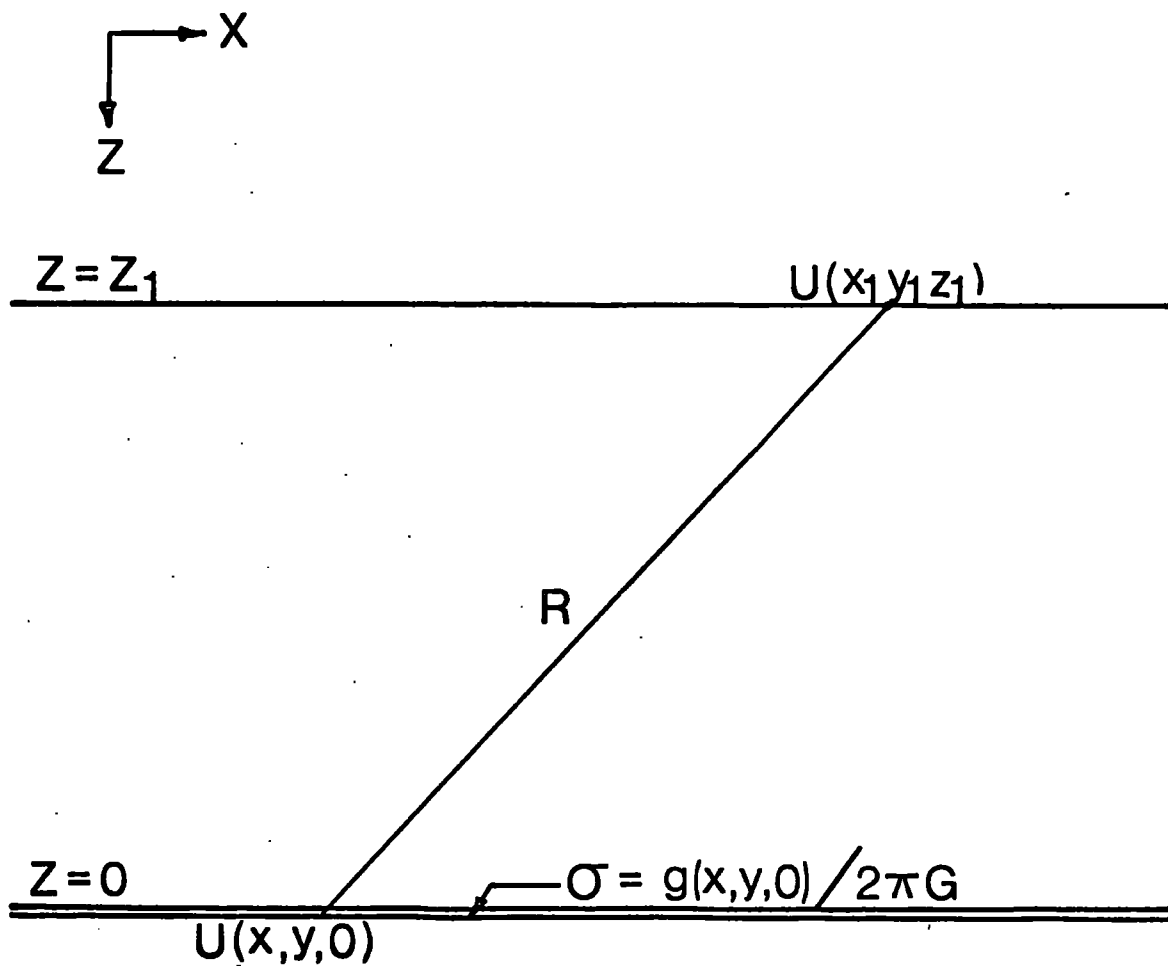


Fig. 1-1. The body  $M$  and the surface density distribution on the plane  $Z=0$  produce identical gravity anomalies on  $Z=Z_1$

$$\begin{aligned} \sigma(x,y) &= g(x,y) / 2\pi G & (1-5) \\ z = 0 & \quad z = 0 \end{aligned}$$

Since the potentials of the two systems are identical, the gravitational fields will also be identical. Thus the gravitational field due to some mass distribution M can be synthesized by a variable surface density distribution at the level of observation, or between that level and the top surface of M.

In practice we find that we can have the surface density distribution deeper than the top of M and that we can have various sections of the distribution at different depths. Indeed, Roy (1962) has pointed out that if we allow the sign of  $\sigma(x,y)$  to vary, there is no limit on the depth of the surface density distribution. However, in the present work we require  $\sigma(x,y)$  to be a stable non-oscillating function and this places an effective limit on the depth of the distribution (Chapter 2).

We can thus write the general equation for the gravitational attraction of an arbitrary body:

$$g(x_1, y_1, 0) = G \int_{-\infty}^{\infty} \int_{-\infty}^{\infty} \int_0^{\infty} \frac{\rho(x, y, z) \cdot z \cdot dx \cdot dy \cdot dz}{((x-x_1)^2 + (y-y_1)^2 + z^2)^{3/2}} \quad (1-6)$$

where  $\rho$  = density and  $z \geq 0$

in the form:

$$g(x_1, y_1, 0) = G \int_{-\infty}^{\infty} \int_{-\infty}^{\infty} \frac{\sigma_h(x, y) \cdot h \cdot dx \cdot dy}{((x-x_1)^2 + (y-y_1)^2 + h^2)^{3/2}} \quad (1-7)$$

where  $\sigma_h$  = variable surface density  
at  $z = h$  ( $h \geq 0$ )

In this work we shall be primarily concerned with two-dimensional interpretation, that is, the geological structures determined from geophysical anomaly profiles are assumed to extend to infinity normal to the vertical plane of the profile. In practice two types of interpretational problems arise.

1) To determine from the gravity anomaly the density of a body of known space form.

2) To determine the space form of a body of known density.

If we then consider a gravity anomaly measured along the horizontal x-axis, caused by an underlying two dimensional mass we have:

$$g(x_1) = \int_{-\infty}^{\infty} \sigma(x) \cdot K(d_1(x), d_2(x), (x_1-x)) dx. \quad (1-8)$$

where  $z = d_1(x)$  and  $z = d_2(x)$  define the top and bottom surfaces of the source body, the density is  $\sigma(x)$  and  $K$  is a kernel function depending on  $d_1, d_2$  defining the gravitational attraction of the source body assuming unit density

The first problem is linear since  $K$  is independent of  $\sigma$  (Bott, 1967). The second problem, that of determining  $d_1$  and  $d_2$  is non-linear and ambiguous unless either  $d_1$  or  $d_2$  is known. In Chapter 2 successive linear approximations are used to solve the non-linear problem for the unambiguous case.

1-3 The Magnetic Equivalent Layer.

Throughout this work the assumption will be made that total field magnetic anomalies are measured in the direction of the ambient field and that this direction is constant over the length of any magnetic anomaly profile considered. The first assumption will be true if  $F_0 \gg F$  where  $F_0$  is the ambient field and  $F$  is the maximum value of the anomaly in question. Since  $F_0$  is of the order of  $2-5 \times 10^5$  gamma this assumption will be valid for the majority of magnetic anomalies. The second assumption holds true for all profiles considered in this work.

Let us again consider a rectangular Cartesian coordinate system with positive z-axis pointing downwards. It is assumed that a source distribution of magnetisation  $M$  causing a magnetic anomaly  $F(x,y,0)$  on the plane  $z = 0$ , lies entirely below  $z = 0$ . Since total field magnetic anomalies will obey Laplace's equation we can obtain an expression for the magnetic anomaly on the plane  $z = z_1$  ( $z_1 < 0$ ) from Green's Theorem

$$F(x_1, y_1, z_1) = \frac{1}{2\pi} \cdot \int_{-\infty}^{\infty} \int_{-\infty}^{\infty} \frac{F(x, y, 0) \cdot z \cdot dx \cdot dy}{((x_1 - x)^2 + (y_1 - y)^2 + z^2)^{3/2}} \quad (1-9)$$

Thus if we express  $F(x,y,0)$  in terms of a sheet of variable surface magnetisation at  $z = 0$  we will have the magnetic equivalent layer.

Direct comparison of integrals, as used in the gravity case, is not possible here as the corresponding integral to (1-2) and (1-4) contain variables not common to both, due to the dipole nature of the magnetic field.

An expression for the dipole layer, for the two dimensional case, can however be obtained using pseudo-gravity calculations (Bott, Smith and Stacey, 1966) or Fourier convolution (Bott, 1967). Bott's (1967) expression for a magnetic anomaly in terms of a coating of magnetic moment per unit area over the plane of observation is:

$$J(x) = \frac{1}{2\pi^2} \int_{-\infty}^{\infty} (\log |x' - x| \cos\beta + \frac{\pi}{2} \text{sign}(x' - x) \sin\beta) F(x') \cdot dx' \quad (1-10)$$

where  $\beta = (\sigma + \mu)$  and  $\mu =$  the dip of the body magnetisation vector in the plane of the profile,  $\sigma =$  dip of the Earth's field in the plane of the profile,  $J(x) =$  surface magnetisation.

It is thus possible to synthesize a magnetic anomaly due to an unknown distribution of magnetisation, by an equivalent layer of variable surface magnetisation.

The linear and non-linear problems described in section 1-2 are again encountered in magnetic interpretation.

We have:

$$F(x_1) = \int_{-\infty}^{\infty} J(x) \cdot K(d_1(x), d_2(x), \beta, (x_1 - x)) \cdot dx \quad (1-11)$$

where  $z = d_1(x)$  and  $z = d_2(x)$  define the top and bottom surfaces of the source body,  $J =$  magnetisation and  $K$  is a kernel function depending on  $d_1, d_2$  and  $\beta$  defining the magnetic anomaly of the source body assuming unit magnetisation.

The linear problem of determining  $J(x)$  knowing  $d_1(x)$  and  $d_2(x)$  has been previously examined (Bott, 1967; Hutton, 1970; Emilia and Bodvarsson, 1970). The non-linear problem of determining  $d_1$  or  $d_2$  knowing the other and the magnetisation is examined in Chapter 3.



CHAPTER 2

THE MATRIX METHOD APPLIED TO GRAVITY INTERPRETATION

2-1 Introduction

In this chapter computer programs which have been developed to solve the non-linear problem of determining the space form of a body resulting in a specified gravity anomaly are described. A matrix technique is employed to obtain a solution to the problem for the overdetermined case by successive linear approximations. The method employed is extended from a method suggested by Bott and programmed by Tanner (1967), which assumes the observed gravity anomaly to result from a body that can be built up from a set of rectangular blocks and has a horizontal upper or lower surface and uniform density contrast.

In the method developed the outline of the causative body is approximated to a continuous smooth curve by a set of trapezia (with no restriction that the top surface should be horizontal for "basin-like bodies) so that the computed model is geologically realistic. The technique has been further extended to permit the determination of the space-form of bodies having lateral density variations, for adjacent bodies having different density contrasts (of either sign) so that interfering anomalies can be interpreted, and for 'infinite' structures, resulting in a change of anomaly level.

A method of three dimensional analysis has also been developed based on the matrix technique using rectangular prisms.

In the methods presented, the ambiguity mentioned in Chapter 1 is removed by constraining the density of the model and either all or part of one surface. Any computed model is unique under these constraints.

## 2-2 Previous Work

The inverse problem in gravity interpretation of determining the space form of a geological structure, knowing the gravity anomaly it produces, can be approached in two ways.

The first (indirect) method consists of estimating the structure from available information (if any) and computing its gravity anomaly, either by using graticules (e.g. Heiland,<sup>1940</sup> or a computer method (Talwan; et.al., 1959; Bott, 1969). The computed anomaly is then compared with the observed, and modifications are made to the model by trial and error until the residuals become tolerable.

The second (direct) method, involves using techniques of automatically adjusting the body parameter to obtain a best fit and is therefore more objective. (e.g. Bott, 1960; La. Porte, 1963; Tanner, 1967).

The method developed in this chapter is considered to be an improvement on these techniques. Realistic geological models of one or more open or closed bodies can be rapidly computed from a knowledge of the resultant gravity anomaly.

## 2-3 Application of the Matrix Technique.

Consider a gravity anomaly measured along the horizontal  $x$  - axis, caused by an underlying two-dimensional distribution of mass with its strike direction perpendicular to the  $x$  - axis (Fig. 2-1(a)). The  $z$  - axis points vertically downwards and the observed

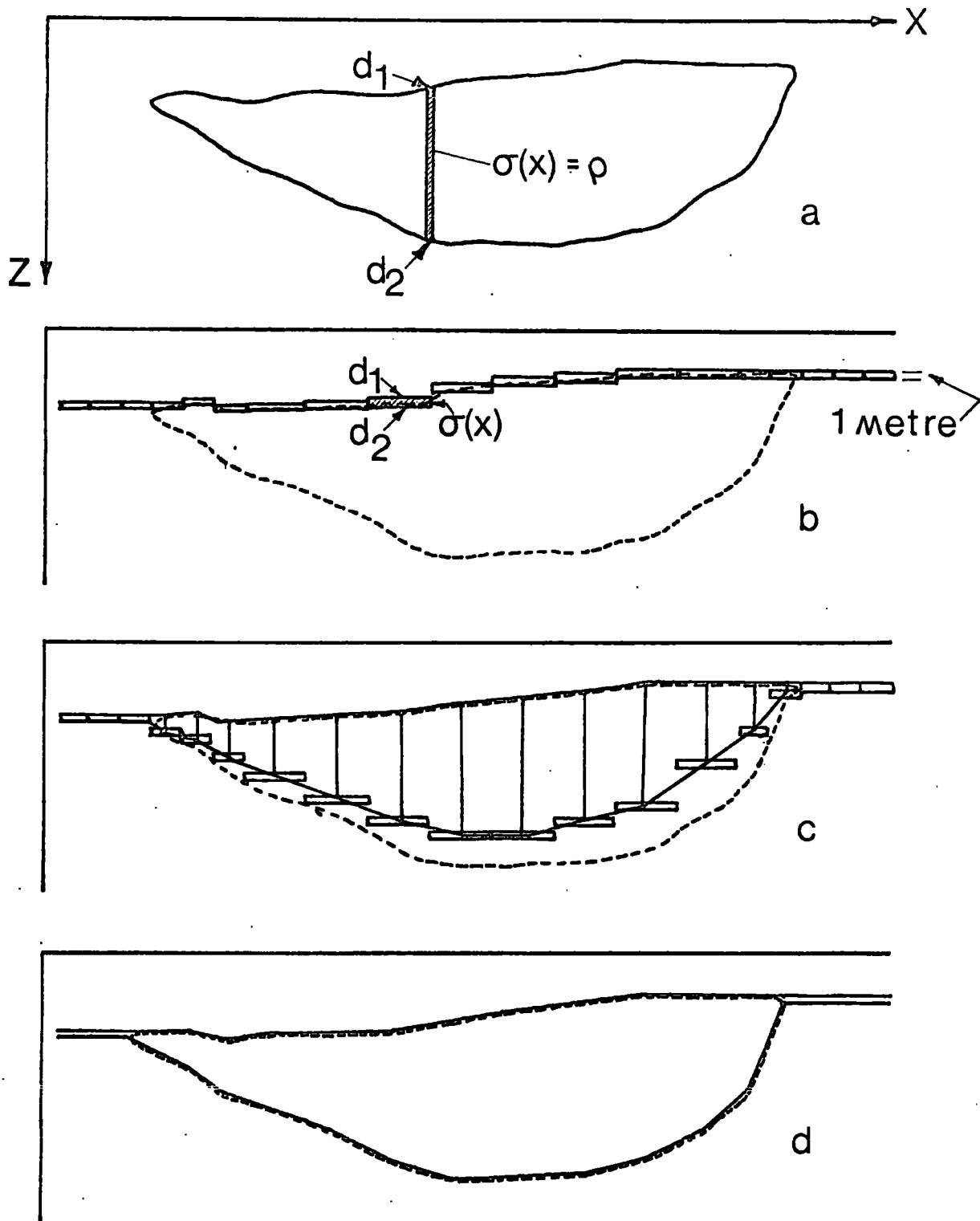


Fig.2-1. The application of the matrix method to determine the space form of a body with inward sloping contacts.

anomaly at  $(x,0)$  is  $g(x)$ . Having shown that a gravity anomaly can be synthesized by an equivalent layer, we approximate the equivalent layer by a layer of finite thickness with upper and lower bounds  $d_1(x)$  and  $d_2(x)$  respectively (Fig. 2-1(b)). If the variable mass/unit area of this layer is  $\sigma(x)$ , then the expression for the gravity anomaly due to the layer either on or above it is:

$$g(x) = \int_{-\infty}^{\infty} \sigma(x') \cdot K((x' - x), d_1(x'), d_2(x')) \cdot dx' \quad (2-1)$$

where  $K$  is a kernel function defining the gravity anomaly due to the body assuming unit density.

As stated in Chapter 1 if  $d_1(x)$  and  $d_2(x)$  represent the true upper and lower boundaries of the causative body  $\sigma(x)$  will be the true density (say  $\rho$ ) and can be found by solving a linear integral equation. Fig 2-1(a) illustrates this case.

However the problem of determining either  $d_1(x)$  or  $d_2(x)$ , knowing the other and  $\sigma(x)$ , is non-linear. The method employed is to fix the unknown surface ( $d_1(x)$  or  $d_2(x)$ ) arbitrarily and to solve for the required values of  $\sigma(x)$  that synthesize the observed gravity anomaly  $g(x)$ . An estimate of the unknown surface can then be made by assuming a linear relationship between body thickness and density, if the correct homogeneous density of the body is specified.

If we subdivide the equivalent layer (over a sufficient length to allow the anomaly to be synthesised)

into a finite number of "blocks" such that an assumption of constant mass/area<sup>unit</sup> for any block is valid, we can approximate equation (2-1) by:

$$g_i = \sum_{j=1}^n K_{ij} \sigma_j \quad (i = 1 \text{ to } m) \quad (2-2)$$

where  $g_i$  is the observed gravity  
 $\sigma_j$  is the mass/area and  $K_{ij}$  is  
the gravity anomaly at the  $i$ th  
observation point due to the  
 $j$ th block assuming unit density.

If  $m > n$  then equation (2-2) has the least squares solution

$$\sigma = (K^T K)^{-1} K^T g$$

det  $K \neq 0$  (2-3)

using matrix notation. We can thus compute the best set of values of surface mass for the  $n$  blocks to produce the observed anomaly at the  $m$  specified points.

### 2-3-1. Computer Method for a Body with Inward Sloping Contacts

A series of blocks 1 metre thick and of specified width are placed along the estimated, or known top surface, of the anomalous body. If the lateral extent of the body is not known the blocks should be extended under the entire observed gravity profile. The specified top surface need not be horizontal. Equation (2-3) is then solved to find the best fitting series of values of mass/area for the blocks to satisfy the observed anomaly, the number of anomaly points being greater than, or equal to, the number of blocks specified. The depth to the bottom surface of each block is then computed by assuming a linear relationship between

density and thickness of block:

$$d_2 (j^{\text{th}} \text{ block}) = d_1 (j^{\text{th}} \text{ block}) + \frac{\text{mass/area}(j^{\text{th}} \text{ block})}{\text{specified density}} \quad (2-4)$$

the three-dimensional density of the body having been specified.

The gravity anomaly of the calculated model is computed by considering each side of each trapezium in turn and using the formula for the gravity anomaly due to a semi-infinite slab (Heiland, 1940, page 153).

$$g = 2 G \rho \left[ -(x_1 \sin i + z_1 \cos i)(\sin i \log r_2/r_1 + \cos i (\phi_2 - \phi_1)) + z_2 \phi_2 - z_1 \phi_1 \right] \quad (2-5)$$

see Fig.(2-2)

Each side is taken to be the end of a semi-infinite slab and each is considered in turn going round each trapezium in an anticlockwise sense. The formula takes a negative sign if the side under consideration shows a decrease in depth. The resultant sum is the gravity anomaly due to each trapezium. This is the method used by Bott (1969) for computing the gravity anomaly due to an arbitrarily shaped body. The centre of gravity of each trapezium is then found and an end-correction for each block is computed using Nettleton's (1940) method, thus allowing three-dimensional structures to be approximated.

The computed anomaly will deviate from the observed for two reasons:

- 1) The assumption of a linear relationship between density and thickness is not valid.

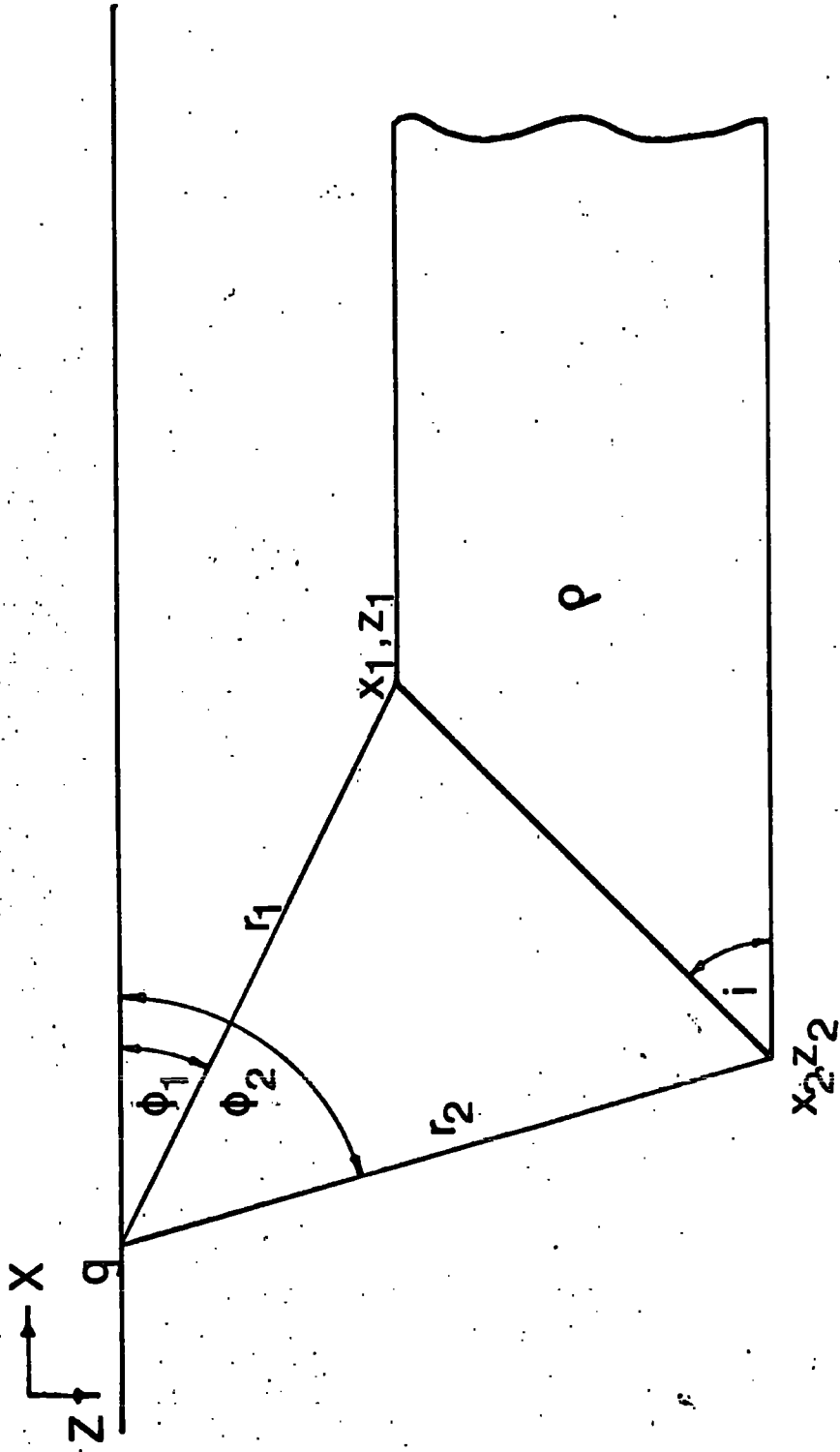


Fig. 2-2. Notation used for the gravity formula at a point due to a semi-infinite slab of rock density  $\rho$ .

2) In changing to the smooth outline model the mass distribution and the total mass are changed. Repeated adjustments are therefore made to the model until the difference between the observed and calculated anomalies is minimised. This is done by placing a horizontal block one blockwidth wide and 1 metre thick beneath each lower corner of the body (Fig. 2-1(c)). Equation (2-3) is then solved for these blocks as before, only using the residual (observed-calculated) gravity anomaly. The new dimensions of the trapezia are then calculated using the relationship:

$$d_2'(j) = d_2(j) + \frac{\text{mass/area (j)}}{\text{specified density}} \quad (2-6)$$

Although equation (2-6) again assumes a linear relationship, the change in thickness will be relatively small and the assumption approaches validity. Repeated iterations are carried out until the residuals between the observed and calculated gravity anomalies become tolerable. Five to ten iterations are usually required.

#### 2-3-2 Computer Methods for a Body with Outward Sloping Contacts

The program for outward sloping contact bodies differs from the previous method only in the following respects.

Only one point on the top surface need be specified as a flat lower surface is assumed. A series of blocks, 1 metre thick and of specified width are placed at the level of the specified top surface point. The best fitting set of values of mass/area for these blocks, to satisfy the observed anomaly, is found by solving



equation (2-3) and the lower surface is calculated using the relationship:

$$d(\text{bottom}) = d(\text{specified}) + \frac{\text{mass/area (K}^{\text{th}} \text{ block)}}{\text{specified density}} \quad (2-7)$$

where the  $K^{\text{th}}$  block is centred about the specified point and the three dimensional density is specified.

The top corners of the trapezia are then computed using the relationship

$$d_{\text{top}}(j^{\text{th}} \text{ block}) = d_{\text{bottom}} - \frac{\text{mass/area}(j^{\text{th}} \text{ block)}}{\text{specified density}} \quad (2-8)$$

$$J \neq K.$$

To make successive adjustments blocks are placed at the top points of the computed model, with the exception of the specified point, which is left unadjusted. The bottom surface is also adjusted and has a one metre thick block placed along its length. The adjustment equations are:

$$d'_{\text{top}}(j) = d_{\text{top}}(j) - \frac{\text{mass/area}(j)}{\text{specified density}} \quad (2-9)$$

$$J \neq K.$$

for the upper surface and:

$$d'_{\text{bottom}} = d_{\text{bottom}} + \frac{\text{mass/area (K}^{\text{th}} \text{ block)}}{\text{specified density}} \quad (2-10)$$

where the  $K^{\text{th}}$  block underlies the bottom surface.

See Fig. (2-3).

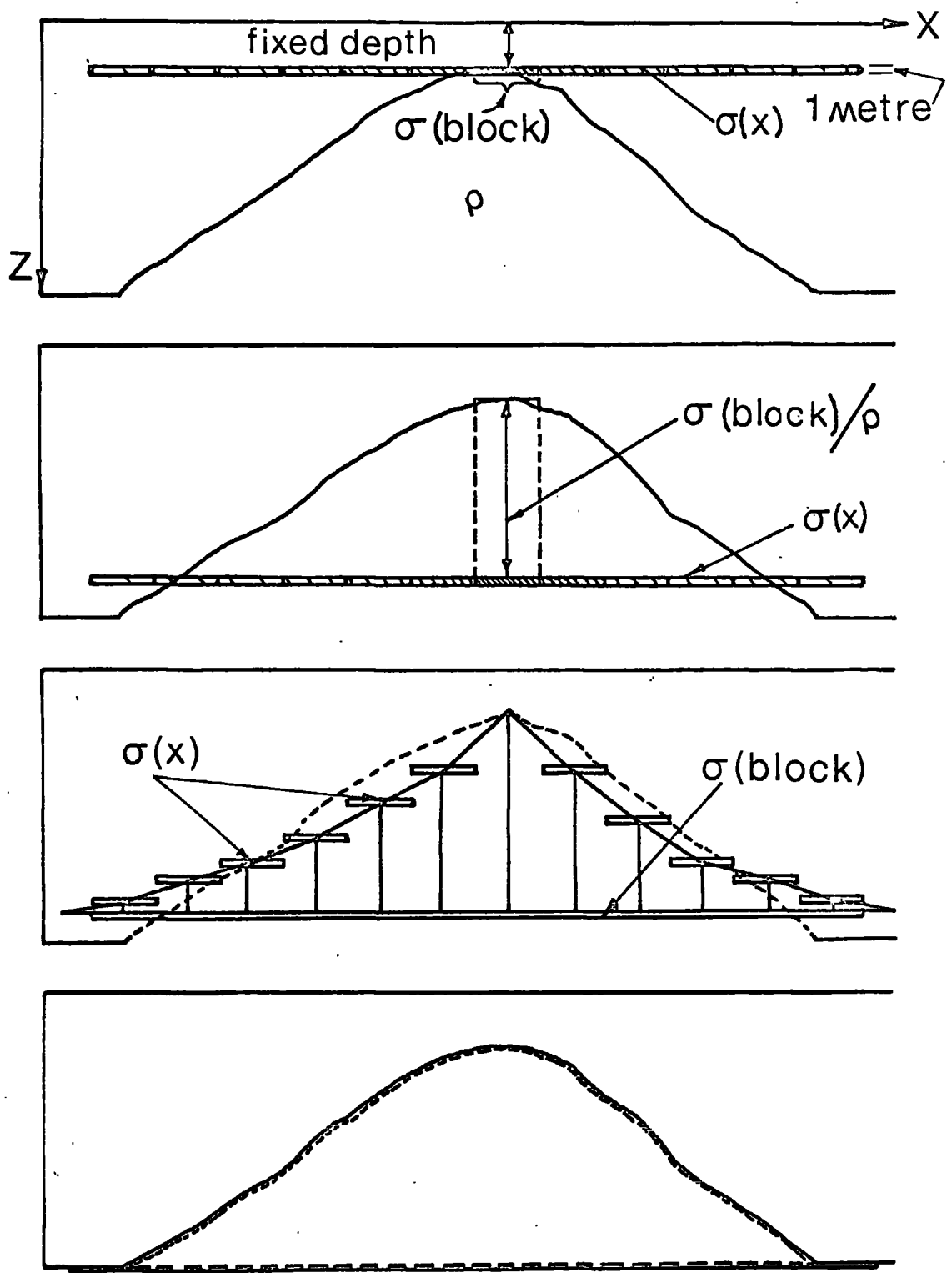


Fig.2-3. The application of the matrix method to determine the space form of a body with outward sloping contacts.

### 2-3-3 Method of Solution

Equation (2-3) is solved using a pre-written Fortran subroutine (I.B.M. 1968). The subroutine 'LLSQ' obtains a least-squares solution to an over-determined system of linear equations using a Householder transform technique - decomposing the coefficient and anomaly matrices into upper triangular forms and computing a solution by back substitution. The over-determined system is chosen in preference to the completely determined system, as a large number of individual anomaly values may then be used to produce a good overall representation of the observed data. This is not possible with an exactly determined system as the number of blocks that may be used is limited by stability considerations (see section 2-5-1).

### 2-3-4 Available Programs.

Two programs written in PL/1 GRAVIT 1 and GRAVIT 2 are available for the inward and outward sloping contact cases respectively. Data specifications, listings and general instructions for use are given in Appendix 1.

## 2-4 Examples of the Applications of the Programs

### 2-4-1 Test Data

To test the programs, gravity anomalies due to two bodies were computed using a program available at Durham (GRAVN, Bott, 1969). The space forms of the bodies were then recomputed from the gravity anomalies using the automatic programs.

#### 2-4-1-1 Outward Sloping Contact Model.

The gravity anomaly and source body are shown at Fig. (2-4). The depth to point A on the top surface of

Fig.2-4. Test body and resultant gravity anomaly  
for the program GRAVIT2.

Fig.2-5. Test body and resultant gravity anomaly  
for the program GRAVIT1.

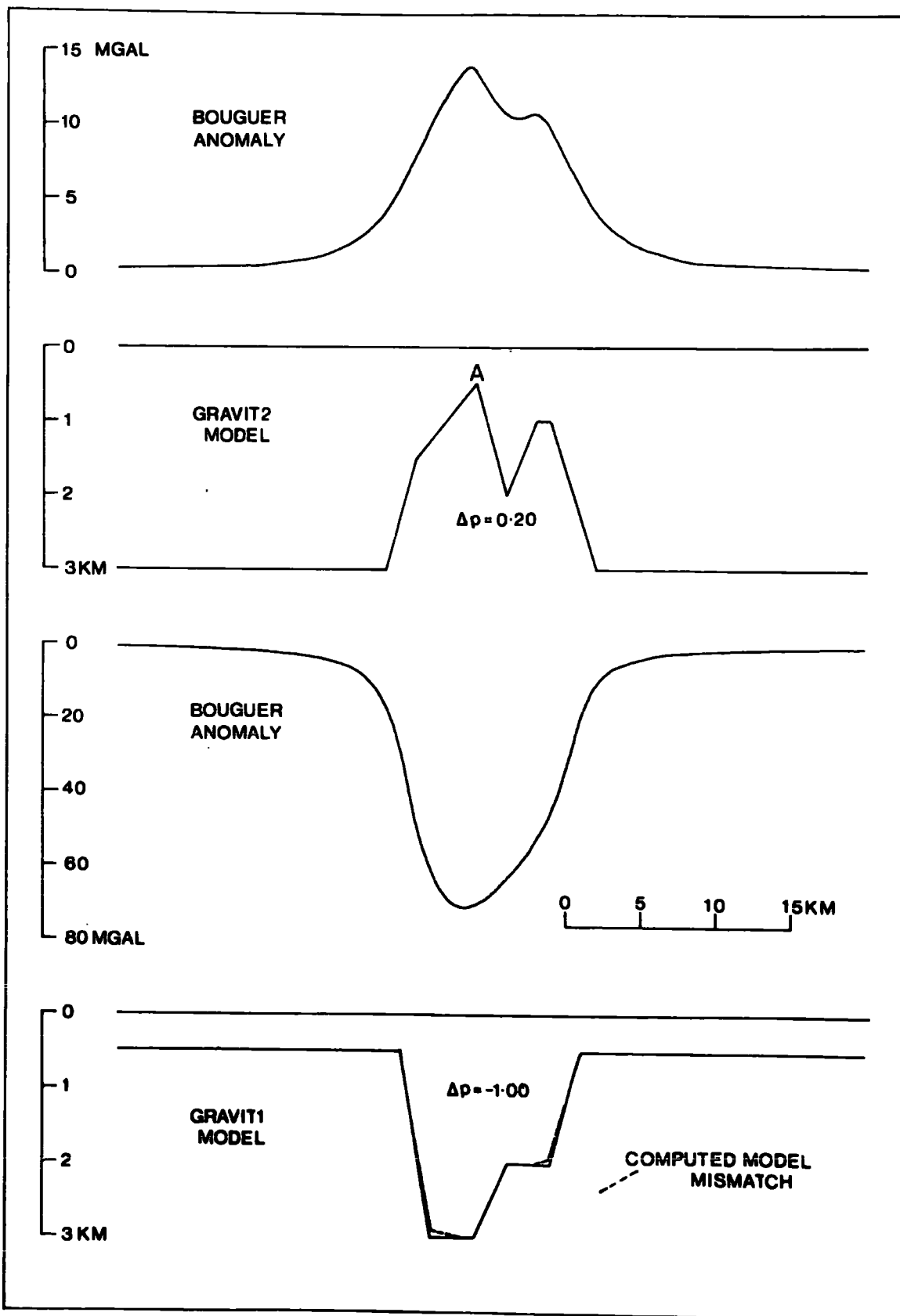


TABLE 2-1.

BATH

MODEL 1-1-1

ESTIMATE 20      UPPER SURFACE      500      DENSITY      0.20

BLOCK	LT	RT	LU	RU	LL	RL
1	18000	19000	3009	2266	3010	3010
2	19000	20000	2266	1508	3010	3010
3	20000	21000	1508	1253	3010	3010
4	21000	22000	1253	1006	3010	3010
5	22000	23000	1006	757	3010	3010
6	23000	24000	757	500	3010	3010
7	24000	25000	500	1261	3010	3010
8	25000	26000	1261	2013	3010	3010
9	26000	27000	2013	1507	3010	3010
10	27000	28000	1507	1005	3010	3010
11	28000	29000	1005	998	3010	3010
12	29000	30000	998	1683	3010	3010
13	30000	31000	1683	2341	3010	3010
14	31000	32000	2341	3009	3010	3010

LOCATION	OBSERVED	CALCULATED	RESID.
0	0.2	0.2	0.0
5000	0.3	0.3	-0.0
10000	0.6	0.6	0.0
11000	0.7	0.7	-0.0
12000	0.9	0.9	-0.0
13000	1.0	1.0	0.0
14000	1.3	1.3	-0.0
15000	1.7	1.7	-0.0
16000	2.2	2.2	-0.0
17000	3.0	3.0	-0.0
18001	4.2	4.2	-0.0
18500	5.0	5.0	0.0
19001	5.9	5.9	0.0
19500	7.0	7.0	0.0
20001	8.0	8.0	-0.0
20500	9.1	9.1	0.0
21001	10.1	10.1	-0.0
21500	11.1	11.1	0.0
22001	11.9	11.9	-0.0
22500	12.7	12.7	0.0
23001	13.4	13.4	-0.0
23500	13.8	13.7	0.0
24001	13.6	13.6	0.0
24500	12.7	12.7	-0.0
25001	11.8	11.8	0.0
25500	11.0	11.0	-0.0
26001	10.6	10.6	-0.0
26500	10.4	10.4	-0.0
27001	10.4	10.4	-0.0
27500	10.5	10.5	0.0
28001	10.6	10.6	0.0
28500	10.3	10.3	-0.0
29001	9.7	9.7	0.0
29500	8.8	8.8	0.0
30001	7.7	7.7	-0.0

30500	6.6	6.6	-0.0
31001	5.6	5.6	0.0
31500	4.8	4.8	-0.0
32001	4.0	4.0	-0.0
33000	2.9	2.9	-0.0
34000	2.1	2.1	-0.0
35000	1.6	1.6	0.0
36000	1.3	1.3	-0.0
37000	1.0	1.0	-0.0
38000	0.8	0.8	-0.0
39000	0.7	0.7	0.0
40000	0.6	0.6	0.0
45000	0.3	0.3	0.0
50000	0.2	0.2	0.0

END OF MODEL 1-1-1-0

END OF DATA

the body and the density contrast were specified. The model computed using GRAVIT 2 show excellent agreement with the true source body. The depth to the base was in error by 10 metres in 3 kms, the maximum error in the computed top surface was 13 metres the rest being less than 6 metres. All residuals were less than 0.05 mgal. The computer results are shown at Table 2-1.

#### 2-4-1-2 Inward Sloping Contact Model.

The top surface and the density contrast of the body were specified. The anomaly and the true and computed bodies are shown at Fig. (2-5). Only five of the computed anomaly values had an error in excess of 0.1 mgal (maximum error 0.3 mgal) in a total amplitude of 70 mgal. The maximum error in a bottom surface co-ordinate was 120 metres (in 3 km.) with the majority accurate to within 40 metres. The increase in error from the previous example is due to a decrease in resolving power when computing deeper coordinates. The computed body is, however an extremely good fit to the true structure Fig. (2-5). The program GRAVIT 1 was used.

For both models the computer time used was of the order of 30 secs.

#### 2-4-2 Field Data

The programs have been widely used in the interpretation of the gravity surveys discussed in Chapters 5 and 6 and examples of the application of the programs to field data need not be given here.



2-5 Limitations of the Method

2-5-1. Resolving Power

Two distinct phenomena affect the resolving power of the programs. The first is the amplification in amplitude experienced in downward continuation by the high frequency components of any anomaly. As shown by equation (1-1) the calculation of the equivalent layer involves downward continuation of the anomaly from the level of observation to the level of the layer. It can be shown, (e.g. Bott and Hutton, 1970) that downward continuation of any frequency component of an anomaly by an amount equal to the wavelength of that component increases its amplitude by a factor of 538. Thus unless some smoothing technique is introduced, the amplification of the short wavelength components of the gravity anomaly causes instability in the downward continued function. Such high frequency components are invariably present due to errors in the observed values of the gravity anomaly.

The second effect is that of ill-conditioning. As stated in section (2-3) the least squares solution to the gravity problem is given by:

$$\sigma = (K^T K)^{-1} K^T g \quad (2-11)$$

however a computational solution to this equation is not always forthcoming. The normal matrix  $(K^T K)$  is notorious for being poorly or ill-conditioned. An excellent example of this phenomenon is the Läuchli (1961) matrix cited by Anderssen (1969)

$$K = \begin{bmatrix} 1 & 1 & 1 \\ e & 0 & 0 \\ 0 & e & 0 \\ 0 & 0 & e \end{bmatrix} \quad \dots \quad K^T K = \begin{bmatrix} 1+e^2 & 1 & 1 \\ 1 & 1+e^2 & 1 \\ 1 & 1 & 1+e^2 \end{bmatrix}$$

If, because of round-off errors and the size of  $e$ , the computer evaluation of  $1+e^2 = 1$  then  $K^T K$  has rank 1 and  $[K^T K]^{-1}$  does not exist.

The problem encountered with the gravity kernel matrix is not usually as extreme as that cited above, but poor conditioning does occur. If just some elements of normal  $K$  are small, the solution will be unstable.

i.e. if  $g = K_o \sigma_{TRUE}$

then the residuals from the least squares solution are given by:

$$r = K (\sigma_{TRUE} - \sigma_{COMPUTED})$$

Hence if some elements of  $K$  are very small a large difference can exist between  $\sigma_{TRUE}$  and  $\sigma_{COMPUTED}$ , but  $r$  the criterion for 'goodness of fit', will still be small.

Both of the phenomena mentioned above impose a restriction on the minimum width of any block used to form the equivalent layer at a given depth. As an approximate rule the width of any block must be at least as great as its depth beneath the observation level. In this way the high frequency components are not resolved by the block model and in addition normal  $K$  contains no small elements.

However, this restriction imposes a severe limitation on the method when working at depths of the order of 30 km below the level of observation i.e. determining the shape of deep structures or the crust mantle interface. A computer program has been written to overcome this deficiency.

2-5-1-1 The Variable Block Coordinate Program.

This program which is basically similar to those described previously operates in the following way:

1) The anomaly is overlaid by a series of blocks, at the specified depth, whose widths exceed this depth, ensuring that the layer overlaps the margins of the body by at least three blockwidths. This can be done by inspection of the anomaly.

2) The best fitting model is produced in the usual way using this block configuration.

3) The program then shifts the whole block system to the right (say) by a specified fraction of a block width (usually 1/10th).

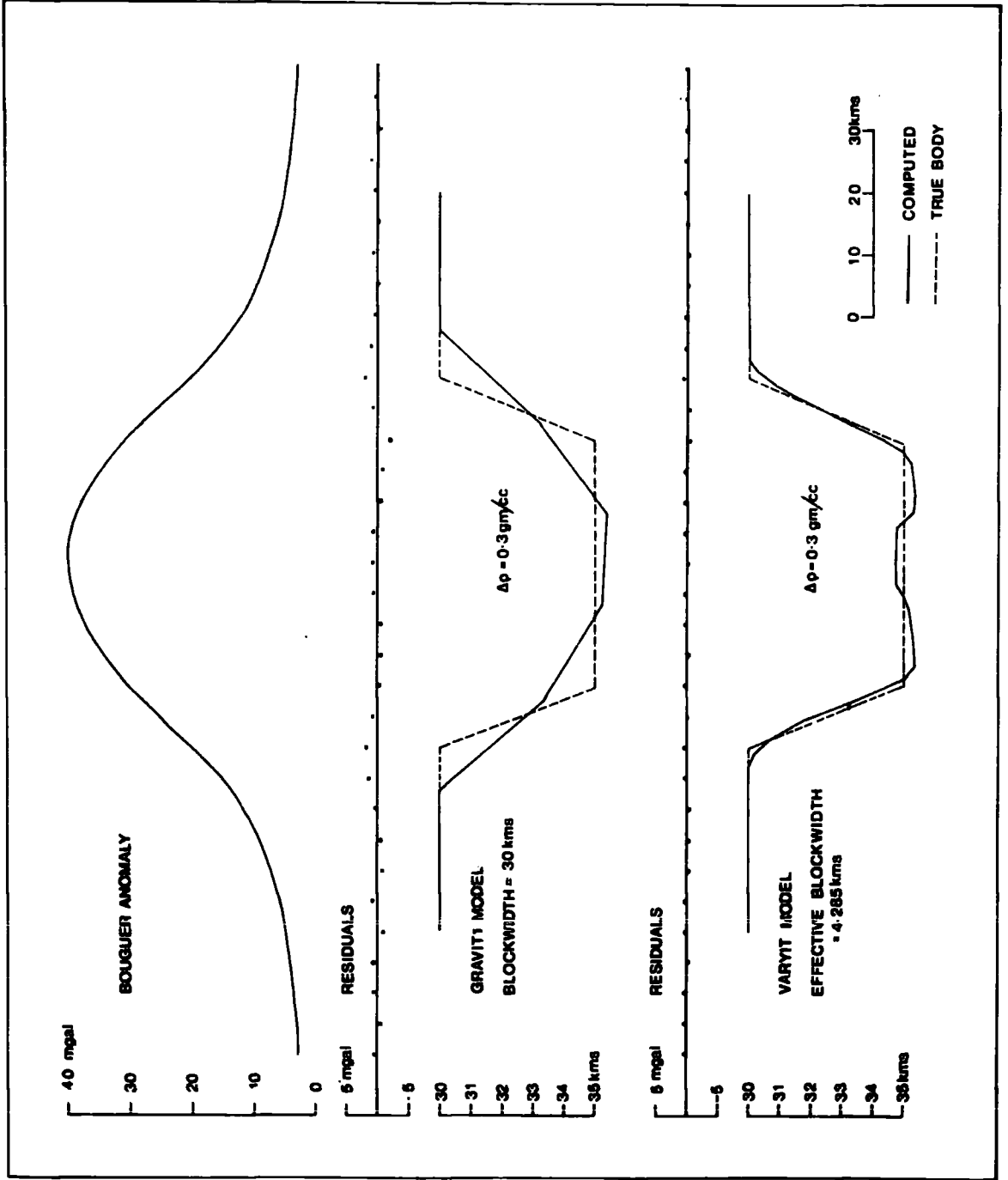
4) The space form is again computed using this new block configuration.

5) This process is repeated until the block margins are again at their original relative location (i.e. 9 times in above case.)

6) The locus of the body points computed, delineates the body shape and the gravity anomaly of the locus is computed and compared with the observed.

In this way the effective block width is reduced and much of the resolving power is regained. An example

Fig. 2-6. Illustration of the increase in resolving power obtained using the VARYIT program



of the program's use is shown at Fig.(2-6). The program written is called VARYIT. Specifications and listing are given in Appendix 1.

## 2-5-2 Infinite Structures

Often we wish to use the programs to compute the form of 'infinite' structures. An example is the computation of the crust-mantle interface across a continental margin when its depth is known at one point. Such 'open ended' anomalies have an effective vertical discontinuity and can be considered to behave like a ~~step-function~~ in the region of the discontinuity. It is well known that when a given function with a vertical discontinuity is approximated by a partial sum of components (e.g. frequency components in Fourier analysis) large discrepancies occur in the vicinity of the discontinuity (e.g. Hsu, 1967 page 320). This effect is known as Gibb's Phenomenon. Infinite anomalies cannot be analysed by the programs because of this effect -- violent oscillations occur in the region of the discontinuity, (the last specified anomaly value in this case), and the model is meaningless.

An example of this phenomenon in practice is shown at Fig. (2-7(b)). The problem is overcome by cosine tapering the observed curve. The result of this procedure is shown at Fig. (2-7(a)). In general when dealing with infinite anomalies the following procedure is adopted:

- 1) The 'open ended' anomaly is extrapolated at its maximum level for five blockwidths beyond the last


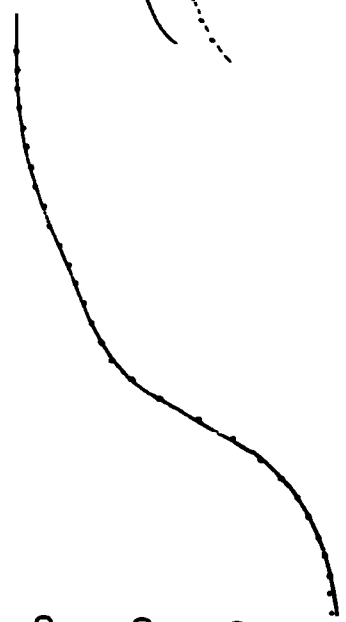
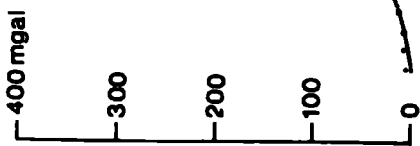
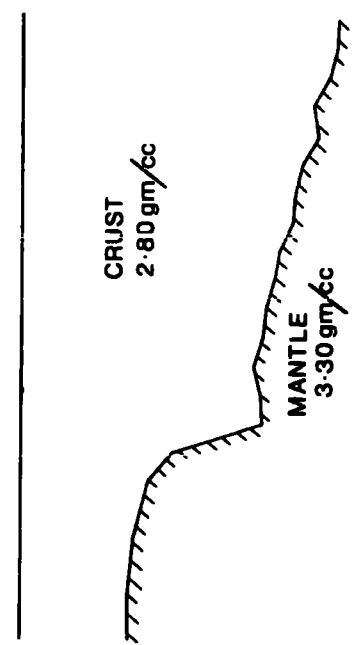
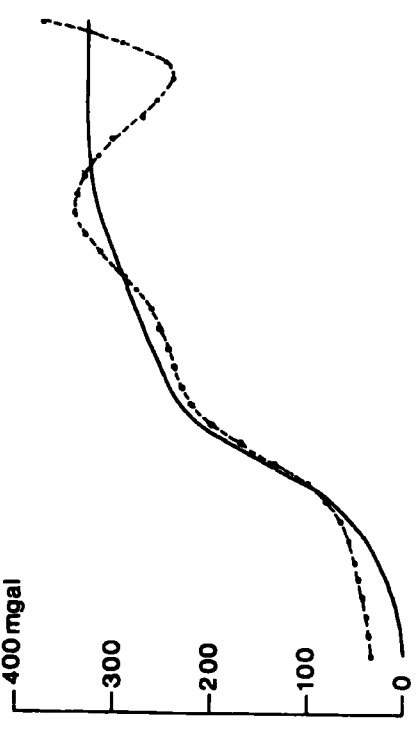


Fig. 2-7. Illustration of the effect of tapering a gravity anomaly over an "infinite" structure. The data used is from a line crossing the Sierra Leone continental margin. (see Chapter 6.)

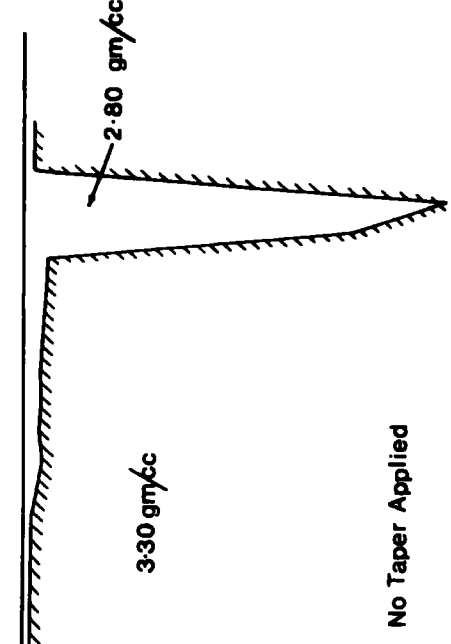
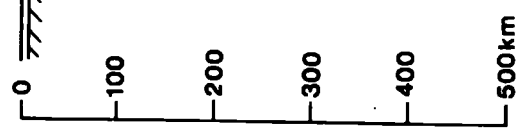
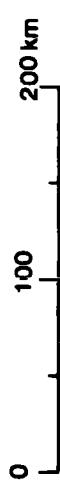
**BOUGUER ANOMALY**



OBSERVED  
COMPUTED



Taper Applied to Data





anomaly point to be fitted.

2) A cosine taper is applied to the end of the anomaly for a distance equal to the anomaly length. Alternatively the anomaly can be mirrored after extrapolation. Errors will obviously occur in the region of the last few anomaly points before the extrapolation, but these are usually found to be well within the limits of tolerance.

#### 2-5-3 Interfering Anomalies.

Adjacent bodies (having the same density contrast, or different contrasts of either sign) causing interfering anomalies can be analysed using the matrix method. The density of each block is read into the program as an array and the procedure used is as before. Bodies with a known lateral variation in density contrast can also be treated in this way.

#### 2-5-4 Steep Body Contacts

The fact that the body is built up of trapezia will obviously limit the maximum body gradients that can be handled, when consideration is given to the condition laid down in section (2-5-1). A facility to vary the blockwidths along the length of any model has been written into the programs and in this way steep shallow structures can be determined even for a body with a large over-all depth. The VARYIT program must however be used if the steep structure is at depth.

#### 2-6 Conclusions

The programs developed provide a fast and widely applicable method of computing realistic geological

models from gravity data. In general, low residuals result, and in cases where they do not, through lack of resolving power, the residuals can usually be reduced to a tolerable level by fine modification of the model using a direct program (e.g. GRAVN -- Bott, 1969).

2-7 Extension of the Method to Three Dimensions

Applying two dimensional analysis to three dimensional structures invariably leads to an underestimate of the body dimensions. However with the application of end corrections the errors will be tolerable in the light of uncertainties about the density and location of the causative body. The exception to this will be bodies that have a small strike length normal to the observed gravity profile or roughly circular structures, when errors may well become significant. The matrix method has been extended to three dimensions so that a reliable interpretation may be made in these cases.

2-7-1 Calculation of the Gravity Anomaly due to a Three Dimensional Rectangular Prism.

A computer program 'PRISM' has been written to calculate the gravity anomaly due to a prism at any point on a surface above the top of the prism. This program is then used as a subroutine in the automatic interpretation programs, but it could also be used to compute the gravity anomaly due to some arbitrarily shaped three-dimensional structure by dividing the structure into a number of small rectangular prisms.

The basic equation used is that of Hāz (1953) cited by Nagy (1966) for the gravity anomaly due to any

rectangular prism.

$$g(0,0,0) = G_p (-a \log(b+r) - b \log(a+r) + \text{catan } \frac{a \cdot b}{c \cdot r})$$

$$\begin{vmatrix} a_2 & b_2 & c_2 \\ a_1 & b_1 & c_1 \end{vmatrix} \quad (2-12)$$

$$\text{where } r = (a^2 + b^2 + c^2)^{\frac{1}{2}}$$

An explanation of the coordinates is given at Fig.(2-8)

The expansion of equation (2-12) is laborious and will not be given here, it can be obtained from the program listing (Appendix 1) if required.

The two programs written GRAVIT 3 (For bodies with inward sloping contacts) and GRAVIT 4 (outward) are essentially identical to their two dimensional counterparts, but a brief description is given below.

#### 2-7-2 Inward Sloping Contact Program

A series of rectangular prisms 100 metres thick are placed under the known or estimated top surface of the causative body. The increased thickness of the equivalent layer approximation as compared to the two dimensional case is necessary because of the smaller gravity anomaly due to a prism compared with a 'block' infinite in one direction. The gravity anomaly due to a 1 metre thick rectangular prism of unit density would be extremely small at some observation points for most practical models, and a conditioning problem would arise. The elementary prisms used for successive iterations must also have this increased thickness, however, this does not affect the resolving power of the program.

The method of iteration is identical to that outlined in section 2-3-1. Three iterations are usually sufficient.

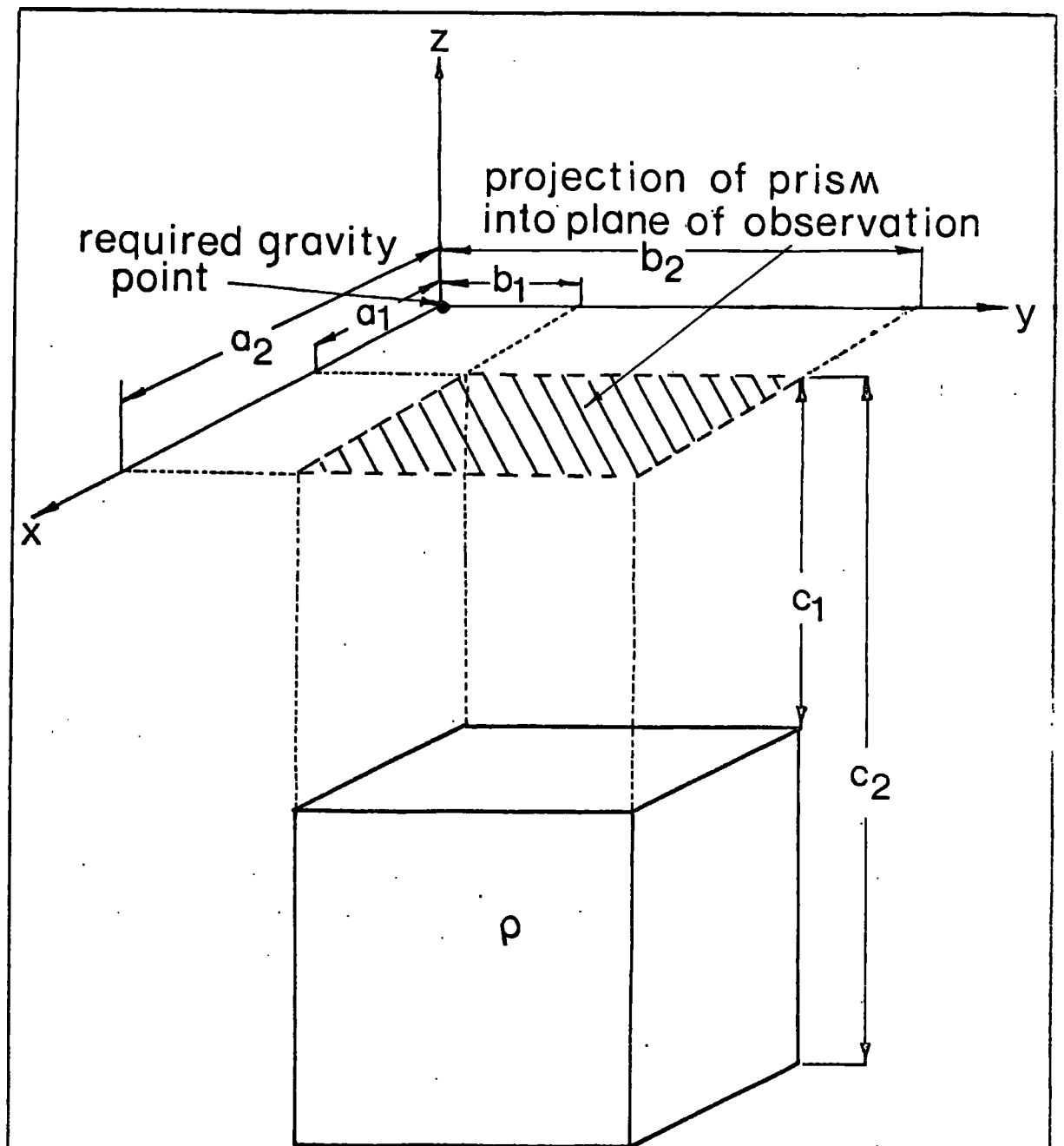


Fig. 2-8. Notation used for the gravity formula at a point due to a rectangular prism

2-7-3 Outward Sloping Contact Program.

One point on the top surface of the body must be specified, a horizontal bottom surface is again assumed. A series of prisms 100 metres thick are placed at the level of the specified top surface point and the bottom surface is computed using equation (2-7). The bottom and top surfaces, with the exception of the specified point, are adjusted by the same method as that used in the two dimensional case. Smoothing of the computed model to form a series of trapezoids is not written into the programs, the final model is built up of rectangular blocks.

2-7-4 Example of the Application of the Programs

Both programs were tested by computing the gravity anomaly due to a three dimensional body using a program <sup>personal communication</sup> THIRDIM (Y. Folkman, 1969) based on the method of Talwani & Ewing (1960). The anomaly was then specified to the automatic programs and the body shape recomputed. A simple example using GRAVIT4 is cited here.

The gravity anomaly due to a 1 km. cube at a depth of 0.5 km. was computed using THIRDIM. The body was then recomputed using four prisms. The depth to the top of one prism was specified. After four iterations of three unknown top surfaces were computed correct to 1 metre and the unknown bottom surface was correct to within 2 metres. The residual anomalies were all 0.01 mgal or less the maximum anomaly value being 3.14 mgal.

2-7-5 Conclusions.

Although the programs have an advantage over the only other method of three dimensional analysis known to the author (Cordell and Henderson, 1968), in that they

rapidly converge to a solution, they have a major drawback, as will any method of three dimensional analysis, in that the computer storage requirement for the analysis of any reasonably sized geological feature is prohibitive. Their use in practice is thus severely limited.

CHAPTER 3

THE MATRIX METHOD APPLIED TO MAGNETIC INTERPRETATION

3-1 Introduction

In contrast to gravity interpretation where space form and density are the only variables, magnetic interpretation is complicated by two additional variable parameters. In addition to shape and intensity of magnetisation, the orientation of the magnetic moment vector in the causative body and the Earth's field direction in the region of measurement all contribute to the anomaly shape. Magnetic interpretation is further complicated by the lack of a direct relationship between anomaly and body shapes. Two main techniques of interpretation have previously been adopted:

3-1-1 Comparison Methods.

The shape of the causative body is assumed, and its anomaly is computed, either using graticules (Pirson, 1940) or a computer program (Talwani and Heirtzler, 1964; Bott, 1969). The computed anomaly is then compared with the observed and the mismatch is noted. Trial and error adjustments are then made, until the residuals between the observed and calculated anomalies become tolerable. This method proves far less simple than is gravity interpretation, and the time required to obtain a solution becomes prohibitive when the polarization direction is unknown.

Alternatively, the anomaly can be matched with master curves of known origin (Hutchinson, 1958; Gay, 1963; Magrath and Hood, 1970). Such master curves are, however, only available for simple bodies such as dykes,

sills, prisms etc.

### 3-1-2 Direct Methods:

Under certain assumptions, such as the basic form of the source body, parameters such as depth and width can be evaluated from a consideration of the anomaly curve parameters. (Bruckshaw and Kuneratnum, 1963; Vaquier et al, 1951).

Other methods involving continuation techniques have been developed by Peters(1949), Henderson and Zeitz (1949) and many commercial companies have methods for estimating depth to magnetic basement (e.g. Hartmann et al, 1961; Naudy, 1970).

### 3-2 Non-Linear Optimisation

Non-linear optimisation techniques (Al-Chalabi, 1970) are the only methods developed to date of delineating an arbitrary body shape directly from the anomaly caused. They work by searching for optimum of a function in the hyperspace of its variable parameters. No information about the direction of magnetisation, regional background field, intensity of magnetisation or body location need be specified for a solution to be obtained, the resulting model being in the form of a two dimensional polygon. Although the methods produce excellent results they do have a serious limitation in that the number of coordinates delineating the causative body must be small if the computation time is not to be prohibitive. The method is thus restricted to simple anomalies.

The matrix methods described in this chapter are capable of handling both simple and complex anomalies and thus fill a very real gap in the available methods



of magnetic interpretation.

### 3-3 Notation

The following notation will be used throughout this chapter.

$F(x,z)$  is any two dimensional total field magnetic anomaly and is assumed to be measured in the direction of the ambient field  $F_0$ . This assumption is valid as long as  $F \ll F_0$ . Magnetic anomalies usually satisfy this condition and thus satisfy Laplace's Equation.

The Earth's field dip is  $I_e$  and its azimuth with respect to the direction of the anomaly profile is  $\alpha_e$  (Fig. 3-1). The dip of the Earth's field in the plane of the profile is given by:

$$\sigma = \arctan (\tan I_e / \cos \alpha_e) \quad (3-1)$$

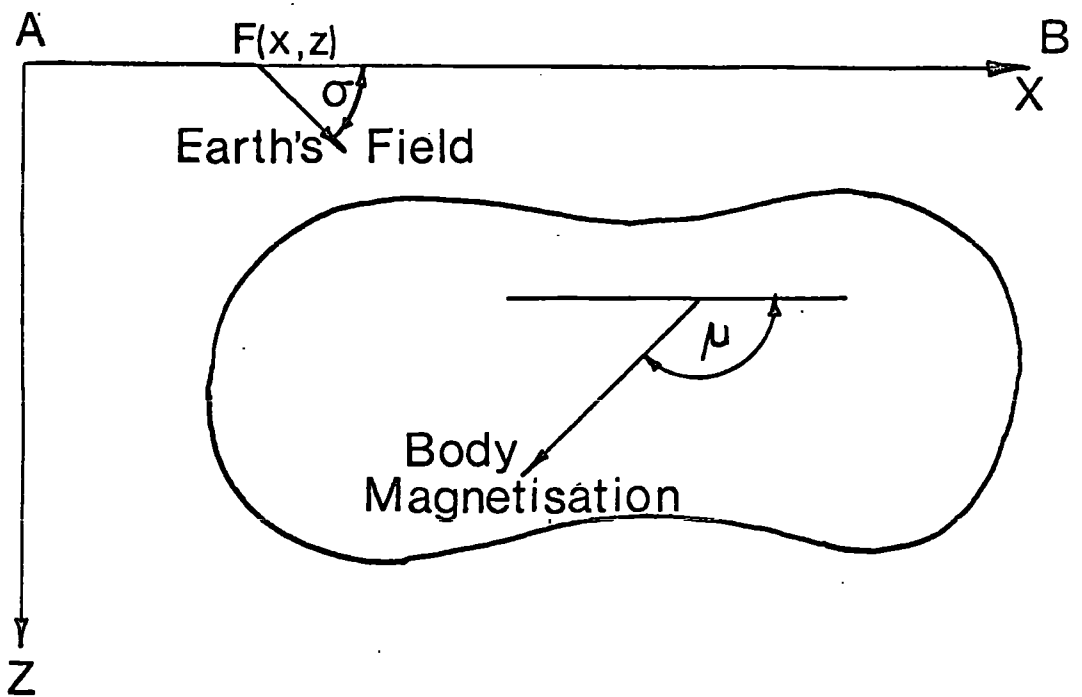
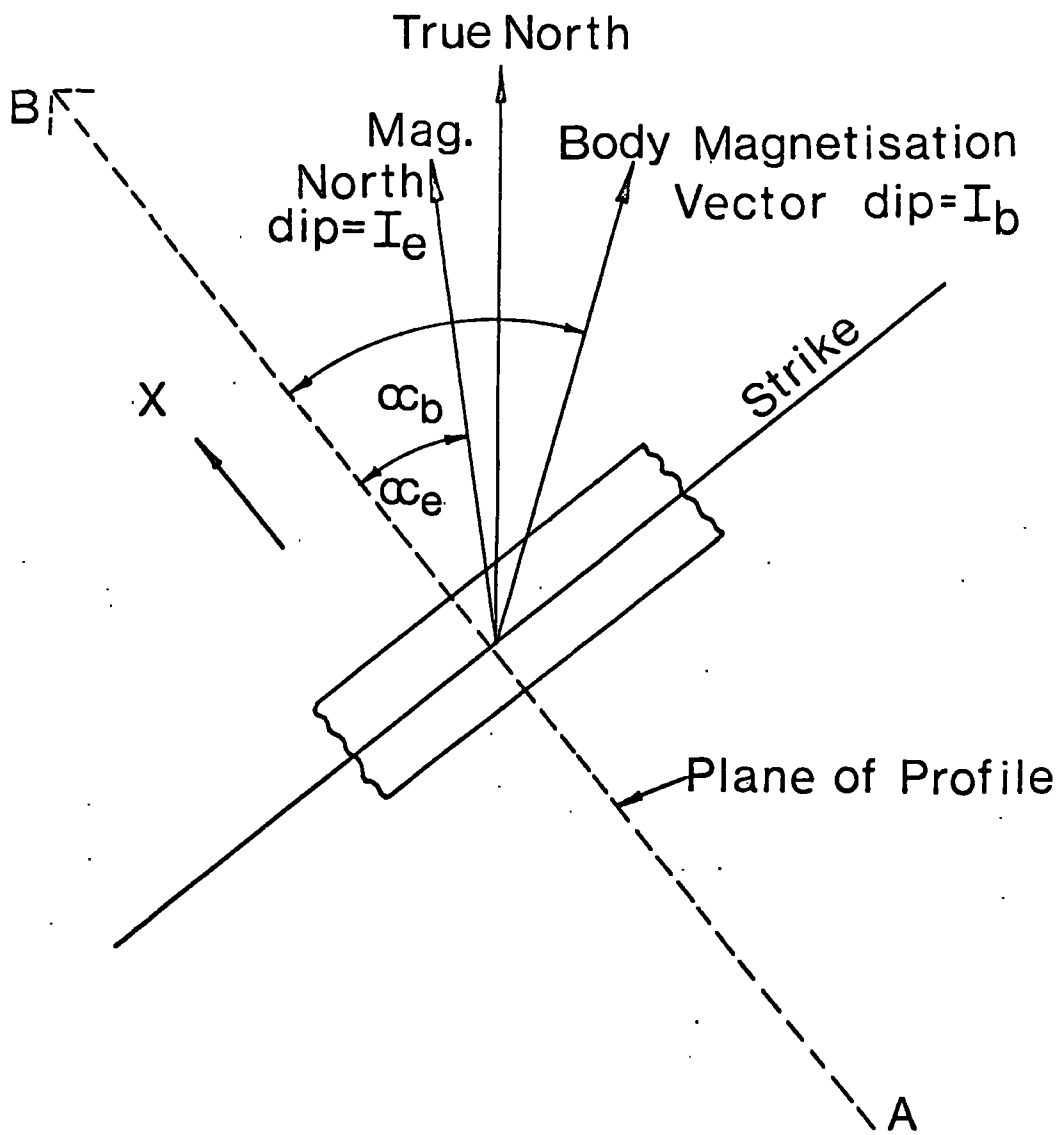
Similarly the body magnetisation vector  $\underline{J}$  ( $J_x, J_y, J_z$ ), has dip  $I_B$ , azimuth  $\alpha_B$ , and dip in the plane of the profile:

$$\mu = \arctan (\tan I_B / \cos \alpha_B) \quad (3-2)$$

### 3-4 Application of the Matrix Technique.

Since the equivalent dipole layer exists for total field magnetic anomalies (Chapter 1), we can apply the matrix method, used in Chapter 2 for gravity interpretation, to solve the inverse problem in magnetics. However inspection of equation (1-10) shows that the magnetic equivalent layer is a function of the angle  $\beta$  ( $\beta = \sigma + \mu$ ), and thus the dip of the body magnetisation in the plane of the anomaly profile must be known before an equivalent layer can be computed.

Fig.3-1. Notation used for the magnetic anomaly due to an arbitrarily shaped, arbitrarily magnetised body.



3-4-1 Determination of the Body Magnetisation Angle

In cases where the causative body outcrops, the magnetic properties of specimens can be used to determine the angle of magnetisation ( $\mu$ ), but in the case of a buried structure, or when the magnetisation of the rocks exposed does not reflect the mean magnetisation of the whole body, we must use the geophysical anomaly to determine the angle.

Bott, Smith and Stacey (1966) used the method of Baranov (1957) to transform a magnetic anomaly to a 'pseudo-gravity' anomaly, and were able to estimate the angle of magnetisation to within a range of some 50 degrees in this way. Various authors have published methods of determining the angle of magnetisation when the body shape is known (e.g. Bhattacharyya, 1966; Watts, personal communication), but no method exists in the literature for determining the angle from a knowledge of the magnetic anomaly alone. This can be achieved by the empirical method described below.

There is associated with any magnetic anomaly an anomalous magnetic moment vector (analogous to the excess mass associated with a gravity anomaly) resulting from the causative body. If this moment be  $\underline{M}$  ( $M_x, M_y, M_z$ ) and if we then consider a two dimensional body in the x,z plane, with area S within this plane and infinite in the y - direction (Fig. 3-2), then the total magnetic moment vector is:

$$M (M_x, M_z) = \iint_S J(x,z) \cdot dx \cdot dz \quad (3-3)$$

where  $J(x,z)$  is the intensity of magnetisation at any point  $(x,z)$  in the body

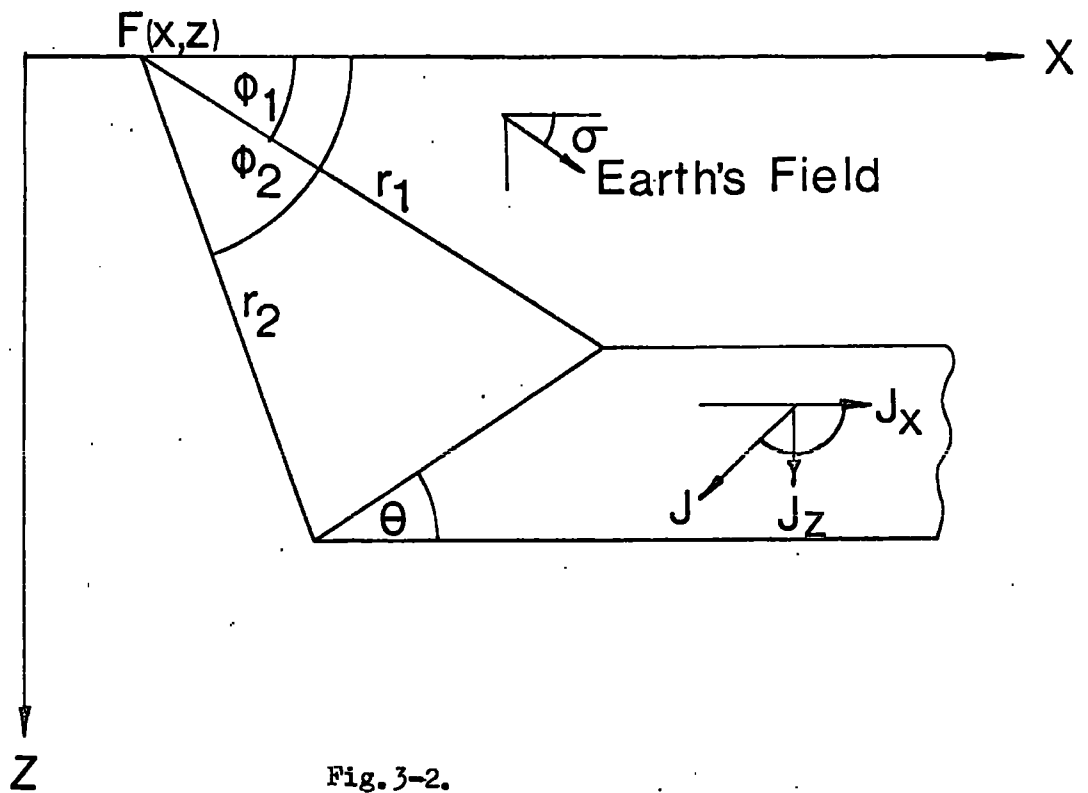
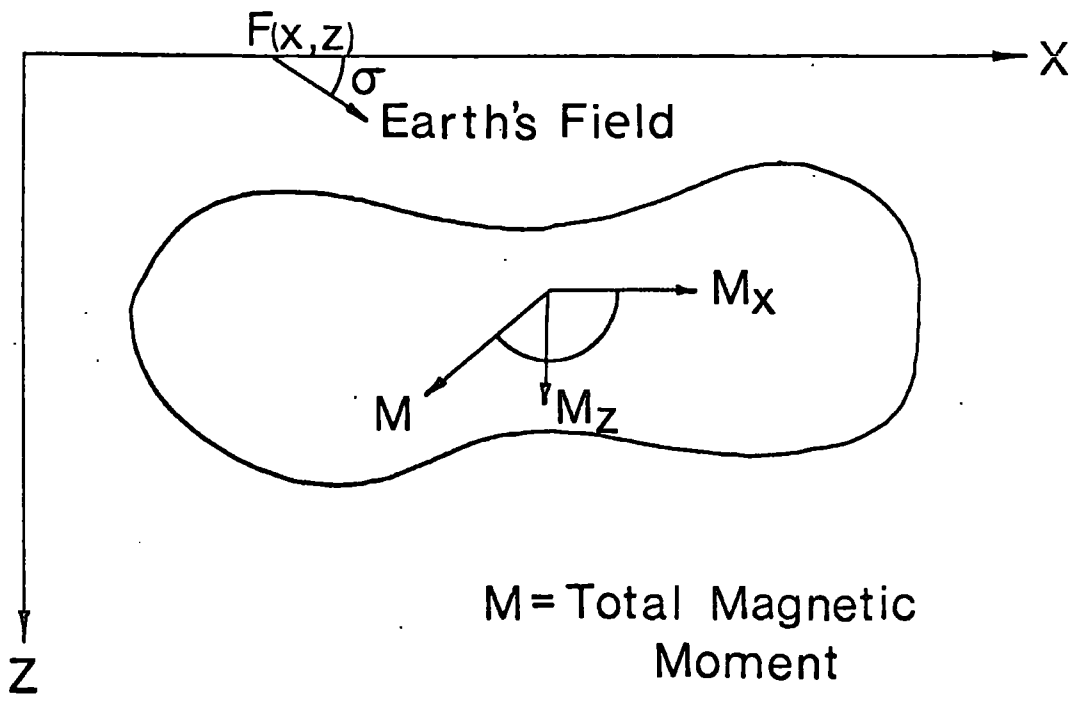


Fig. 3-2.

It can be shown that:

$$M_x = - (\ell J_2 + n J_1)/2 (\ell^2 + n^2) \quad (3-4)$$

and

$$M_z = (n J_2 - \ell J_1)/2 (\ell^2 + n^2) \quad (3-5)$$

where

$$J_1 = \frac{1}{\pi} \int_0^{\infty} x \cdot (F(x) - F(-x)) dx \quad (3-6)$$

and

$$J_2 = \lim_{x \rightarrow \infty} \frac{1}{2} x^2 (F(x) + F(-x)) \quad (3-7)$$

and the vector  $\underline{s} = (\ell, 0, n)$  defines the direction of measurement of  $F$ . (i.e. the ambient field direction)

(Smith - unpublished manuscript  
- see Appendix 2).

Thus the total magnetic moment vector can be represented as a function of the anomaly  $F(x)$  alone, and any set of finite bodies producing the same magnetic anomaly must have the same total magnetic moment. This fact can be used to determine the angle of magnetisation of a finite body using the equivalent layer technique.

### 3-4-1-1. Method

The equivalent layer is approximated by a series of thin blocks underlying the anomaly (with width  $\gg$  depth - see section 3-4-2-1). The magnetic anomaly due to such a block can be calculated at any point on or above the block using the formula for a semi-infinite slab Talwani and Heirtzler, 1964; Bott, 1969)

$$F = \sin I_e (2J_x \sin^2 \theta \log r_1/r_2 + 2J_x \sin \theta \cos \theta (\phi_1 - \phi_2) + 2J_z \sin \theta \cos \theta \log r_1/r_2 - 2J_z \sin^2 \theta (\phi_1 - \phi_2))$$

$$\begin{aligned}
 &+ \cos I_e \sin \alpha_e (2J_x \sin^2 \theta (\phi_1 - \phi_2) - 2J_x \sin \theta \cos \theta \log r_1/r_2 \\
 &+ 2 J_z \sin^2 \theta \log r_1/r_2 + 2 J_z \cos \theta \sin \theta (\phi_1 - \phi_2)) \quad (3-8)
 \end{aligned}$$

see Fig. (3-2)

By subtracting two vertically sided semi-infinite slabs we obtain any desired block. Thus putting  $\Theta = 90^\circ$  in equation (3-8) and rearranging in terms of  $J_x$  and  $J_z$  we obtain the equation for the magnetic anomaly at any point due to any block.

$$\begin{aligned}
 F &= J_x (2 \sin I_e \log r_1/r_2 + 2 \cos I_e \sin \alpha_e (\phi_1 - \phi_2)) \\
 &+ J_z (2 \cos I_e \sin \alpha_e \log r_1/r_2 - 2 \sin I_e (\phi_1 - \phi_2)) \quad (3-9)
 \end{aligned}$$

Thus for a series of blocks making up the equivalent layer approximation we have, using matrix notation:

$$F_i = A_{ij} J_{xj} + B_{ij} J_{zj} \quad (i = 1 \text{ to } N \quad j = 1 \text{ to } M). \quad (3-10)$$

$A_{ij}$  is the magnetic anomaly of the  $j$ th block at the  $i$ th field point assuming unit horizontal magnetisation.  $B_{ij}$  similarly assumes unit vertical magnetisation. The subscript indicates summation. Thus we have

$$\begin{bmatrix} F_1 \\ F_2 \\ F_3 \\ \vdots \\ F_N \end{bmatrix} = \begin{bmatrix} A_{11} & A_{12} & \dots & A_{1M} & B_{11} & B_{12} & \dots & B_{1M} \\ A_{21} & & & & B_{21} & & & \\ \vdots & & & & \vdots & & & \\ A_{N1} & \dots & A_{NM} & B_{N1} & \dots & B_{NM} \end{bmatrix} \begin{bmatrix} J_{x1} \\ J_{x2} \\ \vdots \\ J_{xM} \\ J_{z1} \\ J_{z2} \\ \vdots \\ J_{zM} \end{bmatrix}$$

If  $N > 2M$  then this set of equations has a least squares solution. However the vectors  $J_{xj}$  and  $J_{zj}$  are linearly dependent and the individual values obtained for any element will depend on the dimensions of the equivalent layer approximation used and will thus have no real significance. Nevertheless the mere existence of a solution is sufficient for our purposes since any solution must obey the constraint:

$$\mu = \arctan \left[ \frac{\sum_{j=1}^M J_{zj}}{\sum_{j=1}^M J_{xj}} \right] \quad (3-11)$$

The individual elements are then ignored and equation (3-11) is solved for the angle of magnetisation.

Since it is not necessary to restrain the depth of the equivalent layer, except for the lower limit imposed by the resolving power criterion, it is not necessary to have any knowledge of the depth of the causative body to determine the angle of magnetisation.

No knowledge of the width or intensity of magnetisations is needed and the technique is thus widely applicable. Determinations of the angle of magnetisation can be made when insufficient data is available to determine the space form of the body.\*

### 3-4-1-2 Results Using the Matrix Technique

The magnetic anomalies due to four arbitrarily shaped bodies with different angles of magnetisation were computed using a program available at Durham (MAGN-

\* The magnetic anomaly to be analysed must extend beyond the ends of the equivalent layer approximation.



Bott, 1969). The equivalent layer technique was then used to recompute the angle of magnetisation in each case. For each model the equivalent layer was placed at a series of depths ranging from half the true top surface depth or top point depth, to three times this depth. No assumption about the body width was made, the entire anomaly being underlaid by blocks. The only parameter specified to the program was the Earth's field direction.

In all cases the angle computed was accurate to within 0.05 degrees, a slight variation of computed angle with depth of equivalent layer (of the order of 0.02 degrees) was observed. Further applications of the technique to test and field data are discussed in sections 3-5-1 and 3-5-2.

#### 3-4-1-3 Limitations of the Method

1) Sufficient of the anomaly to be analysed must be specified to permit the problem a meaningful solution. Thus just the main 'lobe' of an anomaly is not sufficient.

2) The technique will not work for bodies that are infinite in the x or z - directions (e.g. dykes, sills etc.) since in these cases angle of magnetisation and geological dip are interchangeable (Bruckshaw and Kunaratnam, 1963)

3) With field data there will always be some uncertainty about the regional background field and if this is large the possible range of angle of magnetisation will also be quite large.

3-4-2 Determination of the Space Form.

Knowing or having determined, the angle of magnetisation, the problem of determining the shape of the anomalous body is similar to that posed by the inverse gravity problem. Two programs have been developed to treat the cases of bodies with inward and outward sloping contacts.

3-4-2-1 Method.

It has been shown in Chapter 1 that a magnetic dipole equivalent layer, producing the identical magnetic anomaly to some unknown distribution of magnetisation exists and we can thus write:

$$F(x_1) = \int_{-\infty}^{\infty} K \left[ (x_1-x), d_1(x), d_2(x), \beta \right] \cdot J(x) \cdot dx. \quad (3-12)$$

where  $J(x)$  is the magnetic moment per unit area bounded by  $d_1(x)$  and  $d_2(x)$  and  $\beta = \sigma + \mu$ .  $K$  is a kernel function depending on  $d_1$ ,  $d_2$  and  $\beta$  defining the magnetic anomaly of the equivalent layer assuming unit magnetisation.

As before, if we subdivide the layer into a finite number of blocks sufficiently small for the assumption of constant magnetisation within a given block to be valid, then equation (3-12) can be approximated by:

$$F_i = \sum_{j=1}^N K_{ij} J_j \quad (3-13)$$

$i = 1$  to  $N$

where  $K_{ij}$  is the anomaly at the  $i$ th field point due to the  $j$ th block assuming unit magnetisation.

If  $n > m$  the solution is given by:

$$J = (K^T K)^{-1} K^T F \quad (3-14)$$

using matrix notation.

The methods of iterating on equation (3-14) are basically the same as those employed in the gravity programs and need not be repeated here. Several minor differences do, however, exist.

1) When calculating the kernel function  $K$  unit magnetisation in the direction of the true body magnetisation vector must be specified for each block.

2) The expansion equations for the gravity case (equations 2-4, 2-6 and 2-7 - 2-10) must all have their final terms multiplied by  $\sin \mu$ .  
e.g. equation 2-4 becomes:

$$d_2 (j^{\text{th}} \text{ block}) = d_1 (j^{\text{th}} \text{ block}) + \frac{J (j^{\text{th}} \text{ block}) \sin \mu}{\text{specified magnetisation}} \quad (3-15)$$

i.e. the assumption is that a linear relationship exists between thickness and magnetisation, in the direction of magnetisation.

3) End corrections are not applied.

4) The magnetic anomaly due to each model is calculated using equation (3-8) after each iteration.

Again the problem is ambiguous and must be constrained if the solution is to be meaningful. In the case of the outward sloping contact program, one point on the top surface and the magnetisation contrast must be specified. In the case of the inward sloping contact program, the top surface (not necessarily flat) and the magnetisation

are fixed. Both programs have the facility for computing the best model for various sets of these parameters, the resulting models can then be accepted or rejected on the grounds of geological feasibility and 'goodness of fit'.

### 3-4-3 Available Programs

Two programs, MAGGIT 1 and MAGGIT 2 have been written, which compute the body magnetisation direction and the space form for the cases of inward and outward sloping body contacts respectively. Solutions can be obtained for a series of values of magnetisations and depths. A further two programs MAGGIT 3 and MAGGIT 4 are for use when it is wished to specify a value or series of values for the dip and azimuth of the body magnetisation vector. Data specifications, listings and general operating instructions are listed in Appendix 1.

### 3-5 Examples of the Application of the Programs.

#### 3-5-1 Test Data

Total field magnetic anomalies resulting from two models, one with inward sloping contacts, one with outward, were computed using a program available at Durham (MAGN -- Bott, 1969). The body shapes were then recomputed using the automatic programs.

#### 3-5-1-1 Model 1. - Outward Sloping Contacts

The depth to the point A (Fig. 3-3(a)) on the top surface of the body and the magnetisation contrast were specified. The peak to peak amplitude of the anomaly is of the order of 4,000 gamma (1 gamma =  $10^{-5}$  Oersted). The computed dip of the body magnetisation vector in the plane of the profile was in error by 0.02 degrees. Of the fifty anomaly values computed only nine had non-zero

Fig.3-3(a). Test body and resultant magnetic anomaly  
for the program MAGGIT2.

Fig.3-3(b). Test body and resultant magnetic anomaly  
for the program MAGGIT1.

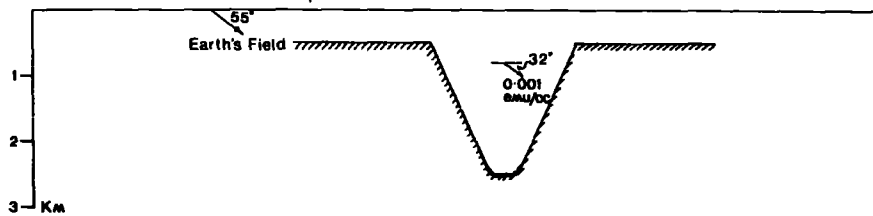
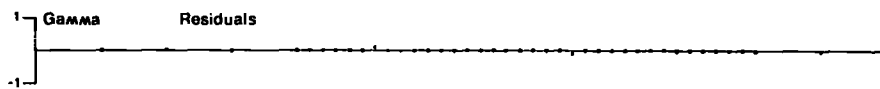
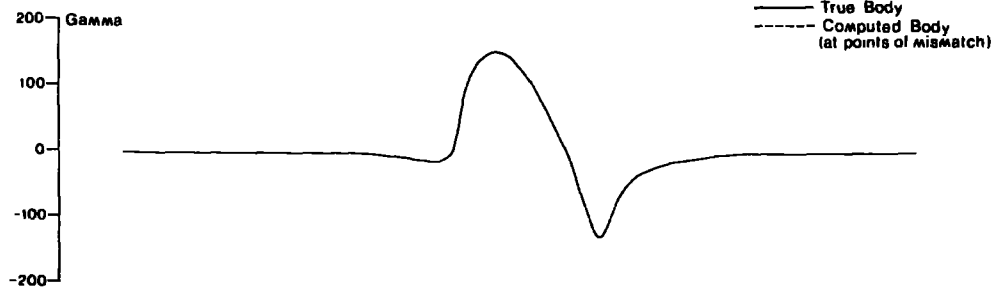
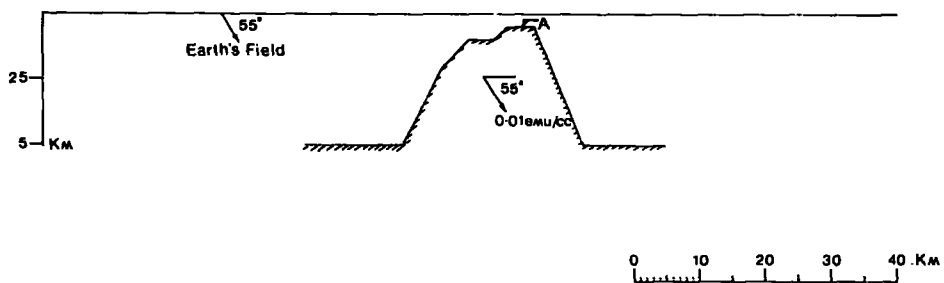
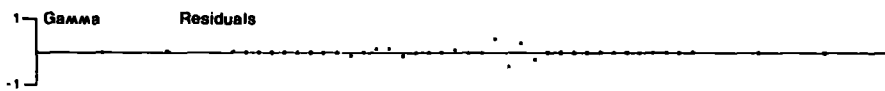
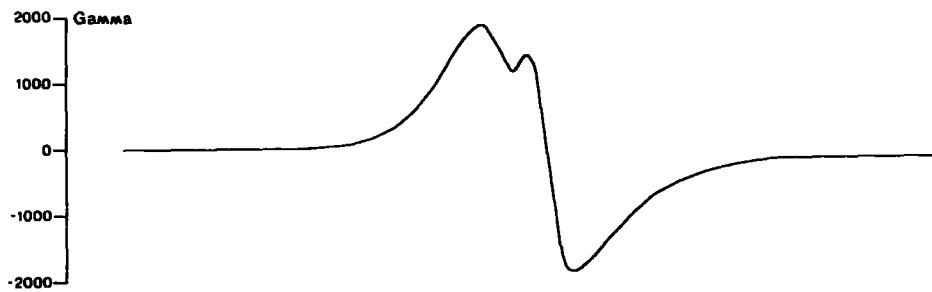


TABLE 3-2.

ESTIMATE 15    MAGNETISATION=.00100    BODY-ANGLE= 30  
 BODY-INCLINATION= 70    FIELD-ANGLE= 45    FIELD-INCLINATION= 45

SIDE	XTOP	XBOT	DTOP	DBOT
1	105500	105500	500	501
2	106500	106500	500	944
3	107500	107500	500	1392
4	108500	108500	500	1823
5	109500	109500	500	2311
6	110500	110500	500	2536
7	111500	111500	500	2517
8	112500	112500	500	2316
9	113500	113500	500	1824
10	114500	114500	500	1392
11	115500	115500	500	943
12	116500	116500	500	501

LOCATION	OBSERVED	CALCULATED	RESID
0	0.0	-0.1	0.1
50000	-0.4	-0.4	-0.0
55000	-0.5	-0.5	-0.0
60000	-0.6	-0.6	-0.0
65000	-0.7	-0.7	-0.0
70000	-0.8	-0.8	0.0
75000	-1.1	-1.1	-0.0
80000	-1.4	-1.4	0.0
85000	-2.0	-2.0	0.0
90000	-3.1	-3.1	-0.0
95000	-5.1	-5.1	-0.0
96000	-5.7	-5.7	0.0
97000	-6.5	-6.5	0.0
98000	-7.5	-7.5	-0.0
99000	-8.6	-8.6	0.0
100000	-10.1	-10.1	0.0
101000	-11.9	-12.0	0.1
102000	-14.3	-14.3	-0.0
103000	-17.0	-17.0	0.0
104000	-19.3	-19.3	-0.0
105000	-8.4	-8.4	-0.0
106000	90.0	90.0	0.0
107000	135.6	135.6	-0.0
108000	148.0	148.0	-0.0
109000	145.7	145.7	-0.0
110000	130.0	130.0	-0.0
111000	103.7	103.7	-0.0
112000	69.2	69.2	-0.0
113000	27.2	27.2	0.0
114000	-19.6	-19.6	-0.0
115000	-70.7	-70.7	0.0
116000	-129.9	-129.8	-0.1
117000	-108.0	-108.0	0.0
118000	-60.5	-60.5	0.0
119000	-39.8	-39.8	0.0
120000	-28.7	-28.7	-0.0
121000	-21.8	-21.8	-0.0

124000	-786.1	-786.1	-0.0
125000	-628.7	-628.7	-0.0
126000	-503.3	-503.3	0.0
127000	-406.0	-406.0	0.0
128000	-331.1	-331.1	-0.0
129000	-273.3	-273.3	-0.0
130000	-228.3	-228.3	0.0
135000	-108.5	-108.5	0.0
140000	-62.0	-62.0	0.0
145000	-39.7	-39.7	0.0
150000	-27.5	-27.5	-0.0
155000	-20.1	-20.1	-0.0
160000	-15.3	-15.3	0.0
165000	-12.0	-12.0	0.0
170000	-9.7	-9.7	-0.0
175000	-8.0	-8.0	-0.0
180000	-6.7	-6.7	-0.0
200000	0.0	-3.7	3.7

END OF MODEL. 1£1£1

END OF DATA



residuals ( $<0.05$  gamma) the largest being 0.4 gamma. The largest error in any body coordinate computed was 2 metres in a total thickness of 4.5 km. . The computed bottom surface was accurate to within 0.5 metres. The results are shown at Table (3-1) and the magnetic anomaly and causative body are shown at Fig. (3-3(a)). The program MAGGIT2 was used.

#### 3-5-1-2 Model 2 - Inward Sloping Contacts

The top surface of the body and the magnetisation contrast were specified. The peak to peak amplitude of the magnetic anomaly is 300 gamma. Of the fifty seven computed anomaly values only two showed non-zero residuals (both 0.1 gamma). The angle of magnetisation computed was accurate to within 0.03 degrees. The corners of the elementary trapezia were chosen so that the model could not produce an exact fit, to test the behaviour of the programs under these conditions. The degree of misfit of the computed body is small Fig.(3-3 (b)). Table 3-2 shows the computed results. The program MAGGIT1 was used.

#### 3-5-1-3 General Remarks

Both of the above solutions took of the order of 30 secs. computer time using NUMAC IBM 360/67 (cf. optimisation, 8 mins.). The advantage of using trapezia to produce a smooth body outline, as opposed to rectangular block is clearly seen by the good fits produced, particularly in the case of building up the top surface of a body. The near surface vertical discontinuities which necessarily result from using rectangular blocks

TABLE 3-1.

MODEL 1.8181

ESTIMATE 14    MAGNETISATION=.01000    BODY-ANGLE= 45

BODY INCLINATION= 45    FIELD-ANGLE= 45    FIELD-INCLINATION= 45

SIDE	XTCP	XBOT	DTOP	DBOT
1	107500	107500	4999	5000
2	108500	108500	4002	5000
3	109500	109500	3000	5000
4	110500	110500	2001	5000
5	111500	111500	1500	5000
6	112500	112500	1000	5000
7	113500	113500	1000	5000
8	114500	114500	1000	5000
9	115500	115500	500	5000
10	116500	116500	500	5000
11	117500	117500	500	5000
12	118500	118500	1400	5000
13	119500	119500	2301	5000
14	120500	120500	3200	5000
15	121500	121500	4102	5000
16	122500	122500	4999	5000

LOCATION	OBSERVED	CALCULATED	RESID
40000	0.0	-3.0	3.0
60000	-4.8	-4.8	0.0
65000	-5.5	-5.5	0.0
70000	-6.4	-6.4	-0.0
75000	-7.3	-7.3	-0.0
80000	-8.2	-8.2	0.0
85000	-8.7	-8.7	0.0
90000	-7.3	-7.3	0.0
95000	2.0	2.0	-0.0
100000	49.3	49.3	0.0
101000	73.0	73.0	0.0
102000	107.2	107.2	0.0
103000	157.0	157.0	-0.0
104000	230.0	230.1	-0.1
105000	336.8	336.8	0.0
106000	489.7	489.6	0.1
107000	700.5	700.4	0.1
108000	974.0	974.1	-0.1
109000	1299.2	1299.2	0.0
110000	1629.4	1629.4	0.0
111000	1872.9	1872.9	-0.0
112000	1913.7	1913.6	0.1
113000	1516.0	1516.0	-0.0
114000	1203.5	1203.5	-0.0
115000	1454.6	1454.2	0.4
116000	833.1	833.5	-0.4
117000	-215.9	-216.2	0.3
118000	-1714.8	-1714.6	-0.2
119000	-1785.7	-1785.7	0.0
120000	-1615.7	-1615.7	0.0
121000	-1405.9	-1405.9	-0.0
122000	-1186.2	-1186.2	0.0
123000	-974.7	-974.7	-0.0

122000	-17.1	-17.1	0.0
123000	-13.9	-13.9	-0.0
124000	-11.5	-11.5	0.0
125000	-9.7	-9.7	-0.0
126000	-8.3	-8.3	-0.0
127000	-7.2	-7.2	-0.0
128000	-6.3	-6.3	-0.0
129000	-5.5	-5.5	0.0
130000	-4.9	-4.9	-0.0
135000	-3.0	-3.0	-0.0
140000	-2.0	-2.0	-0.0
145000	-1.4	-1.4	0.0
150000	-1.1	-1.1	-0.0
155000	-0.8	-0.8	0.0
160000	-0.7	-0.7	-0.0
165000	-0.5	-0.5	0.0
170000	-0.5	-0.5	-0.0
175000	-0.4	-0.4	-0.0
180000	-0.3	-0.3	0.0
185000	-0.3	-0.3	-0.0
190000	-0.2	-0.2	0.0
200000	0.0	-0.2	0.2

END OF MODEL 1#1#1

END OF DATA

---

would certainly produce oscillations in the computed magnetic anomaly, if not complete instability.

3-5-2 Field Data

3-5-2-1 Lesser Antilles Arc Anomaly

This is a marine magnetic anomaly recorded during the 1968 survey by the USC & GSS DISCOVERER. It crosses the trend of the Lesser Antilles (Volcanic) Island Arc into the Venezuelan shelf (Fig. 3-4). The world wide regional program was used to remove the background field. The anomaly, shown at Fig (3-5(b)), is fairly complex and is thus a good test for the technique.

The top surface of the assumed causative body is known from seismic reflection (air-gun) data (Lattimore et al, in press), thus the only unknown to be specified is the magnetisation contrast. Control on this is possible since the depth to magnetic basement is estimated to be between 4 and 5 km . in the Grenada Trough (Fig. 3-4), to the north of the profile, from seismic refraction data (Ewing et al, 1957). Various magnetisations were specified and a value of 0.002 emu/cc was found to satisfy these conditions. The angle of magnetisation is  $84^{\circ}$  down to the north, and since the Earth's field dip is of the order of  $45^{\circ}$  in the plane of the profile, remanent magnetisation must have a significant contribution to the total. The computed space-form of the body is shown at Fig(3-5(c)) and shows good agreement with the seismic reflection data, the rough topography to the north of the main anomaly peak probably being due to the magnetic basement undulations shown.

# Antilles Magnetic Profile

Isobaths in fathoms

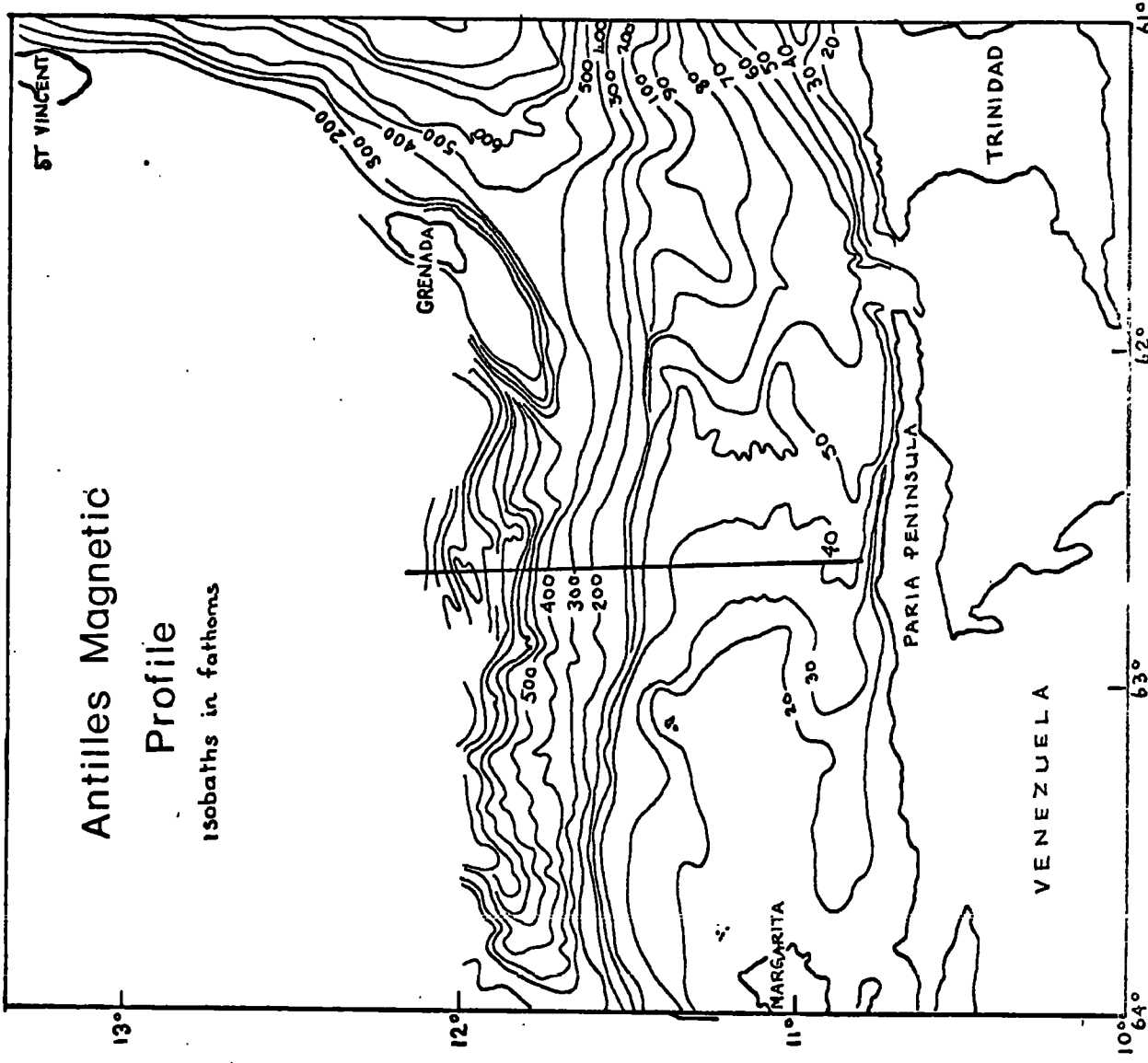


Fig. 3-4. Location of the Lesser Antilles Arc anomaly.

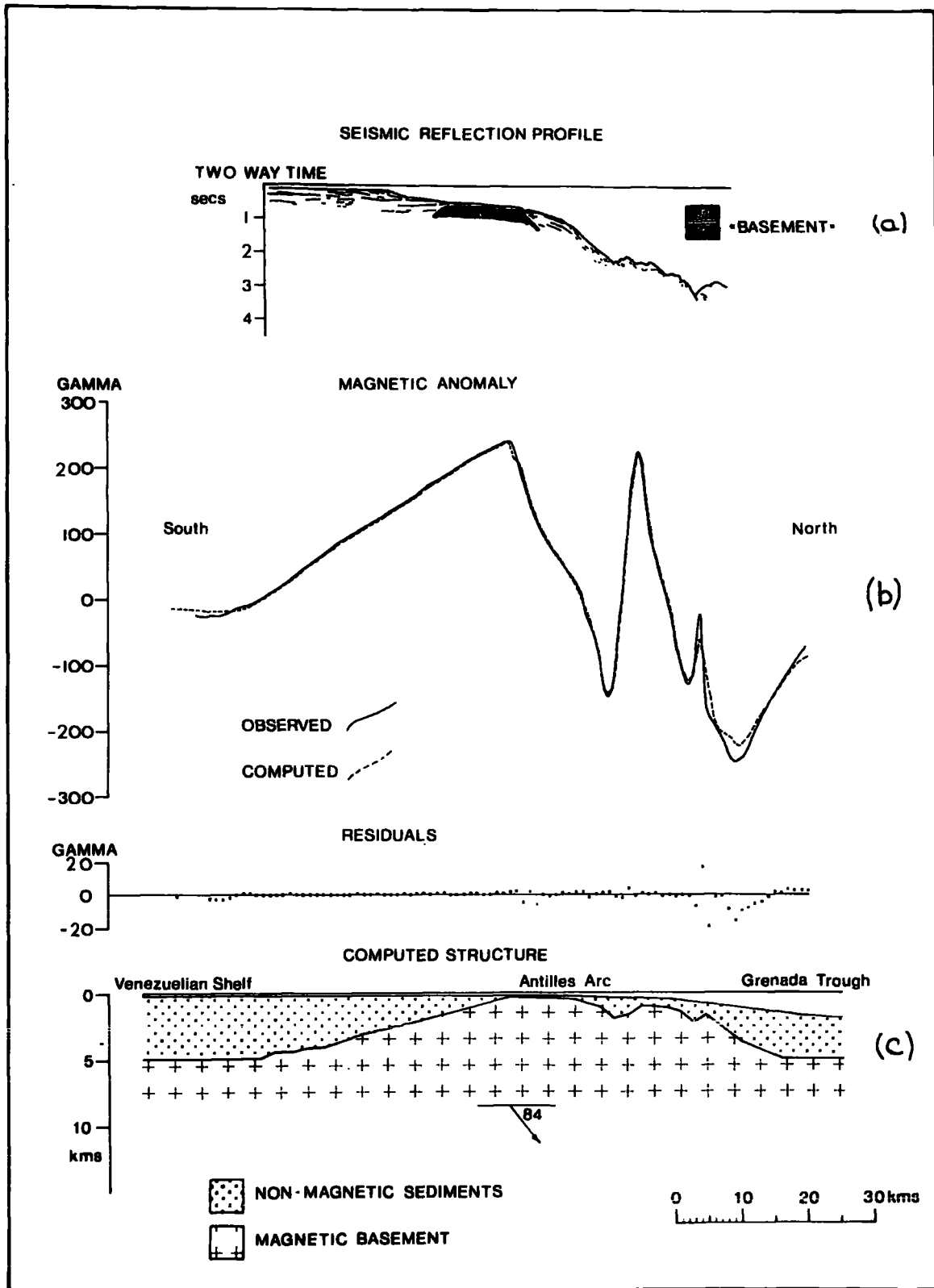


Fig.3-5. The Lesser Antilles Arc Anomaly.

### 3-5-2-2 The Carlisle Anomaly

This anomaly, which is taken from the aeromagnetic map of Great Britain, is centred near the city of Carlisle in N.W. England. Fig.(3-6). The exposed rock at the surface is Triassic conglomerate, sandstone and marl, and thus no surface evidence can be found for the cause of the anomaly. The roughly circular form of the anomaly does however tend to favour an intrusion of some kind rather than basement relief, as the causative feature.

Since the basic form of the causative body is unknown, the magnetic anomaly was analysed using both MAGGIT1 and MAGGIT2, for a series of depths and magnetisations. The results are shown at Fig. (3-7).

Although, for a body with outward sloping contacts, a range of solutions with depth to highest point in the range 2-4.5 km . and magnetisations 0.0008 to 0.006 emu/cc satisfy the observed anomaly within reasonable limits of tolerance, the best fit is produced by a body with a depth of 4 km. and a magnetisation contrast of 0.001 emu/cc.(all residuals  $< 1$  gamma). The form of the body produced is suggestive of a dome-shaped intrusion, probably a basic plug, as 0.001 emu/cc is an unusually high magnetisation for a granite.

A slightly deeper body with a magnetisation contrast of 0.003 emu/cc also produced an excellent <sup>fit</sup> to the observed anomaly (Fig.(3-7(b))). As this model has only 1 km. of relief a basement rise is suggested. However, the direction of magnetisation of the basement to the southwest of this profile is known from the work of Al-Chalabi (1970) and from re-analysis is this chapter(section

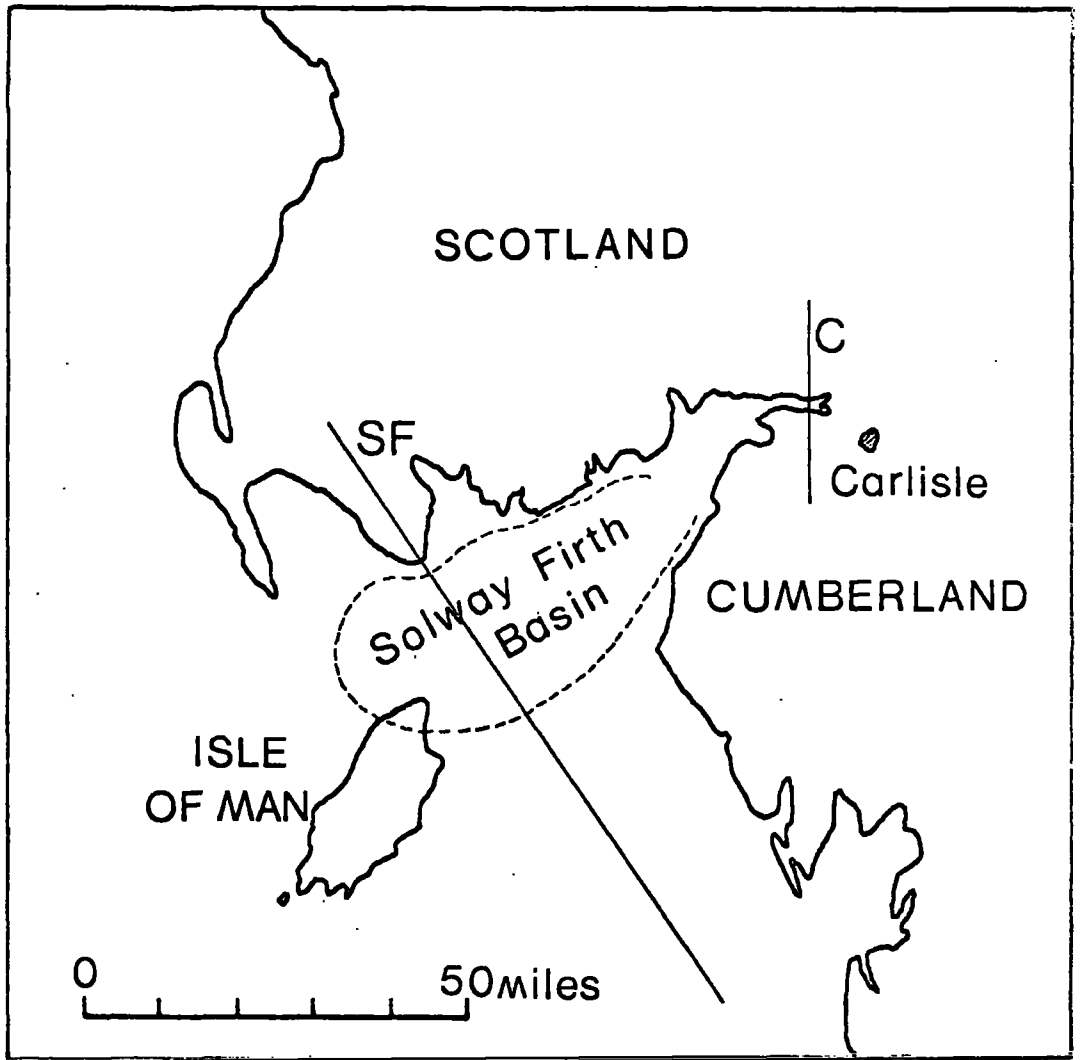
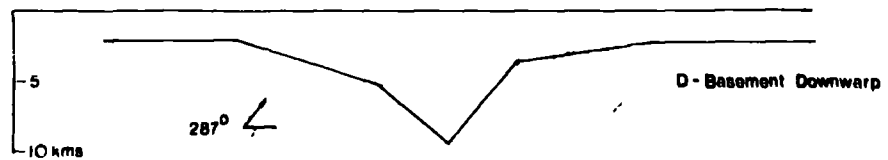
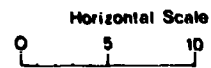
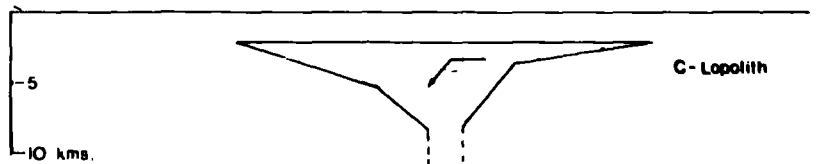
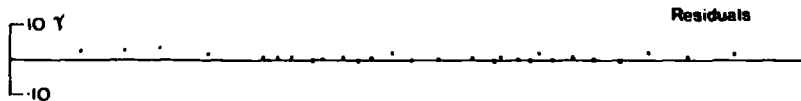
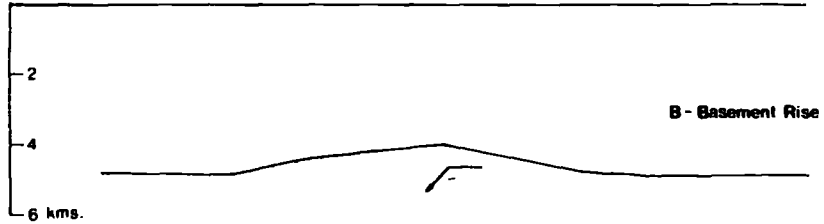
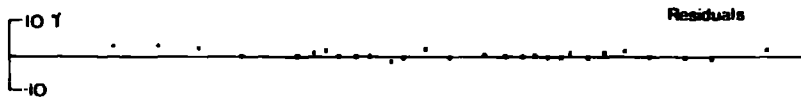
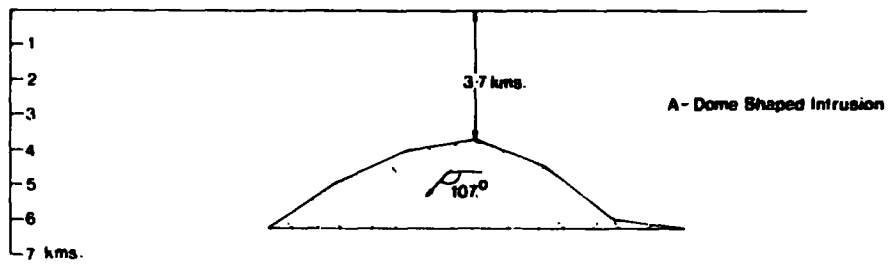
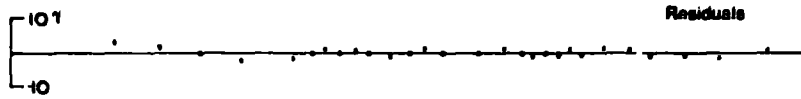
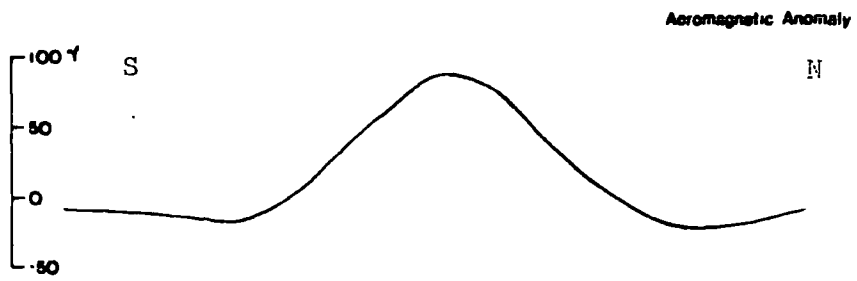


Fig.3-6. Location of the Carlisle (C) and Solway Firth (SF) Magnetic Anomalies.



Fig.3-7. Possible causative structures of the Carlisle anomaly.



(3-5-2-3) to be of the order of  $82^{\circ}$  down to the north. The body causing this anomaly has a computed magnetisation direction of  $107^{\circ}$  (i.e. down to the south). This fact plus the circular nature of the anomaly tend to militate against basement topography as the origin of the anomaly.

The best fit with an inward sloping contact body was obtained with a magnetisation contrast of 0.0005 emu/cc and a depth to top surface of 2.5 km. . Again two possible interpretations exist.

1) The anomaly is caused by a downwarp in the magnetic basement, which must then be magnetised at an angle of  $-73^{\circ}$  (i.e. up to the north) Fig.(3-7(d)).

2) The 'downwarp' contains the material with the higher magnetisation, and the angle of magnetisation is as before  $107^{\circ}$  Fig (3-7(c)) (feeder not computed).

Again we cannot exclude either solution on geological grounds, but basement downwarp is unlikely for the reasons given previously against basement rise.

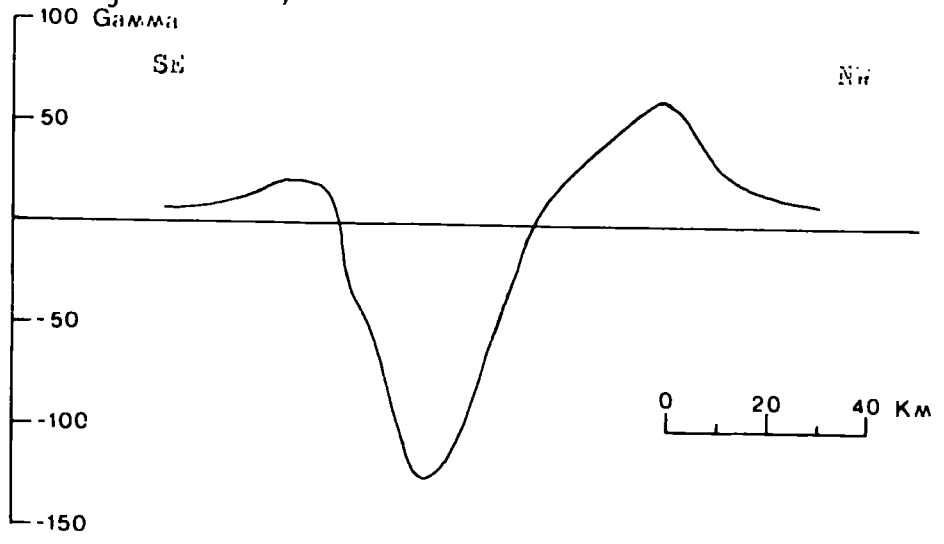
Thus the anomaly would seem to result from either a plug shaped intrusion or a lopolith. In either case it is clear that the body was intruded during a period of reversed polarity, the computed magnetisation direction resulting from a combination of the induced magnetisation (down to the north) and the remanent (up to the south).

### 3-5-2-3 The Solway Firth Anomaly

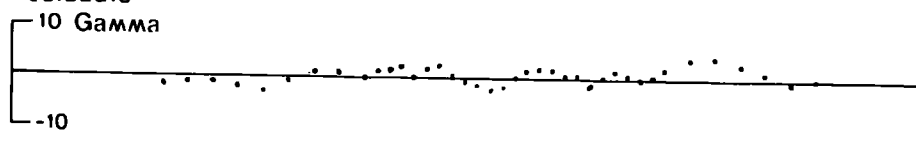
This anomaly is again taken from the Aeromagnetic Map of Great Britain and is chosen to provide a method of comparison between the matrix method and the only other available method, non linear optimisation

Fig. 3-8. The Solway Firth Aeromagnetic Anomaly with possible causative structures

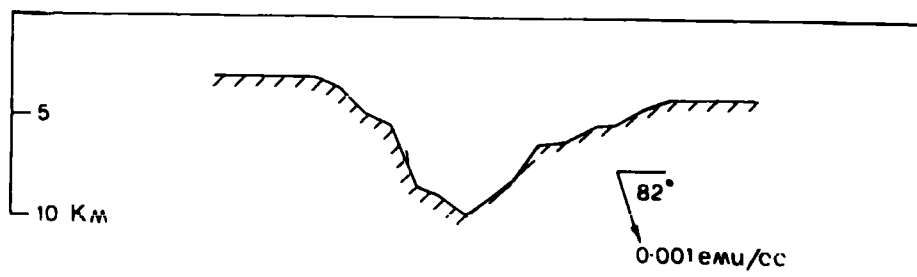
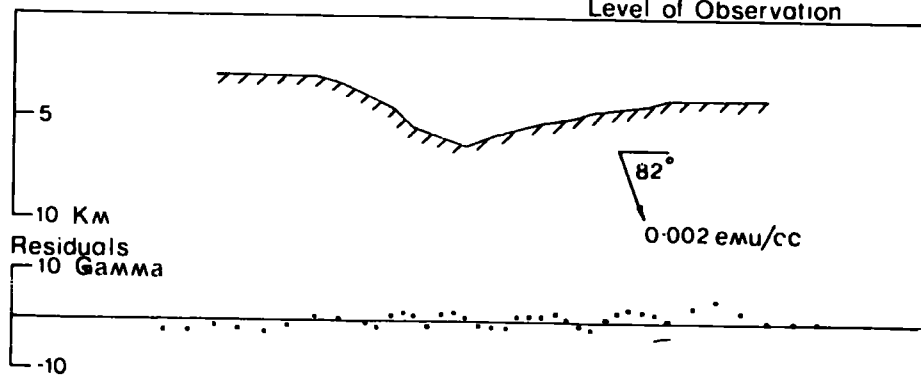
Aeromagnetic Anomaly



Residuals



Level of Observation



(Al-Chalabi, 1970).

The anomaly extends over the Solway Firth and is negative over a region occupied by a sedimentary basin (Fig. (3-6)). The anomaly was first discussed by Bott (1965), who concluded that it cannot be attributed to a magnetisation contrast between the basin and the underlying Paleozoic rocks. Al-Chalabi (1970) interpreted the anomaly in terms of Pre-Cambrian basement relief..

The specified top surface was the same as that used by Al-Chalabi(1970) and a series of magnetisation contrasts in the range 0.0005 to 0.005 emu/cc were specified. The best results were obtained using contrasts of 0.001 and 0.002 emu/cc, the results are shown at Fig. (3-8)..

The angle of magnetisation computed differed by only 1 degree from that found by Al-Chalabi (1970) and the models were in excellent agreement with those obtain by optimisation for the same magnetisation contrasts. The computer time for each model was of the order of 45 secs.

### 3-6 Limitations of the Method

The limitations of the matrix method applied to gravity interpretation (Chapter 2) apply equally to the magnetic programs.

There exists, however, an additional limitation.

#### 3.6.1 Shallow Angle Magnetisation

If the angle of dip of the body magnetisation vector is found to be less than 10 degrees in the plane of the profile the problem of instability in the initial

equivalent layer approximation, due to dependence between the individual magnetisation vectors, is encountered. The problem can be overcome by increasing the initial blockwidth to 5 to 10 times the depth to the equivalent layer approximation, thus reducing the instability, but resulting in an unacceptable loss in resolving power. This in turn can be overcome by using a shifting block coordinate program similar to the VARYIT gravity program (Chapter 2). Although the instability is not entirely removed by this method, a good estimate of the body space form is obtained.

An attempt to overcome the problem using a pseudo-gravity transform technique (Baranov, 1957) was unsuccessful since the transform also becomes unstable under shallow angle conditions.

The second problem associated with shallow angle ( $\mu < 10^\circ$ ) analysis arises in determining the shape of the causative body from the equivalent layer approximation. Since the direction of magnetisation is at a high angle to vertical, the resultant magnitude of the vertical expansion, given by equation (3-15), will be very small, and a correspondingly slow rate of convergence will result.

This is overcome by expanding the body dimensions at an angle shallower than  $90^\circ$  and varying both the x and z coordinates of the unknown surface (Fig 3-9). The choice of expansion angle is governed by the nature of the sin function and the estimated steepest slope of the body, since if the expansion angle is not greater

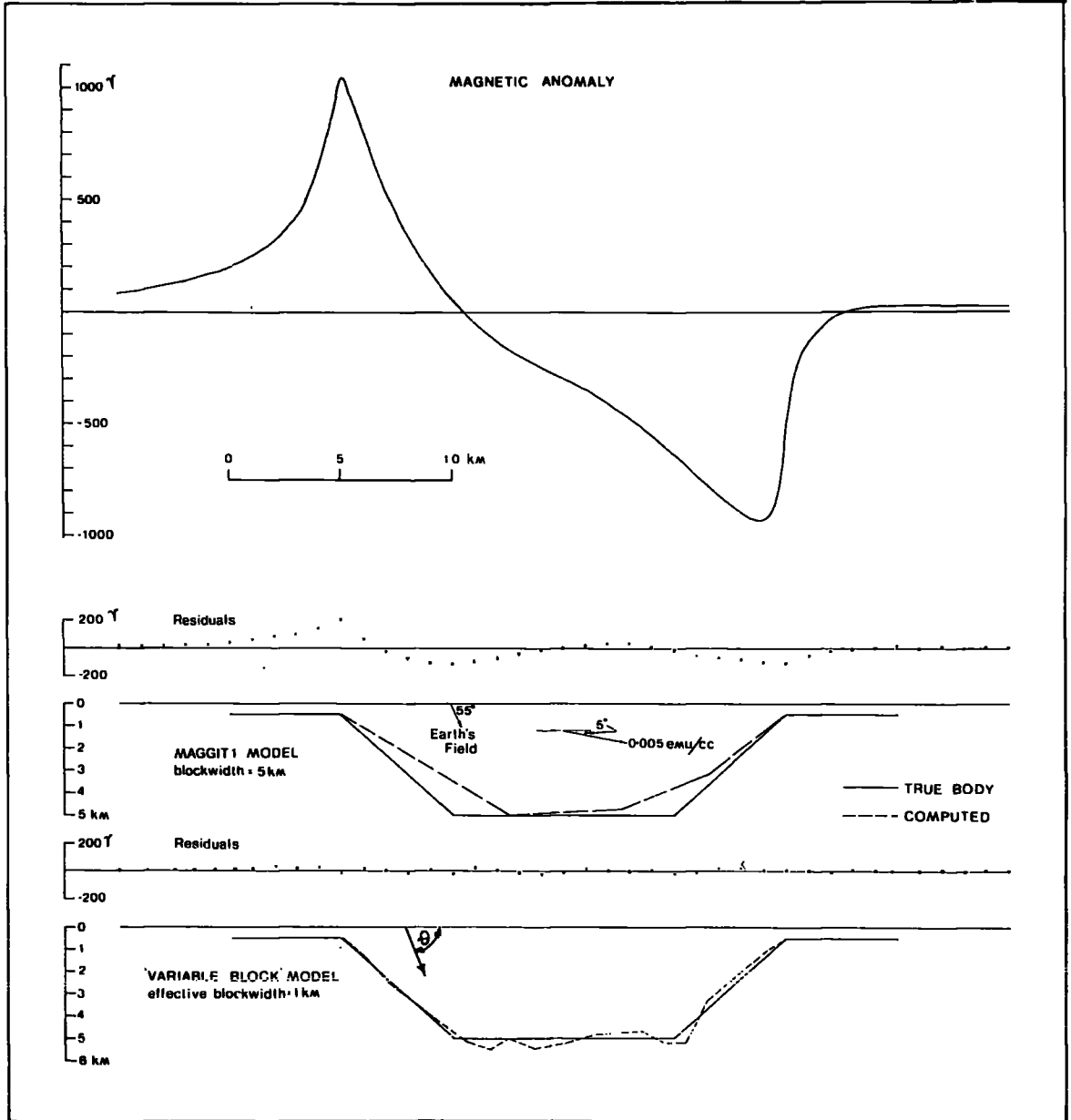


Fig. 3-9.



than the steepest body surface slope, the program will obviously be unable to produce the required body. The general problem of low angle magnetisation is illustrated at Fig. (3-9). An expansion angle of  $60^{\circ}$  has been used throughout.

The equations replacing equation (3-15) and defining the x and z coordinates of the new body point are:

$$d_2 \text{ (jth block)} = d_1 \text{ (jth block)} + \frac{J \text{ (jth block)} \times (\cos \mu \cdot \cos \theta + \sin \mu \cdot \sin \theta) \sin \theta}{\text{specified magnetisation}} \quad (3-16)$$

and:

$$x_2 \text{ (jth)} = x_1 \text{ (jth)} + \frac{J \text{ (jth)} \times (\cos \mu \cdot \cos \theta + \sin \mu \cdot \sin \theta) \cos \theta}{\text{specified magnetisation}}. \quad (3-17)$$

where  $(x_1, d_1)$  are any initial body coordinates,  $(x_2, d_2)$  are the new coordinates and  $\theta =$  expansion angle - see Fig.(3-9).

### 3-7 Other Applications of the Magnetic Equivalent Layer.

Having computed the magnetic equivalent layer the anomaly at any point in space on or above the layer can be found. The method can thus be used for upward and downward continuation, or for recomputing the anomaly on a regular grid for mapping purposes. The problem encountered in many upward continuation methods of requiring at least a series approximation for the anomaly between  $+\infty$  and  $-\infty$  does not arise as the equivalent layer has a finite magnetic anomaly at large distances

from the layer.

### 3-8 Conclusions

The programs developed provide a fast and reliable technique of determining the shape and magnetisation direction of a body, from a knowledge of the magnetic anomaly produced, under certain constraints on the depth and intensity of magnetisation.

The advantage of the matrix method over the only other available method (non-linear optimisation - Al-Chalabi (1970)) is that it is faster (average computer time = 40 secs. cf. optimisation = 8 mins.) and is thus able to handle a large number of body variables and consequently analyse complex anomalies. Interfering anomalies cause by adjacent bodies with different magnetisation contrasts can also be treated.

The advantage of non-linear optimisation over the matrix technique is that it is not necessary to specify the regional field, the magnetisation or the whole anomaly to obtain a solution. Although the last point may be open to criticism in that unless the whole anomaly is specified the model produced is merely the optimum body for the section of the anomaly specified and may have no geological significance, the first two points give the method a real advantage over the matrix technique in many cases.

### 3-9 Extension of the Technique to Three Dimensional Analysis

As stated in Chapter 2, the application of two dimensional analysis to three dimensional structures will lead to an underestimate of the body dimensions

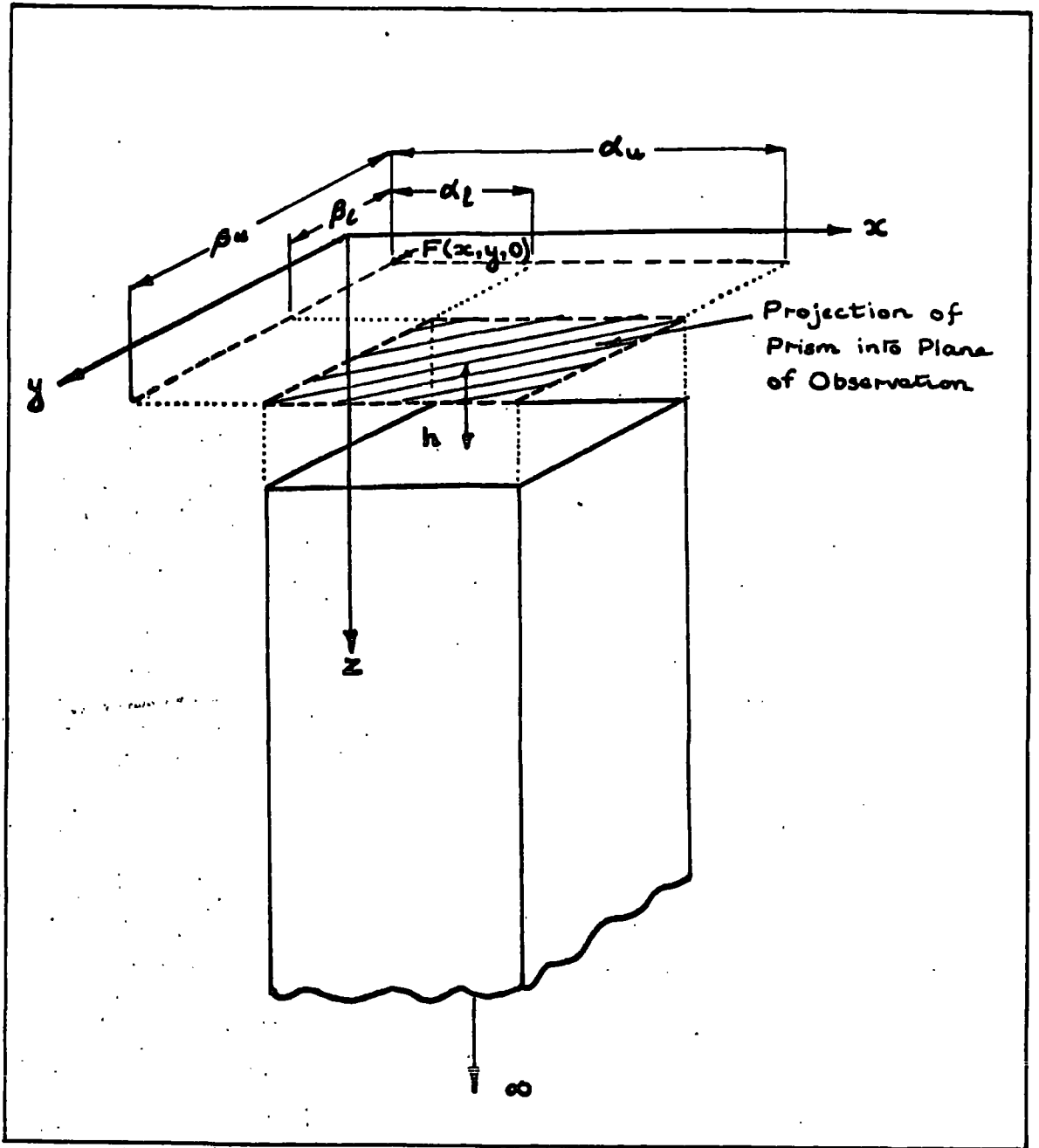


Fig.3-10. Notation used for the magnetic anomaly at a point due to a rectangular prism.

being made..

Three dimensional analysis programs have not been written, but modification of the three dimensional gravity programs for magnetic interpretation is merely a matter of substituting the magnetic prism formula (Bhattacharyya, 1964) for the gravity prism subroutine (PRISM - see Appendix 1). Whether the greatly increased computing time and storage requirement would be justified is open to question. From an examination of the work of Lehmann (1971) on this subject it is <sup>the</sup> present author's opinion that it would not. The formula is given here for completeness and for the information of anyone wishing to employ three dimensional analysis:

$$F(x,y,o) = F_{h_1}(x,y,o) - F_{h_2}(x,y,o) \quad (3-18)$$

where  $F_{h_1}$  and  $F_{h_2}$  are the magnetic anomalies at the point  $(x,y,o)$  due to infinitely thick prisms with depths to top surface  $h_1$  and  $h_2$  respectively ( $h_2 > h_1$ ). The anomaly due to a prism of finite thickness  $h_2 - h_1$  is then obtained from equation (3-18). See Fig. (3-10)

We have:

$$F_{h_1}(x,y,o) = J \left[ \frac{\alpha_{23}}{2} \log \left( \frac{r_o - \alpha_1}{r_o + \alpha_1} \right) + \frac{\alpha_{13}}{2} \log \left( \frac{r_o - \beta_1}{r_o + \beta_1} \right) - \alpha_{12} \log(r_o + h) - \ell L \operatorname{atan} \left( \frac{\alpha_1 \beta_1}{\alpha_1^2 + r_o h + h^2} \right) - m N \operatorname{atan} \left( \frac{\alpha_1 \beta_1}{r_o^2 + r_o h_1 - \alpha_1^2} \right) + n N \operatorname{atan} \left( \frac{\alpha_1 \beta_1}{r_o h} \right) \right] \begin{matrix} \alpha_u \\ \beta_u \\ \alpha_e \\ \beta_L \end{matrix} \quad (3-19)$$

where:

$$\alpha_1 = \alpha - x, \beta_1 = \beta - x, r_o^2 = \alpha_1^2 + \beta_1^2 + h^2$$

and  $\alpha_u$  and  $\beta_u$  are the upper limits and  $\alpha_e$  and  $\beta_e$  are the lower limits of  $\alpha_1$  and  $\beta_1$  respectively.  $e, m, n$  are the direction cosine of the Earth's field vector.

$L, M, N$  are the direction cosines of the body magnetisation vector

and  $\alpha_{12} = Lm + Ml$  ,  $\alpha_{13} = Ln + Nl$  and  $\alpha_{23} = Mn + Nm$ .

CHAPTER 4

THE MEASUREMENT OF GRAVITY AT SEA

4-1 Introduction

Gravity stations at sea are established by measuring the difference in gravity between some fixed location at sea and a land base station where gravity is accurately known. This can be accomplished by using an underwater gravity meter (operated on the ocean bottom), a Vening Meinesz pendulum, or a surface ship meter (mounted in gimbals or on a stable platform). The gravity stations discussed in the present work have all been established using an Askania sea gravimeter mounted on an Anschütz gyrostabilised platform.

Problems arise because the measuring system is itself in motion, resulting in errors which must be taken into account if accurate measurements of the gravity field are to be obtained.

4-2 Vertical Accelerations of the Ship

Since no instrument can distinguish between gravity and vertical accelerations any measurements made at sea will be of gravity plus the vertical acceleration of the ship due to wave motion ( $g + \ddot{z}$ ). These vertical accelerations have an average period of 8-10 seconds and a maximum amplitude of 100,000 mgal. The gravity signal can be considered to have a minimum period of interest of 8-10 minutes. The meter is thus highly damped for high frequencies, to remove the signal due to wave motion and prevent the measuring instrument from hitting its stops, but has low damping for low frequencies. No long period change in  $\dot{z}$  is considered since vertical accelerations.

of the ocean surface due to tides are negligible. The gravimeter then behaves like a simple low-pass filter and some data, at higher frequencies will be lost.

In normal use the Askania sea gravimeter has a time constant of 250 seconds. This introduces a constant time delay of 250 seconds for constant gravity gradients (Graf and Schulze, 1961), but gravity signals with periods of several tens of minutes are distorted as well as delayed (Talwani, 1966). This effect and the effect of non-linearity of the measuring system are usually ignored.

#### 4-3 Horizontal Accelerations of the Ship

##### 4-3-1 Off-Levelling Errors

Dynamic off-levelling errors, caused by a periodic off-leveling of the stable platform in the presence of periodic horizontal accelerations are discussed in this section.

If we consider the stable platform to be off level by an angle  $\Theta$  (Fig. 4-1) the gravimeter will measure:

$$g_M = (g + \ddot{z}_0 \cos (wt + \phi)) \cos \Theta - \ddot{x}_0 \cos (wt + \lambda) \sin \Theta \quad (4-1)$$

where the horizontal acceleration is given by

$$\ddot{x} = \ddot{x}_0 \cos (wt + \lambda) \quad (4-2)$$

and the vertical acceleration by

$$\ddot{z} = \ddot{z}_0 \cos (wt + \phi) \quad (4-3)$$

that is the two accelerations have the same frequency. This condition generally exists to some extent at sea due to the approximately circular motion of water particles

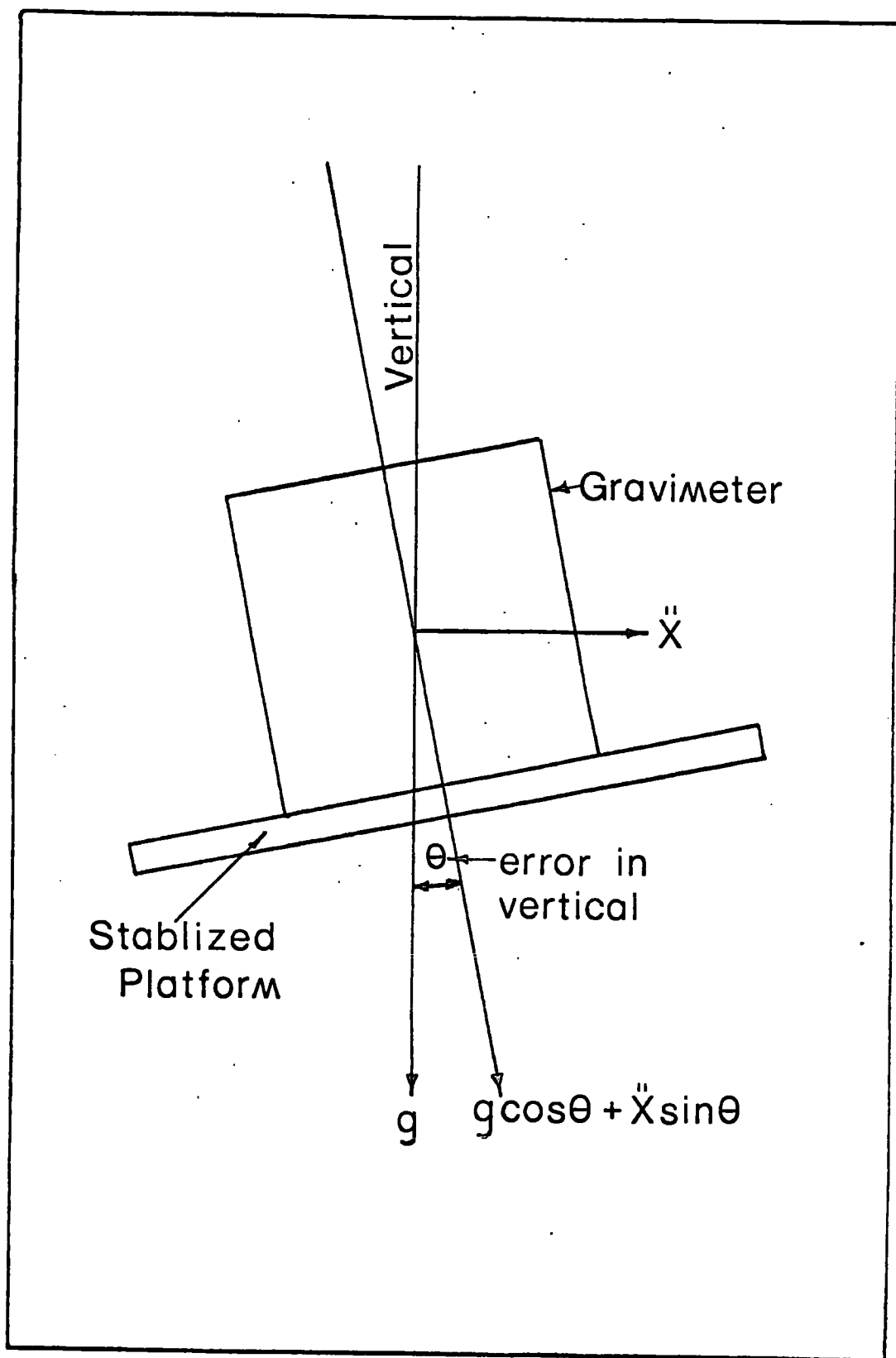


Fig.4-1. Off leveling errors for a sea-gravimeter



in waves.

If we now consider the case where the off-level angle is driven by the vertical accelerations and has the same frequency as the vertical accelerations:

$$\theta = \theta_0 + \theta_1 \cos (wt + \epsilon) \quad (4-4)$$

where  $\theta_0$  = mean table angle.

we have:

$$\begin{aligned} g_M = & (g + \ddot{z}_0 \cos(wt + \phi)) \left( 1 - \frac{\theta_0^2}{2} - \theta_0 \theta_1 \cos(wt + \epsilon) \right) \\ & - \frac{\theta_1^2}{2} \cos^2(wt + \epsilon) - \ddot{x}_0 \cos(wt + \lambda) (\theta_0 + \theta_1 \cos(wt + \epsilon)) \end{aligned} \quad (4-5)$$

Taking the long period time average and assuming  $\ddot{z}_0$  to be damped and therefore  $\ddot{z}_0 \ll g$  we have:

$$g_M = g \left( 1 - \frac{1}{2} \theta_0^2 - \frac{1}{4} \theta_1^2 \right) - \frac{1}{2} \ddot{x}_0 \theta_1 \cos(\lambda - \epsilon) \quad (4-6)$$

If the period of table off-levelling is not equal to the horizontal acceleration period only the term due to non vertical measurement exists in (4-6).

It is found that the level must be maintained to within  $\pm 5'$  if an accuracy of  $\pm 1$  mgal is to be maintained.

#### 4-3-2 Cross Coupling Errors

Cross coupling errors occur if horizontal accelerations act in the direction of the beam with the same period as the vertical motions of the beam.

If the wave motion causes the beam to be displaced by an angle  $\phi$  where:

$$\phi = \phi_0 + \phi_1 \cos (wt + \lambda) \quad (4-7)$$

and the horizontal accelerations are given by:

$$\ddot{x} = \ddot{x}_0 \cos (wt + \epsilon) \quad (4-8)$$

The instantaneous cross coupling is given by:

$$CCI = \ddot{x} \phi \quad (4-9)$$

The time averaged cross coupling is given by:

$$CC = \frac{1}{2} \ddot{x}_0 \phi_1 \cos (\epsilon - \lambda) \quad (4-10)$$

(La Coste, 1967).

This effect is relatively small in calm seas, but values up to 25 mgal have been reported in rough sea states (Talwani, 1966; LaCoste, 1967). A simple computer can be used to measure the effect by monitoring the beam position and measuring the horizontal acceleration exerted on the beam with an accelerometer on the stable platform.

#### 4-4 The Eötvös Effect

A moving object on a rotating earth is subject to a vertical Coriolis acceleration known as the Eötvös effect.

The gravity data must be corrected for this effect which can reach well over 100 mgal.

The Eötvös error is given by:

$$- 7.503 V_E \cos \theta \quad (\text{mgal.}) \quad (4-11)$$

where  $V_E$  is the easterly component of the ship's velocity in knots.

and  $\theta$  = ship latitude

a second order term involving the ships speed ( $0.00415 v^2$ ) is neglected.

Since the effect can be large it is important to

know both the course and speed of the ship accurately, that is, to have accurate navigation.

A 1 knot error in the calculation of the east west speed of the ship, will result in an error of the order of 7 mgal in low latitudes.

#### 4-5 Gravimeter Drift

Sea gravimeters, like their land counterparts are subject to drift of reading with time. This effect is usually considered to vary linearly with time and is corrected for by 'tying in' the meter reading to an established base station on land, at each end of the survey.

#### 4-6 Land Ties

Land ties at either end of a survey leg are necessary to tie down the survey and compute the sea gravimeter drift correction.

A gravity station at the dock alongside the ship is first tied in to an accurately established gravity base station, using a land gravimeter.

The gravity at the ship's location is then determined at sea level. If the dock is solid this consists of a free air correction ( $+0.09406$  mgal/ft.), less the semi-infinite slab correction ( $-0.01703$  mgal/ft. - for an assumed density of 2.67 gm/cc). If the pier is open only the free air correction need be applied. At the same time as the dock station is established, the steady reading of the sea gravimeter is taken.

The survey between land ties can thus be tied down and the sea gravimeter drift since the last land tie

can be calculated. This is done by subtracting the sea gravimeter reading (converted to mgal) from the computed sea level gravity. This quantity, known as the 'zeroed meter gravity' (Z.M.G) is then subtracted from the previously determined Z.M.G. to obtain the drift in mgals between land ties.

This treatment of the problems encountered in measuring gravity at sea has necessarily been brief. Excellent detailed accounts of the problems and errors involved are presented by Talwani (1966) and LaCoste (1967).

CHAPTER 5

INTERPRETATION OF A MARINE GRAVITY SURVEY OF THE CARIBBEAN  
EASTERN MARGIN SOUTH OF ST. VINCENT.

5-1. Introduction

5-1-1 Island Arcs-General

The hypothesis of sea-floor spreading (Deitz, 1961; Hess, 1962) and the complementary 'New Global Tectonics' (Isacks, Oliver and Sykes, 1968), whereby new oceanic crust is being created at the active ocean ridges and crustal loss or shortening is occurring at the deep trenches and regions of active folding and thrusting is now generally accepted by most Earth scientists. Geophysical evidence points to island arcs as being areas of crustal loss. They are regions of great tectonic activity, volcanoes, folding, faulting and the majority of the world's deep and intermediate depth earthquakes are associated with these or similar structures. A deep ocean trench often parallels a volcanic arc on its convex side.

A study of the hypocentres that account for most of the shallow earthquake activity in island arc areas indicates that the earthquakes are situated beneath the landward slope of the associated deep-sea trench and form a zone dipping beneath the arc (Isacks, Oliver and Sykes, 1968). Comparison of seismic waves generated by deep earthquakes and propagated along different paths under Tonga Kermadec arc, demonstrated the existence of a zone of anomalously high seismic velocity and low attenuation of the order of 100 kms. thick in the upper

mantle. This zone, which is bounded on its upper surface by the seismic zone previously mentioned, dips west beneath the arc and extends to a depth of 700 kms. (Oliver and Isacks, 1967). These data are interpreted as underthrusting of the oceanic lithosphere (that part of the crust and upper mantle having high strength) beneath the volcanic arc, the deep sea trench being taken as the locus of underthrusting.

Island arc areas, in general, exhibit three main elements, a deep sea trench, a chain of uplifts lacking young volcanoes and a zone of active volcanoes, although one or more of these features may be absent in some arc areas. The narrow belt of negative gravity anomalies found to the convex side of the volcanic arc (Hess, 1938), the inclined zone of earthquake hypocentres (Isacks, Oliver and Sykes, 1968, Molnar and Sykes, 1969) and the narrow zone of volcanic activity about 150 kms. from the concave side of the trench, all lend support to the theory that island arcs are areas where recycling of the lithosphere occurs.

The volcanic activity is believed to result from partial melting (Ringwood, 1969) under high load pressures and shear stresses (Oxburgh and Turcotte, 1968) of the oceanic crust on the descending plate. This probably involves the partial melting of quartz eclogite from the transformed dry basalt in the lower crust and of amphibolite from the transformed wet upper crust, leaving residual eclogite (Dewey and Bird, 1970). The calc-alkaline magma which is formed erupts on the arc as

andesite and dacite. Lateral variations in magma type, attributed to different depths of formation by Kuno(1965) are observed in the Japan arc.

#### 5-1-2 Lesser Antillean Geology

The islands of the Lesser Antilles, which form one of a series of north-south trending ridges and troughs, separating the Atlantic ocean from the Caribbean basin (Fig. 5-1), form an atypical island arc. No deep trench is found to the convex side of the islands and the arc is in a region of otherwise inactive continental margins where no crustal loss occurs.

North of Dominica the islands can be divided into 'Limestone Caribbees' and 'Volcanic Caribbees'. The geological history of the Limestone Caribbees: (Marie Galante, La Desirade, Grande Terre, Antigua, St. Bartholomew, St. Martin, Anguilla, Dog and Sombrero) is Middle Eocene to Late Oligocene volcanism, followed by erosion, minor intrusions and faulting, then a late Oligocene - Early Miocene cap of shallow water limestone, followed by Late Miocene uplift (Nagle, 1970).

The Volcanic Caribbees (Illes des Saintes, Basse Terre, Montserrat, Nevis, St. Kitts, St. Eustace and Saba) are composed of Late Miocene to Recent Volcanics, with no major intrusions and only few sediments.

To the south of Dominica lie only Volcanic Caribbees (Martinique, St. Lucia, St. Vincent, the Grenadines and Grenada), which have Middle Eocene to Lower Miocene volcanics in addition to the Late Miocene to Recent Volcanics, similar to those of the Volcanic Caribbees

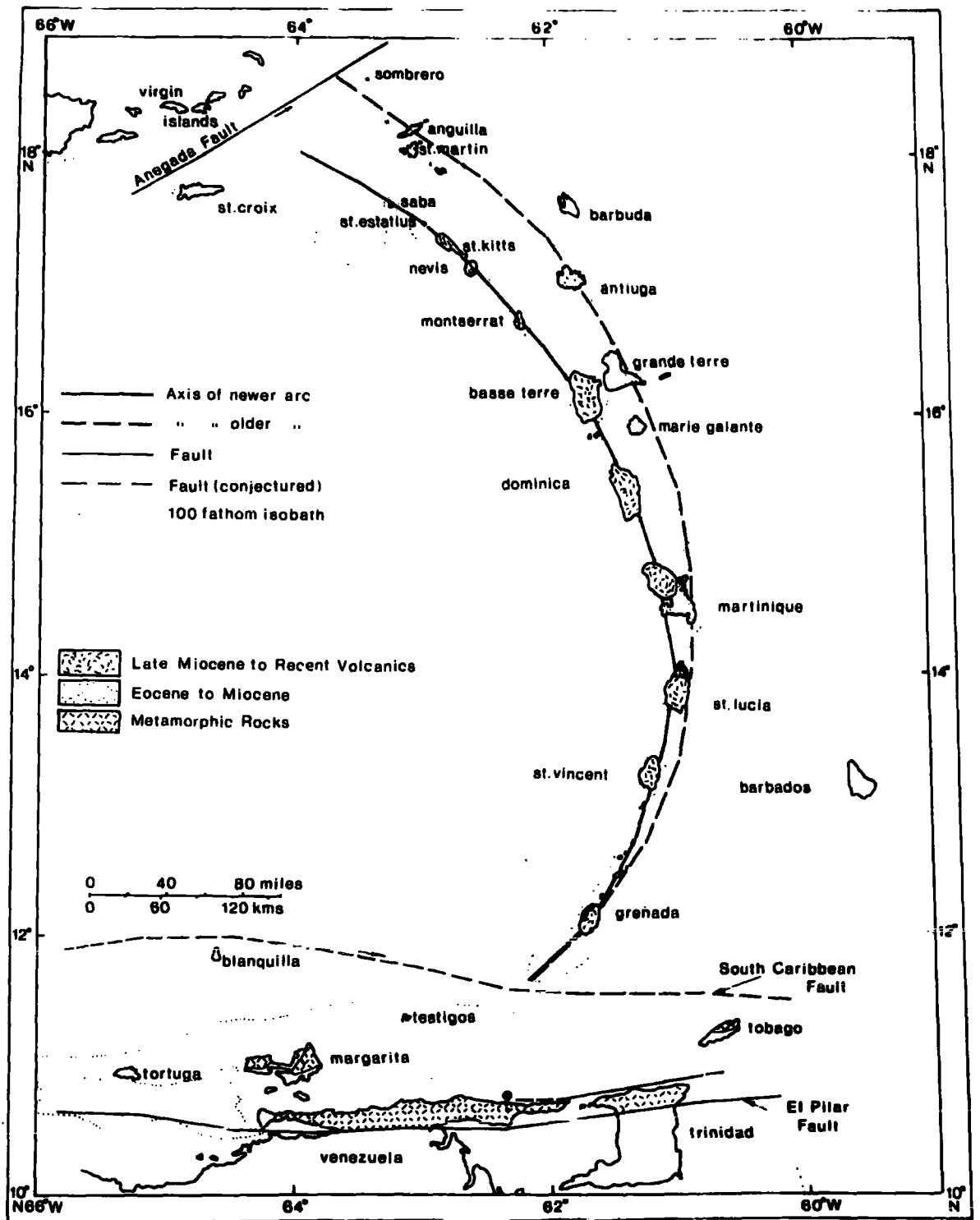


Fig. 5-1. Structural map of the Lesser Antilles. (modified from Martin-Lage, 1965)



north of Dominica (Nagle, 1970).

There have thus been two episodes of volcanism separated by a period of submergence, resulting in the deposition of shallow water limestone.

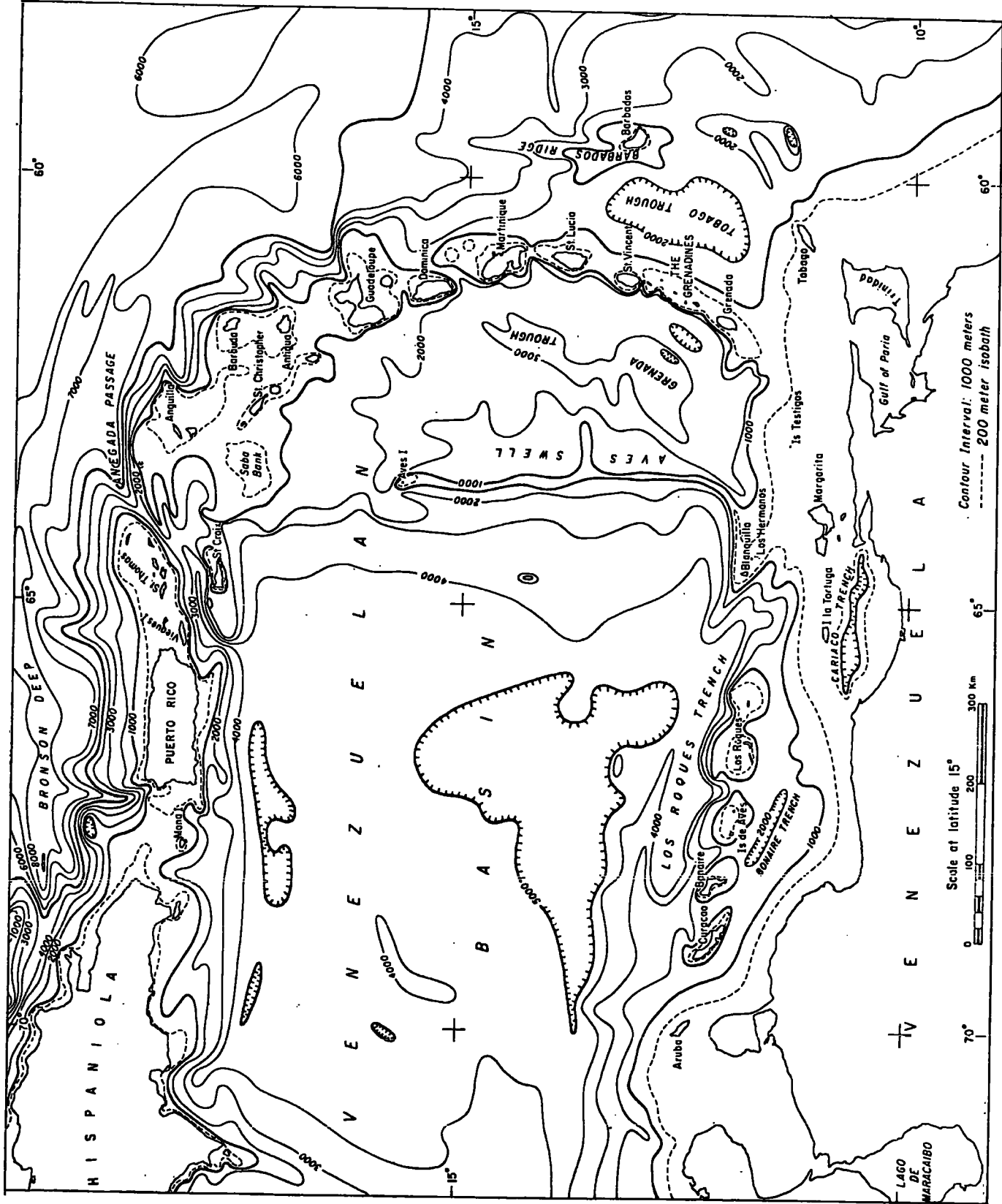
### 5-1-3 Surrounding Framework.

On the Atlantic side of the Lesser Antilles lies, in the north the Puerto-Rico Trench and in the south the Barbados Ridge. Between the island arc and the Barbados Ridge is the Tobago Trough (Fig. 5-2). Interior to the arc is the Grenada Trough and west of this the Aves Swell, which forms the eastern margin of the Venezuelan Basin. To the north of the arc are the islands of the Greater Antilles (Jamaica, Cuba, Hispaniola and Puerto Rico) and to the south the South American continental margin.

### 5-1-3-1 Northern South America, Trinidad and Tobago.

Pre-Mesozoic rocks probably underlie the North Range Mountains of northern Venezuela and Trinidad (Fig 5-1), although their existence has never been proved (Nagle, 1970). The rocks of the North Coast Range form a rigid unit, traceable from the Araya Peninsula in Venezuela, through Trinidad to 59° 50' West (Bassinger et al, in press) and are believed to have been metamorphosed during the Cretaceous - Early Tertiary interval during a series of episodes (Hess, 1960). The range is bounded north and south by fault zones (the southern boundary being the El-Pilar fault) and is comprised, in the east of Venezuela of two major groups of metamorphic rocks, a metasedimentary sequence in the north and an essentially metavolcanic sequence in the south (Nagle, 1970).

Fig. 5-2. Bathymetry of the Caribbean Region. (After Bush and Bush, 1969)



Contour Interval: 1000 meters  
 --- 200 meter isobath

Scale of latitude 15°  
 0 100 200 300 Km

South of the El-Pilar fault thick Mesozoic and Tertiary sediments overlies the Pre-Mesozoic rocks through most of northern Venezuela.

In Trinidad, the North Range Schists are mainly phyllites (Liddle, 1946) identical with the metasediments of northern Venezuela. No metavolcanics, and only a few igneous rocks are found.

In Tobago, the deeply eroded schists of the Main Ridge formation, found in the north of the island resemble the North Range schists of Trinidad in degree of metamorphism and in that they are both isoclinally folded and turned over northwards, (Maxwell, 1948). On the other hand the schists of Tobago are mainly metavolcanic rocks. South of the schist belt on Tobago, is a belt of intrusive and extrusive rocks, occupying more than half the island's area (Maxwell, 1948). This is in contrast to northern Trinidad where igneous activity is only slight.

#### 5-1-3-2. Barbados.

The island of Barbados is a local topographic high element within the complex Barbados Ridge structure. The foundation series of the island is the Eocene Scotland Group (Senn, 1940), a series of sandstones and clays testifying to the proximity of a large land area at this time. Overlying this is the Miocene Oceanic Series containing abyssal deposits (radiolarians) indicating that the Barbados Ridge was a foredeep at this time (Weeks et al., in press) and has since been elevated. Lying above this is Pliocene Globingerina.

marl and limestone (Trenchman, 1933), followed by Recent to Early Pleistocene limestone. At present most of the island is covered by coral rock up to a maximum thickness of 250 ft. Boreholes show that sediments have a thickness in excess of 15,000 ft. under the island.

#### 5-1-4 Previous Geophysical Work.

Seismic refraction experiments in the eastern Caribbean have been interpreted by Ewing et al. (1957) and Officer et al. (1957; 1959).

Gravity measurements have been made by Vening Meinesz (1934; 1948), Ewing (1937), Shurbet and Ewing (1956), Shurbet et al. (1956), Masson Smith and Andrew (1965), Talwani et al. (1959), Andrew et al. (1970) and Bowin (personal communication).

A general description of the nature of the magnetic field in the eastern Caribbean is presented by Ewing et al. (1960).

Bunce et al. (1970) describe several continuous seismic reflection, magnetic and gravity profiles across the eastern margin of the Caribbean and Chase and Bunce (1969) show four seismic reflection profiles to the east of the Barbados Ridge.

Details of the seismicity of the region are presented by Molnar and Sykes (1969).

#### 5-2 Reduction of the Gravity Survey.

##### 5-2-1 Introduction

During the summer of 1968, 4630 km. of seismic reflection profiling, gravimeter, magnetometer and echo sounding observations were made by the U.S.C & G.S.S. DISCOVERER in an area bounded by longitudes 58° 30' West

to 63° 00' West and latitudes 10° 00' North to 12° 30' North, as part of a geophysical investigation of the southern Lesser Antilles and associated structures.

The track chart is shown at Fig. (5-3).

Results and interpretations of various sections of the survey are presented by Lattimore et al., Bassinger et al. and Weeks et al. (all in press).

The gravity data obtained, supplemented by gravity data from Bowin (personal communication), Bush and Bush (1969) and Andrew et al. (1970) are interpreted in this chapter.

Measurements of the gravitational field were made with an Askania Seagravimeter (nr.23) mounted on an Anschutz gyrostabised table. The meter was run in the automatic mode and a cross-coupling computer was not used.

Navigation was by radar and star sights, the estimated probable position of the ship being  $\pm 2$  nautical miles. (R.K. Lattimore - personal communication). The survey was, in the main, run at a speed of 5 knots, although for various reasons, speeds between 2 and 10 knots were used during the cruise.

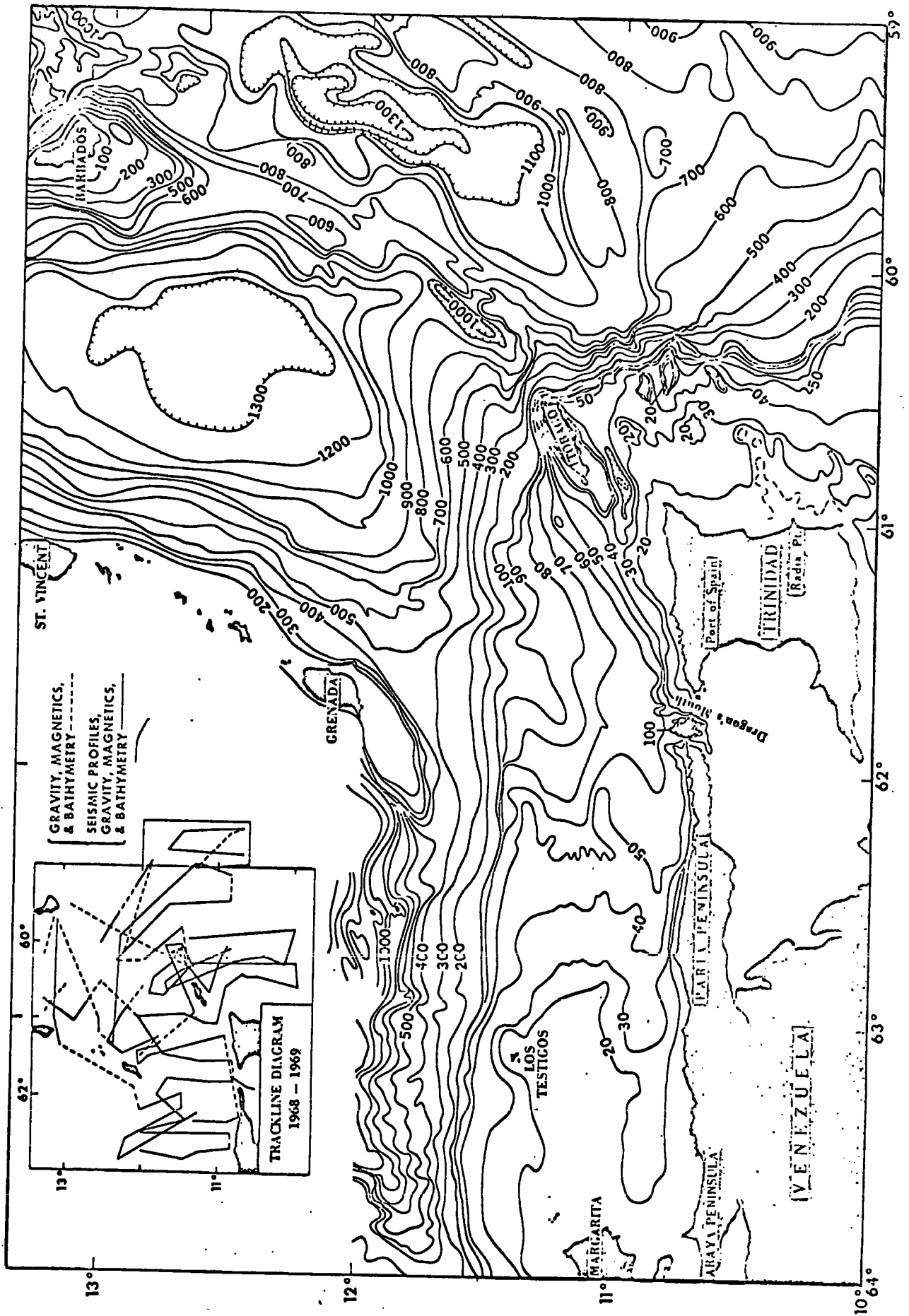
#### 5-2-2 Gravity Base Station

The survey, which was in two legs, was tied into the gravity station at Seawell Airport, Bridgetown, Barbados

BASE GRAVITY = 978.2997 gals.

The dock gravity station established was the same for each land tie. Details of the dock gravity and sea-

Fig.5-3. Trackline Diagram. (After Lattimore et al., in press)





gravimeter zeroed metered reading are given below

SCIENTIFIC DAY	LOCATION OF STATION + ELEV.	GRAVITY (gals)	Z.M.G. (gals)
170	BRIDGETOWN BDS.	978.2951	977.0565
LEG 1	BOLLARD 34 h = 8'		
180	" "	978.2951	977.0506
248	" "	978.2951	977.0585
LEG 2			
266	" "	978.2951	977.0573

Drift rates were thus:

0.59 mgal/day for leg 1.

0.07 mgal/day for leg 2

#### 5-2-3 Navigation

Smooth plots of the navigation fixes were drawn and the ships tracks broken into sections that could reasonably be approximated by constant course and speed.

These fixes were then supplied to a reduction program.

#### 5-2-4 Analogue Records.

The analogue gravity meter records were critically examined and a quantity of the data deemed to be in error as a result of a malfunction of the x - axis accelerometer on the gyrostable table, was rejected. The remaining data was digitised by hand at a maximum interval of 5 mins. (0.75 kms.), less if necessary to delineate the records.

#### 5-2-5 Reduction to Free Air Anomaly.

The free air gravity is computed from the digitised records by applying the meter scaling factor and the Eotvos and drift corrections (Chapter 4). Free air

anomalies are taken as the deviation of these corrected values from the values computed from the 1930 International Gravity Formula.

The reduction was carried out with a computer program, written by P.Grim (personal communication) using the University of Miami's I.B.M. 360/70 computer. The program computes the free air anomaly and navigation fixes as a specified function of distance or time, by linear extrapolation between given data points.

5-2-6 Reduction to Bouguer Anomaly.

The Bouguer correction corrects for the effect of varying bathymetry by effectively replacing the sea water up to sea level with rock of a specified density. Two common densities used for this correction are 2.67 gm/cc, the mean density of <sup>upper</sup> crustal rocks (Woodward and Strange, 1961), or the density of the 'basement' rocks of the region, if these are common to the whole survey area. In the extremely complex area under consideration, it was decided to use the density of the shallowest sedimentary layer (1.80 gm/cc - estimated from P - wave velocities using the relationship of Nafe and Drake, 1963). In this way successively deeper strata have, in general, increasing densities. This is considered a realistic method of making the correction, as well as facilitating the computation of the structure of the region.

The corrections were applied using a program available at Durham (GRAVN; Bott, 1969) which computes the gravitational attraction of an arbitrarily shaped body. Sudden changes in bathymetry prohibit the use of the

simple infinite slab formula (Nettleton, 1940) for making the correction.

5-2-7 Errors

Errors in the observed meter readings will occur due to the off-leveling and cross coupling effects (Chapter 4) errors in navigation, and non-linearity of the meter. Further, operating the meter in the automatic mode results in the attenuation of readings in regions of high field gradient. Some estimate of the errors incurred can be obtained by an examination of the readings at the intersections of track lines (cross-over errors).

The ten cross over errors examined for this survey were less than 10 mgal, the mean error being 6.9 mgal. with a standard deviation of 2.9 mgal. from this mean.

5-3 Description of the Bouguer Anomaly Map

The Bouguer anomaly map (Fig. 5-4) shows two main areas of anomalously high gravitational field. The first, High A, in the north and west of the map shows the curve of the volcanic arc and its extension into the Venezuelan shelf at least as far as  $63^{\circ}$  West. Data for the islands of St. Vincent, the Grenadines and Grenada has not been included but is available (Andrew et al. 1970). Bouguer anomalies up to 195 mgal are observed on these islands. The highest anomaly measured at sea is 110 mgal in the south west of the arcuate high. Although topography accounts for part of the high there is obviously a considerable mass excess associated with the islands. Outside the survey area this high can be traced further north always associated with the volcanic

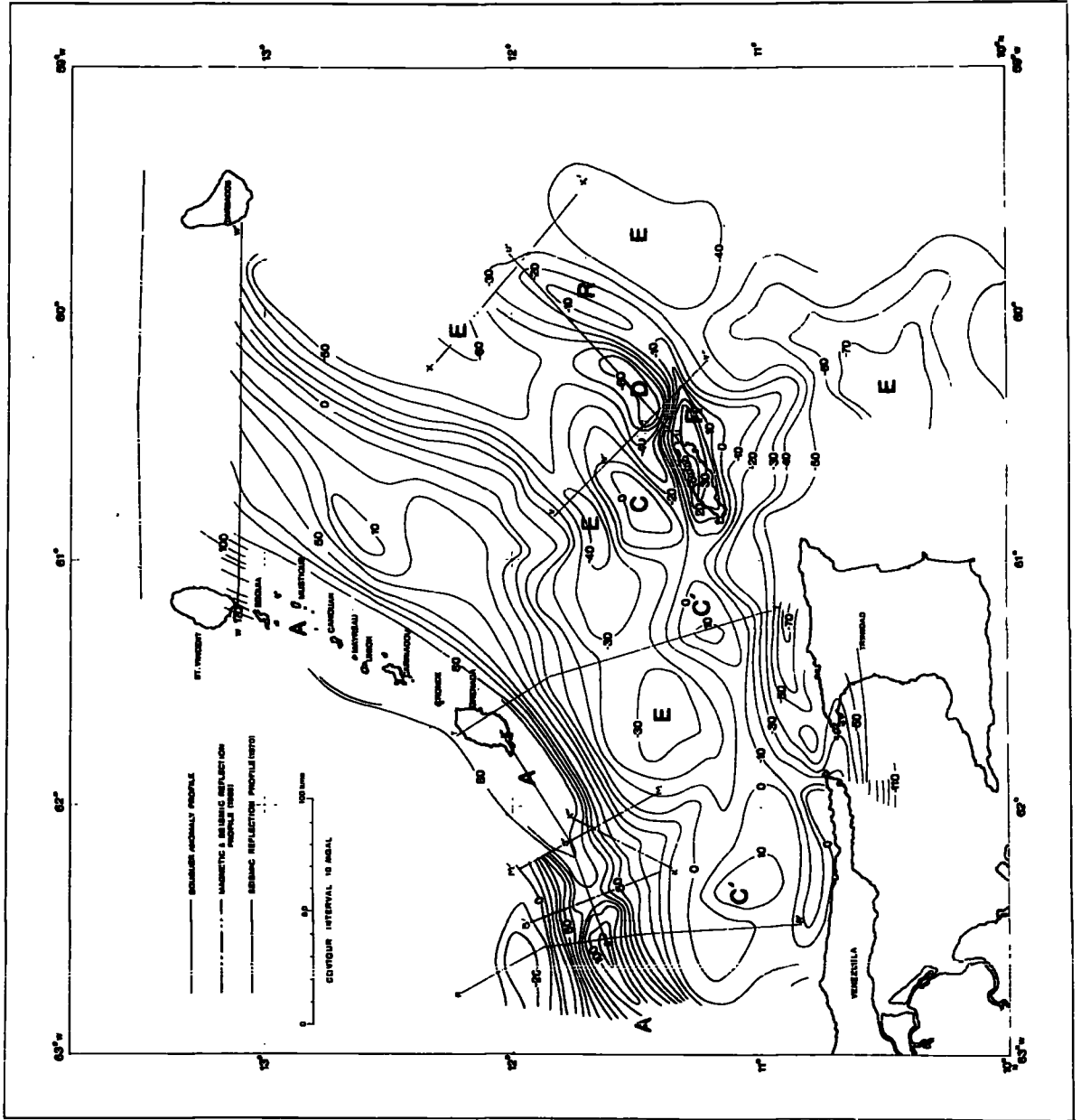


Fig. 5-4. Bouguer Anomaly  
Map of the  
Caribbean Eastern  
Margin South of  
St. Vincent.  
(based on gravity  
tracklines shown  
in Fig. 5-3.)

or ex-volcanic arc (Andrew et al., 1970).

The second main high, in the south and east of the map, is considered to be caused by at least two distinct structural features. High C - C' is later interpreted in terms of shelf structure, High R as a local mass excess within the broad structure resulting in the Bouguer anomaly low (LOW E).

As stated, LOW E is interrupted by HIGH R and forms two distinct 'limbs', one striking from west of Barbados into the Tobago Trough where it decreases in magnitude, dying out around  $61^{\circ} 30'$  West, the other striking first south, with increasing magnitude, then turning west through central Trinidad.

#### 5-4 Interpretation

##### 5-4-1 Profiles R - R' and S - S' and the Extension of the Lesser Antilles Arc into the Venezuelan Shelf.

Profile R - R' (Fig 5-4) strikes roughly north-south at Longitude  $62^{\circ} 30'$  West, from the Venezuelan Shelf off the Paria Peninsula to the Grenada Trough. It includes a Bouguer anomaly high (High A) that is continuous with the arcuate Bouguer anomaly high associated with the Lesser Antilles. The anomaly has a maximum value of 110 mgal. High A coincides with an outcrop of seismic 'basement', <sup>on R-R'</sup> and with a zone of high frequency, high amplitude magnetic anomalies. The outcrop of basement rock is not, however, an extension of the island of Grenada, since seismic reflection profile KB' (Fig.5-4) shows no basement in more than 0.5 sec. of penetration and the magnetic record shows a lack of the characteristic

high frequencies (Lattimore et al., in press). Lattimore et al. (ibid.) suggest that this is probably due to faulting and postulate a N.W. - S.E. trending fault in this area. The gravity evidence also indicates that the basement rock is at depth in this region.

Two interpretations of the Bouguer anomaly high are then possible:

- 1) A fault bounded block of igneous or metamorphic rocks.
- 2) A continuation of the island arc structure into the Venezuelan Shelf.

The second possibility would seem the more probable of the two, taking into consideration the magnitude of the Bouguer anomaly and its continuity with the trend of the main arc anomaly (Fig. 5-4).

A possible structure, that satisfies all the available seismic and gravity evidence, is shown in Fig (5-6). The following initial assumptions were made.

The profile crosses a seismic refraction line shot by Ewing et al. (1957) (line 25 - Fig (5-5)) on the Venezuelan Shelf. The crustal structure at the point of intersection is taken from the refraction data.

The north of the profile extends into the Grenada Trough (Fig. 5-4), but does not cross seismic refraction line 29 (Ewing et al., 1957). However, recent seismic reflection work (Bunce et al., in press) indicates that the sedimentary strata are extremely flat lying in the Grenada Trough, thus in the absence of further information, the crustal structure at the northern end of the profile is taken to be that found under refraction

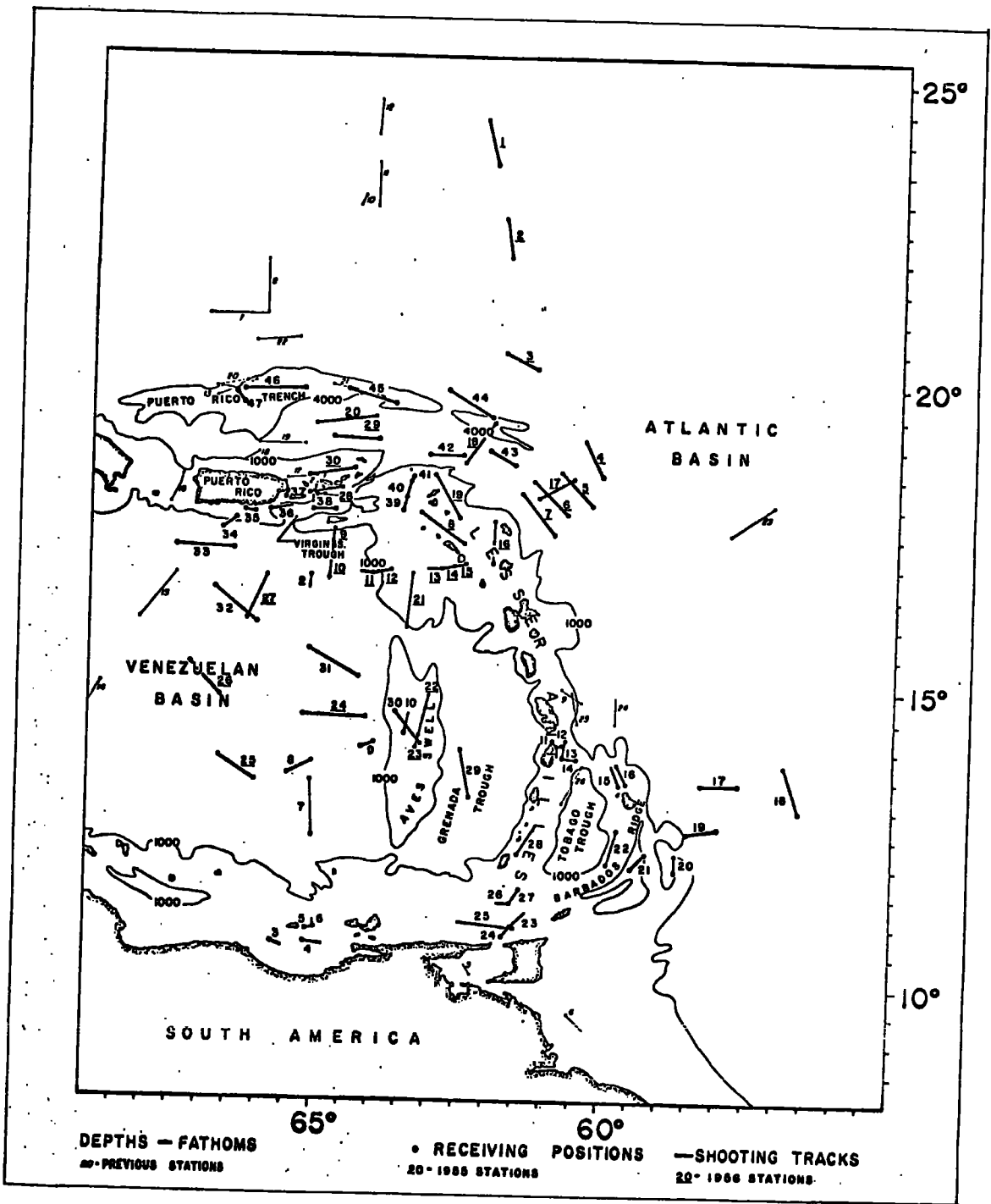


Fig. 5-5. Seismic refraction stations in the Eastern Caribbean.  
 (After Officer et al., 1959)

station 29..

Refraction work in the region of the volcanic islands of the Lesser Antilles (Ewing et al., 1957; Officer et al., 1959) has shown that a layer with velocity 4.0 - 4.4 km/sec. rises above the sediment cover to form the islands. The seismic basement found beneath High A is taken to be the upper surface of this layer.

The density of upper mantle rocks is assumed to be 3.30 gm/cc, other densities are estimated from P - wave velocity - density relationships (Appendix 3) and the densities reported by Andrew et al. (1970). Layers are distinguished on the grounds of seismic velocity and density, not necessarily lithology.

The method of computation was as follows:

A simple initial crustal model was constructed using the available seismic evidence and the resultant gravity anomaly was computed using GRAVN (Bott, 1969). The program GRAVIT 2 was then used to determine the shape of the source body causing High A, assuming a point on the top surface (from reflection data) and a density of 2.6 gm/cc. A thickness of some 9 kms. of the 2.6 gm/cc layer was found to be required to satisfy the Bouguer anomaly and since this is incompatible with the seismic refraction evidence (Ewing et al., 1957) it is clear that this layer alone cannot be responsible for High A.

The most probable explanation is that the 6.4 - 6.8 km/sec. layer, found under most of this region and elevated under the volcanic islands of the Lesser Antilles (Ewing et al., 1957) is also elevated under this extension



of the arc. The depth to this layer is known at the ends of the profile, thus assuming a simple model for the 2.6 gm/cc layer compatible with the seismic evidence, the program GRAVIT 2 was used to determine the required depth to the top surface of the 6.4 - 6.8 km/sec. (2.95 gm/cc) layer beneath High A. A depth of 4.1 km. to the top surface of this layer was found to satisfy the gravity and seismic refraction data. This is in excellent agreement with the depths to this layer found by Ewing et al. (1957) under the islands of the Lesser Antilles.

In the final model a simple outline for the 2.95 gm/cc layer (Fig. 5-6) was assumed and a good fit was obtained to gravity High A, using the program GRAVIT 1 to adjust the upper surface of the 2.6 gm/cc layer.

If constant crustal thickness is assumed the Bouguer anomaly in the north of the profile cannot be produced. It is clear that the Moho is elevated in the Grenada Trough with respect to the Venezuelan Shelf and arc extension. High A intersects the break in shelf slope (100 fathom isobath) and it appears that the Moho remains depressed under the arc structure before rising in the Grenada Trough. The depth to Moho under the Venezuelan Shelf was assumed to be 30 km., this value being obtained from the average Bouguer anomaly on the shelf (recomputed for a density of 2.67 gm/cc) using the relationship of Wollard and Strange (1961), no other evidence being available. The Moho profile (Fig. 5-6) was computed using the program GRAVIT 2 and a depth to Moho <sup>in the Grenada Trough</sup> of 20.5 km. was found to be necessary to satisfy the Bouguer anomaly. Ewing et al. (1957) obtained a velocity of

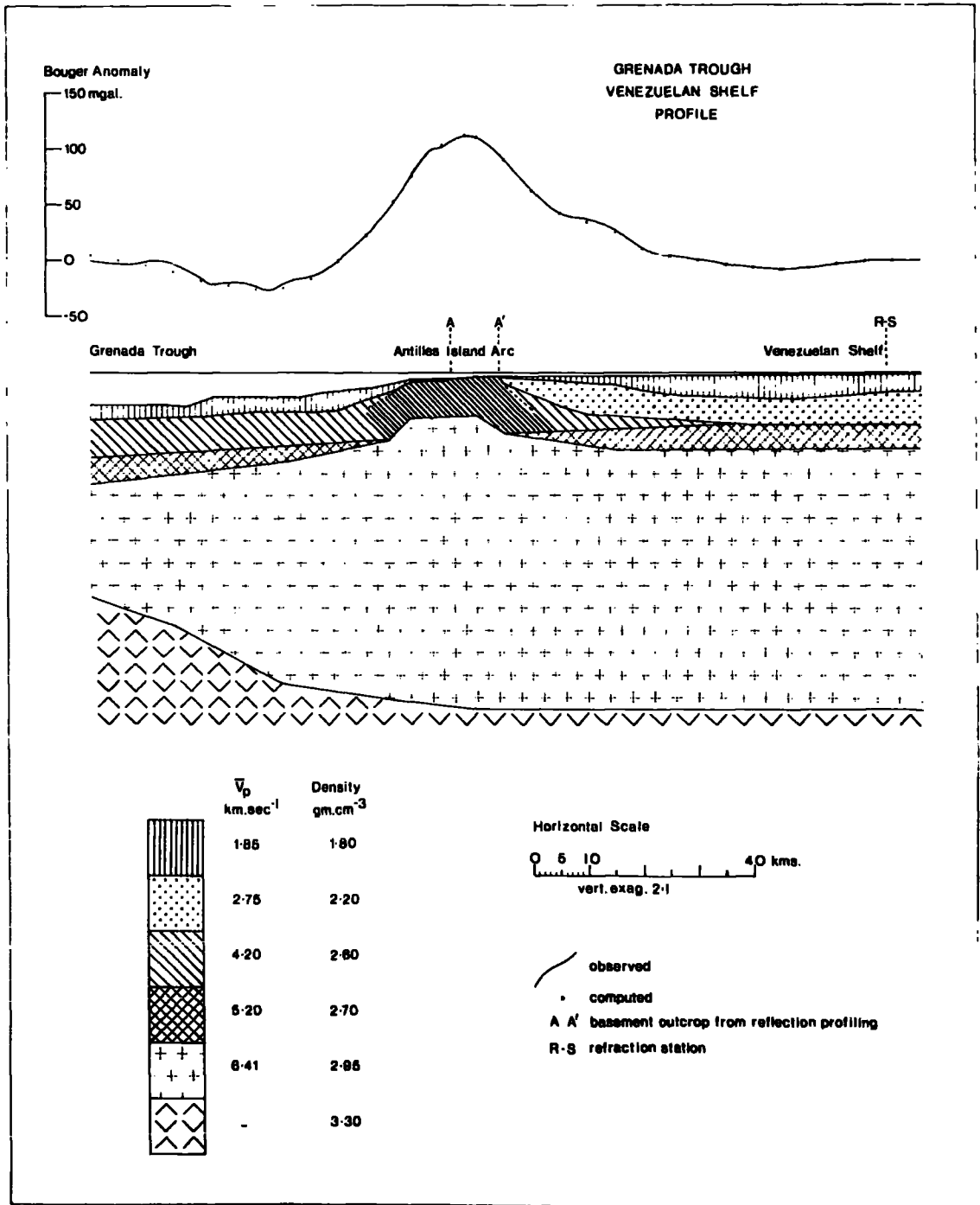


Fig.5-6. Interpretation of Bouguer anomaly profile R-R'.  
Two dimensional structure has been assumed.

7.47 km/sec at a depth of 18.5 km., further north in the Grenada Trough, which they interpreted as possible upper mantle.

Although the Bouguer anomaly does decrease between the coast of Paria and the arc structure, this has been interpreted in terms of crustal structure, rather than a depression of the Moho under the arc structure relative to the Venezuelan shelf. It is shown as a thickening of the sediments on the shelf, although crustal thickening under the arc structure, of (when the evidence from the profile T - T is considered - section 5-4-2) a pinching out of the 5.2 km/sec layer northwards the arc would appear to be equally valid interpretations.

Clearly, because of the large number of unknown layer interfaces, the model presented is in no way unique. It does, however, fit all the available seismic and gravity data and forms a starting model to which modifications can be made should further seismic data become available.

In the region of gravity High A, the 2.6 gm/cc layer has probably been built up by volcanic accumulation (Shown by fine hatching - Fig.5-6), elsewhere it is probably composed of lithified pyroclastics and other sediments. However, other possibilities exist since lithified sediments, volcanic rocks and some metamorphic rocks all have velocities that could lie within the required range. There may also be a lateral variation within the 6.4 - 6.8 km/sec layer, but no detailed evidence is, as yet, available.

The 5.2 km/sec velocity layer underlying the sedimentary strata in the south of the profile can probably

be correlated with the metamorphic rocks of the North Coast Range of Venezuela. (section 5-1-3-1).

-4-1-1 Continuity of the Arc Trend

If the anomaly trend is continued west of  $63^{\circ}$  West, it would pass through the island of Margarita, however, the basement rocks exposed in the north of that island are metamorphic rocks, similar to those of the North Coast Range of Venezuela (Hess and Maxwell, 1953) and it thus seems probable that the arc structure either dies out or is present only at depth west of  $63^{\circ}$  West.

Further west the Dutch islands of Curacao, Bonaire and Aruba, which also have associated Bouguer anomaly highs (Lagaay, 1969), seem not to be related to the Lesser Antilles, being composed of basic tuffs, dykes, sills and larger diorite to granite intrusions (Lagaay, 1969).

It is worthy of note that the continuation of the arc trend to  $63^{\circ}$  West is evidence that the often postulated 'South Caribbean Fault' (e.g. Martin Kaye, 1969 - Fig. 5-1) trending east-west, north of  $11^{\circ}$  North, does not exist.

-4-1-2 Profile S - S'

Profile S - S' (Fig. 5-4) strikes along the crest of Bouguer anomaly High A from  $62^{\circ} 30'$  West to the Grenada Platform at  $62^{\circ} 05'$  West. The anomaly shows a fall of some 35 mgal from its value at the intersection with profile R - R', before rising again towards the Grenada Platform. No data is available between  $62^{\circ} 05'$  West and the island of Grenada, but a proposed model on the evidence

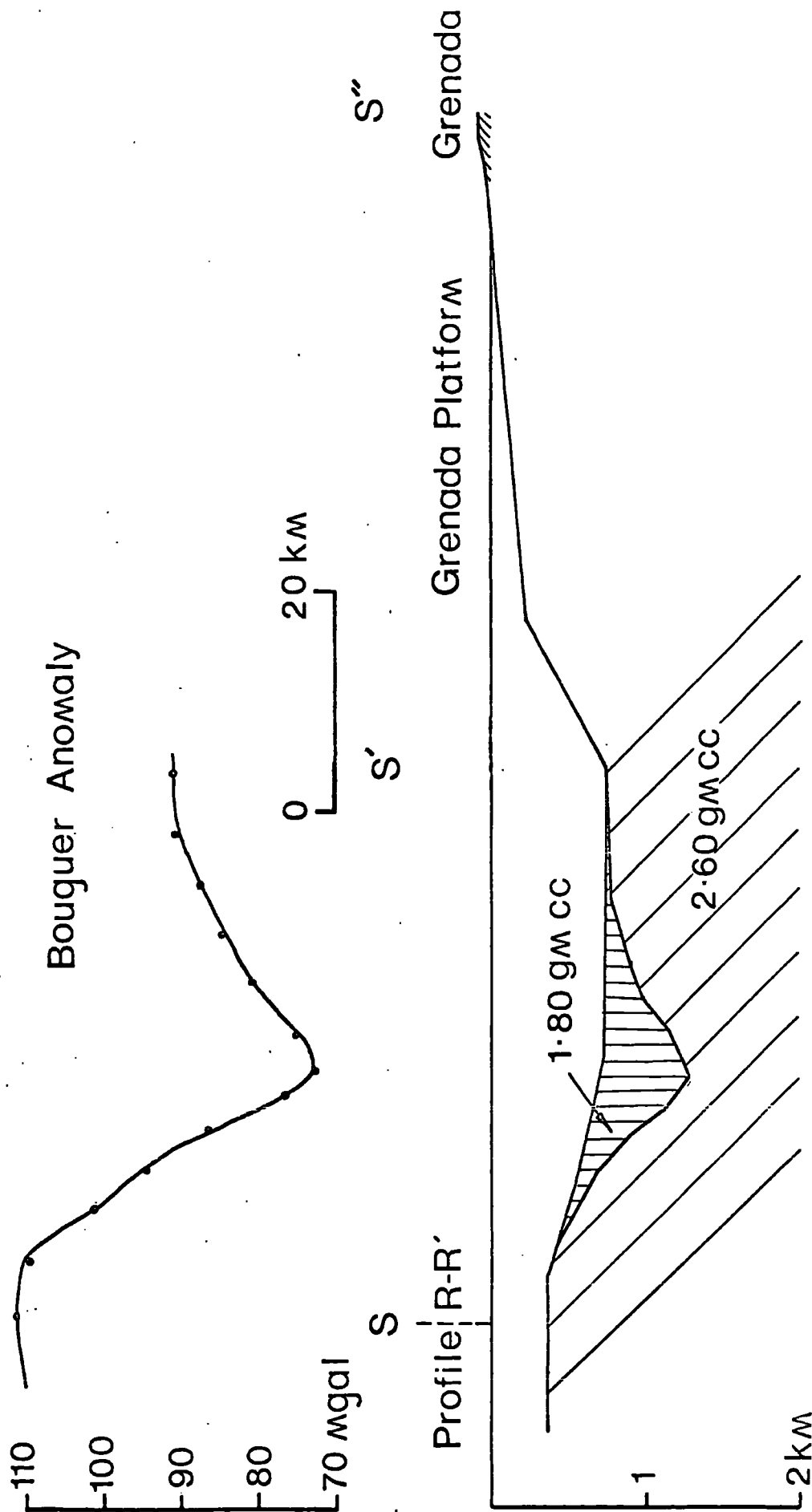


Fig. 5-7. Interpretation of Bouguer anomaly profile S-S'.

available is presented in Fig. (5-7).

The gravity low is assumed to be due to a depression of the 2.6 gm/cc. layer and infilling by low density sediments. No downwarp of the 2.95 gm/cc. layer has been considered.

The program GRAVIT 1 was used to compute the model.

The depression of the 2.6 gm/cc layer could be attributed to faulting or to two centres of volcanism separated by a sediment filled channel. The Bouguer anomaly requires that the 2.6 gm/cc. layer be near to outcrop on the slope of the Grenada Platform. Lattimore et al. (in press) did observed seismic 'basement' in region K'' (Fig. 5-4) on the Grenada Platform slope. Furthermore, these authors' magnetic profile M - M' (Fig. 5-4) has higher frequency content than profile KB', again indicating a rise in crystalline rocks on the slope of the Grenada Platform.

#### 5-4-2 Profile T' - T Trinidad Shelf to Grenada

This profile strikes roughly north-south from the island of Grenada to the continental shelf off Trinidad (Fig. 5-4). The gravity data for the island of Grenada is taken from Andrew et al. (1970).

The profile shows a Bouguer anomaly high of 160 mgal over the island of Grenada decreasing to -27 mgal between the islands before rising again to 12 mgal on the Trinidad shelf (Fig. 5-8). Just north of the coast of Trinidad the Bouguer anomaly falls again to at least -42 mgal. Two isolated readings indicate that the gravity low may reach -70 mgal, but the evidence is not good enough to include these values in profile T'-T. Two land gravity

stations on Trinidad (Bush and Bush, 1969) indicate that the Bouguer anomaly rises again over the North Range, as would be expected, before decreasing again over the sediment filled basin south of the El-Pilar fault (Fig.5-1).

A possible structure, that satisfies all the available seismic and gravity evidence, is shown at Fig.(5-8). The following initial assumptions were made.

The crustal structure determined at two seismic refraction stations crossed by profile T'-T (stations 23 and 27 - Ewing et al., 1957) is assumed.

The structure under Grenada is taken from seismic refraction station 28 (Ewing et al., 1957) adjacent to the island (Fig. 5-5).

When computing the structure of Grenada symmetry of the island along the line of the profile was assumed, no other evidence being available.

An initial assumption of constant crustal thickness along the line of the profile was also made. The method of density determination was as in the previous example.

The method of computation was as follows:

A simple crustal model was constructed using the seismic evidence available and the resultant gravity anomaly was computed using GRAVN (Bott, 1969). Refraction line 28 (Ewing et al., 1957) shows the 4.0 - 4.4 km/sec. layer rising to form the island of Grenada and the 6.4 - 6.8 km/sec. layer at a depth of 4.5 kms. beneath the island. The volcanics of the island are hornblende and hypersthene andesites with recent lava flows of basalt and picrite basalt (Andrew et al., 1970).

A simple model for the lower velocity (2.6 gm/cc.) layer, satisfying the seismic refraction data from stations 28 and 27, was assumed and the program GRAVIT 2 was used to determine the upper boundary of the higher velocity (2.95 gm/cc.) layer, fixing the highest point at 4.5 km<sub>d</sub>. under Grenada. If the crust is of constant thickness along the profile, the 2.95 gm/cc. layer must be at a depth of 9.5 km<sub>d</sub>. beneath refraction station 27 (Fig.5-8). Assuming a smooth outline for the upper surface of the 2.95 gm/cc. layer, the Bouguer anomaly between Grenada and station 27 was reproduced using GRAVIT 2 to determine the upper surface of the 2.6 gm/cc layer between these points (Fig. 5-8).

The 5.1 km/sec. layer found beneath refraction station 23 was not found beneath station 27 and the layer is assumed to pinch out to the north (Fig. 5-8). Similarly only 300 metres of the 4.0 - 4.4 km/sec. layer was found under station 23 and this layer is assumed to pinch out to the south. The Bouguer anomaly between refraction stations 23 and 27 was then produced using the program GRAVIT 1 to determine the lower boundaries of the sedimentary layers.

The 5.1 km/sec. layer found under refraction station 23 can probably be correlated with the metamorphic rocks of the North Range of Trinidad. As mentioned (section 5-1 - 3-1) the North Range of Trinidad is a narrow horst bounded north and south by major fault zones (Fig. 5-1). The decrease in Bouguer anomaly south of refraction station 23 is then interpreted as a basin bounded in the north by a downwarp of the shelf structure and in the south by a major, down to the north, fault. The program



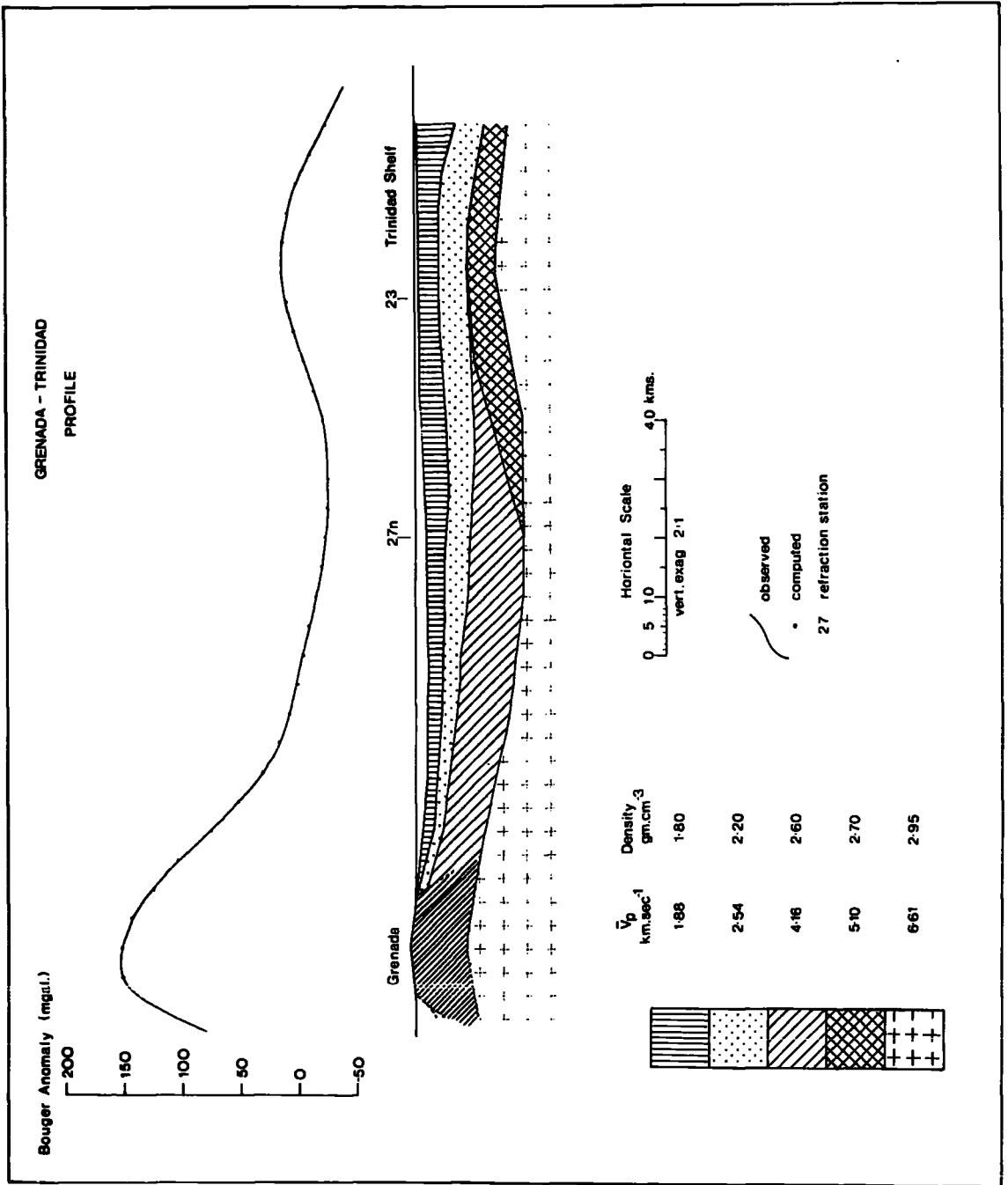


Fig. 5-8. Interpolation of Bouguer anomaly profile T'-T. Two-dimensional structure has been assumed.

GRAVIT 1 was used to match the Bouguer anomaly assuming downwarp of the 5.1 km/sec. (2.7 gm/cc.) layer with an accompanying thickening of low density sediments. A complete model of the basin is not possible because of the lack of gravity data from northern Trinidad.

Inspection of the Bouguer anomaly map (Fig. 5-4) indicates that this basin off the coast of Trinidad shallows to the east and to the west where it appears to die out around  $62^{\circ} 40''$  West.

The major ambiguity in the interpretation is the upper boundary of the 6.4 - 6.8 km/sec. (2.95 gm/cc.) layer under the central region of the profile. Seismic refraction station 27 was heavily shot by Ewing et al. (1957) but no velocity higher than 4.3 km/sec. was obtained from first arrivals. Ewing et al. (1957) estimate the depth to the 2.95 gm/cc. layer may be of the order of 12 kms. from second arrivals.

If a uniformly thick crust is assumed across the profile the depth to the 2.95 gm/cc. layer is 9.5 km. (Fig. 5-8). If, as seems likely, the layer is found to be deeper than 9.5 km., there must be crustal thinning between Trinidad and Grenada. This might be expected as the maximum water depth between the islands is 500 fathoms, and the effect of the mass excess of the volcanic arc is unlikely to cause a depression of the Moho as far south as the shelf onset.

As in the previous example the model is not unique, but is consistent with all the present data. Again it seems probable that lateral variation in the nature of the 2.6 gm/cc. and 2.95 gm/cc. layers exists. The area

of probable volcanic accumulation is shown by fine hatching in Fig. (5-8).

5-4-3 Profiles U-U', V-V'-V'' and W-W' and the Barbados Ridge.

The gravity data presented, plus the seismic reflection work of Bassinger et al. (in press) and the refraction work of Ewing et al. (1957) and Officer et al. (1959) show that, in the area under consideration the Barbados Ridge is a continuous, arcuate structural element, extending from Barbados, south and west to the island of Tobago. West of Tobago the picture becomes confused, but it seems probable that the ridge structure dies out.

5-4-3-1 Gravitational Effect of the Downgoing Lithosphere

Profile W-W' (Fig. 5-4) strikes east-west from the volcanic arc (St. Vincent) to Barbados. Since this is along the direction of assumed lithosphere underthrusting, in this section the likely gravitational field due to the downgoing slab is considered. Our lack of knowledge concerning the behaviour of the lithosphere under the conditions encountered renders any model speculative and imposes an additional uncertainty on an already ambiguous situation. Several firm conclusions can however be drawn.

The gravity models due to a series of models were computed using GRAVN (Bott, 1969). The model presented shows the factors taken into consideration in computing the gravity field (Fig. 5-9).

1) Adopting the model of Funnel and Smith (1968) for the opening of the Atlantic, the rate of underthrusting of the lithosphere is taken to be 1 cm/year.

2) Minear and Toksoz. (1970) describe the temperature

field for a lithosphere plate 80 km . thick, underthrusting at 1 cm/year. Taking into account adiabatic compression, phase changes and shear strain energies, their model shows the average temperature of the slab to be about 100°C. lower than the surrounding mantle..

3) The value for the thermal expansivity of upper mantle rock is taken to be the value for Forsterite given by Thomsen (1967)

$$\frac{1}{P} \left( \frac{dp}{dT} \right)_{pr} = 2.40 \times 10^{-5} \text{ } ^\circ\text{K}^{-1} \quad (5-1)$$

where p = density

T = temperature and subscript

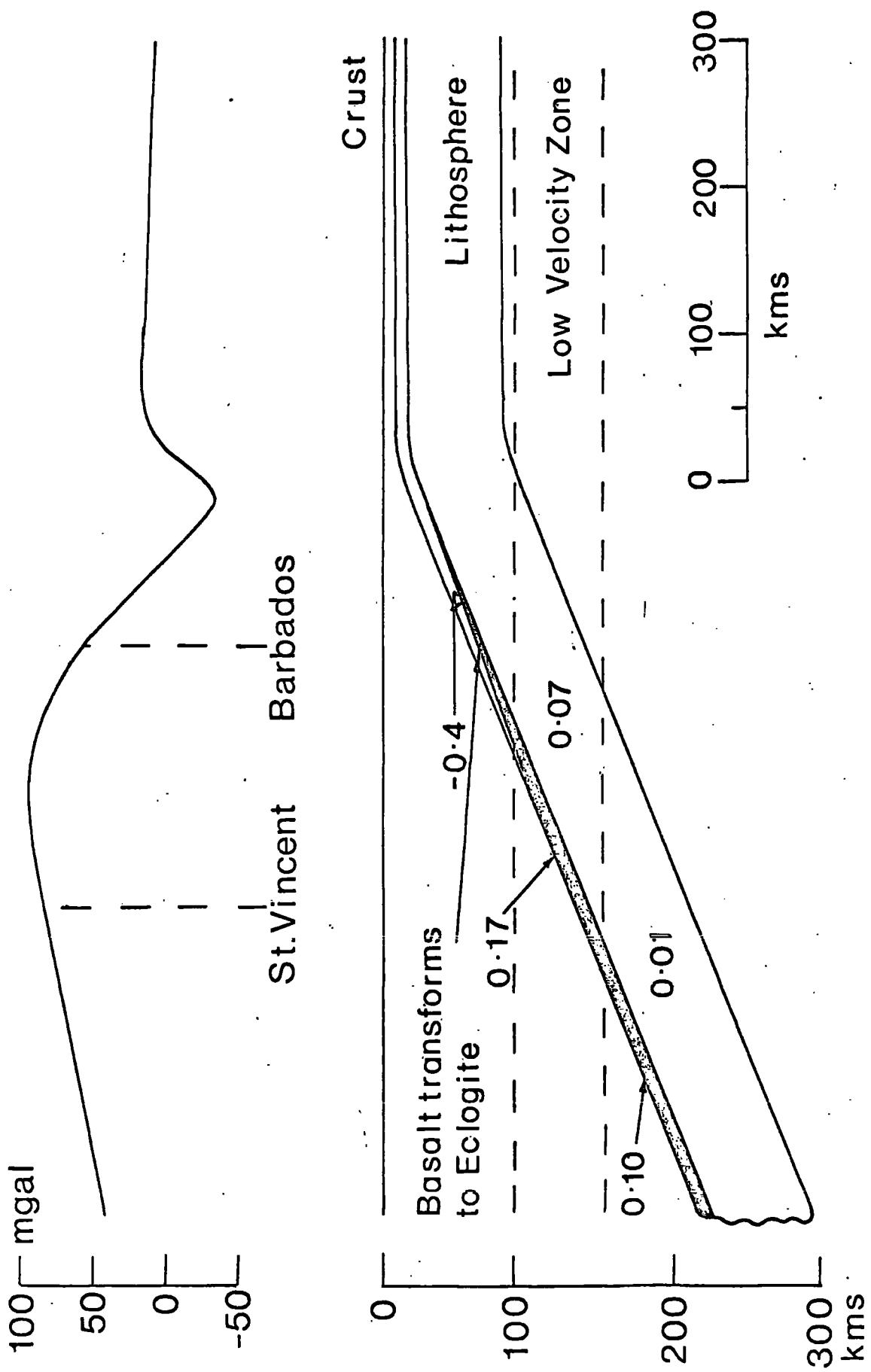
pr indicates a value at constant pressure.

Evaluation of equation (5-1) gives a density contrast between the underthrust lithosphere and surrounding mantle of the order of 0.01 gm/cc.

4) The effect of the lithosphere passing through the low velocity zone of the upper mantle has been considered separately. Anderson (1967), shows the reduction in P - wave velocities under oceanic areas is of the order of 0.7 km/sec. From the work of Birch (1969) this is assumed to result in a reduction in density of 0.07 gm/cc, assuming partial melting in the low velocity zone.

5) The effect of the crustal portion of the lithosphere is also considered. Ringwood (1969) suggests that the transformation of basalt to eclogite will begin "within a few tens of kilometers" in the lower 'dry' crust, with the upper 'wet' crust transforming to amphibolite. Total transition of the crust to eclogite

Fig.5-9. Possible gravitational effect of the downgoing lithosphere.



should however have occurred by a depth of 100 km. (Fitton, personal communication).

The density of eclogite is taken to be 3.5 gm/cc.

6) The point of underthrusting is estimated to be some 100 kms. east of Barbados, from a consideration of seismic reflection (Chase and Bunce, 1969) and refraction (Ewing et al., 1957; Officer et al., 1959) (Figs. 5-16(a) and (b)). The depth of the lithosphere under St. Vincent (and hence its dip) is estimated from the work on Caribbean seismicity (Sykes and Ewing, 1965).

The model and anomaly are shown at Fig. (5-9).

Although this and the other models computed are speculative, the general conclusion can be drawn that, over much of the region between St. Vincent and Barbados, the slab will produce only a low amplitude, long wavelength anomaly. In the vicinity of Barbados however, it seems possible that the crustal section of the lithosphere will make a significant contribution to the broad Bouguer anomaly low observed. Nevertheless, it has been assumed in computing a model of the structure between St. Vincent and Barbados from the gravity data, that the gravitational effect of the downgoing slab can be ignored. Without a detailed knowledge of the behaviour of the lithosphere at depth, this is considered to be the only possible approach.

#### -4-3-2 Profile W-W' St. Vincent to Barbados.

This is an east-west striking profile from the island of Barbados to the volcanic island of St. Vincent. The Bouguer anomaly shows a local high within a broad low in

the vicinity of Barbados (Fig. 5-11) before rising to a 'plateau' value of 50 mgal in the Tobago Trough. Over the island of St. Vincent the anomaly reaches 160 mgal. The rocks on St. Vincent are entirely volcanic, mainly basaltic andesite and basalt, and are correlated with the 4.0 - 4.4 km/sec. layer. The lateral extent of surface outcrop of the volcanic rocks is known from a seismic reflection profile, shot during 1970 from north of St. Vincent to north of Barbados (Fig. 5-10).

The following initial assumptions were made:

Although no refraction data is available from the area of St. Vincent, the refraction lines of Ewing et al. (1957) in the vicinity of the islands immediately to the north and south of St. Vincent (St. Lucia - profiles 11 and 12; Grenada - profile 28 - Fig. (5-5)) all indicate that the depth to the 6.4 - 6.8 km/sec. layer is of the order of 4 kms. A similar value is assumed for St. Vincent.

Profile W-W' intersects refraction line 7 (Ewing et al., 1957) in the Tobago Trough. The crustal structure deduced from the refraction data is assumed at the point of intersection.

Under Barbados the structure is far less certain. Ewing et al. (1957) shot two refraction lines to the north of the island (lines 15 and 16; Fig (5-5)) and one to the south (line 22). Worzel and Ewing (1948) shot a line just west of the island. Most of the stations show large dips and horizontal discontinuities indicating severe folding and faulting. A possible upper crustal structure is estimated using the data from these stations.



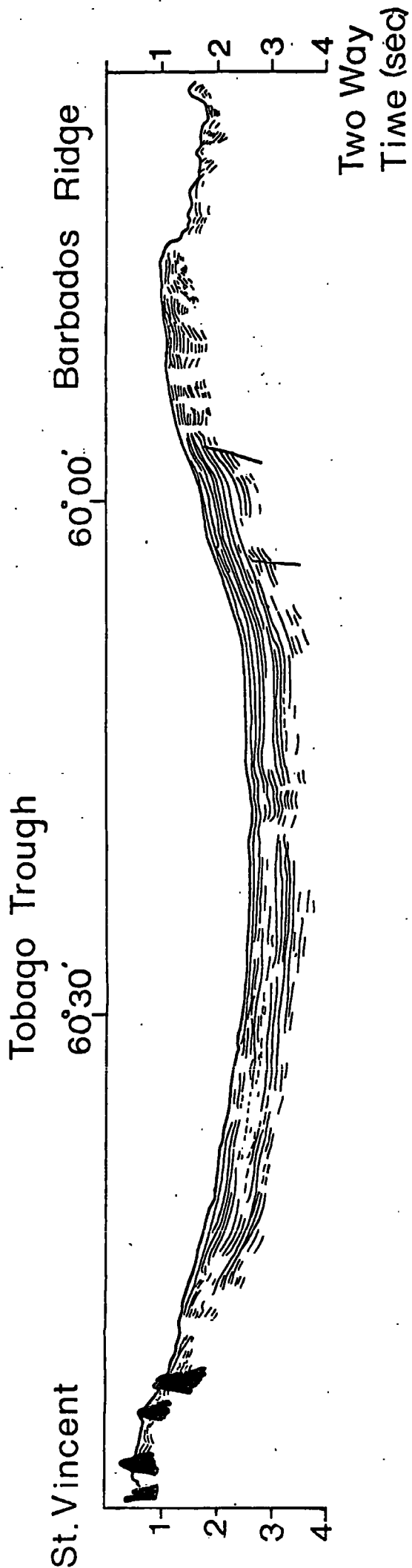


Fig.5-10. Seismic reflection profile from St. Vincent to Barbados.  
 (Bassinger, personal communication)

Fig. (5-11) show a possible structure that satisfies the available seismic and gravity data. The method of computation used was as follows.

A simple crustal model between St. Vincent and refraction station 7 was constructed using the available seismic evidence and assuming east-west symmetry of the structure of St. Vincent (no data west of St. Vincent being available). The gravity effect of the model was computed using GRAVN (Bott, 1969). However, the Bouguer anomaly produced at St. Vincent by the model was of the order of 50 mgal too high with respect to that at refraction station 7 in the Tobago Trough. Since the crustal structure at these two points is known, it is clear that either crustal thickening, or a net decrease in upper mantle density is occurring from the Tobago Trough towards St. Vincent. Computation carried out to determine the gravitational attraction of various 'downgoing slab' models indicates that their effect will be to reduce the Bouguer anomaly at St. Vincent with respect to that of the Tobago Trough, but that the effect is unlikely to be as great as 20 mgal. and will probably be of the order of 10 mgal. Crustal thickening is assumed to be the cause of the required anomaly reduction and although no account is taken of the gravity anomaly due to the downgoing slab, it is clear that crustal thickening would still be necessary if this effect were considered.

In the absence of further information a crustal thickness of 30 km. under the arc was assumed (this

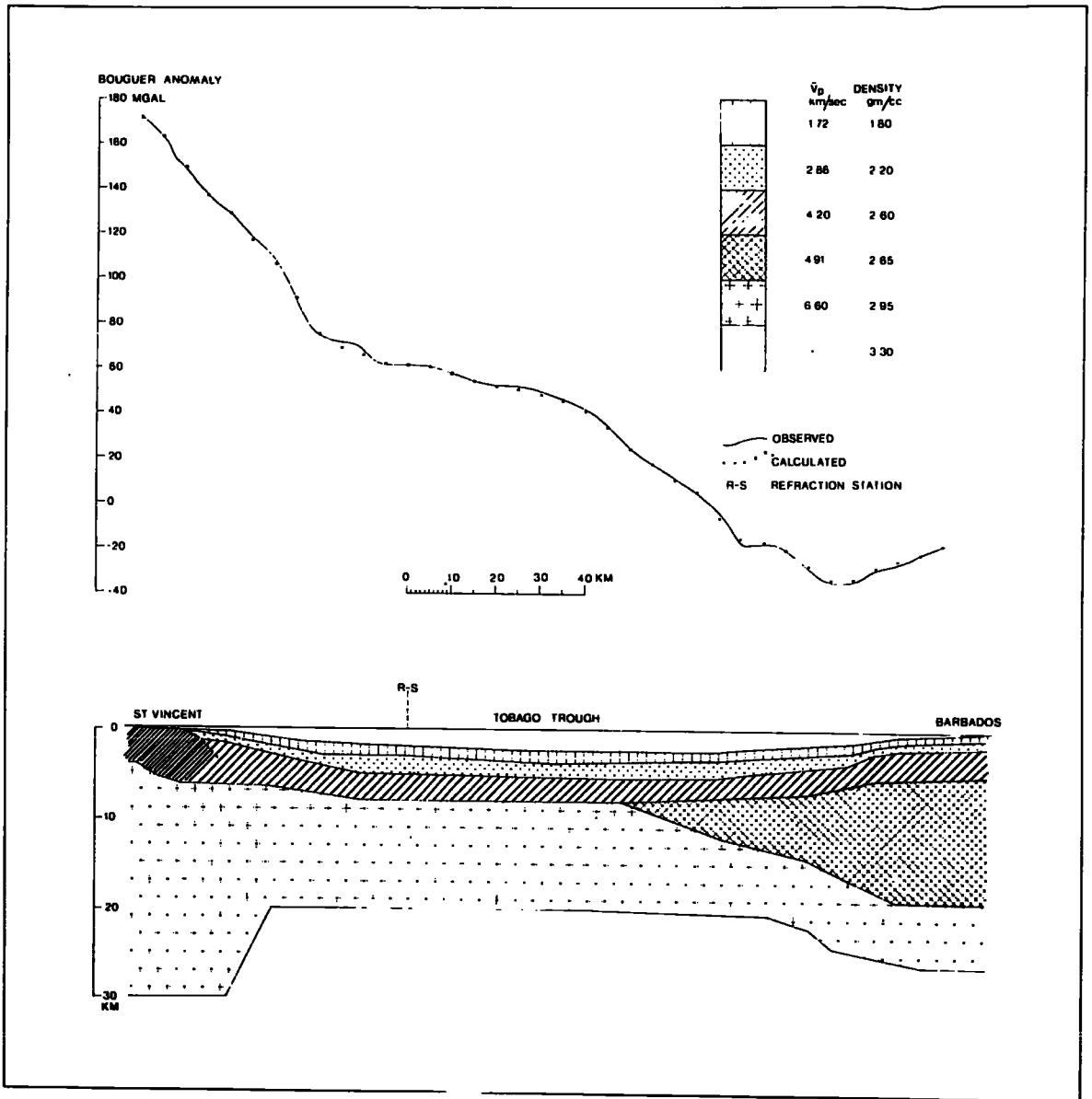


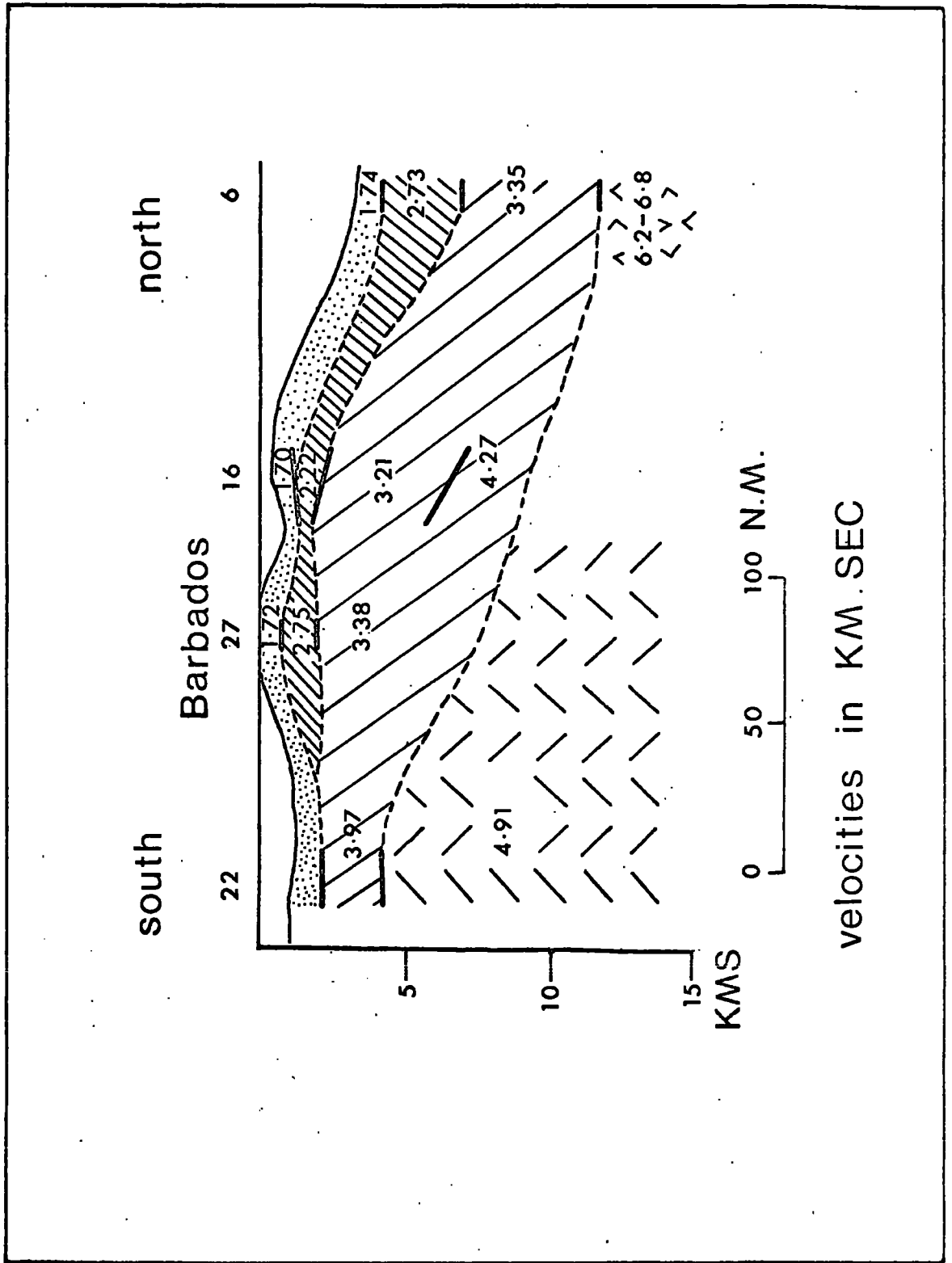
Fig.5-11. Interpretation of Bouguer anomaly profile W-W'

being the value assumed for the extension of the arc structure further south) and the program GRAVIT 1 was used to determine the crust-mantle interface required to satisfy the observed Bouguer anomaly, assuming an upper mantle density of 3.30 gm/cc. A depth to Moho of 20.5 kms. under the Tobago Trough was found to be required. Ewing et al. (1957) put a minimum limit on the depth to the Moho under the Tobago Trough of 16.5 km. A simplified model was then assumed for the crust-mantle boundary and the 2.95 gm/cc. layer upper surface. The program GRAVIT 2 was then used to determine the upper surface of the 2.6 gm/cc. layer necessary to produce the observed Bouguer anomaly (Fig. 5-11). The model may have to be modified when the depth to Moho in the Tobago Trough is determined from seismic refraction.

As previously stated, the structure under Barbados appears complex. Evidence for the distinction between the 2.60 gm/cc. and 2.65 gm/cc. (4.0 and 4.9 km/sec.) layers shown in the gravity model (Fig. 5-11), although well defined south of Barbados, is a little tenuous under the island itself. The refraction profiles show a general decrease in velocity in the various strata from south to north along the ridge (Fig. 5-12).

The gravity data presented, the land gravity data from Barbados (Andrew et al., 1970) and the marine gravity data obtained during 1971 by Durham University (Westbrook-personal communication) show a broad Bouguer anomaly low in the vicinity of the Barbados Ridge, with a local central Bouguer high. The high is attributed to an anticline in the intermediate velocity crustal layers as shown (Fig. 5-11).

Fig. 5-12. Seismic structure along the Barbados ridge . Station locations are given in Fig. 5-5. (After Ewing et al., 1957)



velocities in KM . SEC

Work on the 'downgoing slab' of lithosphere indicates that part of the broad gravity low will probably result from the effect of the crustal (basaltic) section of the lithosphere being thrust into the mantle (before its transformation to eclogite). It is unlikely, however, that this is the only contributory factor. The thickening of the 4.9 km/sec. (2.65 gm/cc.) layer will obviously contribute to the low. A general crustal thickening under the ridge would also appear to be necessary if the estimate of 20.5 kms. of crust in the Tobago Trough is of the right order of magnitude.

The base of the 4.9 km/sec. layer and the base of the crust are both undetermined under Barbados, introducing a further ambiguity. Various models of the crust under Barbados were produced, assuming the upper crustal structure from seismic refraction data, and determining the possible lower boundaries of the 4.9 km/sec. layer and the crust using GRAVN (Bott, 1969) and GRAVIT 1. Fig. (5-11) shows one possible solution. A simple thickening of the crust to 26 km. under Barbados has been assumed and the lower surface of the 4.9 km/sec. (2.65 gm/cc.) layer has been computed using GRAVIT 1.

The implications of the Barbados Ridge structure are discussed in section (5-4-3-5).

-4-3-3 Profile U-U'

Profile U-U' extends S.W. - N.E. from Tobago island to the northern extension of gravity High R (Fig. 5-4). The Bouguer anomaly on Tobago reaches 30 mgal. (Bowin-personal communication) then falls rapidly to - 70 mgal. (Low D) to the north of the island, before rising again

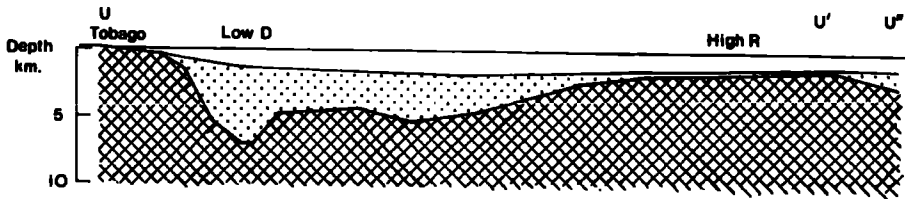
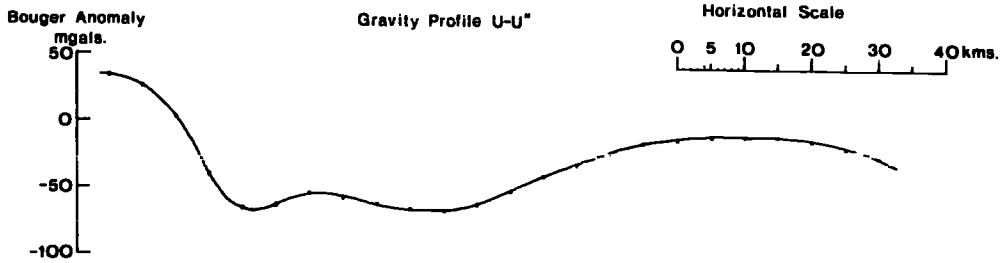
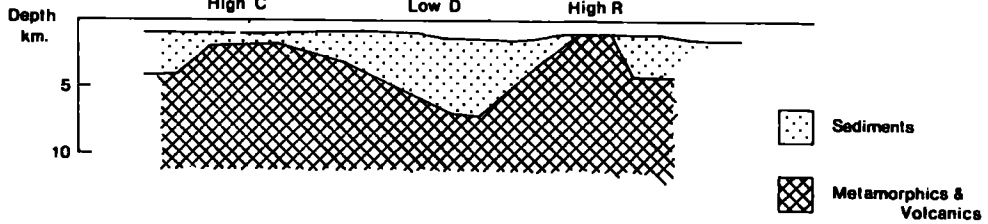
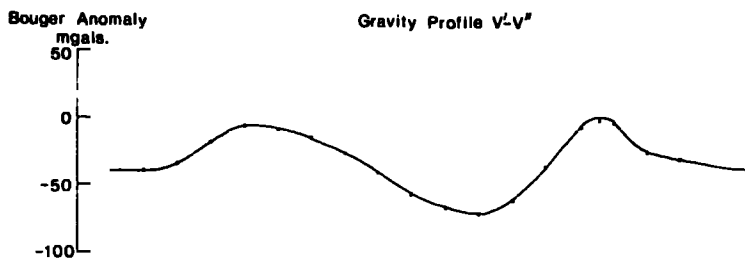
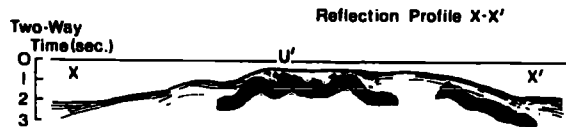
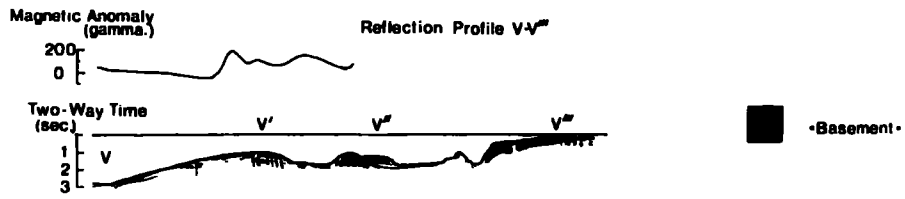
Fig.5-13(a) Seismic reflection and magnetic profiles  
V-V'-V''-V'''.-see Fig.5-4.  
(After Bassinger et al., in press)

Fig.5-13(b) Seismic reflection profile X-U'-X'.  
(After Bassinger et al., in press)

Fig.5-13(c) Interpretation of Bouguer anomaly profile  
V-V'-V''. Two dimensional structure has  
been assumed.

Fig.5-13(d) Interpretation of Bouguer anomaly profile  
U-U'. Two dimensional structure has been  
assumed.





to -17 mgal. (High R).

The north eastern end of profile U-U' coincides with refraction line 22 (Fig 5-5) of Ewing et al., (1957), which shows some 300 metres of sediments overlying the 3.97 km/sec. and 4.91 km/sec. layers.

In the absence of detailed seismic information the 3.97 km/sec. and 4.91 km/sec. velocity layers were taken as having a uniform density of 2.60 gm/cc. Constant crustal thickness along the profile was assumed.

The model shown at Fig. 5-13 (d) was computed using the program GRAVIT 1 assuming a density of 2.2 gm/cc. for the sedimentary layer.

The gravity model is in excellent agreement with the seismic reflection profile (Bassinger et al., in press) which crosses the northern end of U-U' and shows seismic basement near to outcrop in the region of U' (Fig. 5-13 (b)). The density of 2.2 gm/cc. for the sediments in this area was chosen, as the sediments can be seen to plunge beneath the younger beds of the Tobago Trough at point X (Fig. 5-13 (b)).

The magnitude of Bouguer anomaly Low D requires a depth of 7 km. of sediments in a basin, north-east of Tobago. The anomaly gradient suggest that the basin is fault bounded on its southern margin (Fig. 5-4).

#### -4-3-4 Profile V-V'-V''

Profile V-V'-V'' extends N.W. - S.E. along a line east of Tobago (Fig. 5-4). The Bouguer anomaly is -4 mgal. over High C in the north-west of the profile, falls to -70 mgal. (Low D), then rises to 0 mgal. in the south-east of the profile (High R) over the seaward extension of the rocks exposed on Tobago (section 5-1-3-1). A seismic

reflection profile. (Bassinger et al., in press) shows basement outcropping in the region of gravity High R. (Fig. 5-13 (a)).

As in the previous model, a simple contrast between the 2.60 gm/cc. basement and the 2.20 gm/cc sediments is assumed, as is constant crustal thickness. The model shown at Fig. 5-13 (c) was computed using the program GRAVIT 1.

The depth of the sediments in the basin resulting in Low D is 7 km., agreeing with the value previously obtained.

Seismic reflection and magnetic records along the line of the profile (Bassinger et al., in press) are shown at Fig. (5-13 (a)). The reflection profile confirms that Low D results from a faulted basin and shows an anticline in the sedimentary strata, with many minor faults, in the region of High C. The magnetic field is also relatively disturbed in the region of High C.

These data tend to confirm the results of the gravity model which shows High C to be caused by an elevation of the 2.60 gm/cc. layer. The depth shown to the layer may however, be an underestimate. Examination of the Bouguer anomaly map (Fig. 5-4) indicates that the trend of High C may be continuous with High C' to the west, previously interpreted as a shallowing of the 5.1 - 5.1 km/sec. layer. If this geological structure does continue to form High C, the mean density of the rocks in this region should probably be 2.65 - 2.70 gm/cc., resulting in a greater thickness of sediments under High C. The simplified

model is however presented in the absence of detailed seismic information.

-4-3-5 The Barbados Ridge -- Discussion

Although continuity of the gravity trend (Fig. 5-4) and the available seismic data indicate the existence of a continuous structural unit from Tobago to south of Barbados, the featureless magnetic field in the vicinity of Barbados, the variation in the acoustic nature of the seismic (reflection) basement (Bassinger et al., in press) and the complexity of the seismic refraction data along the northern section of the ridge (Ewing et al., 1957) (Fig. 5-12), all militate against a simple extension of the metamorphic and igneous rocks of Tobago, north to Barbados.

That the ridge in the vicinity of Barbados is not due to simply <sup>to</sup> sediment filling of the 'Antillean Trench' is evidenced by the presence of the Oceanic series on Barbados. The abyssal nature of these marls (section 5-1-3-2) indicates that the area of Barbados was once a foredeep and has since been uplifted. This conclusion can also be drawn by an examination of the generalised section across the region by Officer et al., (1959) (Fig. 5-16 (b)).

The Antillean Arc is not alone in having an uplifted sedimentary outer arc and a lack of a deep sea trench. The area of the Kodiak-Alaska Peninsula, which is an extension of the Aleutian Arc, the eastern extension of the Indonesian Arc and the Andaman-Nicobar Arc all show similar structure.

The Andaman-Nicobar Arc has been studied by Peter

et al. (1966) and Weeks et al. (1967). The main elements of the area are shown at Fig. (5-14) and profiles across the structures at Fig. (5-15). As shown the volcanic arc is, in places only poorly developed, but the nature of the gravity field shows a striking resemblance to that of the Antilles Arc, the Nicobar-Andaman sedimentary arc having a mass deficiency similar to that of Barbados and the volcanic arc having a mass excess. The lack of a trench and nature of the sedimentary arc shown by the bathymetric profiles of Fig. (5-15) is remarkably similar to the structure shown by the seismic reflection profile from the Atlantic basin onto the Barbados Ridge (Chase and Bunce, 1969) (Fig. 5-16 (a)). The Java-Sumatra deep sea trench dies out south of the Nicobars.

The fact that the occurrence of a sedimentary arc appears usually to accompany the absence of a deep sea trench is evidence that although simple infilling of the trench due to close proximity to a large sedimentary source, cannot alone explain the sedimentary arc, proximity to such a source would appear to be a necessary condition for the formation of the sedimentary ridge.

A possible source of uplift is pressure exerted by the oceanic lithosphere. It appears probable that although much of the crustal section of the downgoing slab will be dragged down into the mantle, various parts of the crust will be torn from the slab and forced westwards resulting in a *mélange* terrain west of the locus of underthrusting. Flysch filling the 'Antillean Trench' might also be incorporated in this terrain. Takeuchi and Uyeda (1965), suggest that such an area might be the site of low

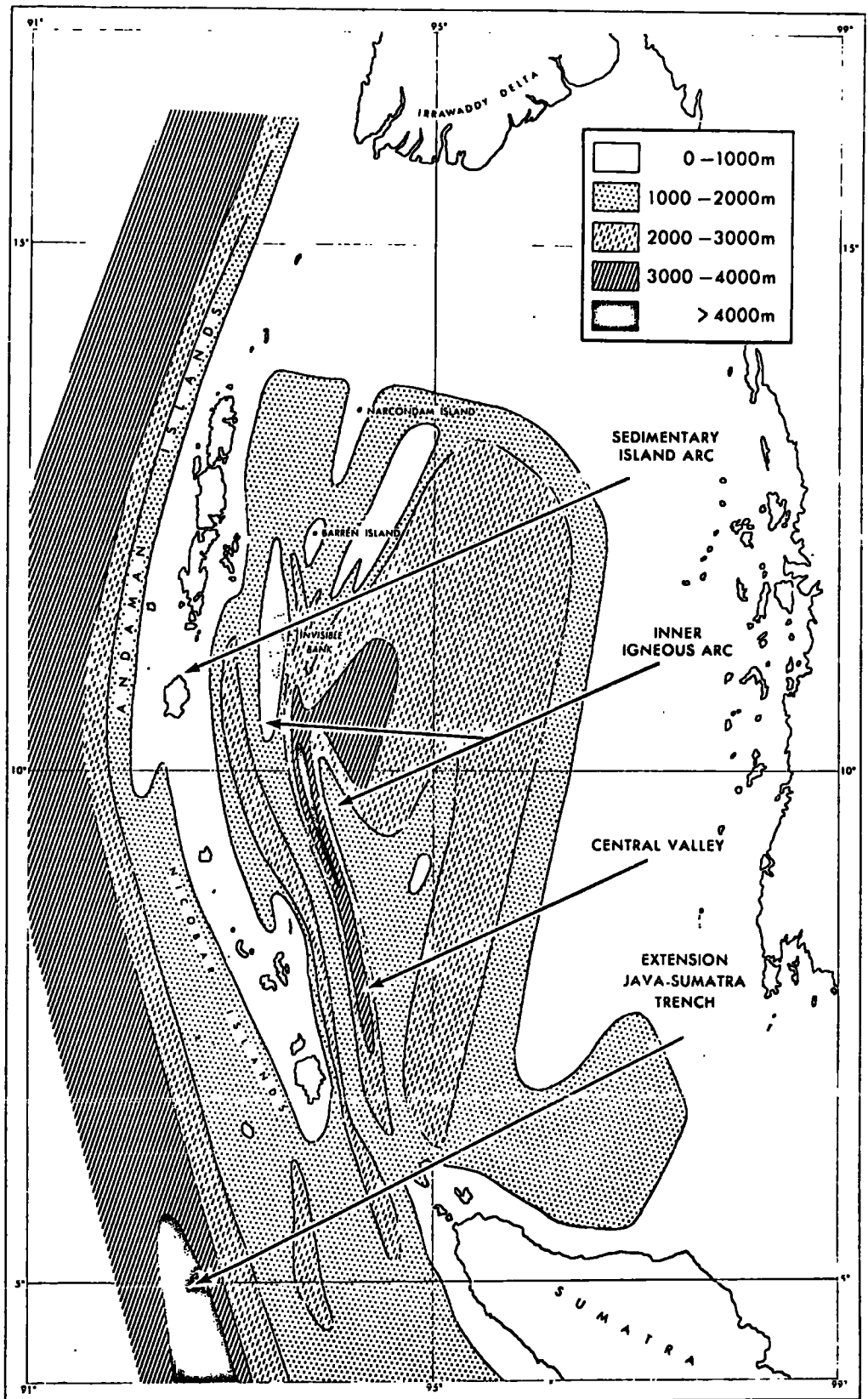


Fig.5-14. Main structural elements of the Andaman-Nicobar Island Arc region. (After Peter et al., 1966)

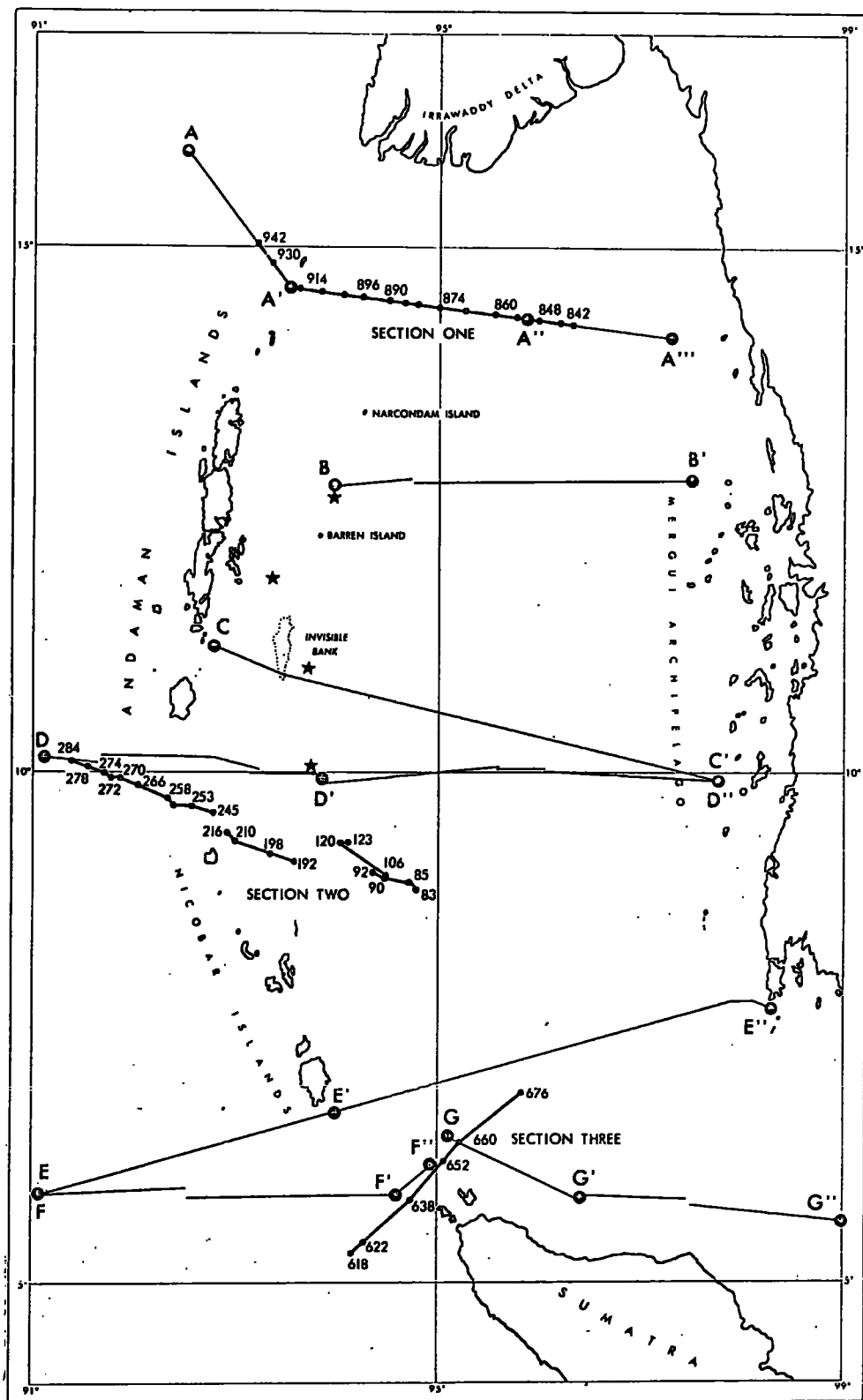


Fig.5-15(a) General location of subbottom profiles and gravity and magnetic profiles. (After Peter et al., 1966)

Fig.5-15(b) Bouguer anomaly profile E-E'-E'' showing the "low" associated with the outer sedimentary arc and a possible interpretation. The volcanic arc is only poorly developed in this region.

Subbottom profile A-A'-A''-A''' showing the highly folded outer sedimentary arc and the inner volcanic arc.

Modified from Peter et al., 1966.



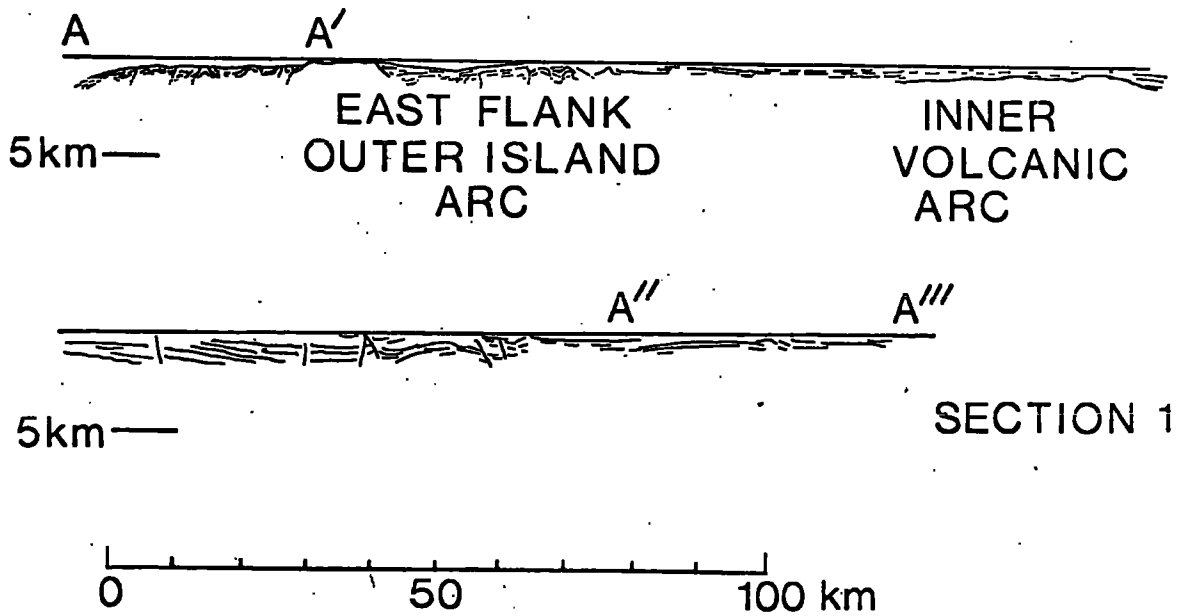
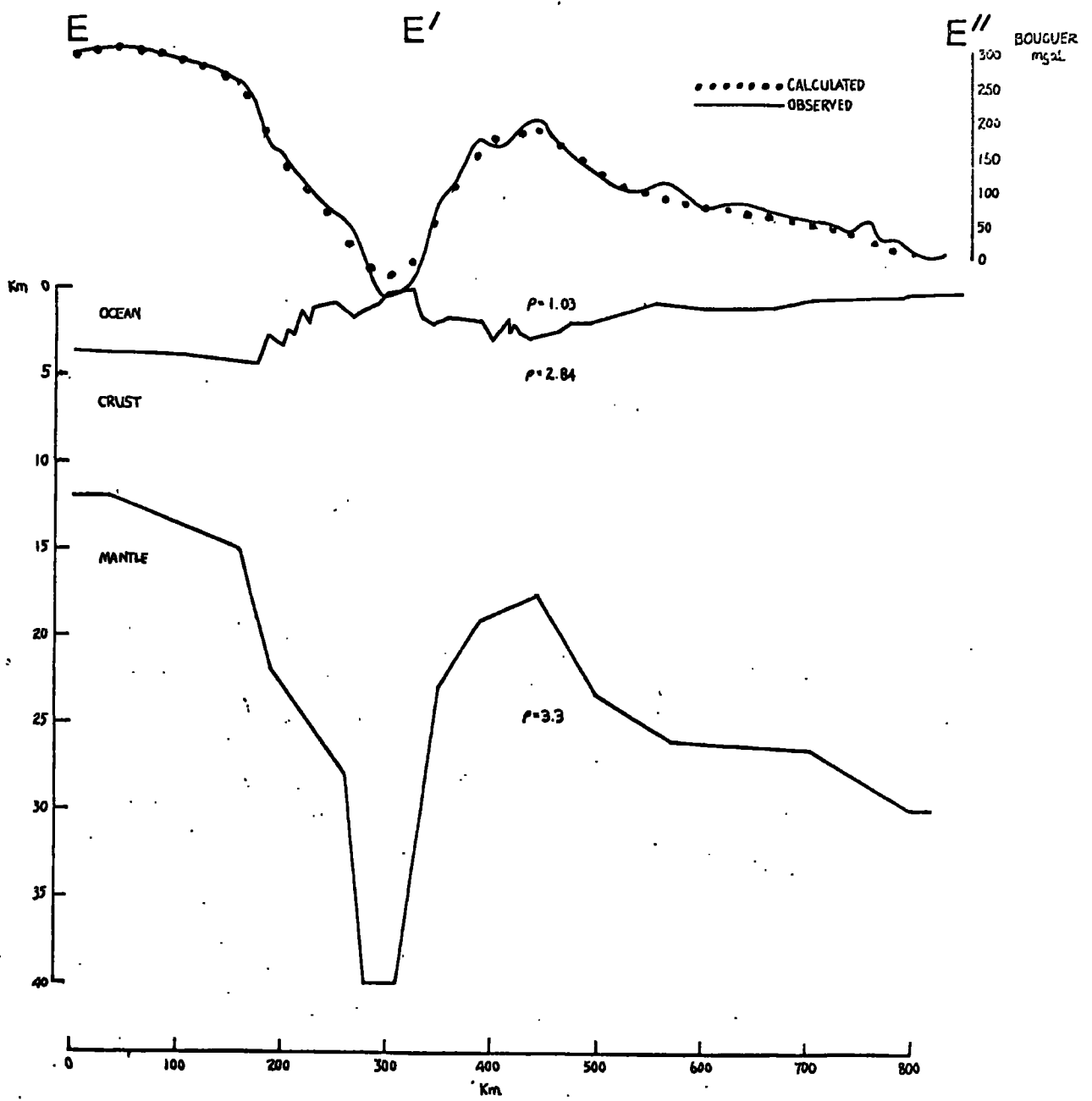
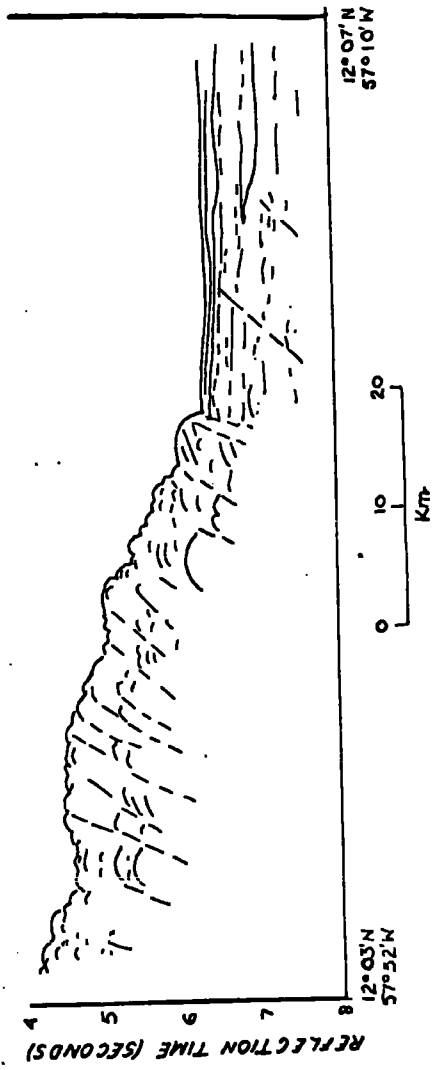
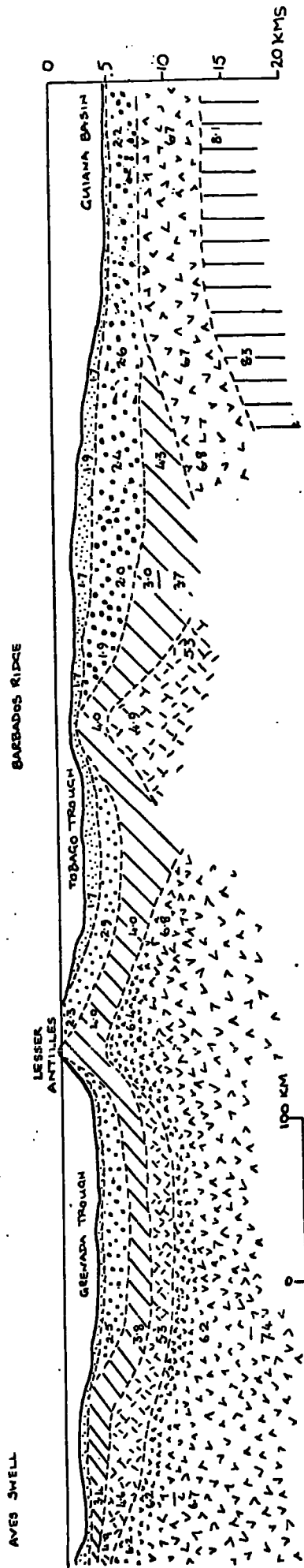


Fig. 5-16(a) Generalised section across the Caribbean Eastern margin  
(After Officer et al., 1959)

Fig. 5-16(b) Continuous seismic reflection profile across the Eastern  
margin of the Barbados ridge southeast of Barbados  
(Modified from Chase and Bunce, 1969)



12° 07' N  
57° 10' W

12° 03' N  
57° 52' W

temperature, high pressure (blueschist) metamorphism. Whether such a mechanism could result in uplift to the west of the locus of underthrusting is open to speculation, certainly the possibility that the area would rise isostatically cannot be excluded. That there has been a vast amount of sediment available is evidenced by the reflection profile of Chase and Bunce (1969) (Fig. 5-16 (a)). In the area shown, east of the underthrusting zone, simple accumulation of flysch would appear to be the only necessary mechanism for the evolution of the ridge, but a detailed knowledge of the strata underlying Barbados will be necessary before the mechanism of evolution of the ridge, west of the underthrusting zone, can be determined.

5-5

#### General Conclusions

1) The crust under the volcanic arc is thicker than that under the adjacent basins (Tobago Trough and Grenada Trough). It also seems probable that there is a crustal thickening under the Barbados Ridge with respect to the Tobago Trough.

2) The Barbados Ridge is a continuous arcuate structural feature from Barbados at least as far south as the shelf off Tobago. In the vicinity of Tobago the roughly east-west striking structure of the metamorphic and igneous rocks exposed on the island is shown by the Bouguer anomaly map (Fig. 5-4) to merge with the N.E. - S.W. trend of the ridge. An irregular outlined Bouguer anomaly high is developed in this region. It is possible that the island of Tobago, and the shelf structure resulting in gravity Highs C' and C, are an expression

of the continuation of the uplift that resulted in the Barbados Ridge into the continental shelf of Trinidad and Venezuela.

3) Weeks et al. (in press) concluded from an examination of anomaly profiles, that the 'South Caribbean Fault' long postulated as the sight of strike slip motion between the Caribbean and South American plates, does not exist. The continuation of High A to  $63^{\circ}$  West, shown by the Bouguer anomaly map (Fig. 5-4) clearly illustrates this conclusion to be correct. Any strike slip motion between the plates must then be attributed to the faults exposed in Trinidad and Venezuela (e.g. El-Pilar Fault - Fig. 5-1). Although Rod (1956) implied a lateral displacement of over 100 km. due to strike slip faulting in northern Venezuela, Metz (1964) could only find 10-15 kms. of strike slip motion along the El-Pilar fault. In addition, work by Ewing et al. (1957) and Ball et al. (1971 - in press) suggest vertical displacements along the southern Caribbean margin, rather than lateral movement.

These data, in addition to the seismic inactivity of northern Venezuela (Molnar and Sykes, 1969), indicate that the South American and Caribbean plates are welded west of the Paria peninsula, and add weight to the theory of Ball et al. (1969), that, rather than right lateral motion between the two plates, relative motion between the lamellae of the Atlantic plate, from the latitude of the Lesser Antilles, to that of the Greater Antilles, results in left lateral shear in the Atlantic and underthrusting at the Lesser Antilles. This theory allows

for welding of the South American and Caribbean plates and is compatible with the relative northward movement of North America with respect to South America proposed by the model of Funnel and Smith (1968).

CHAPTER. 6

INTERPRETATION OF A MARINE GRAVITY SURVEY OF THE SIERRA  
LEONE CONTINENTAL SHELF

6-1 Introduction

6-1-1 Structural Framework of the West African Continental Margin

In pre-Cambrian times a large area of the continent of Africa was affected by a major orogenesis (the 1850  $\pm$  250 m.y. orogenesis) that resulted in the structural differentiation of the continent into four major stable nuclei; The Rhodesia - Transvaal Craton; The Tanzania Craton; The Angola - Kasai Craton and the West African Craton (Fig. 6-1). These are distinct from the surrounding regions of more recent activity (Clifford, 1966). In West Africa, the Ivory Coast, Upper Volta, Mali, Senegal and Mauritania were affected, with widespread metamorphism and intrusion of granites occurring.

In the east of the Sierra Leone - Ivory Coast nucleus ( a nucleus of ancient rocks affected by an orogeny dated at 2500 m.y.) pegmatites and dolerites giving an age of 2000  $\pm$  200 m.y. are found illustrating the wide influence of the event. (Andrew Jones, 1968).

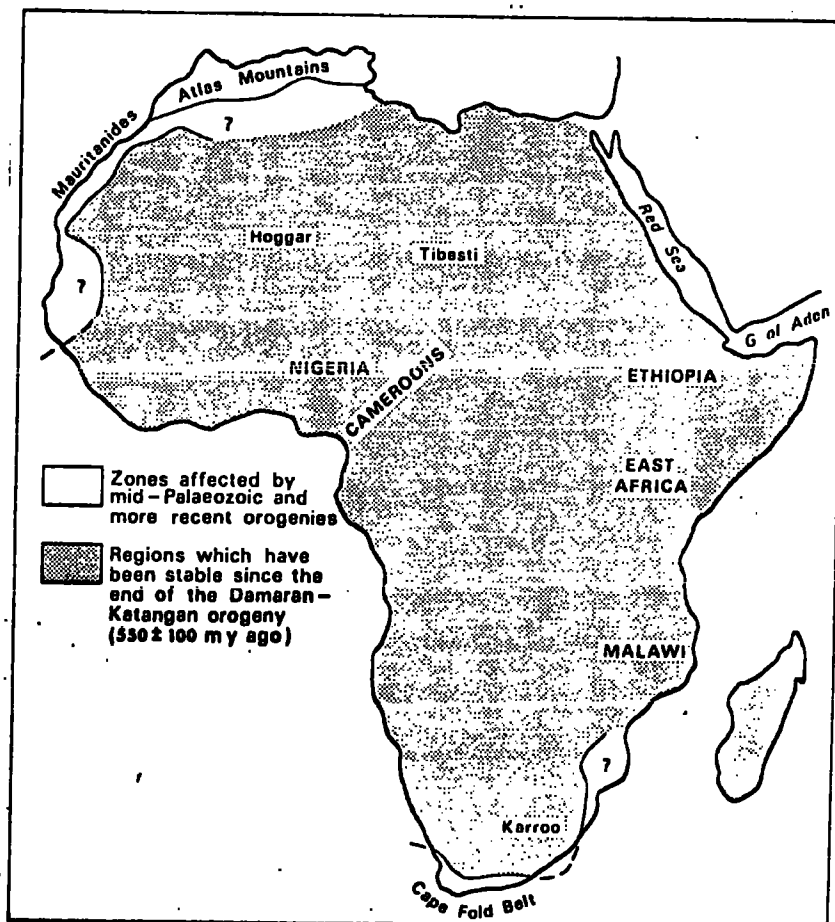
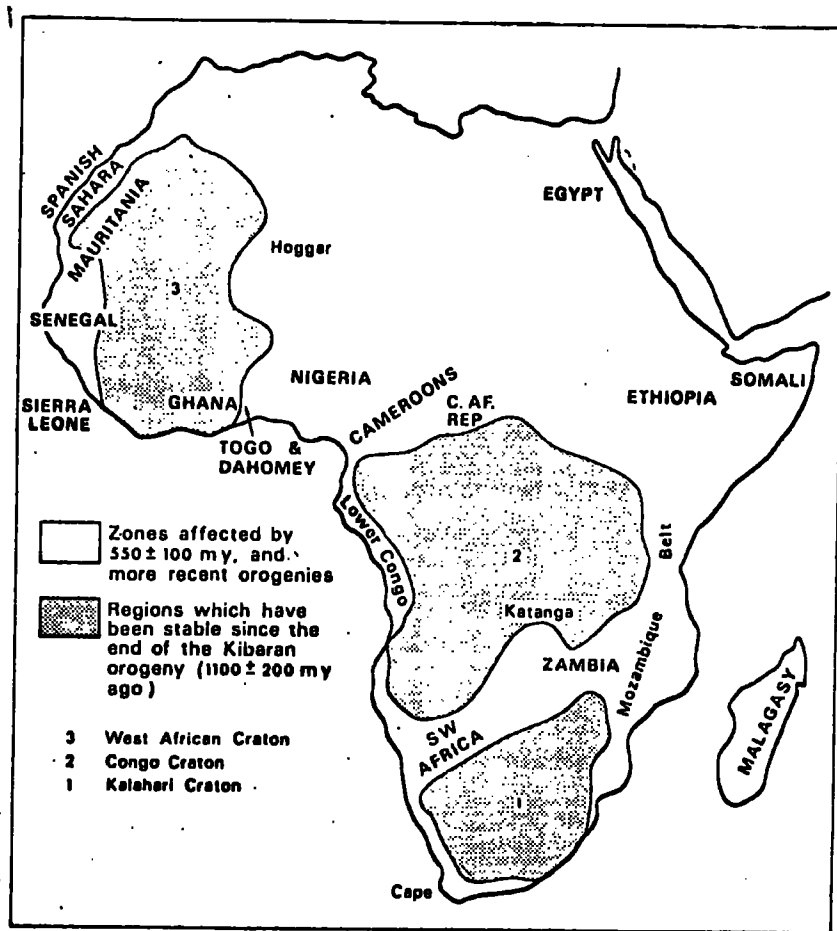
In contrast to these stable areas, a major part of Africa was affected by the 550  $\pm$  100 m.y. or Pan-African orogenesis (Clifford, 1970). In west Sierra Leone it is represented by a well defined orogenic belt extending across the country from south east to north west and into Guinea, where it disappears beneath horizontal sandstones ('grés horizontaux') that pass upwards into fossiliferous Slurian Shales (Rockel River Series - Allen, 1968; Clifford, 1970)

Fig.6-1(a). Regions which have remained stable since the end of the Kibaran Orogeny, distinguished from zones affected by the Pan-African and more recent Orogenies.

Fig.6-1(b). Regions which have been stable since the end of the Pan-African Orogenesis distinguished from zones affected by Hercynian and Alpine Orogenies.

(Modified after Clifford, 1970)





Extending along the western margin of the continent from Morocco to Senegal is an orogenic belt, similar to the marginal belt of Sierra Leone. Evidence for the Pan-African orogeny can be found, but the main fold movements were Hercynian (Sougy, 1962). This belt is known as the Mauritanide Zone (Fig. 6-1 (b)). In post-Hercynian times, westward downwarp of this belt occurred and resulted in the accumulation of Jurassic and Cretaceous sediments along the coastal region (Sougy, 1962).

The southern extension of this Hercynian fold belt shows divergent trends, one south through Guinea, the other west-southwest through Portuguese Guinea (Sougy, 1962). This latter trend falls along the southern flank of the Senegal (Mesozoic and Tertiary) basin (Fig. 6-2). Sheridan et al. (1969) suggested a south-west extension of the Mauritanides onto the continental shelf, south west of the Bijagos Archipelago, where the sediments are thinner than in the basin to the north, and a fault controlled basement arch separating the Senegal basin to the north from the sediments further south. The magnetic evidence does not support this idea (McMaster et al., 1970), a relatively quiet pattern characterising most of the area (Fig. 6-3). However, a relatively abrupt change in magnetic anomaly does occur near 11° North suggesting that the basement is higher, and that the westward deviation of the contour lines for the pre-Mesozoic surface (Sheridan et al., 1969 - Fig. 6-2) could reflect an upwarp in basement rocks along the southern boundary of the Senegal basin (McMaster et al.,

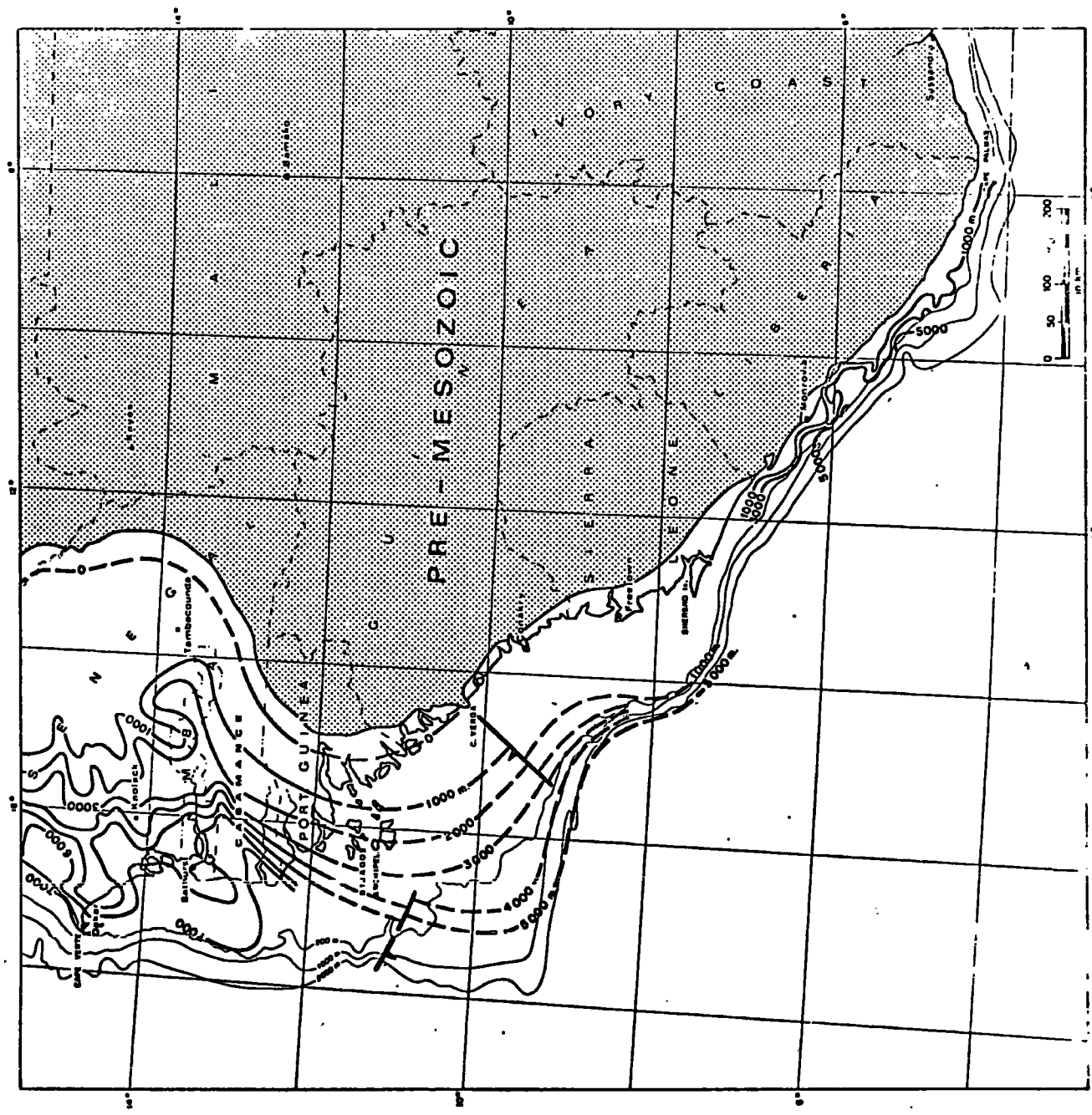
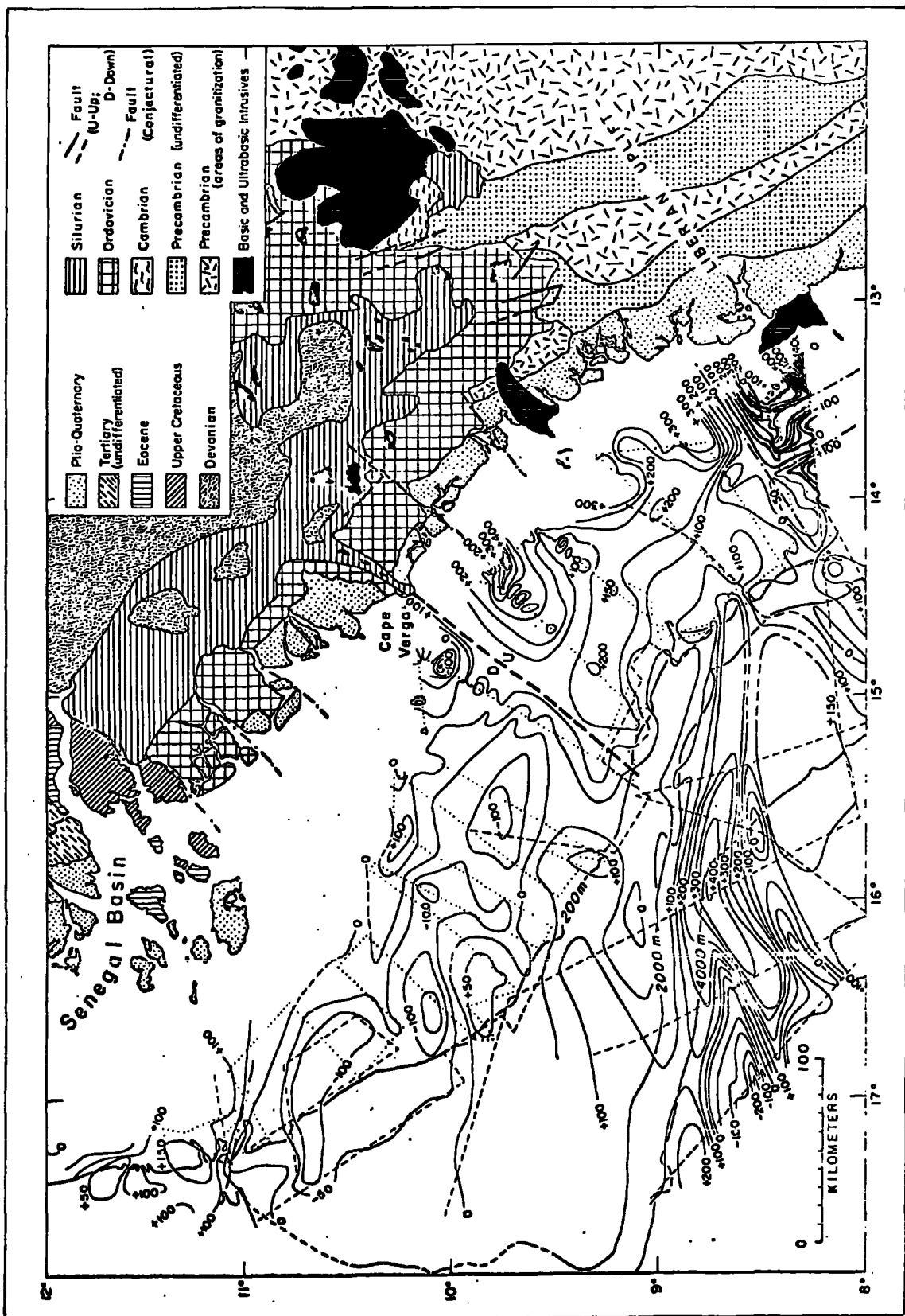


Fig. 6-2. Isobath, map of the Pre-Mesozoic surface between Cape Verde and Cape Palmas (After Templeton, 1971)

Fig.6-3. Total field magnetic anomalies. Contour interval 50 gamma . Dashed and dotted lines designate ship's tracks on different cruises. The geology is adapted from AAGS-UNESCO, 1973. (After McMaster et al., 1971)



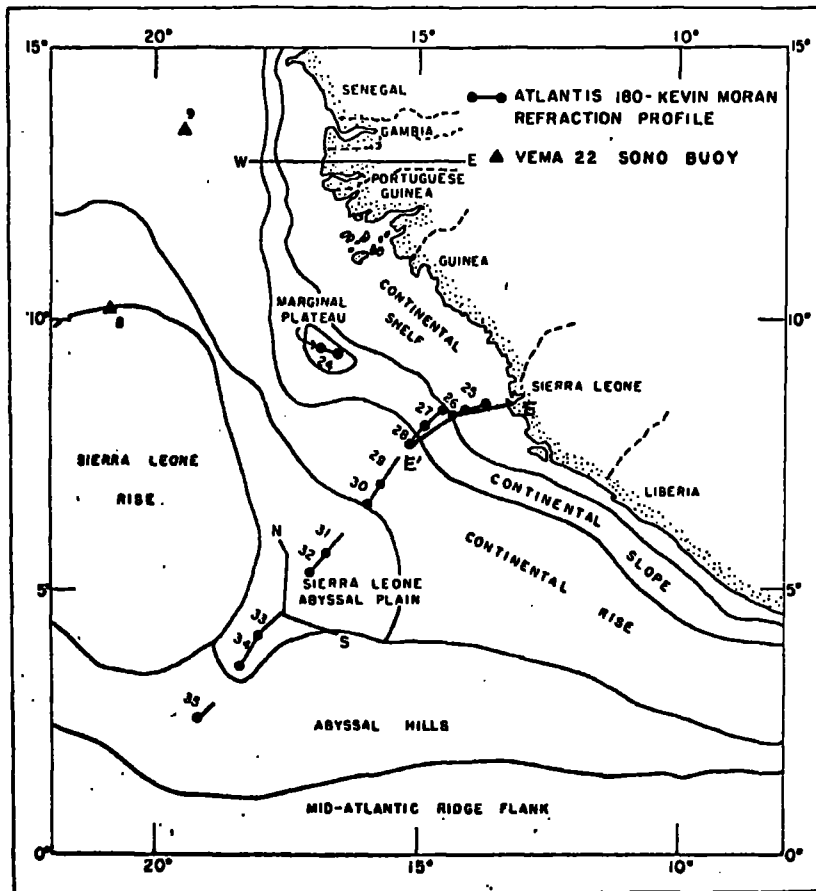


Fig.6-4a Location of seismic refraction profiles and major physiographic provinces. (after Sheridan et al., 1969)

1971).

6-1-2 The Senegal and Sierra Leone Embayments.

The continental shelf of Senegal has been studied in detail by geophysical methods (Aymé, 1965; Tenaille et al., 1960). It would appear that the Mesozoic and Tertiary basins of the Sierra Leone continental shelf and the Senegal and Mauritania shelf, were controlled by regional basement features, with the stable West African craton acting as a hingeline. The subsidence in Senegal may have started as early as Jurassic times, with a general transgression taking place during Albian and Aptian times and continuous subsidence and deposition occurring throughout the Cretaceous (Aymé, 1965).

At the termination of Cretaceous times the sequence is marked by thick Maestrichtian sands in Senegal, indicating the infilling of the basin. Overlying these sands are calcareous marly Tertiary deposits, which continue into Sierra Leone. The Cretaceous sequence is underlain by Paleozoic sediments of Cambrian to Devonian age (Aymé, 1965). These outcrop in Senegal where they consist of Cambrian sandstone followed by graptolitic Silurian shale and terminate in incomplete Devonian sandstone and shale. (Aymé, 1965).

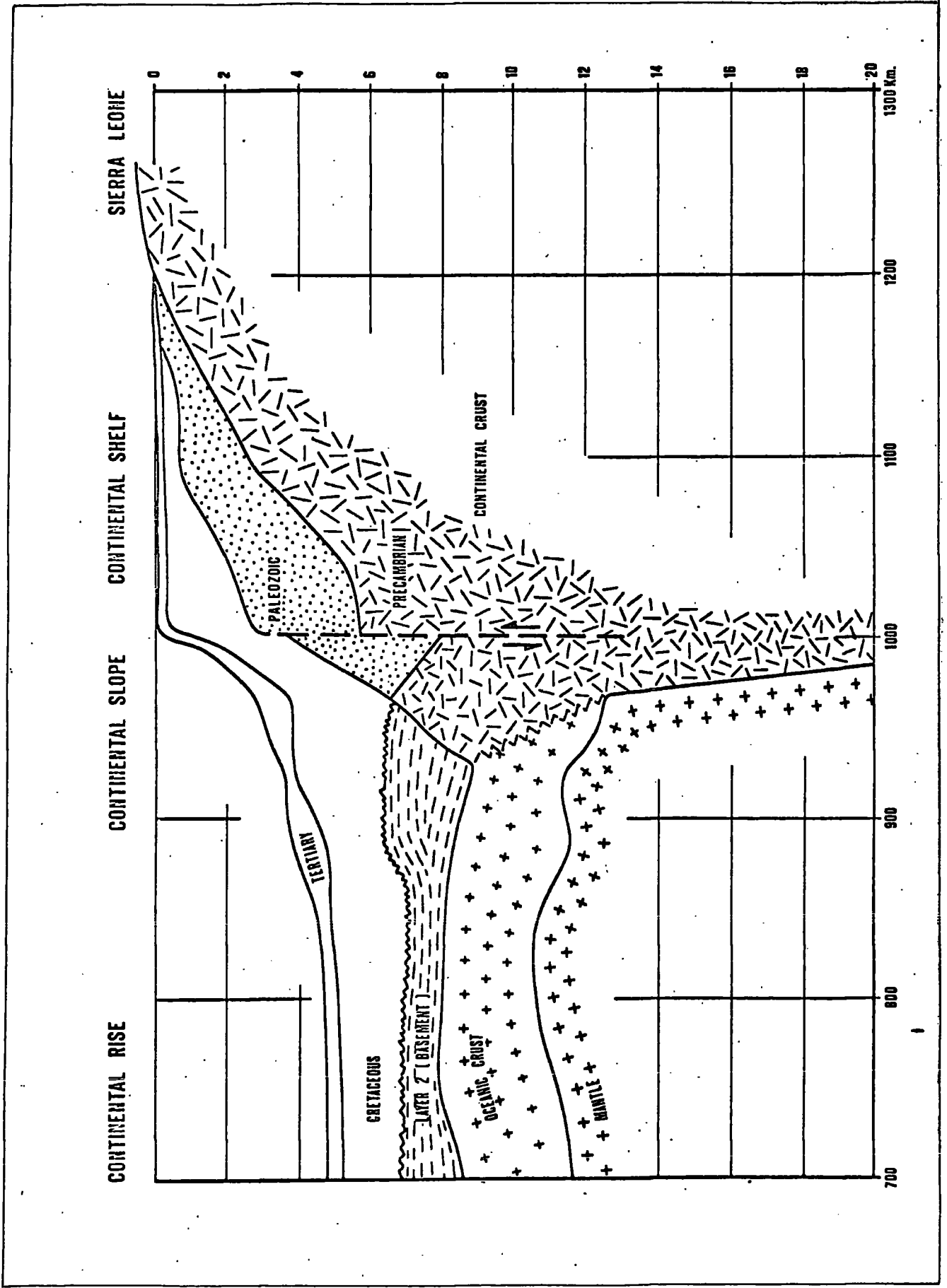
These beds on the Senegal shelf can be correlated with those found on the Sierra Leone shelf by Sheridan et al. (1969) as the result of a two-ship seismic refraction survey (Fig. 6-4)(a+b)

6-1-2-1 Seismic Refraction Results from the Sierra Leone Continental Shelf.

Four distinct layers were recognised on the grounds of velocity by Sheridan et al. (1969)

Fig. 6-4b Interpreted structural section based on refraction data off  
Sierra Leone. (After Sheridan et al., 1969)





1) The shallowest seismic velocity layer (1.6-1.9 km/sec.) was correlated with the Tertiary and Quaternary sediments exposed along the coast of Sierra Leone, Guinea, Portuguese Guinea and Senegal.

2) A 2.2 to 2.7 km/sec. semi consolidated layer correlated with the Cretaceous sediments found on the Senegal shelf.

3) A 5.2-5.4 km/sec. seismic velocity layer correlated with a seaward extension of the Cambrian-Devonian sediments exposed in Guinea.

4) A 6.1-6.5 km/sec. layer correlated with the crystalline pre-Cambrian rocks exposed near the coast of Sierra Leone.

#### 6-1-3 The Geology of Sierra Leone.

Sierra Leone is situated between the latitudes of 7° North and 10° North on the West African coast. The east of the country consists of a series of plateaux up to 6400 ft, while the west is a vast plain. With the exception of a coastal strip of sediments of Pleistocene to Recent age, the country is made up almost entirely of pre-Cambrian rocks, divided into two main geological units, corresponding to morphology (Fig. 6-5).

In the east of the country the Sula Mountains and Kangari, Kambui, Nimini and Gori Hills, consist of sedimentary and igneous rocks, metamorphosed in the granulite facies. These were once part of the old crust before granitisation and are known as the Kambui schists and Mano-Moa granulites. Their relationship to Dahomeyan (the oldest classification of rocks in the region) is unknown, but they are believed to be older than Birrimian (Haughton, 1963) and are surrounded by gran-

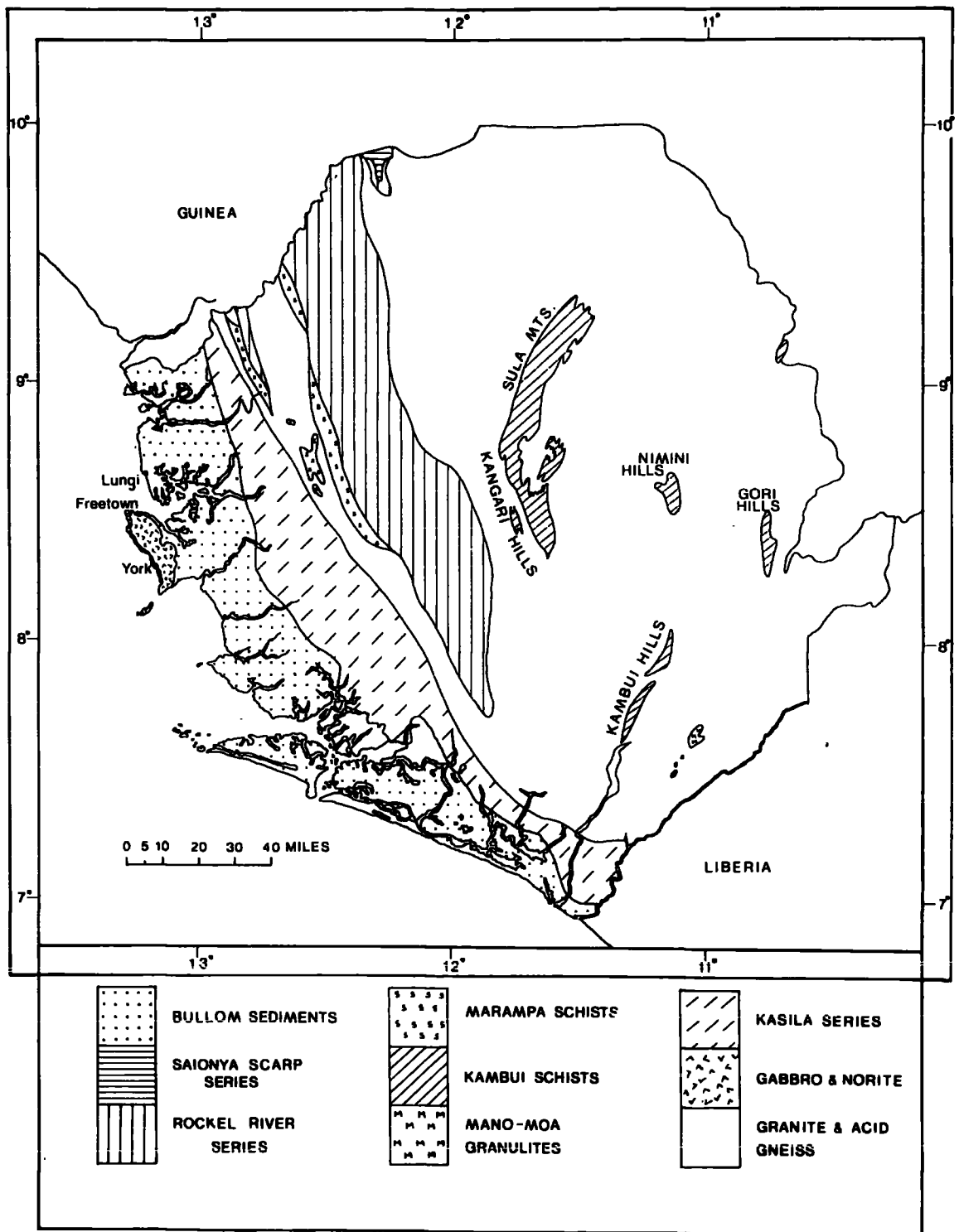


Fig.6-5. Geological Map of Sierra Leone.(After Sierra Leone Geological Survey)

-itic gneisses and granites, which have been intruded into them.

In the western plain area three main groups are distinguished. Firstly the Kasila series, a series of Dahomeyan crystalline schists and gneisses with some granulites, forming a belt some 20 miles wide, running almost parallel to the coast from Guinea through to Liberia. Secondly the Marampa schists, Birrimian metamorphic rocks of sedimentary origin, having subordinate ortho-schists and forming a narrow belt running south from the Guinea border for about 100 miles.

Finally there is a 20 mile wide belt of sedimentary rocks with intercalated lavas and ashes extending for about 140 miles south southeast from the Guinea border known as the Rockel River series. These lie unconformably on the granites and metamorphic rocks and are in turn overlain unconformably by the shales of the Siaonya Scarp series, which are of Silurian age. The Rockel River series has been studied in detail by Allen (1968) who concluded that towards the end of the pre-Cambrian a geosyncline formed at the margin of the West African craton in this area of Sierra Leone. The flat lying Siaonya Scarp series above indicates that deformation of the Rockel River series occurred before the Silurian.

The mountain range of the Freetown peninsula is formed by a layered basic intrusive, known as the Freetown Complex, which is intruded into the highly folded and metamorphosed basement rocks. In the east of the peninsula the contact between the intrusion and basement

is covered by a thin veneer of Pleistocene to Recent sediments, and it is similarly covered by a coastal strip in the west. The outcrop is crescentic in form (Fig. 6-5) indicating the extension of the intrusion under the Atlantic.

On the basis of the layering, Junner (1930) concluded that the complex was lopolithic and not a batholith as had been suggested by Dixey (1922). Junner (1930) also pointed out that, unlike the Bushveld and Sudbury Lopoliths, where the more basic rocks occur at the base of a layered series, with granitic rocks above, the Sierra Leone complex lacked this order, the variation of rock types occurring in cycles.

Wells (1962) studied the structure and petrology of the complex and showed that the layered series can be divided into four major zones in each of which there is a generalised upward sequence from Olivine rich to Plagioclase rich rocks, and within which prominent rhythmic layering can be recognised. Ideally the sequence is from Troctolite to anorthosite or Leucogabbro.

Baker and Bott (1961) carried out a land gravity survey of the Freetown peninsula which confirmed saucer or funnel-shaped space form for the intrusion, with an inward contact dip of 20-30 degrees, centered 8-12 miles W.S.W. of York.

## 6-2 Reduction and Interpretation

### 6-2-1. Introduction

Between the 25th February 1969 and the 21st March 1969 a bathymetric survey of the outer approaches of

Sierra Leone was carried out by H.M.S. Hydra. During this period 11 days were allocated to measurement of the gravitational field. The area of the Sierra Leone continental shelf covered was from the 20 fathom line to the 100 fathom line between latitudes  $8^{\circ} 10'$  North and  $8^{\circ} 55'$  North (Fig. 6-6). East-west lines were run at 5 mile intervals and interlined at  $2\frac{1}{2}$  miles in areas of likely interest. Two north-south cross lines were also run.

Measurements of the gravity field were made with an Askania Seagravimeter mounted on an Anschutz gyro-stable table. The meter was run in the manual mode to obtain the maximum possible accuracy over steep gravity gradients. A cross-coupling computer was not used.

#### 6-2-2 Navigation

Navigational fixes throughout the survey were obtained using Decca Lambda, with stations at Barlo and Shenge on the coast of Sierra Leone (Fig 6-6) opposite the north and south limits of the survey respectively. Both sites were adjacent to trigonometrical stations of Sierra Leone.

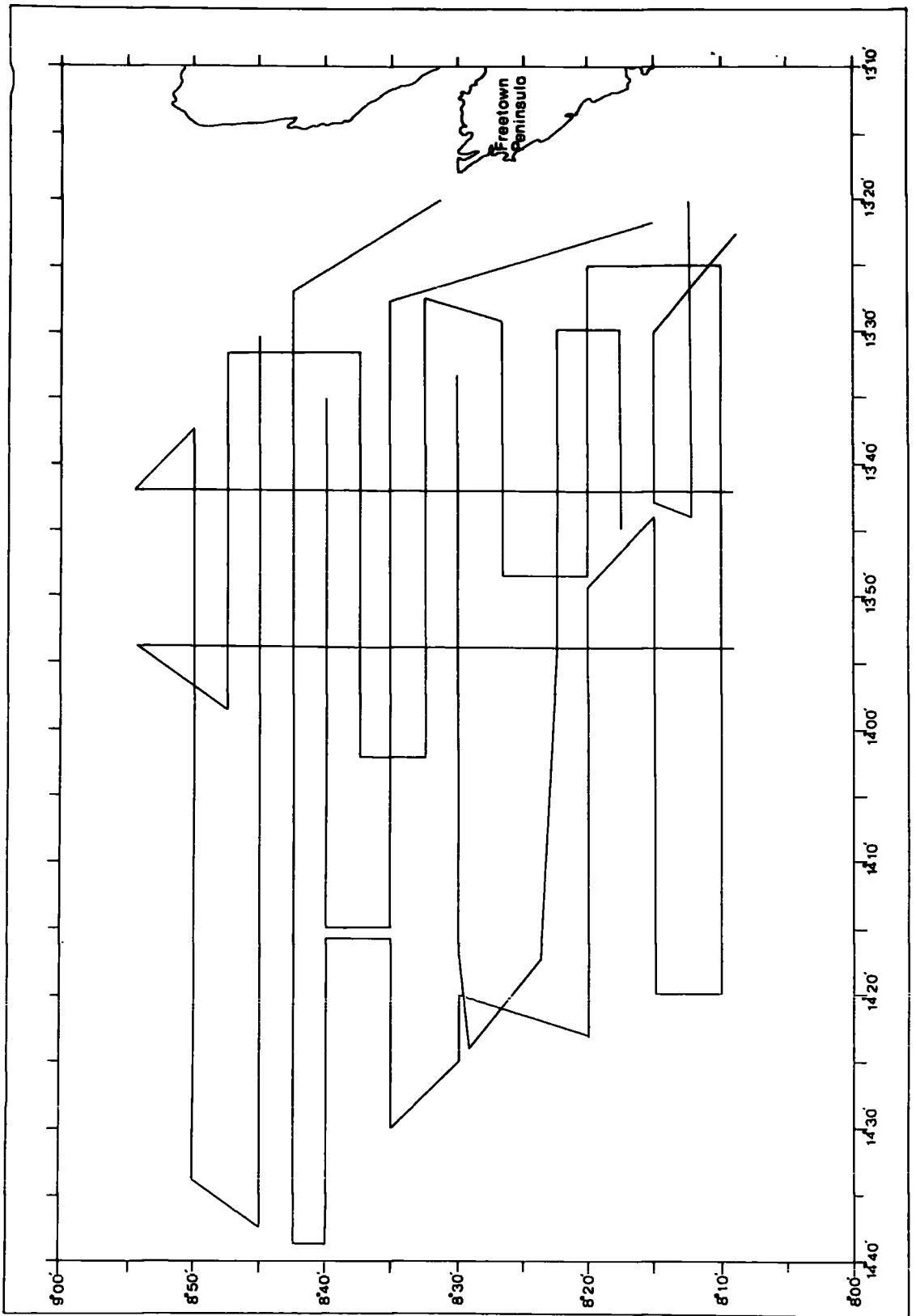
#### 6-2-3 Base Station

The survey was carried out in a single leg and was tied into a base station at Kissy Jetty

$$g = 978.21875 \text{ gals.}$$

this value having been established relative to the station at Lungi airport occupied by Harding (Woollard et al., 1952) during the establishment of the International Gravity Network. The land ties established the drift rate to be 0.2 mgal/day. This was corrected for and the free-air

Fig. 6-6. Trackline diagram of the gravity survey of the Sierra Leone continental margin carried out by H.M.S. HYDRA during 1969.





anomalies computed in the usual way using the International Gravity Formula.

#### 6-2-4 Errors.

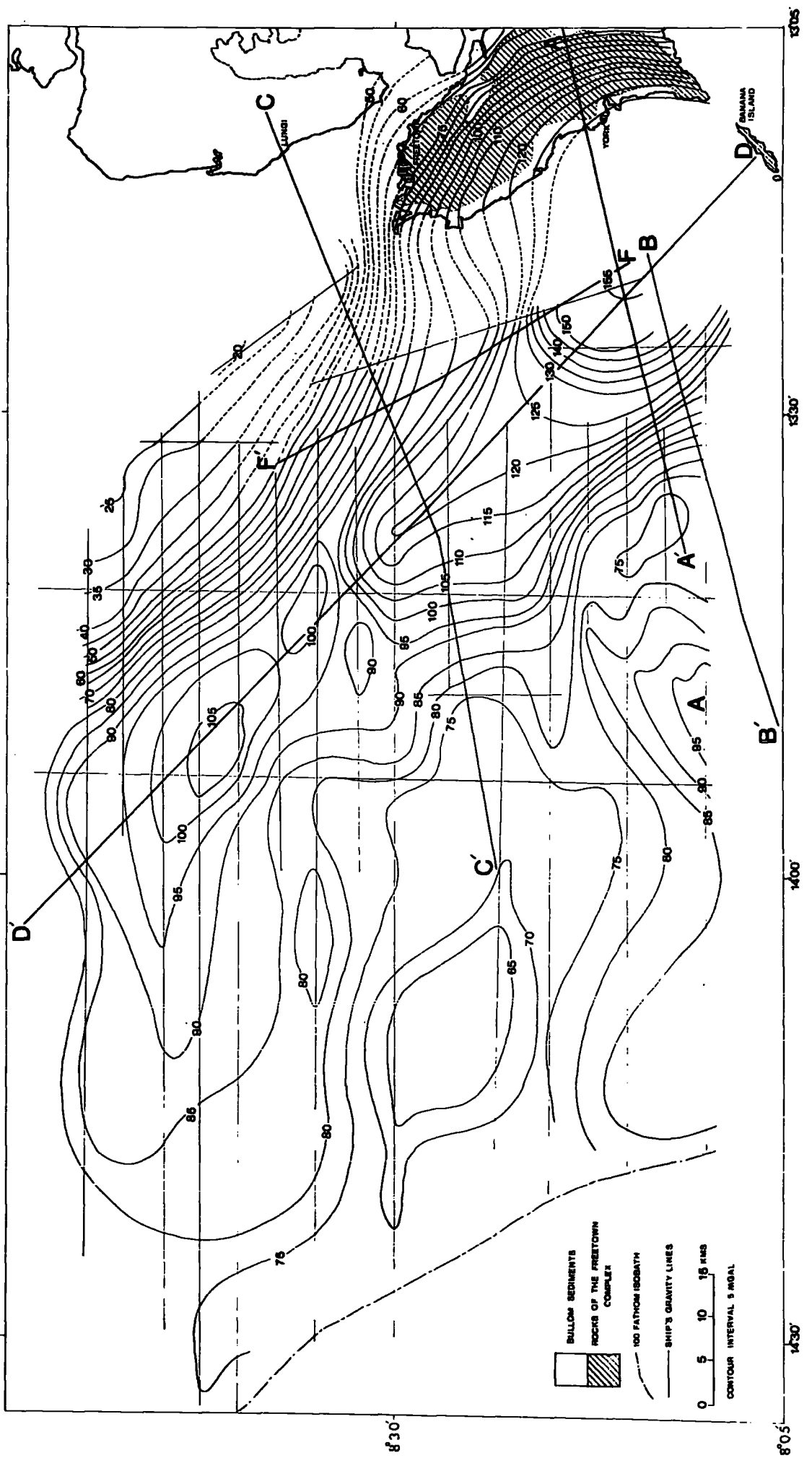
Examination of crossovers shows a mean crossover error of 2.54 mgal with a standard deviation of 2.01 mgal from this mean. The main source of error is attributed to errors in the north-south lines, where the technique of making many small course changes to maintain a constant track on the Lambda Plotter was employed. A bias was given to the east-west readings where discrepancies occurred.

#### 6-2-5 The Bouguer Anomaly Map.

The Bouguer anomaly map was produced using a density of 2.75 gm/cc; the density of the crystalline pre-Cambrian basement rocks which underlie the region. This value is the same as that taken by Baker and Bott (1961) in reducing their land survey, of the Freetown Peninsula, and is arrived at from a consideration of density measurements made by the Geological Survey of Sierra Leone. The corrections were applied using the infinite slab formula (e.g. Nettleton, 1940). This method was considered sufficiently accurate in view of the relatively featureless bathymetry.

The gravity high seen in the east of the Bouguer anomaly map (Fig. 6-7) is associated with the seaward extension of the Freetown Complex. It is apparent that the intrusion is elliptical in plan, with its major axis striking along a N.W. - S.E. line passing through Banana Island, rather than circular as might be expected from the results of the land gravity survey (Baker and Bott, 1961). The maximum observed Bouguer anomaly is 157 mgal

Fig. 6-7. Bouguer anomaly map of the Sierra Leone Continental Shelf.



BULLWOUND SEDIMENTS  
 ROCKS OF THE FREETOWN COMPLEX  
 100 FATHOM ISOBATH  
 SHIP'S GRAVITY LINES  
 0 5 10 15 NMS  
 CONTOUR INTERVAL 5 MGAL

8°05' 8°30' 13°30' 14°00'

at a point 12 miles W.S.W. of York. From a consideration of the gravity gradient it appears most unlikely that the actual maximum Bouguer anomaly is greater than 5 mgal above this.

The other striking feature of the map is the Bouguer anomaly low, paralleling the high on its landward side. Here the minimum observed Bouguer anomaly is 18 mgal. but it is impossible to predict what the actual minimum anomaly will be.

6-2-6 Additional Data.

The main objective of the marine survey was a detailed bathymetric study to ensure safe approach to Freetown for deep draught shipping. This resulted in areas of great interest, from the point of view of the gravitational field being left unsurveyed (Fig. 6-7) and the scope of the interpretation of the geological structure of the shelf was consequently reduced. This deficiency was overcome to some extent by gathering data from other sources:

1) A land gravity survey, carried out by Baker and Bott in 1961, of the Freetown peninsula.

2) A marine gravity traverse over the continental margin of Sierra Leone, carried out for the U.S. Department of Commerce by the U.S.G. & G.S.S. DISCOVERER.

3) A seismic reflection and magnetic survey of the Sierra Leone shelf carried out by McMaster et al. (1970).

4) A seismic refraction survey of the Sierra Leone shelf by Sheridan et al. (1969)

5) Three magnetic profiles obtained by the Royal Navy on the Sierra Leone shelf (H.M.S. Hecla, 1966).

TABLE 2-1.

SAMPLE DENSITY MEASUREMENTS		
Class and Nature of Rock	Locality	Density g./cm. <sup>3</sup>
<i>Surface Weathered Deposits</i>		
Bauxite . . . . .	near Songo	2.21
Ferruginous laterite . . . . .	Samueltown grid (surface)	2.58
Sedimentary laterite . . . . .	" " "	2.45
<i>Sediments (Bullom Series)</i>		
Black clay . . . . .	Samueltown grid (borehole)	1.71
<i>Metamorphic Rocks (?Kasila System)</i>		
Granodiorite-gneiss . . . . .	" " "	2.82
Plagioclase-hornblende-gneiss . . . . .	" " "	2.93
Amphibolite (average of four specimens) . . . . .	Rokell grid (boreholes)	3.01
<i>Freetown Basic Complex</i>		
Gabbro (marginal) . . . . .	Samueltown grid (surface)	2.87
		3.03
Hornblende-gabbro (average of five specimens) . . . . .	Samueltown and Rokell grids (boreholes)	3.08
Troctolitic gabbro . . . . .	Hastings	3.13
Troctolite (average of four specimens) . . . . .	?	3.16*
Olivine-gabbro (average of three specimens) . . . . .	?	3.16*
Norite (average of four specimens) . . . . .	?	3.01*
Anorthosite . . . . .	?	2.72*
<i>Ijolite</i> . . . . .	near Songo	3.05

\* Densities according to Junner (1930); all other densities measured by Geological Survey, Sierra Leone.

(After Baker and Bott, 1961)

TABLE 2-2.

Nature of Rock	<sup>+</sup> P-Wave Velocity (km/sec)	Density (gm/cc)
Tertiary-Quaternary Sediments	1.49-1.51	1.80
Cretaceous Sediments	2.26-2.67	2.20
Cambrian-Devonian Sediments	5.14-5.41	2.60
Pre-Cambrian Crystalline Rocks	6.16-6.59	2.75-2.80
Freetown Complex		
Main Complex	-	3.05-3.15
Anorthosite	-	2.72

<sup>+</sup>P-Wave velocities after Sheridan et al., 1969.

## 6-2-7 Densities

The densities used for the interpretations were arrived at by a consideration of measurements made by the Geological Survey of Sierra Leone and measured P - wave velocities (Sheridan et al., 1969) using velocity density relationships (Appendix 3). Details of measurements of densities made are shown at Table (6-1) and the densities used at Table (6-2).

## 6-2-8 Interpretation

### 6-2-8-1 Profile A-A'

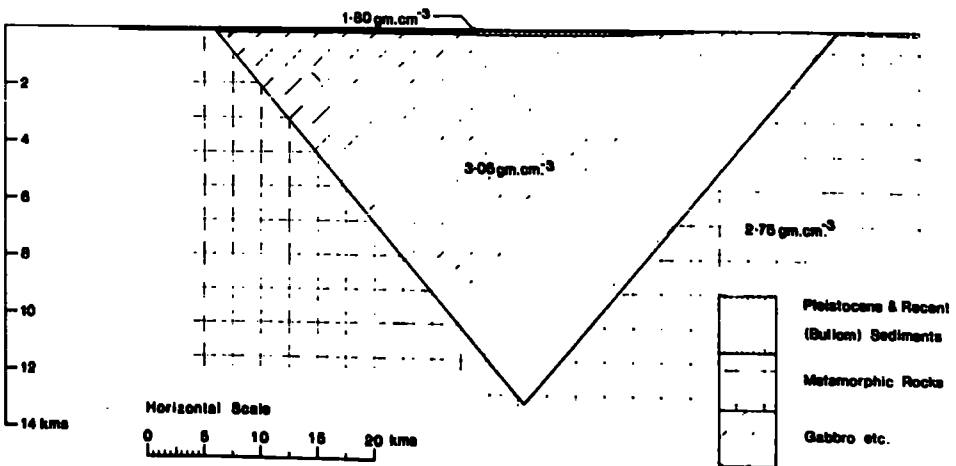
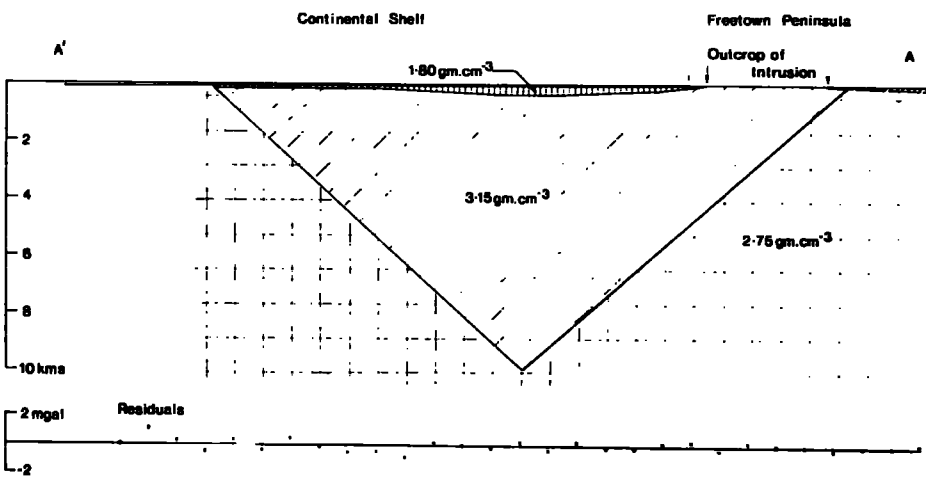
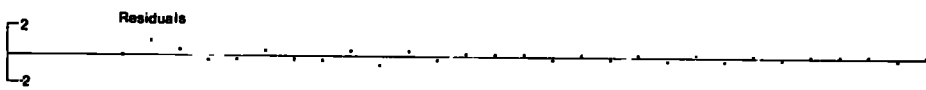
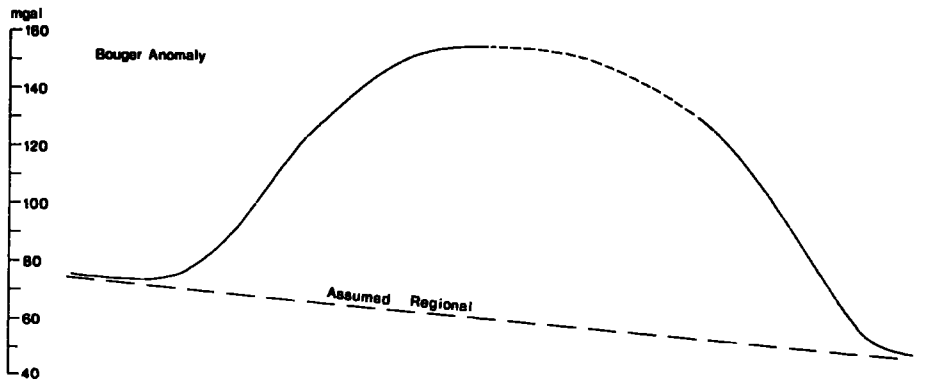
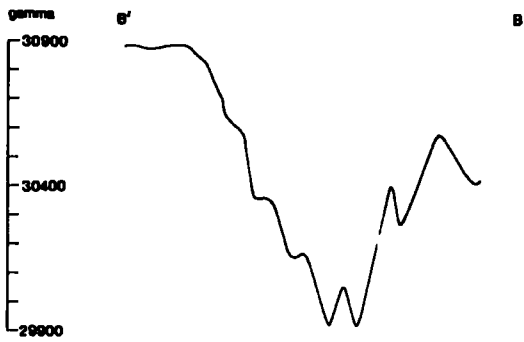
This profile extends roughly east-west from the Freetown peninsula onto the Sierra Leone continental shelf (Fig. 6-7). It includes the data from the land gravity survey, (Baker and Bott, 1961)

The Bouguer anomaly shows a steep increase westwards from its value of 50 mgal in the east of the Freetown peninsula, to 130 mgal at the coast. There is then a gap in the data, but the trends of the data available indicate that this steep increase continues to about 150 mgals, followed by a broad low gradient increase to the maximum observed value of 157 mgal. West of this maximum the anomaly shows a low gradient decrease to 150 mgals before falling off rapidly to 70 mgal in the far west of the profile (Fig. 6-8(b)). The background anomaly over the shelf is difficult to estimate as the major part of the field due to the intrusion covers most of the map. A linear increase in regional field from 55mgal in the east of the Freetown peninsula to 70 mgal on the shelf has been assumed.

Fig. 6-8. Interpretation of Bouguer anomaly profile A-A'.

Two-dimensional structures have been assumed.

The relative lowering of the Bouguer anomaly over the centre of the intrusion has been interpreted in terms of top surface topography.





A magnetic traverse (B-B' - Fig. 6-7) run by H.M.S. Hecla (1966) close to profile A-A' indicates that the top surface of the intrusion is close to the sea bed throughout its length. Intensive bottom sampling west of 13° 30' West showed no surface outcrop of crystalline rock.

As a first assumption, the intrusion was taken to have a sloping top surface 10 metres beneath the sea bed. The program GRAVIT. 1 was then used to determine the bottom surface of the intrusion assuming its density to be 1) 3.05 gm/cc. 2) 3.15 gm/cc.

Although the program reproduced the observed Bouguer anomaly accurately, the 'flattened top' nature of the anomaly resulted in the unidensity models being geologically unacceptable. The two models showed a linear increase in thickness with distance towards centre, associated with the steep sides of the anomaly, but these steep sides resulted in the low gradient central region of the anomaly having to be produced by a shallowing of the bottom surface under the centre of the intrusion.

To produce a geologically more acceptable model the linear sides of the computed models were extrapolated to an apex. The gravity anomalies due to these models were computed using GRAVN (Bott, 1969). As expected, the computed gravity showed excellent agreement with the observed over the steep limbs of the anomaly (residuals less than 1 mgal), but large residuals over the central region.

Assuming this basic space form to be correct, two possible explanations exist for the flattened top nature of the anomaly.

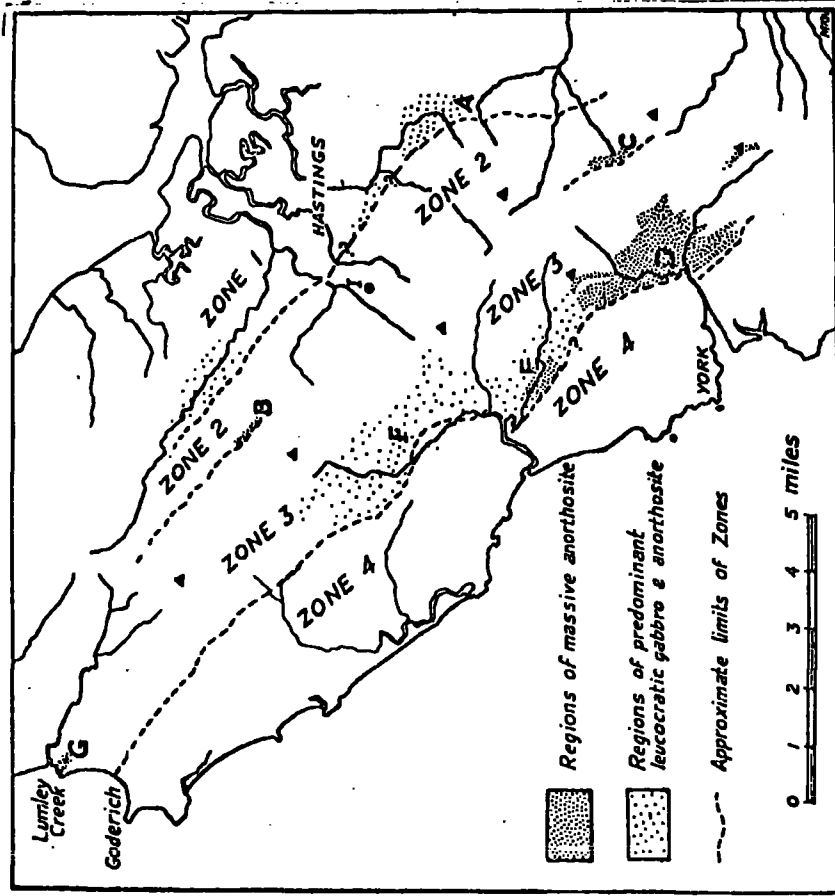
1. Top Surface Relief

The anomaly can be explained by a central sag in the roof of the intrusion accompanied by a thickening of the Pleistocene to Recent sediments. Assuming 'roof sag' the program GRAVIT 1 was used to compute the necessary top surface topography of the intrusion, to produce a good cover-all fit to the observed Bouguer anomaly. Density contrasts between the Bullom sediments and the two specified intrusion densities were used. The results are shown at Fig. (6-8 (c)).

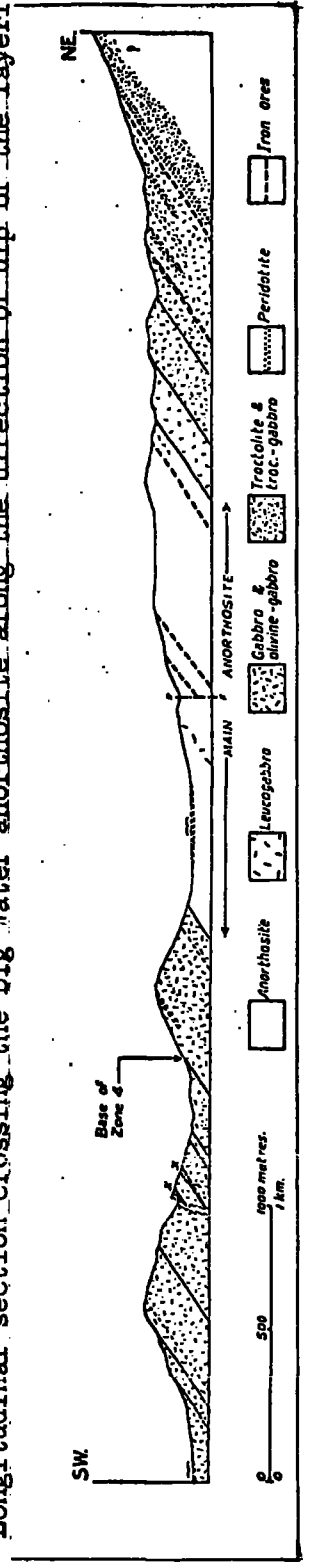
It is impossible to estimate the strike length of the intrusion south of Banana Island, but should the intrusion be found to terminate in the region of the island, the depths shown in Fig. (6-8 (c)) will be underestimates.

It appears from the models that the landward and seaward contact dips are very similar,  $20^{\circ}$  for an intrusion of density 3.15 gm/cc. and  $26^{\circ}$  for 3.05 gm/cc. These values are in good agreement with the dips of the intrusion banding observed on land ( $25^{\circ} - 30^{\circ}$ ) (Wells, 1962). However, variations of density that are known to occur within the intrusion (Table 6-1) and the uncertainty about its true top surface make it impossible to determine with absolute certainty, whether its form is saucer shaped (i.e. a lopolith) or funnel shaped. Modification of the models may be necessary when the

Fig. 6-9.  
 Distribution of the main  
 surveyed anorthositic bodies  
 of the Freetown Complex.



Longitudinal section crossing the Big Water anorthosite along the direction of dip of the layering.



(After Wells and  
 Baker, 1956)

true top surface is determined from seismic evidence.

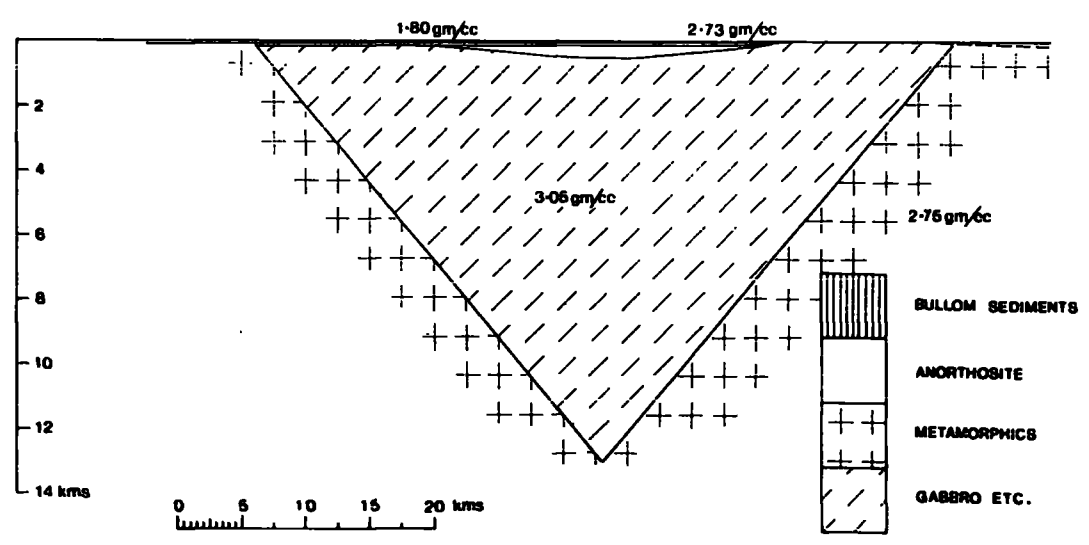
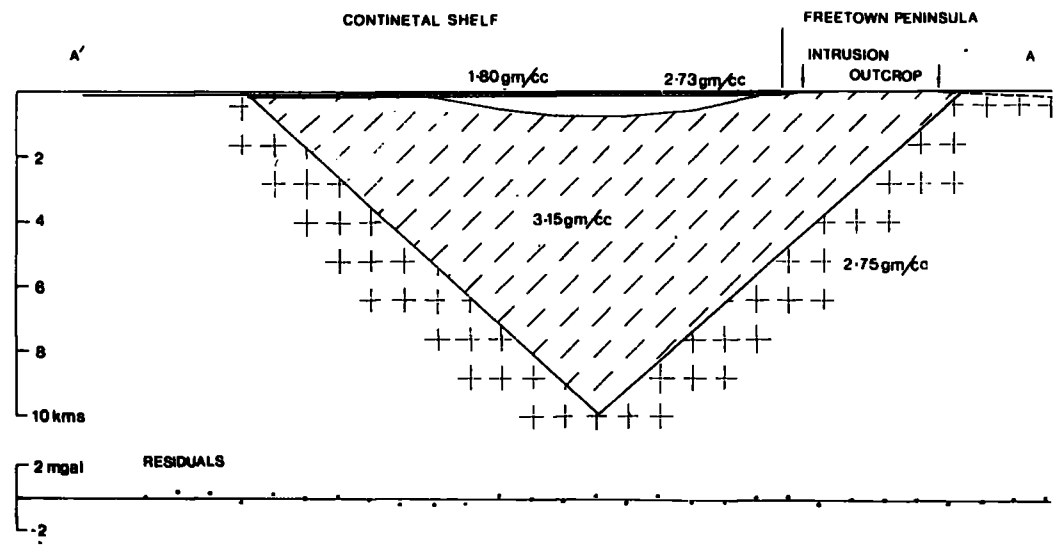
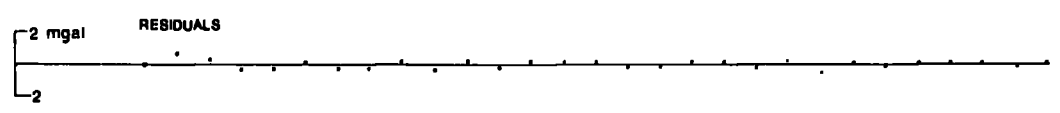
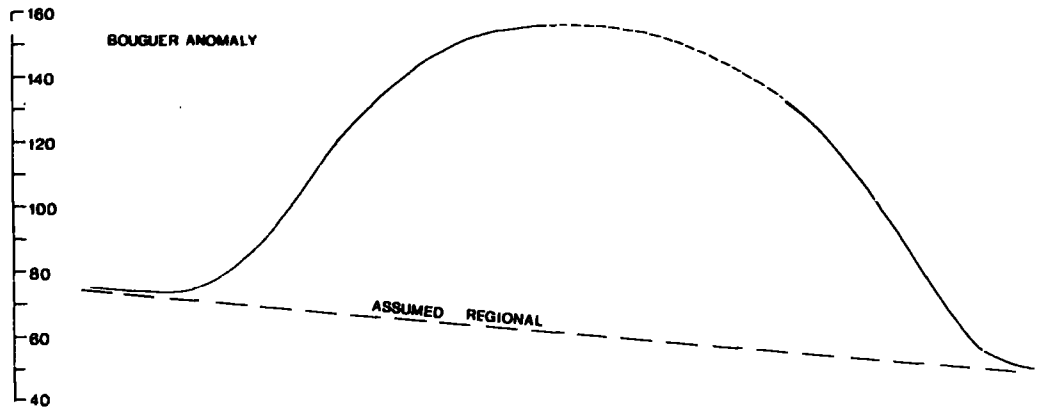
## 2. Density Variations within the Intrusion

As stated earlier, Wells (1962) showed that the layered series of the intrusion can be divided into four major zones in each of which there is generalised upward sequence, ideally from tracholite to anorthosite or leucogabbro (Fig. 6-9). It seems likely from the work of Wells and Baker (1956) and Wells (1962) that each zone represents a separate influx of magma, and that differentiation occurred within each zone, producing the rhythmically layered units. Thus we might expect to find an area of anorthosite, associated with zone 4 (Fig. 6-9) under the centre of the anomaly.

Measurements by Junner (1930) give a density of 2.72 gm/cc. for the anorthosite of the intrusion and Baker and Bott (1961) noted a relative lowering of the Bouguer anomaly over the anorthosite belt of the York pass area.

Using the density for anorthosite given by Junner (1930) and assuming a flat top surface for the intrusion, the shape of the anorthosite mass required to produce the relative lowering of the Bouguer anomaly was computed using the program GRAVIT 1. The models produced are shown at Fig. (6-10). A saucer shaped mass of anorthosite is required with a maximum thickness of 530 metres (intrusion density = 3.05 gm/cc.) or 920 metres (3.15 gm/cc.). This is not unreasonable as the Big Water anorthosite mass has a thickness of the order of 800 metres (Wells and Baker, 1956). As before uncertainties about the body's top surface and strike length may

Fig.6-10. Interpretation of Bouguer anomaly profile A-A'.  
Two-dimensional structures have been assumed.  
The relative lowering of the Bouguer anomaly  
over the centre of the intrusion has been interpreted  
in terms of an anorthosite body.



necessitate modification of the model when more seismic data is available.

6-2-8-2. Profile C-C'

Profile C-C' extends roughly south-west from the coast of Sierra Leone at Lungi and crosses the main gravity high associated with the extension of the Freetown Complex under the Atlantic. (Fig. 6-7).

The Bouguer anomaly decreases seaward from its value at Lungi (43.5 mgal) and although there is a gap in the data, examination of the gradient of the anomaly further west indicates that the anomaly falls to around 20 mgal before rising again to 110 mgal over the extension of the intrusion.

The western section of the profile coincides with two seismic refraction lines shot by Sheridan et al. (1969). In the absence of further information the top surface of the intrusion is assumed to coincide with the high velocity (6.1 km/sec. -- metamorphic rock) layer onset, which underlies the region, as no other sufficiently high velocity layer has been detected above this.

Seismic reflection profiling, coinciding with the eastern section of C-C' was undertaken by the University of Rhode Island (McMaster et al., 1970) and shows crystalline rock at a depth of 300 - 500 metres for about 11 km; along the length of C-C' adjacent to the Freetown peninsula, where the intrusion outcrops (Fig. 6-11 (a)). A steep fall in the seismic basement <sup>to the west</sup> is indicated by its sudden loss as a reflecting horizon.

This coincides with a high amplitude, high gradient magnetic anomaly (Fig 6-3) (McMaster et al., 1970) indicating the highly magnetic nature of the seismic basement. For this reason the seismic basement is taken to be the top surface of the intrusion, in the east of C-C'.

The seismic refraction work (Sheridan et al., 1969) also shows that the Cambrian - Devonian and Cretaceous sediments thicken westwards along C-C'. As these would tend to mask the gravity anomaly due to the intrusion, their gravity effect and the gravity effect of the overlying Tertiary - Quaternary sediments are computed and removed from the observed Bouguer anomaly using GRAVN (Bott, 1969). Sediments thicknesses were taken from Sheridan et al. (1969) and the densities were estimated from P-wave velocities (Table 6-2).

The eastern section of C-C' crosses the N.W. - S.E. striking gravity low. As has been mentioned, the area surveyed does not include the minimum of this low, but this is partially compensated for by choosing the profile to pass through Lungi where the Bouguer anomaly is known (Woollard et al., 1952). In this way an estimate of the magnitude of the low can be made.

The low is attributed to a sedimentary basin of Cretaceous or Tertiary - Quaternary age.

The determination of the space form of the intrusion and adjacent sedimentary basin was carried out using the horizontal variable density program VARYIT as the two anomalies interfere. The top surface of the intrusion





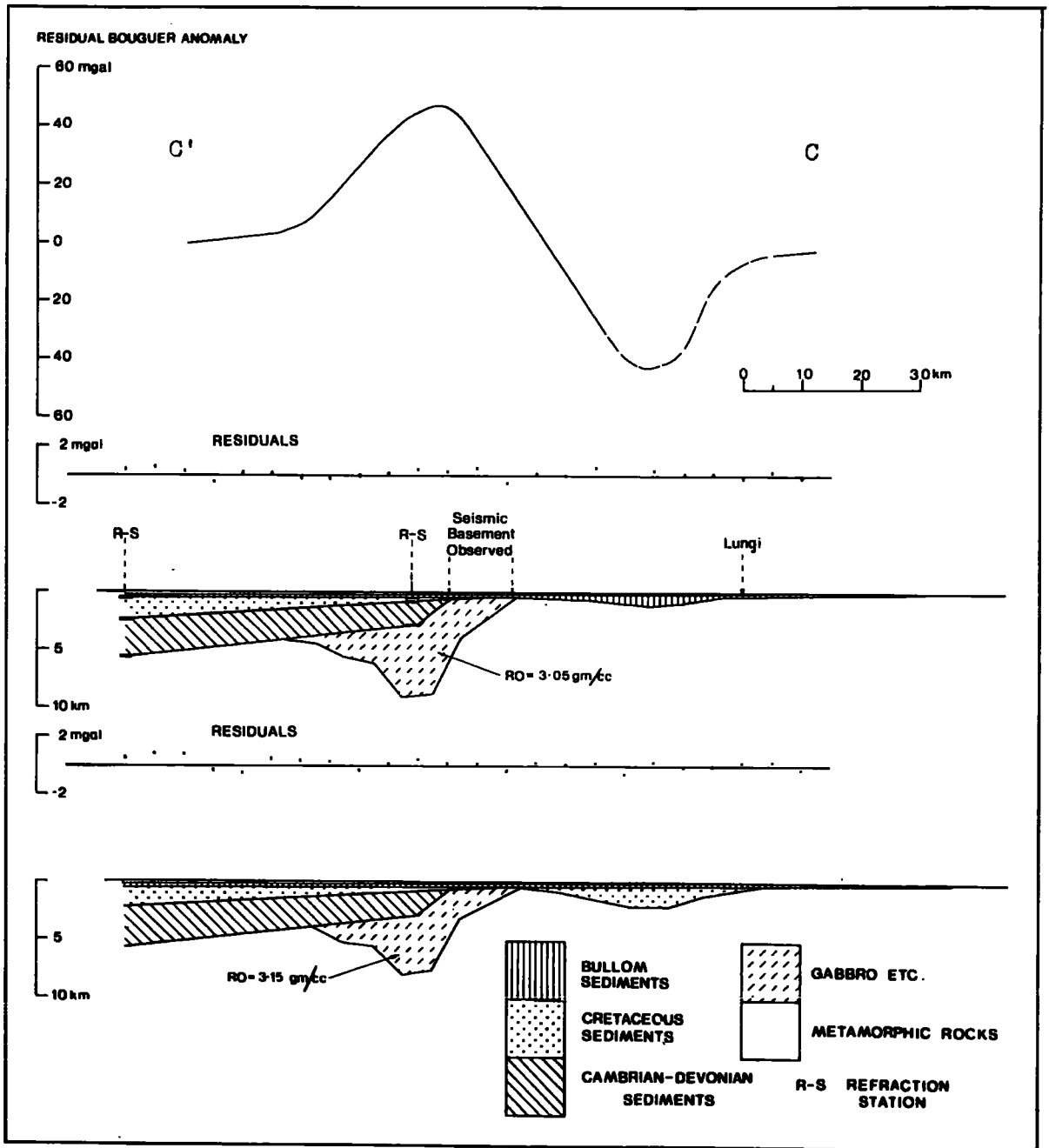


Fig.6-11. Interpretation of Bouguer anomaly profile C-C'. Two-dimensional structures have been assumed.

was estimated from the seismic data discussed and the top surface of the basin from this data and the known extent of the Tertiary - Quaternary sediments on land. As in the previous example densities of 3.05 gm/cc. and 3.15 gm/cc. for the intrusion were considered. The basin was assumed to be formed of either Cretaceous (2.20 gm/cc.) or Tertiary - Quaternary (1.80 gm/cc.) sediments. The models are shown at Fig. (6.11 (b)).

As shown, the intrusion in this region has a splayed top, there being an increase in slope of contact with depth. Both models have a maximum depth less than that computed from profile A-A', indicating, as would be expected, that the centre of the body is approximately under A-A'.

It is impossible, on the available evidence, to rule out either model for the coastal sedimentary basin. Thicknesses of 2 km. of Cretaceous sediments and 1.2 km. of Tertiary-Quaternary sediments are necessary to satisfy the extrapolated Bouguer anomaly low. The Tertiary - Quaternary (Bullom) sediments that form a strip along the coast of Sierra Leone are known to increase in thickness towards the coast in the region around Lungi (Pollett, 1951), but there is no evidence for Cretaceous or older sediments underlying these on the mainland.

As mentioned previously a probable basement rise separates the Senegal and Sierra Leone continental shelf embayments. Extensive geophysical and drilling work

north of this rise reveals up to 3800 metres of Tertiary limestone and more in the area of the Senegal salt dome arc (Aymé, 1965) and there may be a similar accumulation south of the rise on the Guinea and Sierra Leone continental shelves.

However, many areas of the shelf of West Africa also experienced basement downwarp and an accompanying infilling of sediments during Cretaceous times, including the continental shelf of Sierra Leone west of this area. Seismic evidence will be necessary to resolve this problem.

6-2-8-3 Profile F-F'

This profile extends northwards from the centre of the Bouguer anomaly along the line of a magnetic traverse run by H.M.S. Hecla in 1966 (Fig. 6-7). The gravity profile shows a steep decrease from 150 mgal to 100 mgal, followed by a shallow gradient decrease to 70 mgal, then a further steep decrease to 20 mgal over the sedimentary basin discussed in the previous section. The profile crosses the seismic reflection line of McMaster et al. (1970) previously described, and the depth to the top of the intrusion is taken to be 400 metres in the north of the profile from this reflection data. The top surface under the maximum anomaly in the south of the profile, is taken from that found from the analysis of profile A-A', assuming top surface topography to explain the relative lowering of the Bouguer anomaly in this region. The program GRAVIT 1 was then used to determine the bottom surface of the intrusion assuming densities of 3.05 gm/cc and 3.15 gm/cc.

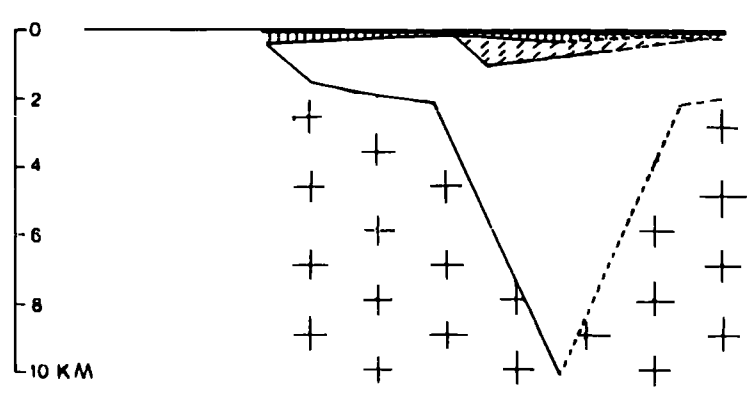
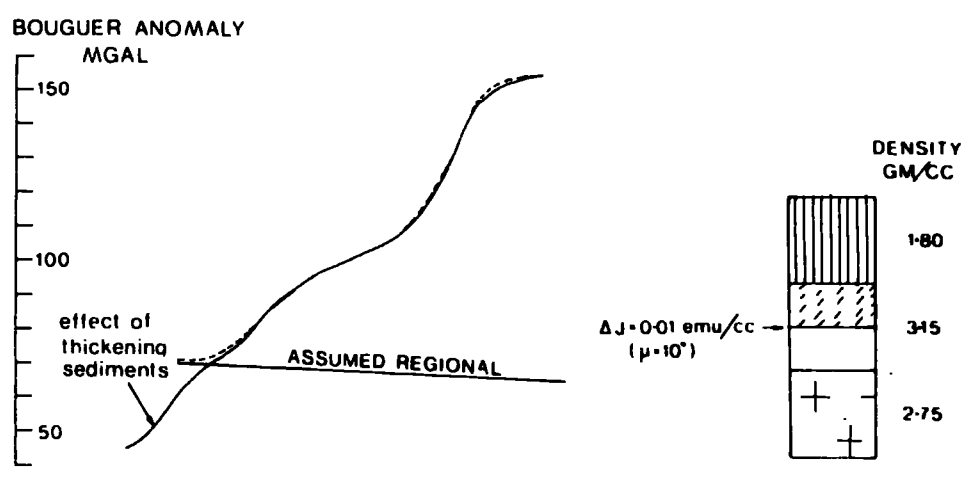
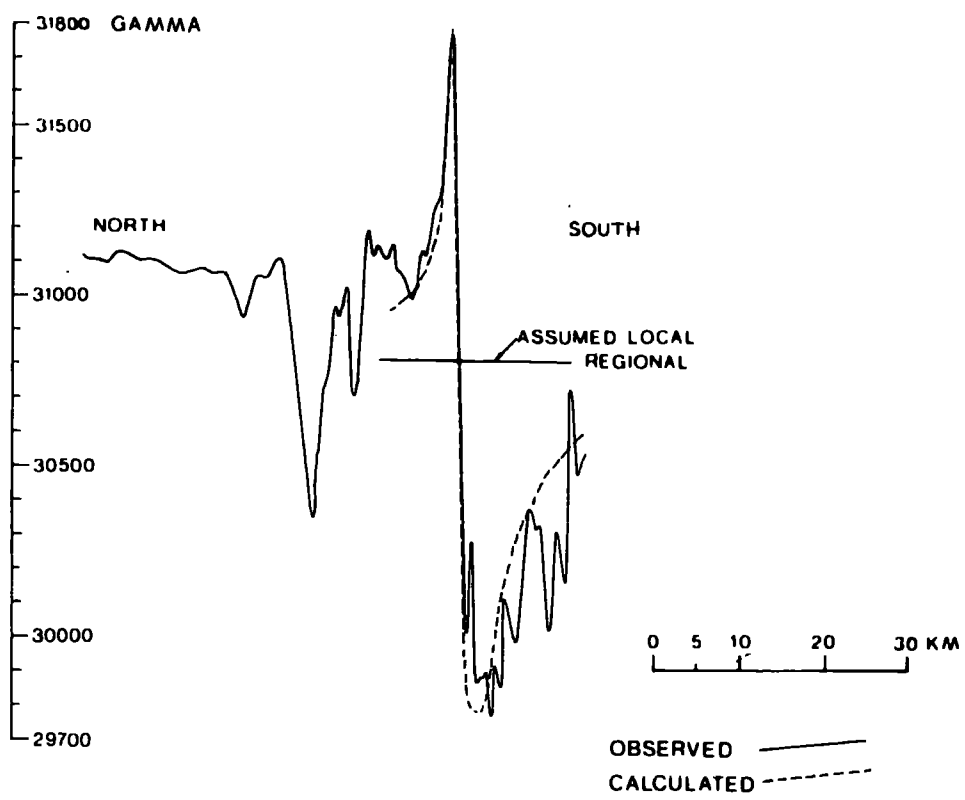
The model is shown at Fig. (6-12). The change in gradient of the Bouguer anomaly is reflected in a steepening of the contact dip of the intrusion with depth, which is suggestive of a funnel-shaped rather than a saucer shaped intrusion. The results are in good agreement with those obtained for profile D-D' at the point of intersection of the profiles.

The margin of the intrusion is marked by the onset of high amplitude, high frequency magnetic anomalies (Fig. 6-12). Further south the magnetic record shows an extremely high frequency magnetic anomaly with a peak amplitude of some 2000 gamma. The gravity and seismic evidence indicate that the cause of the anomaly is not top surface topography, and computations show that the change in slope of the bottom surface of the intrusion, although it coincides with the anomaly, could not produce the high frequency required.

The anomaly has been interpreted as variation in the magnetisation of the intrusion. Computations using MAGN (Bott, 1969), which computes the magnetic anomaly due to an arbitrarily shaped, arbitrarily magnetised body, indicate that the anomaly cannot be produced by a body with a vertical contact, the contact must dip inwards towards the centre of the intrusion.

Determination of the angle of magnetisation was not possible since the anomaly could not be isolated from the interference effects, probably due to minor lateral variations in the magnetisation of the intrusion. The program MAGGIT 3 was thus used to analyse the anomaly

Fig.6-12. Interpretation of Bouguer anomaly and magnetic anomaly profiles F-F'. Two-dimensional structures have been assumed. The magnetic anomaly is interpreted in terms of a wedge-shaped body with a markedly higher or lower magnetisation than the main body of the intrusion. (Symmetry of the main body of the intrusion in the plane of the profile has been assumed in the gravity interpretation.)



specifying a series of magnetisation intensities and dips. The best fitting model (Fig. 6-12) was produced by a saucer shaped body with a slope of  $20^{\circ}$  in the north and  $10^{\circ}$  in the south. The required magnetisation contrast was 0.01 emu/cc at an angle of  $10^{\circ}$  down to the north, which is approximately the direction of the present Earth's field. The magnetic map of McMaster et al. (1970) (Fig. 6-3) indicates that this anomaly is roughly circular and is further evidence for a saucer shaped source body.

The direction and intensity of magnetisation of the body are, of course, relative to those of the rest of the intrusion, and since these are unknown have little significance.

6-2-8-4 Profile D-D'

This profile extends northwest from Banana Island (Fig. 6-7) along the major axis of the plan of the intrusion. It is not possible to produce a rigorous model with the data available, but the speculative model produced (Fig. 6-13) gives a good indication of the extent of the body. No data is available on the top and bottom surfaces of the intrusion, other than that already used so the following assumptions were made:

1. The bottom surface of the intrusion was estimated from the two values for the depth to bottom surface obtained at the intersection of the two 'east-west' profiles with profile D-D', and from the assumption that the steep decrease in Bouguer anomaly in the far north of the profile marks the termination of the intrusion.

2. A constant thickness of Quaternary-Tertiary sediments of 300 metres was assumed along the length of the profile with the exception of the region of Banana Island, where the intrusion outcrops. This assumption would appear to be reasonably valid in the light of the refraction data of Sheridan et al. (1969).

3. A uniform density for the Cretaceous and Cambrian-Devonian sediments was assumed in the absence of any data on their relative thicknesses.

The gravity model was computed using the following procedure.

1. The gravity anomaly due to the assumed Tertiary-Quaternary sediment distribution was computed using GRAVN (Bott, 1969).

2. Using the assumed bottom surface and taking as its top surface the base of the Tertiary-Quaternary sediments the gravity anomaly of the intrusion was computed using GRAVN. The anomaly due to the sediments calculated in (1) was added to this. This model produces an anomaly that is everywhere greater than the observed Bouguer anomaly

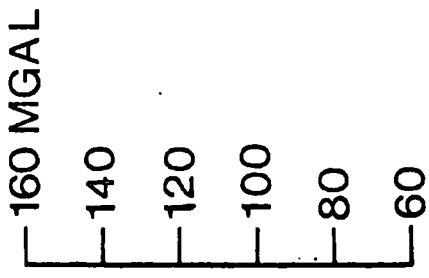
3. The residual anomaly between the observed Bouguer anomaly and that calculated in (2) was taken to be due to surface topography with accompanying thickening of the Cretaceous and Cambrian-Devonian sediments. The required topography was computed using GRAVIT 1 taking a density of 2.35 gm/cc<sup>\*</sup> for the mean sediment density. Reasonable agreement was obtained between the depths to top surface of the intrusion, computed in this model, at the points

\* biased towards the upper sedimentary layer density (2.20 gm/cc.) because of its proximity to the level of gravity observation.

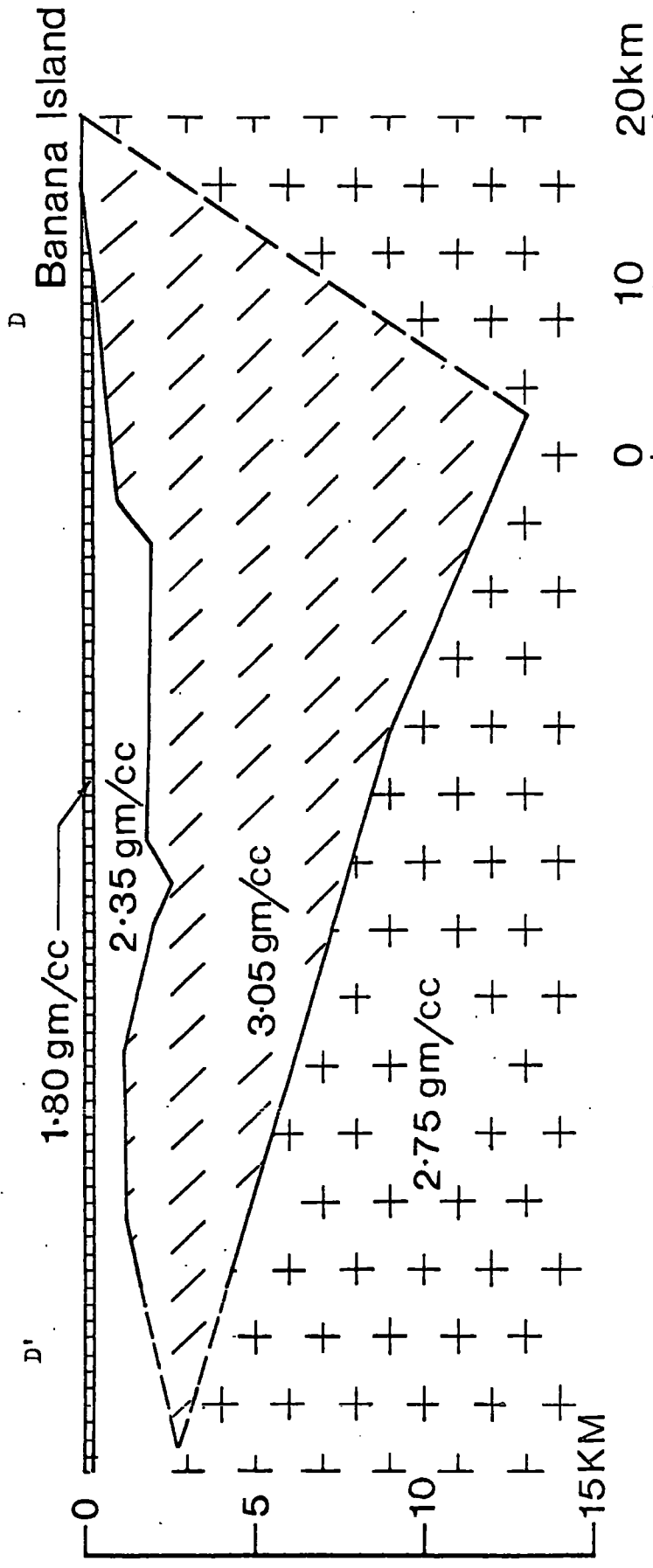
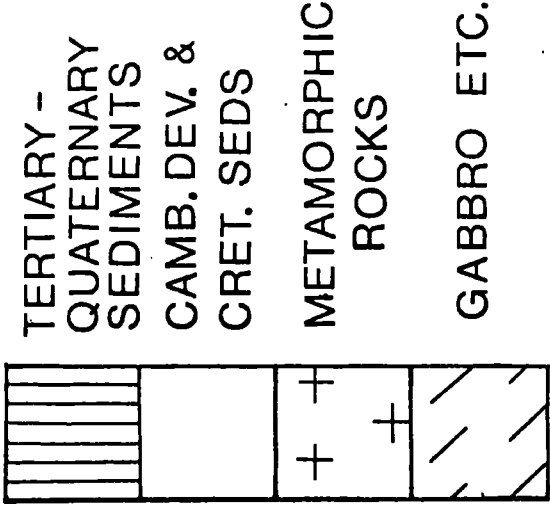
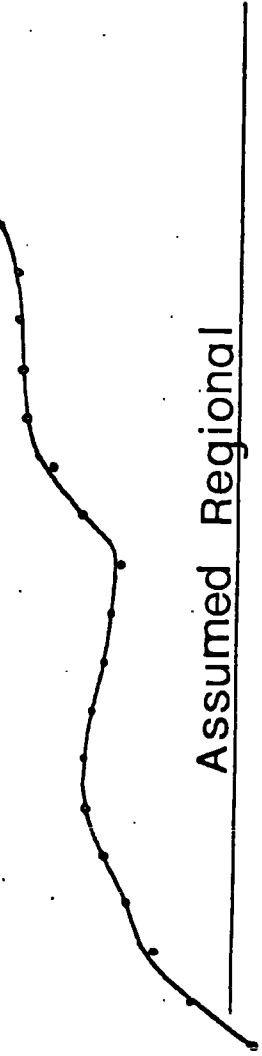


Fig. 6-13. Interpretation of Bouguer anomaly profile D-D'. Two-dimensional structures have been assumed. The southern boundary of the intrusion is taken to be just south of Banana Island.

BOUGUER ANOMALY



— observed  
... calculated



of intersection with the 'east west' profiles, and those previously obtained from the 'east west' profile analyses.

Several different bottom surfaces for the uncontrolled northern section of the profile were used in repeated computations.. The model shown (Fig. 6-13) assumes a density of 3.05 gm/cc for the intrusion. In view of the uncertainties in the model, end corrections have not been applied and a two dimensional structure is thus assumed. This will result in the depths shown being underestimates, but the model nevertheless illustrates the likely basic form of the intrusion.

3-2-8-5 Profile E-E'

This profile extends westwards from the Freetown peninsula across the Sierra Leone continental margin and onto the abyssal plain (Fig. 6-4). It includes the gravity data (unpublished) from the U.S. Department of Commerce Survey (Fig. 6-14 (a)), which was run close to the refraction lines of Sheridan et al. (1969).

The gravity anomaly due to the upper crustal layers was computed using GRAVN (Bott, 1969) taking the thicknesses from the refraction data and estimating the densities from P-wave velocities (Appendix 3). The density contrasts with the lower crustal layer were used thus producing a crust of uniform density.

The depth to the Moho is known in the far west of E-E' from the work of Sheridan et al. (1969) (Station 28 - Fig. 6-14 (b)). Assuming a constant density contrast between the crust and upper mantle, the crust-mantle boundary was computed using GRAVIT 1, the method described

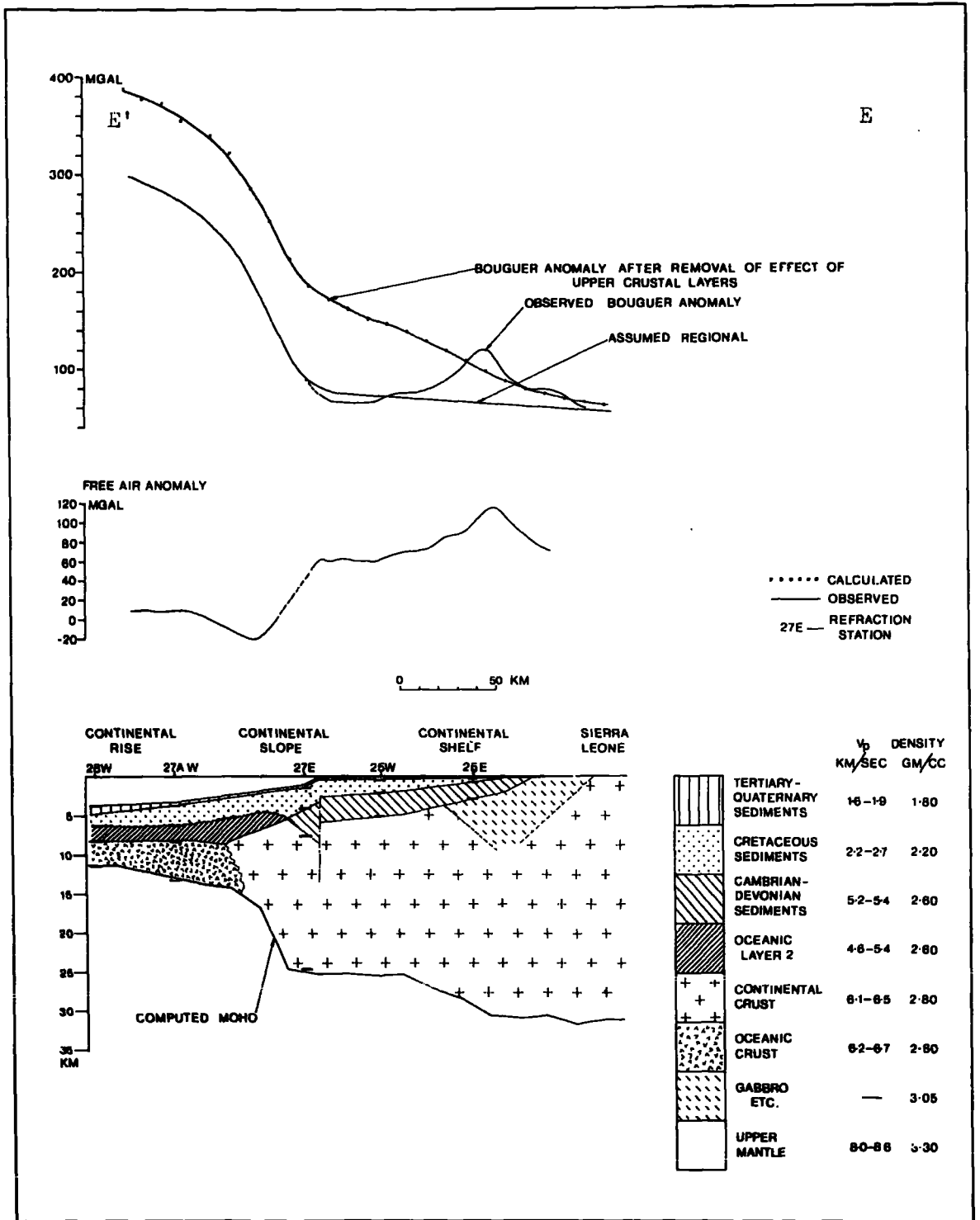


Fig.6-14. Interpretation of Bouguer anomaly profile E-E'. Two-dimensional structures have been assumed.  
 (crustal structure after Sheridan et al., 1969)

in Chapter 2 for analysing infinite anomalies being applied. A mean density for the crustal rocks of 2.80 gm/cc was employed, and a series of densities of the upper mantle in the range 3.25 - 3.45 gm/cc were specified. Control on the density is possible since Sheridan et al. (1969) obtained a depth to Moho of 24.41 km. at station 27 (Fig. 6-14 (b)) east of station 28. The program GRAVIT 1 gives at depth of 24.8 km. at station 27 using an upper mantle density of 3.30 gm/cc. The depth to Moho under the coast of Sierra Leone is computed to be 30.5 km. for this density (Fig. 6-14 (b)).

### 6-3 Summary and Discussion

The Freetown Complex, which forms the mountain range of the Freetown peninsula on the coast of Sierra Leone is a funnel shaped or saucer shaped intrusion, having an elongate elliptical plan and extending for at least 110 km. north-west from the Freetown peninsula. Its extension south of the Freetown peninsula is unknown. The intrusion has its greatest depth to base at a point 20 km. W.S.W. of York and in this region the body appears to have east-west symmetry with a width of 55 km. and a maximum depth between 10 and 13 km.

To the north the intrusion thins and has a funnel like form probably terminating as a sheet-like body in the far north-west of the Bouguer anomaly map (Fig. 6-7).

The magnetic and seismic evidence indicate that the intrusion has a roughly north-south trending fault along much of its length, which appears to die out to the south.

The relative lowering of the Bouguer anomaly over

the centre of the intrusion is attributed to either a saucer-shaped layer of anorthosite or central sag of the intrusion roof. The magnetic evidence indicates that concentric with this is a saucer-shaped layer of rocks with a markedly different magnetisation from the surrounding rock. Both of these structures may be related to the zoned nature of the intrusion (Wells, 1962), although no evidence is as yet available on land for any magnetisation contrast between the zones. Baker and Bott (1961) did however remark on the highly variable magnetisation of the intrusion.

Krause (1963) attributed a circular plan to the body and suggest that it was of meteoric origin. Although the shape and size of the body preclude the possibility that the body is itself of meteoric origin, Harrison (1954) has pointed out that an impact of sufficient violence could act as a trigger to release latent volcanism within the Earth's crust of sufficient magnitude to obliterate all trace of the impact, including the original circular form. Although this possibility cannot be discarded there is no evidence to support the theory.

Baker and Bott (1961) draw attention to the apparent eastward rise of the background anomaly to the east of the peninsula, and point out that crustal downwarp under the intrusion is a possible explanation. A similar rise is not observed on the seaward side of the intrusion, however the westward thickening of the sedimentary strata would tend to mask any such anomaly. When the gravity anomaly due to the thickening sediments is removed, and

the residual anomaly is interpreted in terms of crustal thickening (section 6-2-8-5) the Moho is found to be deeper under the intrusion than under the shelf to the west. How much, if any, of this thickening is due to isostatic compensation of the igneous intrusion, as opposed to the normal thickening which occurs at a continental margin is impossible to deduce. Isostatic anomalies for the intrusion, assuming Airy's theory were computed for depths of compensation in the range 30 km. to 50 km. assuming a density contrast of 0.5 gm/cc between the crust and upper mantle. The calculated increase in anomaly was less than that observed by Baker and Bott (1961) for all the models used, even when allowance was made for the gravity anomaly due to the marginal Bullom sediment thickness. It is therefore quite possible that the body is in fact overcompensated, however Baker and Bott (1961) point out that an alternative explanation for the background anomaly rise would be regional change of the basement density.

The sedimentary basins occurring on either side of the intrusion on the Sierra Leone shelf suggest that the intrusion has acted as a stable block, resisting down-warp, but being susceptible to faulting. The basin developed to the north and east of the intrusion has been assumed to be of either Cretaceous or Tertiary age and may mark the onset of a northward thickening basin on the Sierra Leone and Guinea shelves bounded in the north by the postulated basement rise off Portuguese Guinea.

The other feature of note is the gravity high in the south west of the Bouguer anomaly map (Fig. 6-7 - High A). Only the onset of the high has been recorded, but the magnetic traverse by H.M.S. Hecla (1966) shows a high amplitude, high frequency anomaly in this region, suggesting another intrusion or possibly a rise in the metamorphic basement rocks. Further evidence is however needed before a firm conclusion can be drawn on this point.



APPENDIX 1

SPECIFICATIONS AND LISTINGS FOR COMPUTER PROGRAMS

CONTENTS

The program	GRAVIT 1
" "	GRAVIT 2
" "	GRAVIT 3
" "	GRAVIT 4
" "	VARYIT
" "	PRISM
" "	MAGGIT 1
" "	MAGGIT 2
" "	MAGGIT 3
" "	MAGGIT 4

PROGRAM NAME: GRAVIT 1

FUNCTION: This program determines the space form of a two dimensional body with inward sloping contacts producing a given gravity anomaly. The top surface of the body (not necessarily horizontal) and the uniform density contrast must be specified.

INPUT FORMAT:

CYCLE

'MODELNAME'

ITER

N

M

P3

R0

TT

POS

MAO

XX1

Y1

Y2

DATA NOTES:

CYCLE is the number of gravity anomalies to be analysed and therefore the number of sets of data.

'MODELNAME' Each new set of data must commence with a name of up to 60 characters, enclosed in single quotation marks

ITER is the number of iterations performed by the program (Try 10.)

N is the number of blocks used for the initial equivalent layer approximation (see GENERAL NOTES)

M is the number of anomaly values specified ( $M \geq N$ ).

P3 is the number of density contrasts to be tried for the model.

R0 is an array of P3 density contrasts.

TT is an array of N points defining the depth to each block of the initial equivalent layer approximation.

POS is an array of M x - coordinates defining the points at which the anomaly is specified.

MA0 is an array of M gravity anomalies at the x - coordinates defined by POS.

XX1 is an array of N + 1 x - coordinates defining the margins of the blocks of the equivalent layer approximation.

Y1 and Y2 are arrays of length N defining the strike length of each block in either direction normal to the plane of the profile.

GENERAL NOTES: The user must define a set of blocks along the known or estimated top surface of the body. If the width of the structure is unknown the whole anomaly should be underlain by blocks. The depths defined in TT are the depths at the mid point of each block, The width of any block must be at least as great as its depth. If the observed anomaly has a steep gradient the minimum block-width should be used.

Lengths are in kilometres, anomalies in milligals and the densities.

OUTPUT: For each anomaly analysed the model produced after the specified number of iterations is printed out as are the observed, calculated and residual anomalies.

SUBROUTINES:

SUBR 1: Supervises the setting up of the kernel array and the least squares problem.

SUBR 2: Sets up the trapesoidal coordinates.

SUBR 3: Computes the gravity anomaly due to each model after each iteration.

SUBR 4: Computes the gravity anomaly due to any equivalent layer block.

```

GRAVIT1:PROC OPTIONS (MAIN); /* GESS LAVING 1969 */
DCL(ITERATION,CCOUNT,N,M,P3,RR) FIXED BIN (31),
MODELNAME CHAR (60) VARYING;
GET LIST (CYCLE) ;
LOOP1:DO COUNT=1 TO CYCLE;
GET LIST(MODELNAME,ITERATION,N,M,P3);
BEGIN ;
DCL(MAC(M,1),(AO,AC,POS)(M),(Y1,Y2,D1,D2,CTT,TT,LSIDE,
RSIDE)(N),(XX1,LS,RS,LET,RCT,LDB,RDB,Z1,Z2)(N+1),
(XX,ZT,ZB)(N+2),SCENS(N,1),KK(N,M),RO(P3))FLOAT BIN,
ROUND FLOAT BINARY,(K,J,I,AA,G) FIXED BIN; RCLND=0.00001;
DCL Z(N) FLOAT BIN;
GET LIST(RC,TT,PCS,MAC); PCS=POS*1000; TT=TT*1000;
DO I=1 TO M; MAO(I,1),AC(I)=ABS(MAC(I,1)); END;
RO=ABS(RO);
GET LIST(XX1,Y1,Y2);
XX1=XX1*1000; Y1=Y1*1000; Y2=Y2*1000;
DO I=1 TO N;
Z(I)=XX1(I+1)-XX1(I);
END;
DO I=1 TO N+1;
IF I=1 THEN RSIDE(I-1)=XX1(I);
IF I=N+1 THEN LSIDE(I)=XX1(I); END;
DO Q=1 TO P3;
C1=TT; CTT,C2=TT+1;
DO I=1 TO M; MAC(I,1)=AO(I); AC(I)=0; END;
AA=1;
CALL SUBR1(N,M,MAC,KK,PCS,LSIDE,RSIDE,SCENS,
C1,C2,FINISH,AA);
DO I=1 TO N;
D2(I),CTT(I)=TT(I)+SCENS(I,1)/RC(Q);
IF CTT(I)<TT(I)+1 THEN D2(I),CTT(I)=TT(I)+1; END;
CALL SLER2 (N,C1,C2,ZT,ZB,XX1,XX,Z1,Z2,Y1,Y2,Z);
CALL SLBR3 (ZT,ZB,XX,PCS,AC,RO(Q),N,M,Z1,Z2,AA);
DO I=1 TO M; MAO(I,1)=AO(I)-AC(I); END;
L1: DO AA=1 TO ITERATION;
D1=CTT; D2=CTT+1;
CALL SUBR1(N,M,MAC,KK,PCS,LSIDE,RSIDE,SCENS,
C1,C2,FINISH,AA);
DO I=1 TO N;
D1(I)=TT(I); CTT(I),D2(I)=CTT(I)+SCENS(I,1)/RC(Q);
IF CTT(I)<TT(I) THEN CTT(I),D2(I)=TT(I)+1; END;
CALL SUBP2 (N,C1,C2,ZT,ZB,XX1,XX,Z1,Z2,Y1,Y2,Z);
CALL SLBR3 (ZT,ZB,XX,PCS,AC,RO(Q),N,M,Z1,Z2,AA);
DO I=1 TO M; MAO(I,1)=AO(I)-AC(I); END;
IF AA=ITERATION THEN DO;
PUT LIST (MODELNAME) PAGE;
PUT EDIT ('MODEL',CCOUNT,'_',Q) (A,F(2),A,F(1)) SKIP(2);
PUT EDIT ('ESTIMATE',AA,'DENSITY',RO(Q)+ROUND
(A,F(3),X(3),A,F(6,2)) SKIP(2);
PUT EDIT ('BLOCK','LT','RT','LU','RU','LL','RL')
(A,X(4),A,X(7),A,X(7),A,X(7),A,X(7),A,X(7),A) SKIP(2);
DO I=1 TO N+1;
PUT EDIT (I,XX(I),XX(I+1),ZT(I),ZT(I+1),ZB(I),ZB(I+1))
(F(2),6 F(9,C)) SKIP(1); END;
PUT LIST ('LOCATION OBSERVED CALCULATED RESID')

```

```

SKIP(4); DO I=1 TO M;
PUT EDIT (POS(I),AC(I),AC(I),FAC(I,1))
(F(7,0),F(10,1),F(13,1),F(16,1)) SKIP(1);
END LL;
FINISH:PUT EDIT('END OF MODEL',COUNT,'-',Q)
(A,F(3),A,F(1)) SKIP(3);
END LCOP;
PUT LIST ('END OF DATA') SKIP(3);
STOP;
SUBR1:PROC(A,R,B,KK,LOC,LS,RS,S,DD,CDD,LL,TIMEX);
DCL((B,C)(R,7),(LS,RS,DD,CDD)(A),G(A,1),
(HH,KK)(A,R),LOC(R))
FLOAT BIN, (A,R,I,J,TIMEX) FIXED BIN(31),AUX(2,A) FLOAT
BIN, IPIV(A) FIXED BIN(31), (II,IER) FIXED BIN(31);
X FLOAT BIN, LL LABEL;
DO I=1 TO R;
DO J=1 TO A;
IF DD(J)<2.5 THEN DO;
X=0.5*(CDD(J)-DD(J));
DD(J)=2.5; CDD(J)=DD(J)+X;
IF ABS(LOC(I)-LS(J))<0.1 | ABS(LOC(I)-RS(J))<0.1
THEN LOC(I)=LOC(I)+1; END;
CALL SUBR4 (KK(J,I),LOC(I),LS(J),RS(J),DD(J),CDD(J));
END; END;
HH=KK; C=B;
II=1; AI=0.0001;
CALL LLSQ(HF(1,1),C(1,1),R,A,II,S(1,1),IPIV(1),AI,
IER,AUX(1,1));
IF IER =/=0 THEN DO;
PUT LIST ('PROC UNSUCCESSFUL') SKIP(2);
GO TO LL; END;
END SUBR1;
SUBR2:PROC(H,T,CT,ZT,ZB,LS,XX,ZZ1,ZZ2,YY1,YY2,V);
DCL(N) FIXED BIN(31);
DCL V(N) FLOAT BIN;
DCL((LS,ZZ1,ZZ2)(N+1),(T,CT,YY1,YY2)(N),(XX,ZT,ZB)(N+2))
FLOAT BIN;
DO I=2 TO N+1;
XX(I)=LS(I-1)+V(I-1)/2;
ZT(I)=T(I-1); ZB(I)=CT(I-1); END;
XX(N+2)=LS(N+1)+V(N)/2; ZT(1)=T(1);
ZT(N+2)=T(N); ZB(1)=ZT(1)+1; ZB(N+2)=ZT(N+2)+1;
ZZ1(N+1)=YY1(N); ZZ2(N+1)=YY2(N);
DO I=1 TO N; ZZ1(I)=YY1(I); ZZ2(I)=YY2(I); END;
END SUBR2;
SUBR3:PROC(ZT,ZP,XS,LOC,ACS,RO,N,M,E1,E2,AA);
DCL AA FIXED BIN;
DCL(N,M) FIXED BIN(31);
DCL((XS,ZB,ZT)(N+2),(E1,E2)(M+1),(LCC,CAS,ACS)(M),
(X,Z,C,S)(5)) FLOAT BIN,(P1,P2,RO,XC,ZC,W,H,X1,Z1,R1,
X2,Z2,R2,F1,F2,KCF,A,CDRK) FLOAT BIN;
ACS=0; ROH=RO*0.15728; CAS=0;
DO I=1 TO N+1;

```

GRAVITI:PROC OPTICNS (MAIN); /\* GESS LAVING 1969 \*/

```
IF I=1 THEN ZB(I)=(ZB(I-1)+ZB(I)+ZB(I+1))/3;
X(I),X(2),Z(5)=XS(I); X(3),X(4)=XS(I+1);
Z(1),Z(5)=ZT(I); Z(2)=ZB(I); Z(3)=ZB(I+1);
Z(4)=ZT(I+1);
XC=X(1)+0.333*(Z(2)-Z(1)+2*(Z(3)-Z(4)))
*(X(3)-X(1))/(Z(2)-Z(1)+Z(3)-Z(4));
ZC=0.25*(Z(1)+Z(2)+Z(3)+Z(4));
DO J=1 TO M;
A=(XC-LCC(J))**2+ZC**2;
P1=SQRT(A+LJ(I)**2);
P2=SQRT(A+E2(I)**2);
CORR=0.5*(E2(I)/P2+E1(I)/P1);
X1=X(1)-LCC(J); Z1=Z(1); R1=X1**2+Z1**2;
FI1=(1.5708-ATAN(X1,Z1));
DO K=1 TO 4;
X2=X(K)-LCC(J); Z2=Z(K+1); R2=X2**2+Z2**2;
FI2=(1.5708-ATAN(X2,Z2));
H=SQRT((X(K)-X(K+1))**2+(Z(K+1)-Z(K))**2);
S(K)=(Z(K+1)-Z(K))/H; C(K)=(X(K)-X(K+1))/H;
W=0.5*S(K)*LOG(R2/R1)+C(K)*(FI2-FI1);
CAS(J)=CAS(J)+ROH*(Z2*FI2-Z1*FI1-W*(X1*S(K)+Z1*C(K)));
XJ=X1; ZJ=Z2; R1=R2; FI1=FI2; END;
ACS(J)=ACS(J)+CAS(J)*CORR; CAS(J)=0;
END SUBR3;
SUBR4:PROC(GEX,X,LTX,RT,UP,LQ);
DCL(GEX,X,LTX,RT,UP,LQ,X1,X2,F2) FLOAT BIN;
X1=LTX-X; X2=RT-X; F2=UP*UP+X1*X2;
IF F2=0 THEN F2=1.5708;
ELSE F2=ATAN(UP*(X2-X1)/F2);
IF F2<0 THEN F2=F2+3.14159;
GEX=0.02668*(LQ-UP)*F2;
END SUBR4;
END GRAVITI;
```

PROGRAM NAME: GRAVIT 2

FUNCTION: This program determines the space form of a two dimensional body with outward sloping contacts producing a given gravity anomaly. One point on the top surface and the uniform density contrast must be specified. A horizontal bottom surface is assumed.

INPUT FORMAT:

CYCLE

'MODELNAME'

ITER

N

M

P3

RR

BLOCK

RC

US

POS

MAO

XX1

Y1

Y2

DATA NOTES:

CYCLE

'MODELNAME'

N

As in GRAVIT 1

M

P3



RR is the number of different estimates of depth to the top surface point.

BLCK is the number of the block, counting from the left whose mid point depth is specified.

RO as in GRAVIT 1.

US is an array of RR depths to the mid point of the specified block.

POS

MAO

XX1.           As in GRAVIT 1

Y1.

Y2

For other notes see GRAVIT 1 specification.

GRAVITE:PROC OPTIONS (MAIN); /\* GESS LAVING 1969 \*/

```
GRAVITE:PROC OPTIONS (MAIN); /* GESS LAVING 1969 */
DCL(ITERATION,COUNT,N,M,BLOCK,P3,RR) FIXED BIN (31);
MODELNAME CHAR (60) VARYING;
GET LIST (CYCLE);
LECP1:DO COUNT =1 TO CYCLE;
SET LIST (MODELNAME,ITERATION,N,M,P3,RR,BLOCK);
BEGIN;
DCL(MAC(N,1),SDENS(N,1),KK(N,M),(AO,AC,POS)(M),(Y1,Y2,D1,
D2,CTT,TT,LSIDE,RSIDE)(N),(XX1,LS,RS,LDT,ROT,LDB,RDB,
Z1,Z2)(N+1),(XX,ZT,ZB)(N+2),RO(P3),US(RR)) FLOAT BIN,
(ROUND,S) FLOAT BIN,
(K,J,I,AA,Q,TTT) FIXED BIN;
DCL Z(N) FLOAT BIN;
ROUND=0.00001;
GET LIST(RO,US,POS,MAO);
DO I=1 TO M; MAC(I,1),AO(I)=ABS(MAO(I,1)); END;
DO I=1 TO N;
Z(I)=XX1(I+1)-XX1(I); END;
RO=ABS(RO);
POS=POS*1000; US=US*1000;
GET LIST(XX1,Y1,Y2);
XX1=XX*1000; Y1=Y1*1000; Y2=Y2*1000;
L1:DO I=1 TO N+1;
IF I=1 THEN RSIDE(I-1)=XX1(I);
IF I=N+1 THEN LSIDE(I)=XX1(I);
END L1;
DO TTT=1 TO RR;
DO Q=1 TO P3;
LSIDE(BLOCK)=RSIDE(BLOCK-1);
RSIDE(BLOCK)=LSIDE(BLOCK+1);
DO I=1 TO N;
TT(I),D1(I)=JS(TTT);
CTT(I),D2(I)=US(TTT)+1;
END;
DO I=1 TO M;
MAC(I,1)=AO(I);
AC(I)=0;
END;
AA=1;
CALL FORM(N,M,MAC,KK,POS,LSIDE,RSIDE,SDENS,D1,D2,FINISH,
AA);
CTT(BLOCK),D2(BLOCK)=US(TTT)+SDENS(BLOCK,1)/RO(Q);
DO I=1 TO N;
IF I=BLOCK THEN DO;
D2(I),CTT(I)=CTT(BLOCK);
D1(I),TT(I)=CTT(BLOCK)-SDENS(I,1)/RO(Q);
END; END;
CALL CHANGE(N,D1,D2,ZT,ZB,XX1,XX,Z1,Z2,Y1,Y2,Z);
CALL CALCTRAP(ZT,ZB,XX,POS,AC,RO(Q),N,M,Z1,Z2);
DO J=1 TO M; MAC(I,1)=AC(I)-AC(I); END;
DO AA=1 TO ITERATION;
LSIDE(BLOCK)=LSIDE(1);
RSIDE(BLOCK)=RSIDE(N);
DO I=1 TO N;
IF I=BLOCK THEN DO;
D2(I)=TT(I)-1;
```

```

D2(I)=TT(I);
END;
ELSE DO;
D1(I)=CTT(I);
D2(I)=CTT(I)+1;
END; END;
CALL FURM(N,M,MAO,KK,PCS,LSIDE,RSIDE,SDENS,
D1,D2,FINISH,AA);
D1(BLOCK)=CTT(BLOCK);
CTT(BLOCK),D2(BLOCK)=CTT(BLOCK)+SDENS(BLOCK,1)/RD(Q);
DO I=1 TO N;
IF I=BLOCK THEN DO;
TT(I),D1(I)=TT(I)-SDENS(I,1)/RD(Q);
CTT(I)=CTT(BLOCK);
END;
IF TT(I)>CTT(BLOCK)-1 THEN TT(I),D1(I)=CTT(BLOCK)-1;
IF I=BLOCK & TT(I)<1 THEN TT(I),D1(I)=1;
D2(I)=CTT(BLOCK);
END;
D1(BLOCK)=US(TTT);
LSIDE(BLOCK)=RSIDE(BLOCK-1);
RSIDE(BLOCK)=LSIDE(BLOCK+1);
CALL CHANGE(N,D1,D2,ZT,ZB,XX,XX,Z1,Z2,Y1,Y2,Z);
CALL CALCTRAP(ZT,ZB,XX,PCS,AC,RC(Q),N,M,Z1,Z2);
DO I=1 TO N; MAO(I,1)=AO(I)-AC(I); END;
IF AA=ITERATION THEN DO;
PUT LIST(MODELNAME) PAGE;
PUT EDIT('MODEL',COUNT,'-',TTT,'-',Q)(A,F(2),A,F(1),A,
F(2)) SKIP(2);
PUT EDIT('ESTIMATE',AA,'UPPER SURFACE',US(TTT),
'DENSITY',RD(Q)+ROUND)(A,F(3),X(3),A,F(6),X(3),A,
F(6,2)) SKIP(2);
PUT EDIT('BLOCK','LT','RT','LU','RU','LL','RL')
(A,X(4),A,X(7),A,X(7),A,X(7),A,X(7),A,X(7),A) SKIP(2);
DO I=1 TO N+1;
PUT EDIT(I,XX(I),XX(I+1),ZT(I),ZT(I+1),ZB(I),ZB(I+1))
(F(3),6 F(9,0)) SKIP(1); END;
PUT LIST
('LOCATION OBSERVED CALCULATED RESID')
SKIP(4);
DO I =1 TO M;
PUT EDIT (POS(I),AO(I),AC(I),AO(I)-AC(I))
(F(7,0),F(10,1),F(13,1),F(11,1)) SKIP(1);
END; END; END;
FINISH:PUT EDIT('END OF MODEL',COUNT,'-',TTT,'-',Q,'-',W)
(A,F(3),A,F(1),A,F(2),A,F(1)) SKIP(3);
END LOOP;
PUT LIST ('END OF DATA') SKIP(3);
PUT PAGE;
STOP;
CALCTRAP:PROC(ZT,ZB,XS,LCC,ACS,RC,H,M,E1,E2);
DCL (H,M) FIXED BIN(31);
DCL(ZT(N+2),ZB(N+2),XS(N+2),LCC(M),ACS(M),E1(N+1),CAS(M),
E2(N+2),X(5),Z(5),C(5),S(5)) FLOAT BIN;

```

```

(P1,P2,RO,XC,ZC,W,H,X1,Z),R1,X2,Z2,RO,F11,F12,ROH
,A,CORR) FLOAT BIN;
ACS=0; ROH=RO*C.013328;
CAS=0;
DO I=1 TO N+1;
X(1),X(2),X(5)=XS(I); X(3),X(4)=XS(I+1);
Z(1),Z(5)=ZT(I); Z(2)=ZB(I); Z(3)=ZB(I+1);
Z(4)=ZT(I+1);
XC=X(1)+0.3333*(Z(2)-Z(1)+2*(Z(3)-Z(4)))
*(X(3)-X(1))/(Z(2)-Z(1)+Z(3)-Z(4));
ZC=0.25*(Z(1)+Z(2)+Z(3)+Z(4));
DO J=1 TO M;
A=(XC-LOC(J))**2+ZC**2;
P1=SQRT(A+E1(I)**2);
P2=SQRT(A+E2(I)**2);
CORR=0.5*(E2(I)/P2+E1(I)/P1);
X1=X(1)-LOC(J); Z1=Z(1); R1=X1**2+Z1**2;
F11=(1.5708-ATAN(X1,Z1));
DO K=1 TO 4;
IF ABS(X(K+1)-LOC(J))<0.1 THEN LOC(J)=LOC(J)+1;
X2=X(K+1)-LOC(J); Z2=Z(K+1); R2=X2**2+Z2**2;
F12=(1.5708-ATAN(X2,Z2));
H=SQRT((X(K)-X(K+1))**2+(Z(K+1)-Z(K))**2);
S(K)=(Z(K+1)-Z(K))/H; C(K)=(X(K)-X(K+1))/H;
W=0.5*S(K)*LOG(R2/R1)+C(K)*(F12-F11);
CAS(J)=CAS(J)+ROH*(Z2*F12-Z1*F11-W*(X1*S(K)+Z1*C(K)));
X1=X2; Z1=Z2; R1=R2; F11=F12;
END;
ACS(J)=ACS(J)+CAS(J)*CORR;
CAS(J)=0;
END; END;
END CALCTRAP;
CHANGE:PROC (N,T,CT,ZT,ZB,LS,XX,ZZ1,ZZ2,YY1,YY2,V);
DCL N FIXED BIN (31);
DCL V(N) FLOAT BIN;
DCL (LS(N+1),XX(N+2),ZT(N+2),ZB(N+2),T(N),CT(N),
ZZ1(N+1),ZZ2(N+1),YY1(N),YY2(N)) FLOAT BIN;
DO I=2 TO N+1 ;
XX(I)=LS(I-1)+V(I-1)/2;
ZT(I)=T(I-1);
ZB(I)=CT(I-1);
END;
XX(1)=LS(1)-V(1)/2;
XX(N+2)=LS(N+1)+V(N)/2;
ZB(2)=CT(1); ZB(N+2)=CT(N);
ZT(1)=ZB(1)-1;
ZT(N+2)=ZB(N+2)-1;
ZZ1(N+1)=YY1(N);
ZZ2(N+1)=YY2(N);
DO I=1 TO N;
ZZ1(I)=YY1(I);
ZZ2(I)=YY2(I);
END;
END CHANGE;

```

GRAVIT2:PROC OPTICS (MAIN); /\* GESS LAVING 1969 \*/

```
FORM : PROC (A,R,B,KK,LOC,LS,RS,G,DD,CDD,LL,TIMEX) ;
  DCL (A,C) FIXED BIN (31),
  (TIMEX,I,J) FIXED BIN,
  IPIV(A) FIXED BIN (31), AUX(2,A) FLOAT BIN, (I,IER)
  FIXED BIN (31),
  LL LABEL,
  X FLOAT BIN,
  (B(R,1),KK(A,R),HH(A,A),GG(A,1),DD(R,1),LOC(R),
  LS(A),RS(A),G(A,1),CD(A),CDD(A),P(A),HH(A,R),C(R,1))
  FLOAT BIN ;
S1:DO I=1 TO R;
S2:DO J=1 TO A;
  IF DD(J)<2.51 THEN
S3:DO;
  X=0.5*(CDD(J)-DD(J));
  DD(J)=2.5; CDD(J)=CC(J)+X;
  IF ABS(LOC(I)-LS(J))<0.1 | ABS(LOC(I)-RS(J))<0.1
  THEN LOC(I)=LOC(I)+1;
  END S3;
  CALL CALCSH (KK(J,I),LOC(I),LS(J),RS(J),DD(J),CDD(J));
END S2; END S1;
HH=KK; C=B ;
II=1 ; AI=0.0001 ; G=0;
CALL LLSQ(HH(1,1),C(1,1),R,A,II,G(1,1),IPIV(I),AI,
IER,AUX(1,1));
END FORM;
CALCSH:PROC (GEX,X,LTX,RT,UP,LD);
  DCL (GEX,X,LTX,RT,UP,LO) FLOAT BINARY,
  (X1,X2,F2) FLOAT BINARY;
  X1=LTX-X; X2=RT-X;
  F2=UP*UP+X1*X2 ;
  IF F2=0 THEN F2=1.5708;
  ELSE F2 =ATAN((UP*(X2-X1))/F2);
  IF F2<0 THEN F2=F2+3.14159;
  GEX=0.02668*(LO-UP)*F2;
  END CALCSH;
END GRAVIT2;
```

PROGRAM NAME: GRAVIT 3

FUNCTION: This program determines the space form of a three dimensional body with inward sloping contacts producing a given two dimensional gravity anomaly. The top surface of the body on the uniform density contrast must be specified.

INPUT FORMAT:

N

M

NN

MM

ITER

X1

Y1

XS

YS

XCD

YCD

US

RO

AG

'MODELNAME'

DATA NOTES:

N is the number of anomaly points in the x-direction.

M is the number of anomaly points in the y-direction.

NN is the number of rectangular prisms in the x-direction.

MM is the number of rectangular prisms in the y-direction.

$$N \times M \gg NN \times MM$$

ITER as in GRAVIT 1.

X1 is the x-coordinate of the first anomaly point see Fig. (A1-1).

Y1 is the y-coordinate of the first anomaly point.

XS is the distance between any two successive anomaly point x-coordinates.

YS is the distance between any two successive anomaly point y-coordinates.

XCD is the x-coordinate of the first rectangular prism.

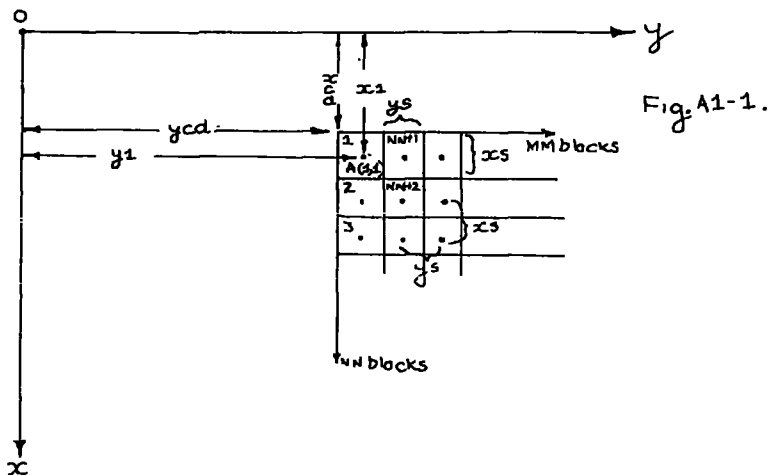
YCD is the y-coordinate of the first rectangular prism.

US is the depth to the top surface of the body.

RO is the density contrast of the body.

AO is the gravity anomaly array (AO (x,y)).

'MODELNAME' as in GRAVIT 1.



GENERAL NOTES: As for GRAVIT 1.

SUBROUTINE:

PRISM: Computes (a) the kernel matrix and (b) the gravity

GRAVIT:PROC OPTIENS (HAI); /\* GLESS LAVING 1970 \*/

```
CRAVITB:PROC OPTIENS (HAI); /* GLESS LAVING 1970 */
DECL (P,M,AB,NN,MM,C,B,ITER,II,IER) FIXED BIN(31);
GET LIST (H,M,NN,MM,ITER);
BEGIN;
DECL ((XL,YL)(N*M),(SX,SY,D1,D2,TT,CTT)(MM*MM),A(B),(AO,AC)
(N*M),MAO(N*M,1),G(NN*MM,1),(X,XX,Y,YY,Z,ZZ,XCD,YCD,XL,YL,XS,
YS,RO,US),KK(M*MM,M*M),AUX(2*N*MM,1)) FLOAT BIN, MODELNAME
CHAR(60) VARYING, IPIV(M*MM) FIXED BIN(31);
GET LIST (XL,YL,XS,YS,XCD,YCD,US,RO,AO);
DO I=1 TO N*M; MAO(I,1)=AO(I); END;
GET LIST (MODELNAME);
C=N*M; F=NN*MM;
DO I=1 TO B; TT(I)=US; CTT(I)=TT(I)+0.001;
END;
DO I=1 TO N;
IF I=1 THEN XL(I)=X; ELSE XL(I)=XL(I-1)+XS;
END;
DO J=1 TO M-1;
DO I=1 TO N;
XL(I+J*M)=XL(I);
END; END;
DO I=1 TO N;
YL(I)=Y;
END;
AB=(M-1)*N;
DO I=1 TO AB;
YL(I+N)=YL(I)+YS;
END;
DO I=1 TO NN;
IF I=1 THEN SX(I)=XCD; ELSE SX(I)=SX(I-1)+XS;
END;
DO J=1 TO MM-1;
DO I=1 TO NN;
SX(I+J*MM)=SX(I);
END; END;
DO I=1 TO NN;
SY(I)=YCD;
END;
AB=(MM-1)*NN;
DO I=1 TO AB;
SY(I+MM)=SY(I)+YS;
END;
ROH=1; AI=0.0001;
CALL PRISM(C,B,KK,XL,YL,SX,SY,TT,CTT,ROH,AC,XS,YS);
AC=0; II=1;
CALL LLSQ(KK(1,:),MAO(1,1),C,B,II,G(1,1),IPIV(1),AI,IER,
AUX(1,1));
PUT SKIP LIST ('SURFACE MASSES');
PUT LIST (G);
DO I=1 TO B;
CTT(I)=(TT(I)+G(I,1)/RO)*0.001;
IF CTT(I)<TT(I)+0.001 THEN CTT(I)=TT(I)+0.001; END;
CALL PRISM(C,B,KK,XL,YL,SX,SY,TT,CTT,RO,AC,XS,YS);
DO I=1 TO C;
MAO(1,1)=AO(I)-AC(I); END;
DO AA=1 TO ITER;
```



```

DO I=1 TO B;
D1(I)=CTT(I); D2(I)=CTT(I)+0.1; END; I1=1;
CALL PRISM(C,B,KK,XL,YL,SX,SY,D1,D2,ROH,AC,XS,YS);
AC=0; AI=0.001;
CALL LLSQ(KK(1,1),MAQ(2,1),C,B,I1,G(1,1),IPIV(1),AI,IER,
AUX(1,1));
PUT SKIP LIST ('SDENS');
PUT LIST(G);
DO I=1 TO B;
CTT(I)=CTT(I)+(G(I,1)/RO)*0.1;
IF CTT(I)<TT(I)+0.001 THEN CTT(I)=TT(I)+0.001; END;
CALL PRISM(C,B,KK,XL,YL,SX,SY,TT,CTT,RO,AC,XS,YS);
DO I=1 TO C;
MAQ(I,1)=AD(I)-AC(I); END;
PUT LIST ( MODELNAME ) PAGE;
PUT EDIT('ESTIMATE',AA,'DENSITY=',RO,'GM/CC') (A,F(3),X(3),A,
F(4,2),A) SKIP(2);
PUT EDIT ('BLOCK','X-LEFT','X-RIGHT','Y-LEFT','Y-RIGHT','TOP',
'BOTTOM') (A,X(7),A,X(7),A,X(7),A,X(7),A,X(7),A,X(7),A) SKIP(2);
DO I=1 TO B;
PUT EDIT (I,SX(I),SX(I)+XS,SY(I),SY(I)+YS,TT(I),CTT(I))
(F(3),6 F(14,3)) SKIP(1); END;
PUT LIST('X-LOCATION Y-LOCATION OBSERVED CALCULATED
RESIDUAL') SKIP(4);
DO I=1 TO C;
PUT EDIT (XL(I),YL(I),AD(I),AC(I),MAQ(I,1)) (F(7,3),X(8),
F(7,3),X(4),F(10,2),F(13,2),X(7),F(11,2)) SKIP (1);
END;
PUT LIST ('END OF MODEL') SKIP(3);
END;
PRISM:PROC(C,B,KK,XL,YL,SX,SY,T,CT,ROD,AC,XS,YS);
DCL A(8) FLOAT BIN;
DCL (C,B) FIXED BIN (31);
DCL (IT,CT)(B) FLOAT BIN,ROD FLOAT BIN;
DCL (KK(B,C),(SX,SY)(B),(XL,YL,AC)(C)) FLOAT BIN;
AC=0; KK=0;
DO I=1 TO C;
DO K=1 TO B;
Z=T(K); ZZ=CT(K);
IF SX(K)>=XL(I) THEN DO;
X=ABS(SX(K)-XL(I));
IF X=0 THEN X=0.001;
XX=X+XS; END; ELSE DO;
X=ABS(XL(I)-SX(K)-XS);
IF X=0 THEN X=0.001;
XX=X+XS;
END;
IF SY(K)>=YL(I) THEN DO;
Y=ABS(SY(K)-YL(I)); IF Y=0 THEN Y=0.001;
YY=Y+YS; END; ELSE DO;
Y=ABS(YL(I)-SY(K)-YS);
IF Y=0 THEN Y=0.001;
YY=Y+YS; END;
DDO=SQRT(X**2+Y**2+ZZ**2); DDT=SQRT(XX**2+YY**2+ZZ**2);

```

```
GRAVIT3:PROC OPTIONS (MAIN); /* GESS LAVING 1970 */
```

```
OTT=SQRT(X**2+YY**2+ZZ**2); OTD=SQRT(X**2+YY**2+Z**2);  
TTT=SQRT(XX**2+YY**2+ZZ**2); TTD=SQRT(XX**2+YY**2+Z**2);  
TDD=SQRT(XX**2+Y**2+Z**2); TCT=SQRT(XX**2+Y**2+ZZ**2);  
  A(1)=ATAN(XX*Y,Z*TD); A(2)=ATAN(X*YY,Z*CTD);  
  A(3)=ATAN(X*Y,Z*DD); A(4)=ATAN(XX*YY,Z*TTD);  
  A(5)=ATAN(X*Y,ZZ*DD); A(6)=ATAN(XX*YY,ZZ*TTT);  
  A(7)=ATAN(XX*Y,ZZ*TD); A(8)=ATAN(X*YY,ZZ*OTT);  
ANS=6.66667*ROD*(XX*LOG(((Y+TD)*(Y+TD))/((Y+TD)*(Y+TT))) +  
X*LOG(((Y+DD)*(Y+DD))/((Y+DD)*(Y+DD))) +  
YY*LOG(((X+TD)*(X+TD))/((X+DD)*(X+TT))) +  
Y*LOG(((X+DD)*(X+TD))/((X+DD)*(X+TD))) +  
  Z*(A(1)+A(2)-A(3)-A(4))+ZZ*(A(5)+A(6)-A(7)-A(8)));  
  KK(K,1)=ANS;  
AC(1)=AC(1)+ANS;  
END;  
END;  
END PRISM;  
END GRAVIT3;
```

anomaly due to each model after each iteration.

N.B. N,M,NN,MM, < 15 for an I.B.M. 360.

PROGRAM NAME: GRAVIT 4

FUNCTION: This program computes the space form of a three dimensional body with outward sloping contacts producing a given two dimensional gravity anomaly. One point on the top surface of the body and the uniform density contrast must be specified.

INPUT FORMAT:

N	}	as in GRAVIT 3
M		
NN		
MM		
ITER		
X1		
Y1		
XS		
YS		
XCD		
YCD		
US		
RC	}	as in GRAVIT 3
AC		
BLOCK		
'MODELNAME'		

DATA NOTES:

US is the depth to the top surface of the specified block.

BLOCK is the number of the specified block counting in the x-direction.

OTHER notes as for GRAVIT 3.

GRAVJ14:PROC OPTIONS (MAIN); /\* GESS LAVING 1970 \*/

```
GRAVIT4:PROC OPTIONS (MAIN); /* GESS LAVING 1970 */
DCL (N,M,AB,NI,MM,C,P,ITER,II,IER) FIXED BIN(31);
DCL MODELNAME CHAR (60) VARYING;
GET LIST (MODELNAME);
GET LIST (N,M,NI,MM,ITER);
BEGIN;
DCL LLL FIXED BIN;
DCL ((XL,YL,AD,AC)(N*M),(SX,SY,D1,D2,TT,CTT)(NN*MM),MAO(N*M,1)
,G(NN*MM,1),KK(NN*MM,N*M),AUX(2*NN*MM,1),(XCD,YCD,X1,Y1,XS,YS,
RD,US))FLOAT BIN,MODELNAME CHAR(60) VARYING,IPIV(NN*MM)
FIXED BIN(31),BLOCK FIXED BIN;
GET LIST (X1,Y1,XS,YS,XCD,YCD,US,RD,AD,BLOCK);
DO I=1 TO N*M; MAO(I,1)=AD(I); END;
LLL=10000;
C=N*M; B=NN*MM;
DO I=1 TO B; TT(I)=US; CTT(I)=US+0.001; END;
DO I=1 TO N;
IF I=1 THEN XL(I)=X1; ELSE XL(I)=XL(I-1)+XS;
END;
DO J=1 TO M-1;
DO I=1 TO M;
XL(I+J*N)=XL(I);
END; END;
DO I=1 TO M;
YL(I)=Y1;
END;
AB=(M-1)*N;
DO I=1 TO AB;
YL(I+N)=YL(I)+YS;
END;
DO I=1 TO NN;
IF I=1 THEN SX(I)=XCD; ELSE SX(I)=SX(I-1)+XS;
END;
DO J=1 TO MM-1;
DO I=1 TO MM;
SX(I+J*NN)=SX(I);
END; END;
DO I=1 TO NN;
SY(I)=YCD;
END;
AB=(MM-1)*NN;
DO I=1 TO AB;
SY(I+MM)=SY(I)+YS;
END;
RDH=1; AJ=0.0001;
CALL PRISM(C,B,KK,XL,YL,SX,SY,TT,CTT,RDH,AC,XS,YS,LLL);
AC=0; II=1;
CALL LSQ(KK(1,1),MAO(1,1),C,B,II,G(1,1),IPIV(1),AI,IER,
AUX(1,1));
PUT SKIP LIST ('SURFACE MASSES');
PUT LIST (G);
CTT(BLOCK),D2(BLOCK)=US+(G(BLOCK,1)/RD)*0.001;
DO I=1 TO B;
IF I=BLOCK THEN DO;
D2(I),CTT(I)=CTT(BLOCK);
D1(I),TT(I)=CTT(I)-(G(I,1)/RD)*0.001;
```

RAVIT4:PREC OPTIONS (MAIN); /\* GESS LAVING 1970 \*/

```
IF TT(I)<0.001 THEN TT(I)=0.001;
IF TT(I)>CTT(I)-0.001 THEN TT(I)=CTT(I)-0.001;
END; END;
CALL PRISM(C,B,KK,XL,YL,SX,SY,TT,CTT,RO,AC,XS,YS,LLL);
DO I=1 TO C;
MAO(I,1)=AO(I)-AC(I); END;
DO AA=1 TO ITR;
DO I=1 TO B;
IF I=BLOCK THEN DO;
D1(I)=TT(I)-0.001;
D2(I)=TT(I);
END;
ELSE DO;
D1(I)=CTT(I);
D2(I)=CTT(I)+0.001;
END; END;
CALL PRISM(C,B,KK,XL,YL,SX,SY,D1,D2,ROH,AC,XS,YS,BLOCK);
AC=0; AI=0.0001;
CALL LLSQ(KK(I,1),MAO(I,1),C,B,II,G(I,1),IPIV(I),AI,IER,
AUX(I,1));
PUT SKIP LIST ('SDENS');
PUT LIST(G);
D1(BLOCK)=CTT(BLOCK);
CTT(BLOCK),D2(BLOCK)=CTT(BLOCK)+(G(BLOCK,1)/RO)*0.001;
DO I=1 TO B;
IF I=BLOCK THEN DO;
TT(I),D1(I)=TT(I)-(G(I,1)/RO)*0.001;
CTT(I)=CTT(BLOCK);
END;
IF TT(I)>CTT(BLOCK)-0.001 THEN TT(I),D1(I)=CTT(BLOCK)-0.001;
IF TT(I)<0.001 THEN TT(I),D1(I)=0.001;
D2(I)=CTT(BLOCK);
END;
D1(BLOCK)=US;
CALL PRISM(C,B,KK,XL,YL,SX,SY,TT,CTT,RO,AC,XS,YS,LLL);
DO I=1 TO C;
MAO(I,1)=AO(I)-AC(I); END;
PUT LIST (MODELNAME) PAGE;
PUT EDIT ('ESTIMATE',AA,'DENSITY=',RO,'GM/CC') (A,F(3),X(3),A,
F(4,2),A) SKIP(2);
PUT EDIT ('BLOCK','X-LEFT','X-RIGHT','Y-LEFT','Y-RIGHT','TOP',
'BOTTOM') (A,X(7),A,X(7),A,X(7),A,X(7),A,X(7),A) SKIP(2);
DO J=1 TO B;
PUT EDIT (I,SX(I),SX(I)+XS,SY(I),SY(I)+YS,TT(I),CTT(I))
(F(3),6 F(14,3)) SKIP(1); END;
PUT LIST ('X-LOCATION' Y-LOCATION OBSERVED CALCULATED
RESIDUAL') SKIP(4);
DO I=1 TO C;
PUT EDIT (XL(I),YL(I),AO(I),AC(I),MAO(I,1)) (F(7,3),X(8),
F(7,3),X(4),F(10,2),F(13,2),X(7),F(11,2)) SKIP (1);
END;
PUT LIST ('END OF MODEL') SKIP(3);
END;
PRISM:PROC (C,B,KK,XL,YL,SX,SY,T,CT,RO,AC,XS,YS,BLOCK);
```

```

DCL I LOCK FIXED BIN ;
      DCL A(8) FLOAT BIN;
DCL (C,B) FIXED BIN (31);
      DCL (T,CT)(B) FLOAT BIN, RCC FLOAT BIN;
      DCL (KK(B,C),(SX,SY)(B),(XL,YL,AC)(C)) FLOAT BIN;
AC=0;
  DO I=1 TO C;
    DO K=1 TO B;
      Z=T(K); ZZ=CT(K);
      IF K=BLCK THEN DO;
        IF SX(1)>=XL(1) THEN DO;
          X=ABS(SX(1)-XL(1)); IF X=0 THEN X=0.001;
          XX=ABS(XL(1)-SX(B)-XS); END;
        ELSE DO;
          X=ABS(XL(1)-SX(B)-XS); IF X=0 THEN X=0.001;
          XX=ABS(XL(1)-SX(1)); END;
        IF SY(1)>=YL(1) THEN DO;
          Y=ABS(SY(1)-YL(1)); IF Y=0 THEN Y=0.001;
          YY=ABS(YL(1)-SY(B)-YS); END;
        ELSE DO;
          Y=ABS(YL(1)-SY(B)-YS); IF Y=0 THEN Y=0.001;
          YY=ABS(YL(1)-SY(1)); END;
        END;
      ELSE DO;
        IF SX(K)>=XL(1) THEN DO;
          X=ABS(SX(K)-XL(1));
          IF X=0 THEN X=0.001;
          XX=X+XS; END; ELSE DO;
          X=ABS(XL(1)-SX(K)-XS);
          IF X=0 THEN X=0.001;
          XX=X+XS;
        END;
        IF SY(K)>=YL(1) THEN DO;
          Y=ABS(SY(K)-YL(1)); IF Y=0 THEN Y=0.001;
          YY=Y+YS; END; ELSE DO;
          Y=ABS(YL(1)-SY(K)-YS);
          IF Y=0 THEN Y=0.001;
          YY=Y+YS; END;
        END;
      ODD=SQRT(X**2+Y**2+Z**2); ODT=SQRT(X**2+Y**2+ZZ**2);
      OTT=SQRT(X**2+YY**2+ZZ**2); OTO=SQRT(X**2+YY**2+Z**2);
      TTT=SQRT(XX**2+YY**2+ZZ**2); TTC=SQRT(XX**2+YY**2+Z**2);
      TDD=SQRT(XX**2+Y**2+Z**2); TOT=SQRT(XX**2+Y**2+ZZ**2);
      A(1)=ATAN(XX*Y,Z*ODD); A(2)=ATAN(X*YY,Z*OTO);
      A(3)=ATAN(X*Y,Z*ODT); A(4)=ATAN(XX*YY,Z*TTD);
      A(5)=ATAN(X*Y,ZZ*ODT); A(6)=ATAN(XX*YY,ZZ*TTT);
      A(7)=ATAN(XX*Y,ZZ*TDD); A(8)=ATAN(X*YY,ZZ*OTT);
      ANS=(0.66667*RCC*(XX*LOG(((Y+TDD)*(Y+TDD))/((Y+TDD)*(YY+TTT)))+
        X*LOG(((Y+ODD)*(YY+OTT))/((YY+ODD)*(Y+ODT)))+
        YY*LOG(((XX+TDD)*(X+OTT))/((X+ODD)*(XX+TTT)))+
        Y*LOG(((X+ODD)*(XX+TOT))/((X+ODT)*(XX+TDD)))+
        Z*(A(1)+A(2)-A(3)-A(4))+ZZ*(A(5)+A(6)-A(7)-A(8)));
      KK(K,I)=ANS;
      AC(I)=AC(I)+ANS;
    
```

GRAVIT4:PPCC OPTICS (MAIN); /\* GPSS LAMTIG 1970 \*/

END;

END;

END PRISM;

END GRAVIT4;

PROGRAM NAME: VARYIT

FUNCTION: This program determines the space form of a two dimensional body when the top surface is too deep to use the GRAVIT 1 or GRAVIT 2 programs. The program can also handle more than one body with different density contrasts (of either sign) resulting in interfering anomalies or a body with a know lateral variation in density. The top surface and density contrast of the body or bodies must be specified.

INPUT FORMAT:

CYCLE

'MODELNAME'

ITER

LIMIT

N

M

P3

BB

TH

RO

TT

XX1

Y1

Y2.

DATA NOTES

CYCLE

'MODELNAME' as in GRAVIT 1

ITER

LIMIT defines the required goodness of fit to the observed anomaly. (Try 0.5 mgal).



N as in GRAVIT 1

M " " "

P3 is the number of sets of N density contrasts for each block.

BB is the reciprocal of the fraction of a block width required for good body resolution (e.g. if 1/10th of blockwidth is necessary then BB = 10).

TH = 1 if block-shifting is required.

RO is a P3 x N array of block density contrasts.

TT

XX1 as for GRAVIT 1

Y1

Y2

Other notes as for GRAVIT 1.

IT:PROC OPTIONS (MAIN);

```
VARYIT:PROC OPTIONS (MAIN);
  DCL (LIMIT) FLOAT BIN,
      (ITERATION,COUNT,N,M,P3,RR,W,BB,TH,ww)
  FIXED BIN (31),
  NPAGE: FIXED DECIMAL INITIAL (1),
  TITL CHAR (26) INITIAL ('VAR-DENS-BODY'),
  UNITS CHAR (23) INITIAL ('MGAL,METRES,GM/CU CM'),
  MODELNAME CHAR (60) VARYING,
  PAGERWORD CHAR (4) INITIAL ('PAGE');
  PUT EDIT (TITL,PAGERWORD,NPAGE) (A,X(84),A,F(3)) PAGE;
  PUT EDIT (UNITS)(A) SKIP(2);
  SET LIST (CYCLE);
LOOP1:DO COUNT =1 TO CYCLE;
  GET LIST (MODELNAME);
  NPAGE=NPAGE+1;
  GET LIST (ITERATION,LIMIT,N,M,P3,RR,BB,TH) ;
  TH=TH*1000;
BEGIN1: DCL (MAC(M,1),SDENS(N,1),KK(N,M),AG(M),AC(M),POS(M),
  Y1(N),Y2(N),D1(N),D2(N),CTT(N),TT(N),LSIDE(N),RSIDE(N),
  SN(N),TY(N),R(M),DO(M,1),GG(N,1),MN(N,N),US(RR),RO(P3,N),
  XX1(N+1)) FLOAT BIN,
  (ROUND,S) FLOAT BIN,
  (FLOW,LINES,K,J,J,AA,CONTROL,TTT,Q) FIXED BIN;
  ROUND=0.00001;
  /*
  DO I=1 TO P3;
  DO J=1 TO N;
  GET LIST (RO(I,J));
  END; END;
  DO I=1 TO N;
  GET LIST (TT(I));
  TT(I)=TT(I)*1000;
  END;
  /*
  DO I=1 TO M;
  GET LIST (POS(I),MAC(I,1));
  POS(I)=POS(I)*1000;
  AG(I)=MAC(I,1) ;
  END;
  /*
S1: DO I=1 TO N+1;
  IF I=N+1 THEN DO;
  GET LIST (XX1(I));
  END;
  ELSE DO;
  GET LIST (XX1(I),Y1(I),Y2(I));
  END S1;
  XX1=XX1*1000; Y1=Y1*1000; Y2=Y2*1000;
  /*
REPEAT:DO W=0 TO BB;
  DO I=1 TO N+1;
  IF W=0 THEN WW=0;
  ELSE WW=1;
  XX1(I)=XX1(I)+(WW*TH)/(BB+1);
  IF I=1 THEN DO;
  RSIDE(I-1)=XX1(I);
```

VARY IT; PROC OPTIONS (MAIN);

```
END;
IF I=N+1 THEN DO;
LSIDE(I)=XX1(I);
END; END;
/*
DO Q=1 TO P;
DO I=1 TO N;
TT(I),D1(I)=TT(I);
CTT(I),D2(I)=TT(I)+1;
END;
/*
DO I=1 TO M;
MAO(I,1)=AO(I);
AC(I)=0;
END;
/*
PUT EDIT (MODELNAME,PAGEWORD,NPAGE) (A,X(50),A,F(3))
PAGE;
NPAGE=NPAGE+1;
AA=1;
CALL FORM (N,M,MAO,KK,POS,LSIDE,RSIDE,SDENS,Y1,Y2,D1,D2,
FINISH,TY,SN,AA);
DO I=1 TO N;
D2(I),CTT(I)=TT(I)+SDENS(I,1)/RO(Q,1);
IF CTT(I)<TT(I)+1 THEN D2(I),CTT(I)=TT(I)+1;
END;
IF FLOW=100 THEN DO;
CALL CALCUL (N,M,POS,LSIDE,RSIDE,RO(Q,*),Y1,Y2,D1,D2,AC,
TY,SN);
CALL RESIDUAL (M,MAO,AO,AC,LIMIT,CONTROL,FLOW);
END;
S2:DO AA=1 TO ITERATION;
IF FLOW=100 THEN DC;
DO I=1 TO N;
D1(I)=TT(I);
D2(I)=CTT(I);
END; END;
DO I=1 TO N;
D1(I)=CTT(I);
D2(I)=CTT(I)+1;
END;
CALL FORM (N,M,MAO,KK,POS,LSIDE,RSIDE,SDENS,Y1,Y2,D1,D2,
FINISH,TY,SN,AA);
S3:DO I=1 TO N;
D1(I)=CTT(I);
IF FLOW=100 THEN DC ;
IF AA=1 THEN DO;
D2(I),CTT(I)=TT(I)+(CTT(I)-TT(I))*(SDENS(I,1)/RO(Q,1));
D1(I)=TT(I);
END;
ELSE DO;
IF ABS(SDENS(I,1)-RO(Q,1))>0.001 THEN
CTT(I),D2(I)=CTT(I)+(CTT(I)-TT(I))*((SDENS(I,1)-RO(Q,1))
/RO(Q,1));
```

VARY IF: PROC OPTIONS (MAIN);

```
END; END;
ELSE CTT(I),D2(I)=CTT(I)+SDENS(I,1)/RO(Q,1);
IF CTT(I)<TT(I) THEN CTT(I),D2(I)=TT(I)+1;
END S3;
CALL CALCUL (N,H,POS,LSIDE,RSIDE,RC(Q,*),Y1,Y2,D1,D2,
AC,TY,SN);
IF AA=3 & LINES=100 THEN FLOW=0;
CALL RESIDUAL (M,MAC,AC,AC,LIMIT,CONTROL,FLOW);
S=0; IF FLOW =0 THEN DO;
DO I=1 TO M;
R(I)=MAC(I,1)**2;
S=S+R(I);
END; END;
/*
IF AA=ITERATION THEN DO;
PUT EDIT (PASSWORD,NPAGE)(X(110),A,F(3)) PAGE;
HPAGE =NPAGE+1;
END;
PUT EDIT ('MODEL',CCUNT)(A,F(2)) SKIP(2);
PUT EDIT ('ESTIMATE',AA) (A,F(3)) SKIP(2);
PUT LIST
('CLOCK LEFT RIGHT MED UPPER LOWER DENSITY')
SKIP(2);
DO I=1 TO M;
PUT EDIT (I,LSIDE(I),RSIDE(I),(LSIDE(I)+RSIDE(I))/2,
TT(I),CTT(I),RD(Q,1)) (F(3),5 F(9,0),F(9,2)) SKIP(1);
END;
PUT LIST
('LOCATION OBSERVED CALCULATED RESIDUAL') SKIP(4);
DO I=1 TO M;
IF FLOW=100 THEN
PUT EDIT (POS(I),AO(I),AC(I),AO(I)-AC(I))
(F(7,0),F(10,1),F(13,1),F(11,1)) SKIP(1);
ELSE
PUT EDIT (POS(I),AC(I),AC(I),MAC(I,1))
(F(7,0),F(10,2),F(13,1),F(11,1)) SKIP(1);
END;
PUT EDIT('VARIANCE=',S/M) (A,F(4,2)) SKIP(4);
IF CONTROL=C THEN GO TO FINISH;
END S2;
FINISH: PUT EDIT ('END OF MODEL',CCUNT) (A,F(3)) SKIP (3);
END; END;
END LOOP1;
PUT LIST ('END OF DATA') SKIP(3);
PUT PAGE;
STOP;
ENDCOR: PROCEDURE(LOO,PP,UU,VV,XX,YY);
DCL(LOO,PP,UU,VV,XX,YY)FLDAT BINARY ;
/*
IF VV<.1 THEN LOO=1 ;
ELSE DO;
IF UU >YY THEN LOO=1/SQRT(1+UU/VV**2);
ELSE LOO=1/SQRT(1+YY/VV**2);
END;
END;
```

VARYI1:PROC OPTICS (MAIN);

```
/*
IF XX<0.1 THEN PP=1;
ELSE DO;
IF UU>YY THEN PP=1/SQRT(1+UU/XX**2);
ELSE PP=1/SQRT(1+YY/XX**2);
END;
END ENDCOR;
/*
```

```
-----
INVTAN:PROCEDURE(MM,D,PP,QQ);
DCL(MM,D,PP,QQ)FLOAT BINARY;
MM=QQ*QQ+D*PP;
IF MM=0 THEN MM=1.5708;
ELSE MM=ATAN((QQ*(PP-D))/MM);
IF MM<0 THEN MM=MM+3.14159;
END INVTAN;
/*
```

```
-----
CALCBLOCK:PROCEDURE(ATT,RHO,A,B,D,C,E,F,G,H,TY,SIG);
DCL(ATT,RHO,A,B,D,C,E,F,G,H,TY,SIG)FLOAT BINARY;
IF TY=0 THEN ATT=SIG*RHO*0.01334*((-A*0.5*LOG((A*A+C*C)
/(A*A+D*D))+B*0.5*LOG((B*B+C*C)/(B*B+D*D))+C*E-D*F)*((G+H)
)*0.5);
ELSE ATT=RHO*0.02668*(C-D)*F;
END CALCBLOCK;
/*
```

```
-----
SORTOUT:PROCEDURE(GEX,DE,X,LTX,RT,UP,LO,E1,E2,TYPE,SGN);
DCL(GEX,DE,X,LTX,RT,UP,LO,E1,E2,TYPE,SGN)FLOAT
BINARY, (X1,X2,C1,C2,F1,F2)FLOAT BINARY;
/*
X1=LTX-X;
X2=RT-X;
IF TYPE=0 THEN DO;
CALL ENDCOR(C1,C2,((X-D*0.5*(LTX+RT))**2+(UP**2)),E1,E2,
(((0.5*(RT+LTX)-LTX)*0.5)**2+(UP**2)));
END; ELSE DO;
CALL ENDCOR(C1,C2,((X-D*0.5*(LTX+RT))**2+(0.5*(UP+LO))**2),
E1,E2,(((0.5*(RT+LTX)-LTX)*0.5)**2+(0.5*(UP+LO))**2));
CALL INVTAN(F1,X1,X2,LO); END;
CALL INVTAN(F2,X1,X2,UP);
CALL CALCBLOCK(GEX,DE,X1,X2,UP,LO,F1,F2,C1,C2,TYPE,SGN);
END SORTOUT;
/*
```

```
-----
DECIDE:PROCEDURE(AB,T1,T2,SNE,TIM);
DCL AB FIXED BINARY(31),
(T1(AB),T2(AB),SNE(AB),TIM(AB))FLOAT BINARY,
I FIXED BINARY, X FLOAT BINARY;
/*
```

VAR Y1 T:PROC LPTI CHS (MAIN);

```
SHE=1 ;
TIM=1 ;
S1:DO I=1 TO AB;
  IF (0.5*(T1(I)+T2(I)) >=2*ABS(T1(I)-T2(I))) |
  ((ABS(T1(I)-T2(I))<=1) & (T1(I)<2.51) & (T2(I)<2.51))
  THEN S2: DO;
    TIM(I)=0 ;
    IF (T2(I)>T1(I)) & (T1(I)<2.51) THEN
S3:DO ; X=0.5*(T2(I)-T1(I));
    T1(I)=2.5; T2(I)= T1(I)+X;
    END S3;
    ELSE S4: DO;
    IF (T2(I)<T1(I)) & (T2(I)<2.51) THEN
S5: DO; X=0.5*(T1(I)-T2(I));
    T2(I)= 2.5 ; T1(I)=T2(I)+X ;
    END S5; ELSE
S6: DO;
    T1(I)= 0.5*( T1(I) + T2(I));
    END S6; END S4; END S2;
    ELSE
S7: DO;
    IF T2(I)<T1(I) THEN S8:
    DO; X=T1(I); SNE(I)=-1 ;
    T1(I)=T2(I);
    T2(I)=X;
    END S8; END S7; END S1;
  END DECIDE ;
/*
```

---

```
*/
CALCUL:PROCEDURE (A,R,LOC,LS,RS,H,L1,L2,DD,CDD,ACS,T,SI);
  DCL(A,R,I,J) FIXED BIN(31), CAL FLOAT BIN,
  (LS(A),RS(A),L1(A),L2(A),DD(A),CDD(A),ACS(R),LOC(R),SI(A)
  ,T(A),H(A))FLOAT BIN;
  CALL DECIDE (A,DD,CDD,SI,T);
S1:DO I=1 TO R;
S2:DO J=1 TO A;
  IF CDD(J)=-DD(J) THEN
S3:DO;
  CALL SORTOUT(CAL,H(J), LOC(I),LS(J),RS(J),DD(J),CDD(J),
  L1(J),L2(J),T(J),SI(J));
  ACS(I)=ACS(I)+CAL;
  END S3; END S2; END S1;
END CALCUL;
/*
```

---

```
*/
FORM:PROC(A,R,B,KK,LOC,LS,RS,G,L1,L2,DD,CDD,LL,T,SI,
  TIMEX);
  DCL(A,R,IER,I1) FIXED BIN(31), (I,J,K,D2) FIXED BIN,
  (H,DEFS,D3) FLOAT BINARY ,
  LL LABEL ,
  IPIV(A) FIXED PIN(31), AUX(2,A) FLOAT BIN,
  (P(R,I),KK(A,R),KN(A,A),GG(A,1),
```

VARY IT:PROC OPTIONS (MAIN);

```
OO(R,1),LOC(R),LS(A),RS(A)
,G(A,1),L1(A),L2(A),DD(A),CDD(A),T(A),SI(A),P(A),
FH(A,R),C(R,1))
FLOAT BIN ;
DENS=1;
CALL DECIDE (A,DD,CDD,SI,T);
S1:DO J=1 TO A;
S2:DO I=1 TO R;
IF DD(J)<2.51 & ABS(LOC(I)-LS(J)) <0.1 | DD(J)<2.51
& ABS(LOC(I) - RS(J))< 0.1 THEN LOC(I) =LOC(I)+1 ;
CALL SORTOUT (KK(J,1),DENS,LOC(I),LS(J),RS(J),DD(J),
CDD(J),L1(J),L2(J),T(J),SI(J));
END S2; END S1;
HH=KK ; C=B ;
II=1 ; AI=0.0001 ;
CALL LLSQ(HH(1,1),C(1,1),R,A,II,S(1,1),IPIV(1),AI,IER,
AUX(1,1));
IF IER /= 0 THEN DO ;
PUT LIST ('PROC UNSUCCESSFUL') SKIP(2);
GO TO LL ;
END ;
IF TIME X=1 THEN DO;
PUT LIST ('SURFACE MASS') SKIP(3);
PUT EDIT ((G(I,1) DO I=1 TO N)) (8 F(12,4)) SKIP(1);
END;
END FORM ;
/*
```

\*/

```
RESIDUAL:PROCEDURE (R,MA,D,C,LIM,CON,FLOW);
DCL R FIXED BIN (31), (CON,I,FLOW) FIXED BIN,
LIM FLGAT BINARY,
(MA(R,1),D(R),C(R)) FLOAT BINARY ;
CON=0;
DO I=1 TO R ;
MA(I,1)=D(I)-C(I);
IF ABS(MA(I,1))>LIM THEN CON=1;
IF FLOW=100 THEN MA(I,1)=MA(I,1)+C(I);
END RESIDUAL;
END VARYIT;
```

PROGRAM NAME: PRISM

FUNCTION: This program computes the gravity anomaly due to any three dimensional body by dividing the body into a set of rectangular prisms.

INPUT FORMAT:

N

M

NN

MM

X1

Y1

XS

YS

XCD

YCD

D1

D2

RO

as in GRAVIT 3

DATA NOTES

D1 and D2 are the top and bottom surface (NN x MM) arrays.

RO is the density contrast of the body.



PRISM:PROC OPTIONS(MAIN);

```
PRISM:PROC OPTIONS(MAIN);
DCL (I,M,AB,NN,C,B,ITER,I,IER) FIXED BIN(31);
GET LIST(N,I,NN,MM);
BEGIN; DCL ((XL,YL) (N*MM), (SX,SY,DZ,D1) (NN*MM) FLOAT BIN,
A(B) FLOAT BIN, (XX,X,YY,Y,ZZ,Z,XCD,YCD,X1,Y1,XS,YS,RO)) FLOAT
BIN; DCL AC(N*M) FLOAT BIN; AC=0;
GET LIST (X1,Y1,XS,YS,XCD,YCD,D1,D2,RO);
DO I=1 TO N;
IF I=1 THEN XL(I)=X1; ELSE XL(I)=XL(I-1)+XS;
END;
DO J=1 TO M-1;
DO I=1 TO N;
XL(I+J*I)=XL(I);
END; END;
DO I=1 TO N;
YL(I)=Y1;
END;
AB=(M-1)*N;
DO I=1 TO AB;
YL(I+I)=YL(I)+YS;
END;
DO I=1 TO NN;
IF I=1 THEN SX(I)=XCD; ELSE SX(I)=SX(I-1)+XS;
END;
DO J=1 TO MM-1;
DO I=1 TO NN;
SX(I+J*NN)=SX(I);
END; END;
DO I=1 TO NN;
SY(I)=YCD;
END;
AB=(MM-1)*NN;
DO I=1 TO AB;
SY(I+I)=SY(I)+YS;
END;
C=N*M; B=NN*MM;
DO I=1 TO C;
AC=0;
DO K=1 TO B;
Z=D1(K); ZZ=D2(K);
IF SX(K)>=XL(I) THEN DO;
X=ABS(SX(K)-XL(I));
IF X=0 THEN X=0.001;
XX=X+XS; END; ELSE DO;
X=ABS(XL(I)-SX(K)-XS);
IF X=0 THEN X=0.001;
XX=X+XS;
END;
IF SY(K)>=YL(I) THEN DO;
Y=ABS(SY(K)-YL(I)); IF Y=0 THEN Y=0.001;
YY=Y+YS; END; ELSE DO;
Y=ABS(YL(I)-SY(K)-YS);
IF Y=0 THEN Y=0.001;
YY=Y+YS; END;
DDD=SQRT(X**2+Y**2+Z**2); CDT=SQRT(X**2+Y**2+ZZ**2);
OTT=SQRT(X**2+YY**2+ZZ**2); OTD=SQRT(X**2+YY**2+Z**2);
```

```
PRISM:PRCC OPTIONS(MAIN);
```

```
TTT=SQRT(XX**2+YY**2+ZZ**2); TTD=SQRT(XX**2+YY**2+Z**2);
TCC=SQRT(XX**2+Y**2+Z**2); TOT=SQRT(XX**2+Y**2+ZZ**2);
A(1)=ATAN(XX*Y,Z*TOO); A(2)=ATAN(X*YY,Z*CTC);
A(3)=ATAN(X*Y,Z*OOT); A(4)=ATAN(XX*YY,Z*OTO);
A(5)=ATAN(X*Y,ZZ*OOT); A(6)=ATAN(XX*YY,ZZ*TTT);
A(7)=ATAN(XX*Y,ZZ*TOT); A(8)=ATAN(X*YY,ZZ*OTT);
ANS=6.66667*RO*(XX*LOG(((Y+TD)*(Y+TOT))/((Y+TOO)*(YY+TTT)))+
X*LOG(((Y+OCC)*(YY+OTT))/((YY+OTO)*(Y+OOT)))+
YY*LOG(((X+TTO)*(X+CTT))/((X+OTC)*(XX+TTT)))+
Y*LOG(((X+OOT)*(XX+TOT))/((X+OOT)*(XX+TCC)))+
Z*(A(1)+A(2)-A(3)-A(4))+ZZ*(A(5)+A(6)-A(7)-A(8)));
AC(I)=AC(I)+ANS;
END;
PUT LIST (AC(I));
END;
END PRISM;
```

PROGRAM NAME: MAGGIT 1

FUNCTION: This program determines the angle of magnetisation and space form of a body with inward sloping contacts producing a given total field magnetic anomaly. The top surface of the body and the magnetisation contrast must be specified. The body is assumed to be two dimensional.

INPUT FORMAT:

CYCLE  
'MODELNAME'  
ITER  
N.  
M  
P3  
RO  
EI  
FA  
TT  
POS.  
AO  
XX1

DATA NOTES:

CYCLE is the number of anomalies to be analysed, therefore the number of sets of data.

'MODELNAME' each new set of data must commence with a name of up to 60 characters enclosed in single quotation marks..

ITER is the number of iterations performed by the program (try 10)

N is the number of blocks used for the initial equivalent layer approximation (see GENERAL NOTES).

M is the number of anomaly values specified ( $M \geq N$ ).

P3 is the number of magnetisation contrast to be tried for the model.

R0 is an array of P3 magnetisation contrasts.

FI is the dip of the earth's field vector in the direction of magnetic north at the location of the anomaly profile.

FA is the azimuth of the earth's field vector. That is the angle, measured in an anticlockwise sense, between the strike of the body and magnetic north.

TT is an array of N points defining the depth to each block of the initial equivalent layer approximation.

POS is an array of M x-coordinates defining the points at which the anomaly is specified.

A0 is an array of M magnetic anomalies at the x-coordinates defined by POS.

XX1 is an array of N+1 x-coordinates defining the margins of the blocks of the equivalent layer approximation.

Y1 and Y2 are arrays of length N defining the strike length of each block in either direction normal to the plane of the profile.

GENERAL NOTES: The user must define a set of blocks along the known or estimated top surface of the body. If the width of the structure is unknown the whole anomaly should be underlain by blocks. The depths

defined in TT are the depth to top surface at the mid point of each block. The width of any block must be at least as great as its depth.

Lengths are in kilometres, anomalies in gamma and magnetisations in e.m.u./cc.

OUTPUT:

For each anomaly analysed the angle of magnetisation, the model produced after the specified number of iterations and the observed, calculated and residual anomalies are printed out.

SUBROUTINES:

SUBR 1: Computes the vectors for the determination of the angle of body magnetisation.

SUBR 2:: Set up the trapezoidal coordinates.

SUBR 3: Computes the magnetic (total field) anomaly due to each model after each iteration.

SUBR 4: Computes the magnetic anomaly due to any equivalent layer block.

SUBR 5: Supervises the setting up of the kernel array and the least squares problem.

N.B. The origin of the coordinate system defining the body and anomaly must be at the more southerly end of the anomaly profile. i.e. x increases northwards.

MAGNET:PROC OPTIONS (MATH); /\* GESS LAVING 1970 \*/

```
MAGNET:PROC OPTIONS (MATH); /* GESS LAVING 1970 */
DCL (ITERATION,COUNT,N,M,P3,RE,11,1FR) FIXED BIN (41),
MODELNAME CHAR (60) VARYING;
  DCL (H1) FIXED BIN (31);
  GET LIST (CYCLE);
  LOOP1: DO COUNT=1 TO CYCLE;
  GET LIST (MODELNAME,ITERATION,N,M,P3);
  BEGIN; DCL (MAC(H,1), (AO,AC,POS) (M), (D1,D2,TT,CTT,LSIDE,RSIDE,
Z) (N), XX1 (H+1), (XX,BXX,ZB,ZT) (H+2), RDENS (2*N,1), RO (P3),
KK (2*N,H), SDENS (H,1), BR (H,M)) FLOAT BIN, (K,I,J,AA,Q) FIXED
BIN, (INC,ANG,ING,SN,SSN) FLOAT BIN;
  GET LIST (RO,FI,FA,TT,POS,AO);
  POS=POS*1000; TT=TT*1000;
  GET LIST (XX1);
  XX1=XX1*1000;
  DO I=1 TO N;
  Z(I)=XX1(I+1)-XX1(I); END;
  DO I=1 TO M;
  MAC(I,1)=AO(I);
  AC(I)=0;
  END;
  D1=TT; D2,CTT=TT+100;
  DO I=1 TO N+1;
  IF I=1 THEN RSIDE(I-1)=XX1(1);
  IF I=N+1 THEN LSIDE(I)=XX1(I);
  END;
  CALL SUBR1(N,M,MAC,KK,POS,LSIDE,RSIDE,RDENS,D1,D2,FINISH,
  AA,FI,FA);
  SN=0; SSN=0;
  DO I=1 TO N;
  SN=SN+RDENS(I,1); END;
  DO I=N+1 TO 2*H;
  SSN=SSN+RDENS(I,1); END;
  ING=ATAN2(SSN,SN);
  ANG=90;
  DO Q=1 TO P3;
  CALL SUBR5(H,M,MAC,BB,POS,LSIDE,RSIDE,SDENS,D1,D2,FINISH,
  AA,ANG,ING,FI,FA); DO I=1 TO N;
  D2(I),CTT(I)=TT(I)+(SDENS(I,1)/RO(Q))*SIND(ING);
  IF CTT(I)<TT(I)+1 THEN D2(I),CTT(I)=TT(I)+1; END;
  CALL SUBR2(N,D1,D2,ZT,ZB,XX1,XX,Z);
  DO I=2 TO H+1; BXX(I)=XX(I);
  END; BXX(1)=XX(1); BXX(N+2)=XX(N+2);
  CALL SUBR3(ZT,ZB,XX,POS,AC,RO(Q),N,M,FI,FA,ANG,BXX,
  ING); DO I=1 TO M; MAC(I,1)=AO(I)-AC(I); END;
  L1:DO AA=1 TO ITERATION; D1=CTT; D2=CTT+100;
  CALL SUBR5(N,M,MAC,BB,POS,LSIDE,RSIDE,SDENS,D1,D2,FINISH,
  AA,ANG,ING,FI,FA); DO I=1 TO N; D1(I)=TT(I);
  CTT(I),D2(I)=CTT(I)+(SDENS(I,1)/RO(Q))*SIND(ING);
  IF CTT(I)<TT(I) THEN CTT(I),D2(I)=TT(I)+1; END;
  CALL SUBR2(N,D1,D2,ZT,ZB,XX1,XX,Z);
  CALL SUBR3(ZT,ZB,XX,POS,AC,RO(Q),N,M,FI,FA,ANG,BXX,
  ING); DO I=1 TO M; MAC(I,1)=AO(I)-AC(I); END;
  IF AA=ITERATION THEN DO; PUT LIST (MODELNAME) PAGE;
  PUT EDIT ('MODEL',COUNT,'_',Q) (A,F(2),A,F(1))
  SKIP(2); PUT EDIT ('ESTIMATE',AA,'MAGNETISATION',
```

```

RO(0), 'PODY ANGLE=' , ANG, 'BCDY INCLINATION=' , INC,
'FIELD-ANGLE=' , FA, 'FIELD-INCLINATION=' , FI) (A, F(3), X(3), A,
F(6), X(2), A, F(3), X(2), A, F(3), X(2), A, F(3), X(2), A, F(3))
SKIP(2); PUT EDIT('SIDE', 'XTOP', 'XBOT', 'DTOP', 'DBOT')
(A, X(3), A, X(5), A, X(6), A, X(5), A) SKIP(2);
DO I=1 TO N+2; PUT EDIT(1, XX(I), BXX(I), ZT(I), ZB(I))
(F(3), 4 F(9, 0)) SKIP(1); END; PUT LIST
('LOCATION OBSERVED CALCULATED RESID')
SKIP(4); DO I=1 TO M;
PUT EDIT (POS (I), AO(I), AC(I), MAO(I, 1)) (F(7, 0), F(10, 1),
F(13, 2), F(11, 1)) SKIP(1); END L1;
FINISH: PUT EDIT('END OF MODEL', COUNT, '_ ', Q)
(A, F(3), A, F(1)) SKIP(3); END LOOP1;
PUT LIST ('END OF DATA') SKIP(3); STOP;
SUBR1:PROC(A, R, H, KK, LOC, LS, RS, G, DD, CDD, LL, TIMEX,
FI, FA);
DCL((B, C)(R, 1), (LS, RS, DD, CDD)(A), G(2*A, 1), KK(2*A, R),
LOC(R) FLOAT BIN, (A, R) FIXED BIN (31),
(1, J, TIMEX) FIXED BIN,
(XX, ZZ) (A, R) FLOAT BIN, H FIXED BIN (31),
(II, IER) FIXED BIN (31), IPIV(2*A) FIXED BIN (31),
AUX(4*A, 1) FLOAT BIN, (X, ANG, INC, FI, FA) FLOAT BIN, LL
LABEL; DO I=1 TO R; DO J=1 TO A; IF DD(J)<2.51 THEN DO;
X=0.5*(CDD(J)-DD(J)); DD(J)=2.5; CDD(J)=DD(J)+X;
IF ABS(LOC(I)-LS(J)) < 0.1 | ABS(LOC(I)-RS(J)) < 0.1 THEN
LOC(I)=LOC(I)+1; END; END; END;
ANG=90; INC=0;
CALL SUBR4(XX, LOC, DD, CDD, A, R, ANG, INC, FI, FA, LS, RS);
INC=90;
CALL SUBR4(ZZ, LOC, DD, CDD, A, R, ANG, INC, FI, FA, LS, RS);
DO I=1 TO A; DO J=1 TO R;
KK(I, J)=XX(I, J); KK(I+N, J)=ZZ(I, J); END; END; H=2*A;
C=B; II=1; AI=0.0001;
CALL LLSQ(KK(1, 1), C(1, 1), R, H, II, G(1, 1), IPIV(1), AI, IER,
AUX(1, 1));
IF IER/=0 THEN DO; PUT EDIT('PROC UNSUCCESSFUL', IER)
(A, F(3)) SKIP(2); GO TO LL; END; END SUBR1;
SUBR2:PROC(N, T, CT, ZT, ZB, LS, XX, V);
DCL (N) FIXED BIN (31);
DCL (LS(N+1), (T, CT)(N), (XX, ZT, ZB)(N+2)) FLOAT BIN,
V(N) FLOAT BIN;
DO I=2 TO N+1;
XX(I)=LS(I-1)+V(I-1)/2;
ZT(I)=T(I-1); ZB(I)=CT(I-1); END; XX(1)=LS(1)-V(1)/2;
XX(N+2)=LS(N+2)+V(N)/2;
ZT(1)=T(1); ZT(N+2)=T(N);
ZB(1)=ZT(1)+1; ZB(N+2)=ZT(N+2)+1; END SUBR2;
SUBR3:PROC(ZT, ZB, XS, LOC, ACS, RO, N, M, FI, FA, ANG, XB, INC);
DCL (N, M) FIXED BIN(31);
DCL((ZT, ZB, XS)(N+2), (EA, EB, LOC, ACS)(N), (X, Z, C, S)(2*N+5),
(ANG, INC, FI, FA, RO)) FLOAT BIN; ACS=0;
DCL XR(N+2) FLOAT BIN;
PX=COSD(INC)*SIND(ANG); PZ=SIND(INC); PXE=CUSD(FI);
PZE=SIND(FI); E=SIND(FA);

```

```

DO I=1 TO N+2; Z(I)=ZB(I); X(I)=XB(I); END;
DO J=N+2 BY -1 TO 1; Z(2*N+5-I)=ZT(I);
X(2*N+5-I)=XS(I); END; Z(2*N+5)=Z(1); X(2*N+5)=X(1);
DO J=1 TO M; EA(J)=0; EB(J)=0; DO I=1 TO 2*N+4;
H=SQRT((X(I)-X(I+1))**2+(Z(I+1)-Z(I))**2);
S(I)=(Z(I+1)-Z(I))/H; C(I)=(X(I)-X(I+1))/H;
X1=X(I)-LOC(J); X2=X(I+1)-LOC(J); Z1=Z(I); Z2=Z(I+1);
B=X1/Z1; D=X2/Z2; H=B-D; B=1+B*D; A=ATAN(H,B);
H=0.5*LOG((X2**2+Z2**2)/(X1**2+Z1**2));
EA(J)=EA(J)+RD*200000*S(I)*(A*S(I)-H*C(I));
EB(J)=EB(J)+RD*200000*S(I)*(H*S(I)+A*C(I)); END;
DH=(PX*EA(J)+PZ*EB(J))*E; DZ=PX*EB(J)-PZ*EA(J);
ACS(J)=PX*DH+PZ*DZ; END; END SUBR3;
SUBR4:PROC(KK,XS,DD,CDD,N,M,ANG,INC,FI,FA,LS,RS);
DCL (N,K) FIXED BIN (31);
DCL (C,S,X,Z)(5),(LS,RS)(N),(ANG,INC,FI,FA),
(EA,EB,XS)(M),(DD,CDD)(N),KK(N,M) FLOAT BIN;
PX=COSD(INC)*SIND(ANG); PZ=SIND(INC); PXE=COSD(FI);
PZE=SIND(FI); E=SIND(FA);
DO I=1 TO N;
DO J=1 TO M;
X(1),X(2),X(5)=LS(I);
X(3),X(4)=RS(I);
Z(1),Z(4),Z(5)=DD(I);
Z(2),Z(3)=CDD(I);
DO K=1 TO 4;
X1=X(K)-XS(J); X2=X(K+1)-XS(J); Z1=Z(K); Z2=Z(K+1);
H=SQRT((X(K)-X(K+1))**2+(Z(K+1)-Z(K))**2);
S(K)=(Z(K+1)-Z(K))/H; C(K)=(X(K)-X(K+1))/H;
B=X1/Z1; D=X2/Z2; H=B-D; B=1+B*D; A=ATAN(H,B);
H=0.5*LOG((X2**2+Z2**2)/(X1**2+Z1**2));
EA(J)=EA(J)+200000*S(K)*(A*S(K)-H*C(K))*0.01;
EB(J)=EB(J)+200000*S(K)*(H*S(K)+A*C(K))*0.01; END;
DH=(PX*EA(J)+PZ*EB(J))*E;
DZ=PX*EB(J)-PZ*EA(J);
KK(I,J)=PX*DH+PZ*DZ; END; END; END SUBR4;
SUBR5:PROC(A,R,B,KK,LOC,LS,RS,G,DD,CDD,LL,TIMEX,ANG,INC,
FI,FA);
DCL ((B,C)(R,1),(LS,RS,DD,CDD)(A),G(A,1),(HH, <K)(A,R),
LOC(R)) FLOAT BIN,(A,R) FIXED BIN (31);
(I,J,TIMEX) FIXED BIN;
(II,IER) FIXED BIN (31), IPIV(A) FIXED BIN (31);
AUX(2*A,1) FLOAT BIN, (X,ANG,INC,FI,FA) FLOAT BIN, LL
LABEL; DO J=1 TO R; DO J=1 TO A; IF DD(J)<2.51 THEN DO;
X=0.5*(CDD(J)-DD(J)); DD(J)=2.5; CDD(J)=DD(J)+X;
IF ABS(LOC(I)-LS(J))<0.1 | ABS(LOC(I)-RS(J))<0.1 THEN
LOC(I)=LOC(I)+1; END; END; END;
CALL SUBR4(KK,LOC,DD,CDD,A,R,ANG,INC,FI,FA,LS,RS);
HH=KK; C=B; II=1; AI=0.0001;
CALL LLSQ(HH(1,1),C(1,1),R,A,II,C(1,1),IPIV(1),AI,IER,
AUX(2,1));
IF IER=0 THEN DO; PUT EDIT('PROC UNSUCCESSFUL',IER)
(A,F(5)) SKIP(2); GO TO LL; END; END SUBR5;
END MAGGIT1;

```



PROGRAM NAME: MAGGIT 2

FUNCTION: This program determines the angle of magnetisation and the space form of a two dimensional body with outward sloping contacts producing a given total field magnetic anomaly. One point on the top surface of the body and the magnetisation contrast must be specified. A horizontal bottom surface is assumed.

INPUT FORMAT:

CYCLE	}	as for MAGGIT 1
'MODELNAME'		
ITER		
N.		
M		
P3		
RR		
BLCK		
RO	}	as for MAGGIT 1
FI.		
FA		
US		
POS	}	as for MAGGIT 1
A0		
XC1		

DATA NOTES:

RR is the number of estimates of depth to specified top surface point to be tried.

BLCK is the number of the block, counting from the left, whose depth is specified.

US is an array of RR depths to the specified block mid point.

For other notes see MAGGIT 1 specification.

PAGE12: PROC OPTIONS (MAIN); /\* GESS LAVING 1970 \*/

```
PAGE12: PROC OPTIONS (MAIN); /* GESS LAVING 1970 */
DCL(ITERATION,COUNT,I,M,P3,RR,I) FIXED BIN (31),
Z FLOAT BIN, MODELNAME CHAR(60) VARYING;
DCL NH FIXED BIN (31), BLOCK FIXED BIN;
GET LIST (CYCLE);
LOOP: DO COUNT=1 TO CYCLE;
GET LIST (MODELNAME,ITERATION,N,M,P3,RR,BLOCK);
PESIN: DCL(MAD(M,I),(AC,AC,POS) (M),(D1,D2,TT,CTT,LSIDE,RSIDE,
Z)(N),(XX1(N+1)),(TXX,XX,ZB,ZT)(N+2),RDENS(2*N,1),RO(P3),
US(RR),KK(2*N,M),SDENS(I,1),BB(N,M)) FLOAT BIN, (K,J,I,AA,Q)
FIXED BIN, (S1,SSN,INC,ANG,ING) FLOAT BIN;
GET LIST (RO,FI,FA,US,PCS,AO);
POS=POS*1000; US=US*1000;
GET LIST(XX1);
XX1=XX1*1000;
DO I=1 TO N; Z(I)=XX1(I+1)-XX1(I); END;
DO TTT=1 TO RR;
DO I=1 TO M;
MAD(I,1)=AO(I);
AC(I)=0;
END;
LSIDE(BLOCK)=RSIDE(BLOCK-1);
RSIDE(BLOCK)=LSIDE(BLOCK+1);
DO I=1 TO M;
TT(I),D1(I)=US(TTT);
CTT(I),D2(I)=US(TTT)+100;
END;
DO I=1 TO N+1;
IF I=1 THEN RSIDE(I-1)=XX1(I);
IF I=N+1 THEN LSIDE(I)=XX1(I);
END;
CALL SUBR5(N,M,MAD,KK,PCS,LSIDE,RSIDE,RDENS,D1,D2,FINISH,
AA,FI,FA);
S1=0; SSN=0;
DO I=1 TO N;
SN=SN+RDENS(I,1); END;
DO I=N+1 TO 2*N;
SSN=SSN+RDENS(I,1); END;
ING=ATAND(SSN,SN);
ANG=90; DO Q=1 TO P3;
AC=0; AA=1;
CALL SUBR6(N,M,MAD,KK,PCS,LSIDE,RSIDE,SDENS,D1,D2,FINISH,AA,
ANG,INC,FI,FA);
CTT(BLOCK),D2(BLOCK)=US(TTT)+(SDENS(BLOCK,1)/RO(Q))
*SIND(ING);
DO I=1 TO N;
IF I=BLOCK THEN DO;
D2(I),CTT(I)=CTT(BLOCK);
D1(I),TT(I)=CTT(BLOCK)-(SDENS(I,1)/RO(Q))*SIND(ING);
IF I=BLOCK & TT(I)<100 THEN TT(I),D1(I)=105;
IF TT(I)>CTT(BLOCK)-1 THEN D1(I),TT(I)=CTT(BLOCK)-1;
END; END;
CALL SUBR2(I,D1,D2,ZT,ZB,XX1,XX,Z);
DO I=2 TO N+1;
TXX(I)=XX(I);
END;
```

```

TXX(1)=XX(1); TXX(N+2)=XX(N+2);
CALL SUBR3(ZT,ZB,XX,POS,AC,RO(Q),N,M,FI,FA,ANG,TXX,ING);
DO I=1 TO M;
MAC(I,1)=AC(I)-AC(1);
END;
LI:DO AA=1 TO ITERATION;
LSIDE(BLOCK)=LSIDE(1);
RSIDE(BLOCK)=RSIDE(N);
DO I=1 TO N;
IF I=BLOCK THEN DO;
D1(I)=TT(I)-100;
D2(I)=TT(I);
END;
ELSE DO;
D1(I)=CTT(I);
D2(I)=CTT(I)+100;
END; END;
CALL SUBR1(H,M,MAO,KK,PCS,LSIDE,RSIDE,SDENS,D1,D2,FINISH,AA,
ANG,ING,FI,FA);
D1(BLOCK)=CTT(BLOCK);
CTT(BLOCK),D2(BLOCK)=CTT(BLOCK)+(SDENS(BLOCK,1)/RO(Q))*
SIND(ING);
DO I=1 TO N;
IF I=BLOCK THEN DO;
TT(I),D1(I)=TT(I)-(SDENS(I,1)/RO(Q))*SIND(ING);
CTT(1)=CTT(BLOCK);
END;
IF TT(I)>CTT(BLOCK)-1 THEN TT(I),D1(I)=CTT(BLOCK)-1;
IF I=BLOCK & TT(I)<100 THEN TT(I),D1(I)=105;
D2(I)=CTT(BLOCK);
END;
D1(BLOCK)=US(TTT);
LSIDE(BLOCK)=RSIDE(BLOCK-1);
RSIDE(BLOCK)=LSIDE(BLOCK+1);
CALL SUBR2(I,D1,D2,ZT,ZB,XX1,XX,Z);
DO I=2 TO N+1;
TXX(I)=TXX(I);
END;
CALL SUBR3(ZT,ZB,XX,POS,AC,RO(Q),N,M,FI,FA,ANG,TXX,ING);
DO I=1 TO M;
MAO(I,1)=AO(I)-AC(1);
END;
IF AA=ITERATION THEN DO;
PUT LIST (MODELNAME) PAGE;
PUT EDIT ('MODEL',COUNT,'_',Q,'_',RR)(A,F(2),A,F(1),A,
F(1)) SKIP(2); PUT EDIT ('ESTIMATE',AA,'MAGNETISATION=',
RO(Q),'BODY ANGLE=',ANG,'BODY INCLINATION=',ING,
'FIELD-ANGLE=',FA,'FIELD-INCLINATION=',FI)(A,F(3),X(3),A,
F(5),X(2),A,F(3),X(2),A,F(3),X(2),A,F(3),X(2),A,F(3))
SKIP(2); PUT EDIT ('SIDE','XTOP','XBCT','DTOP','DBOT')
(A,X(3),A,X(5),A,X(6),A,X(5),A) SKIP(2);
DO I=1 TO N+2; PUT EDIT (I,TXX(I),XX(I),ZT(I),ZB(I))
(F(3),4 F(9,0)) SKIP(1); END; PUT LIST
('LOCATION OBSERVED CALCULATED RESID')

```

```

SKIP(4); DO I=1 TO N;
PUT EDIT (PB(I),AD(I),AC(I),MAO(I,1)) (F(7,0),F(10,1),
F(13,1),F(17,1)) SKIP(1); END LI;
FINISH: PUT EDIT('END OF MODEL',COUNT,'_',Q,'_',RR)
(A,F(3),A,F(1),A,F(1)) SKIP(3); END LOOPI;
PUT LIST ('END OF DATA') SKIP(3); STOP;
SUBR1:PROC(A,B,B,KK,LOC,LS,RS,G,DD,CDD,LL,TIMEX,ANG,INC,
FI,FA);
DCL((B,C)(R;1),(LS,RS,DD,CDD)(A),G(A,1),(HH,KK)(A,R),
LOC(R)) FLOAT BIN,(A,R) FIXED BIN (31),
(1,J,TIMEX) FIXED BIN,
(I,IER) FIXED BIN (31), IPIV(A) FIXED BIN (31),
AUX(*A,1) FLOAT BIN, (X,ANG,INC,FI,FA) FLOAT BIN, LL
LABTL;
CALL SUBR4(KK,LOC,DD,CDD,A,R,ANG,INC,FI,FA,LS,RS);
HH=KK; C=B; I=1; AI=0.0001;
CALL LLSQ(HH(I,1),C(I,1),R,A,I,G(1,1),IPIV(I),AI,IER,
AUX(1,1));
IF IER=0 THEN DO; PUT EDIT('PROC UNSUCCESSFUL',IER)
(A,F(3)) SKIP(2); GO TO LL; END; END SUBR1;
SUBR2:PROC(N,T,CT,ZT,ZB,LS,XX,V);
DCL (N) FIXED BIN (31);
DCL (LS(N+1),(T,CT)(N),(XX,ZT,ZB)(N+2)) FLOAT BIN,
V(N) FLOAT BIN; DO I=2 TO N+1;
XX(I)=LS(I-1)+V(I-1)/2;
ZT(I)=T(I-1); ZB(I)=CT(I-1); END;
XX(1)=LS(1)-V(1)/2;
XX(N+2)=LS(N+1)+V(N)/2;
ZB(1)=CT(1);
ZB(N+2)=CT(N);
ZT(1)=ZB(1)-1; ZT(N+2)=ZB(N+2)-1;
END SUBR2;
SUBR3:PROC(ZT,ZB,XS,LOC,ACS,RO,H,M,FI,FA,ANG,XT,INC);
DCL (N,M) FIXED BIN (31);
DCL((ZT,ZB,XS)(N+2),(FA,EB,LOC,ACS)(M),(X,Z,C,S)(2*N+5),
(ANG,INC,FI,FA,RO)) FLOAT BIN; ACS=0;
DCL XT(N+2) FLOAT BIN;
PX=COSD(INC)*SIND(ANG); PZ=SIND(INC); PXE=COSD(FI);
PZE=SIND(FI); E=SIND(FA);
DO I=1 TO N+2; Z(I)=ZB(I); X(I)=XS(I); END;
DO I=N+2 BY -1 TO 1; Z(2*N+5-1)=ZT(I);
X(2*N+5-1)=XT(1); END; Z(2*N+5)=Z(1); X(2*N+5)=X(1);
DO J=1 TO M; EA(J)=0; EB(J)=0; DO I=1 TO 2*N+4;
H=SQRT((X(I)-X(I+1))**2+(Z(I+1)-Z(I))**2);
S(I)=(Z(I+1)-Z(I))/H; C(I)=(X(I)-X(I+1))/H;
X1=X(I)-LOC(J); X2=X(I+1)-LOC(J); Z1=Z(I); Z2=Z(I+1);
B=X1/Z1; D=X2/Z2; H=B-D; B=1+D*D; A=ATAN(H,B);
H=0.5*LOG((X2**2+Z2**2)/(X1**2+Z1**2));
EA(J)=EA(J)+RO*200000*S(I)*(A*S(I)-H*C(I));
EB(J)=EB(J)+RO*200000*S(I)*(H*S(I)+A*C(I)); END;
DH=(PX*EA(J)+PZ*EB(J))*E; DZ=PX*EB(J)-PZ*EA(J);
ACS(J)=PXE*DH+PZE*DZ; END; END SUBR3;
SUBR4:PROC(KK,XS,DD,CDD,H,M,ANG,INC,FI,FA,LS,RS);
DCL(N,M) FIXED BIN (31);

```

MACGIT2: PROC OPTIONS (MAP); /\* GELS LAVING 1970 \*/

```

DCL ((C,S,X,Z)(5),(LS,RS)(4),(ANG,INC,FI,FA),
      (EA,EB,XS)(3),(DD,CDD)(2),KK(I,M)) FLOAT BIN;
PX=COSD(LOC)*SINC(ANG); PZ=SIND(LOC); PXE=COSD(FI);
PZF=SIND(FI); F=SINC(FA);
DO I=1 TO 4;
  X(1),X(2),X(5)=LS(I);
  X(3),X(4)=RS(I);
  Z(1),Z(4),Z(5)=DD(I);
  Z(2),Z(3)=CDD(I);
  DO J=1 TO M; EA(J)=0; EB(J)=0; DO K=1 TO 4;
    X1=X(K)-XS(J); X2=X(K+1)-XS(J); Z1=Z(K); Z2=Z(K+1);
    H=SQRT((X(K)-X(K+1))**2+(Z(K+1)-Z(K))**2);
    S(K)=(Z(K+1)-Z(K))/H; C(K)=(X(K)-X(K+1))/H;
    B=X1/Z1; D=X2/Z2; H=B-D; B=1+B*D; A=ATAN(H,B);
    H=0.5*LOG((X2**2+Z2**2)/(X1**2+Z1**2));
    EA(J)=EA(J)+0.0000*S(K)*(A*S(K)-H*C(K))*0.01;
    EB(J)=EB(J)+2.0000*S(K)*(H*S(K)+A*C(K))*0.01; END;
    DH=(PX*EA(J)+PZ*EB(J))*F;
    DZ=PX*EB(J)-PZ*EA(J);
    KK(I,J)=PXE*DH+PZF*DZ; END; END; END SUBR4;
  SUBR5:PROC(A,R,B,KK,LOC,LS,RS,G,DD,CDD,LL,TIMEX,
            FI,FA);
    DCL ((B,C)(R,1),(LS,RS,DD,CDD)(A),G(2*A,1),KK(2*A,R),
          LOC(R)) FLOAT BIN,(A,R) FIXED BIN(31);
    (I,J,TIMEX) FIXED BIN;
    (XX,ZZ)(A,R) FLOAT BIN, H FIXED BIN;
    (II,IER) FIXED BIN(31), IPIV(2*A) FIXED BIN(31);
    AUX(4*A,1) FLOAT BIN, (X,ANG,INC,FI,FA) FLOAT BIN, LL
    LABEL; DO I=1 TO R; DO J=1 TO A; IF DD(J)<2.51 THEN DO;
      X=0.5*(CDD(J)-DD(J)); CD(J)=2.5; CDD(J)=DD(J)+X;
      IF ABS(LOC(I)-LS(J))<0.1 | ABS(LOC(I)-RS(J))<0.1 THEN
      LOC(I)=LOC(I)+1; .END; END; END;
    ANG=90; INC=0;
    CALL SUBR4(XX,LOC,CD,CDD,A,R,ANG,INC,FI,FA,LS,RS);
    INC=90;
    CALL SUBR4(ZZ,LOC,DD,CDD,A,R,ANG,INC,FI,FA,LS,RS);
    DO I=1 TO A; DO J=1 TO R;
      KK(I,J)=XX(I,J); KK(1+N,J)=ZZ(I,J); END; END; H=2*A;
      C=B; II=1; AI=0.0001;
      CALL LLSQ(KK(I,1),C(I,1),R,H,II,G(I,1),IPIV(1),AI,IER,
        AUX(I,1));
      IF IER#0 THEN DO; PUT EDIT('PROC UNSUCCESSFUL',IER)
        (A,F(3)) SKIP(2); GO TO LL; END; END SUBR5;
  END MACGIT2;
```

PROGRAM NAME: MAGGIT 3

FUNCTION: This program determines the space form of a two dimensional body with inward sloping body contacts producing a given total field magnetic anomaly. The calculation are carried for a specified series of values of dip and azimuth of the body magnetisation vector. The top surface of the body and its magnetisation contrast must be specified.

INPUT FORMAT:

CYCLE	}	as in MAGGIT 1
'MODELNAME'		
ITER		
N		
M		
P3	}	as in MAGGIT 1
PP		
RO		
FI		
FI		
ANG	}	as in MAGGIT 1
INC		
TT		
POS		
AO		
XX1		

DATA NOTES:

PP is the number of sets of body magnetisation dip and azimuth to be tried.

ANG is an array of PP value of body magnetisation vector azimuth. That is the angle measured in an

anticlockwise sense from the strike of the body to the vertical plane containing the body magnetisation vector.

INC is the dip of the body magnetisation vector in the plane of the vector.

For other notes see MAGGIT 1 specification.



MODEL:PROC OPTIONS (MAIN); /\* GESS LAVING 1970 \*/

```
MAGGITB:PROC OPTIONS (MAIN); /* GESS LAVING 1970 */
  DCL(ITERATION,CONST,N,M,P3,PP) FIXED BIN (31),
  MODELNAME CHAR (60) VARYING; GET LIST(CYCLE);
  LOOP1: DO COUNT=1 TO CYCLE;
GET LIST (MODELNAME,ITERATION,N,M,P3,PP);
  BEGIN; DCL(MAO(P,1),(AO,AC,POS)(M),(D1,D2,CTT,TT,LSIDE,
  RSIDE)(N),(XX1,LS,RS)(N+1),(XX,Z3,ZT)(N+2),SDENS(N,1),
  BXX(N+2),KK(N,M),RG(P3),Z(N),ANG(PP),INC(PP)) FLOAT BIN,
  (FI,FA) FLOAT
  BIN,(K,J,1,AA,Q) FIXED BIN; GET LIST(RO,FI,FA,ANG,INC,
  TT,POS,AO); POS=POS*1000; TT=TT*1000; GET LIST(XX1);
  XX1=XX1*1000; DO I=1 TO N+1; IF I=N THEN RSIDE(I-1)=
  XX1(I); IF I=N+1 THEN LSIDE(I)=XX1(I); END;
DO I=1 TO N; Z(I)=XX1(I+1)-XX1(I); END;
  DO Q=1 TO P3; DO RR=1 TO PP; D1=TT; CTT,D2=TT+100;
  DO I=1 TO N; MAO(I,1)=AO(I); AC(I)=0; END; AA=1;
  CALL SUBR1(N,M,MAO,KK,POS,LSIDE,RSIDE,SDENS,D1,D2,FINISH,
  AA,ANG(RR),INC(RR),FI,FA); DO I=1 TO N;
  D2(I),CTT(I)=TT(I)+(SDENS(I,1)/RG(Q))*SIND(INC(RR));
  IF CTT(I)<TT(I)+1 THEN D2(I),CTT(I)=TT(I)+1; END;
  CALL SUBR2(N,D1,D2,ZT,ZB,XX1,XX,Z);
  DO I=2 TO N+1; BXX(I)=XX(I);
  END; BXX(1)=XX(1); BXX(N+2)=XX(N+2);
  CALL SUBR3(ZT,ZB,XX,POS,AC,RO(Q),N,M,FI,FA,ANG(RR),BXX,
  INC(RR)); DO I=1 TO N; MAO(I,1)=AO(I)-AC(I); END;
  L1:DO AA=1 TO ITERATION; D1=CTT; D2=CTT+100;
  CALL SUBR1(N,M,MAO,KK,POS,LSIDE,RSIDE,SDENS,D1,D2,FINISH,
  AA,ANG(RR),INC(RR),FI,FA); DO I=1 TO N; D1(I)=TT(I);
  CTT(I),D2(I)=CTT(I)+(SDENS(I,1)/RG(Q))*SIND(INC(RR));
  IF CTT(I)<TT(I) THEN CTT(I),D2(I)=TT(I)+1; END;
  CALL SUBR2(N,D1,D2,ZT,ZB,XX1,XX,Z);
  CALL SUBR3(ZT,ZB,XX,POS,AC,RO(Q),N,M,FI,FA,ANG(RR),DXX,
  INC(RR)); DO I=1 TO N; MAO(I,1)=AO(I)-AC(I); END;
  IF AA=ITERATION THEN DO; PUT LIST(MODELNAME) PAGE;
  PUT EDIT ('MODEL',COUNT,'_',Q,'_',RR)(A,F(2),A,F(1),A,
  F(1)) SKIP(2); PUT EDIT ('ESTIMATE',AA,'MAGNETISATION=',
  RO(Q),'BODY-ANGLE=',ANG(RR),'BODY-INCLINATION=',INC(RR),
  'FIELD-ANGLE=',FA,'FIELD-INCLINATION=',FI)(A,F(3),X(3),A,
  F(6,5),X(2),A,F(3),X(2),A,F(3),X(2),A,F(3),X(2),A,F(3))
  SKIP(2); PUT EDIT ('SIDE','XTOP','XROT','DTOP','DBOT')
  (A,X(3),A,X(5),A,X(6),A,X(5),A) SKIP(2);
  DO I=1 TO N+2; PUT EDIT(I,XX(I),BXX(I),ZT(I),ZB(I))
  (F(3),4 F(9,0)) SKIP(1); END; PUT LIST
  ('LOCATION OBSERVED CALCULATED RESID')
  SKIP(4); DO I=1 TO M;
  PUT EDIT (POS(I),AO(I),AC(I),MAO(I,1)) (F(7,0),F(10,2),
  F(3,1),F(11,1)) SKIP(1); END L1;
  FINISH: PUT EDIT ('END OF MODEL',COUNT,'_',Q,'_',RR)
  (A,F(3),A,F(1),A,F(1)) SKIP(3); END LOOP1;
  PUT LIST ('END OF DATA') SKIP(3); STOP;
  SUBR1:PROC(A,R,B,KK,LUC,LS,RS,G,DD,CDD,L1,TIMEX,ANG,INC,
  FI,FA);
  DCL((B,C)(P,1),(LS,RS,DD,CDD)(A),G(A,1),(HH,KK)(A,R),
  LUC(R)) FLOAT BIN,(A,R) FIXED BIN (31),
  (I,J,TIMEX) FIXED BIN,
  (II,IFR) FIXED BIN (31), IPIV(A) FIXED BIN (31),
```

```

AUX(2*4,1) FLOAT BIN; (X,ANG,INC,FI,FA) FLOAT BIN; LL
LABEL; DO I=1 TO R; DO J=1 TO A; IF DD(J)<2.5 THEN DO;
X=0.5*(CDD(J)-CD(J)); CD(J)=2.5; CDD(J)=DD(J)+X;
IF ABS(LOC(I)-LS(J))<0.1 | ABS(LOC(I)-RS(J))<0.1 THEN
LOC(I)=LOC(I)+1; CHD; END; END;
CALL SUBR4(KK,LOC,CD,CDD,A,R,ANG,INC,FI,FA,LS,RS);
H4=KK; C=3; I1=1; A1=0.0001;
CALL LLSG(HH(1,1),C(1,1),R,A,I1,G(1,1),IPIV(1),AI,IER,
AUX(1,1));
IF IER=0 THEN DO; PUT EDIT('PROC UNSUCCESSFUL',IER)
(A,F(3)) SKIP(2); GO TO LL; LND; END SUBR1;
SUBR2:PROC(N,T,CT,ZT,ZB,LS,XX,V);
DCL N FIXED BIN(31);
DCL (LS(N+1),(T,CT)(N),(XX,ZT,ZB)(N+2)) FLOAT BIN,
V(N) FLOAT BIN;
DO I=2 TO N+1;
XX(I)=LS(I-1)+V(I-1)/2;
ZT(I)=T(I-1); ZB(I)=CT(I-1); END;
XX(N+2)=LS(N+1)+V(N)/2;
ZT(N)=T(N); ZT(N+2)=T(N);
ZB(1)=ZT(1)+1; ZB(N+2)=ZT(N+2)+1; END SUBR2;
SUBR3:PROC(ZT,ZB,XS,LOC,ACS,RO,N,M,FI,FA,ANG,XB,INC);
DCL (N,M) FIXED BIN(31);
DCL ((ZT,ZB,XS)(N+2),(EA,EB,LOC,ACS)(M),(X,Z,C,S)(2*N+5),
(ANG,INC,FI,FA,RO)) FLOAT BIN; ACS=0;
DCL XB(N+2) FLOAT BIN;
PX=COSD(INC)*SIND(ANG); PZ=SIND(INC); PXE=COSD(FI);
PZE=SIND(FI); E=SIND(FA);
DO I=1 TO N+2; Z(I)=ZB(I); X(I)=XB(I); END;
DO J=N+2 BY -1 TO 1; Z(2*N+5-J)=ZT(I);
X(2*N+5-I)=XS(I); END; Z(2*N+5)=Z(1); X(2*N+5)=X(1);
DO J=1 TO M; EA(J)=C; EB(J)=0; DO I=1 TO 2*N+4;
H=SQR((X(I)-X(I+1))**2+(Z(I+1)-Z(I))**2);
S(I)=(Z(I+1)-Z(I))/H; C(I)=(X(I)-X(I+1))/H;
X1=X(I)-LOC(J); X2=X(I+1)-LOC(J); Z1=Z(I); Z2=Z(I+1);
B=X1/Z1; D=X2/Z2; H=3-D; B=1+B*D; A=ATAN(H,3);
H=0.5*LOG((X2**2+Z2**2)/(X1**2+Z1**2));
EA(J)=EA(J)+RO*20000*S(I)*(A*S(I)-H*C(I));
EB(J)=EB(J)+RO*20000*S(I)*(H*S(I)+A*C(I)); END;
DH=(PX*EA(J)+PZE*EB(J))*E; DZ=PX*EB(J)-PZE*EA(J);
ACS(J)=PXE*DH+PZE*DZ; END; END SUBR3;
SUBR4:PROC(KK,XS,DD,CDD,N,M,ANG,INC,FI,FA,LS,RS);
DCL (N,M) FIXED BIN(31);
DCL ((C,S,X,Z)(5),(LS,RS)(N),(ANG,INC,FI,FA),
(EA,EB,XS)(M),(CD,CDD)(N),KK(N,M)) FLOAT BIN;
PX=COSD(INC)*SIND(ANG); PZ=SIND(INC); PXE=COSD(FI);
PZE=SIND(FI); E=SIND(FA);
DO I=1 TO N;
X(1),X(2),X(5)=LS(I);
X(3),X(4)=RS(I);
Z(1),Z(4),Z(5)=DD(I);
Z(2),Z(3)=CDD(I);
DO J=1 TO M; EA(J)=0; EB(J)=0; DO K=1 TO 4;
X1=X(K)-XS(J); X2=X(K+1)-XS(J); Z1=Z(K); Z2=Z(K+1);

```

PAJGJ1:PROC OPTIENS (MAIN); /\* GLSS LAMING 1970 \*/

```
H=SQRT((X(K)-X(K+1))**2+(Z(K+1)-Z(K))**2);
S(F)=(Z(K+1)-Z(F))/H; C(K)=(X(K)-X(K+1))/H;
B=X1/Z1; D=X2/Z2; E=B-D; B=1+B*D; A=ATAN(H,0);
H=0.5*LOG((X2**2+Z2**2)/(X1**2+Z1**2));
EA(J)=EA(J)+200000*S(K)*(A+S(K)-H*C(K))*0.01;
EB(J)=EB(J)+200000*S(K)*(H*S(K)+A*C(K))*0.01; END;
DH=(PX*EA(J)+PZ*EB(J))*E;
DZ=PX*F(J)-PZ*A(J);
KK(I,J)=PX*DH+PZ*DZ; END; END; END SUBR4;
END PJJG13;
```

PROGRAM NAME: MAGGIT 4

FUNCTION: This program determines the space form of a two dimensional body with outward sloping contacts producing a given total field anomaly. The calculations are carried out for a specified series of values of dip and azimuth of the body magnetisation vector. The magnetisation contrast of the body and one point on its top surface must be specified. A horizontal bottom surface is assumed.

INPUT FORMAT:

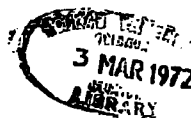
CYCLE	}	as in MAGGIT 2
'MODELNAME'		
ITER		
N		
M		
P3		
RR		
BLCKK		
SS	}	as in MAGGIT 3
RO		
FI		
FA		
ANG		
INC		
US	}	as in MAGGIT 3
POS		
MAO		
XX1		

DATA NOTES:

SS is the number of sets of body magnetisation dip and azimuth to be tried.

US is an array of RR depths to the specified block mid point.

For other notes see MAGGIT 1 specification.



MAGGIT4:PROC OPTICS (MAGIT); /\*GESS LAVING 1970 \*/

```
MAGGIT4:PROC OPTICS (MAGIT); /*GESS LAVING 1970 */
DCL(N,M) FIXED BIN (31);(ITERATION,COUNT,BLOCK,P3,RR,SS)
FIXED BIN; MODELNAME CHAR (60) VARYING;
GET LIST (CYCLE);
LOOPI:DO COUNT=1 TO CYCLE;
GET LIST (MODELNAME,ITERATION,N,M,P3,RR,BLOCK,SS);
BEGIN;DCL(MAO(M,1),SDENS(I,1),KK(N,M),(AC,AC,PCS)(M),(D1,D2,
CTT,TT,LSIDE,RSIDE)(N),(XX1,LS,RS)(N+1),(XX,ZB,ZT)(N+2),
TXX(N+2),AD(P3),US(RR),(ANG,INC)(SS)) FLOAT BIN,(FI,FA)
FLOAT BIN,AA FIXED BIN;
DCL Z(N) FLOAT BIN;
GET LIST (RO,FI,FA,ANG,INC,US,PCS,MAO);
DO I=1 TO M;
AD(I)=MAO(I,1); END;
POS=POS*1000; US=US*1000;
GET LIST(XX1); XX1=XX1*1000;
DO I=1 TO N;
Z(I)=XX1(I+1)-XX1(I); END;
DO I=1 TO N+1;
IF I=1 THEN RSIDE(I-1)=XX1(I);
IF I=N+1 THEN LSIDE(I)=XX1(I);
END;
DO TTT=1 TO RR;
DO Q=1 TO P3;
DO L=1 TO SS;
LSIDE(BLOCK)=RSIDE(BLOCK-1);
RSIDE(BLOCK)=LSIDE(BLOCK+1);
DO I=1 TO N;
TT(I),D1(I)=US(TTT);
CTT(I),D2(I)=US(TTT)+100;
END;
AC=0; AA=1;
CALL SUBR1(N,M,MAO,KK,PCS,LSIDE,RSIDE,SDENS,D1,D2,FINISH,AA,
ANG(L),INC(L),FI,FA);
CTT(BLOCK),D2(BLOCK)=US(TTT)+(SDENS(BLOCK,1)/RO(Q))
*SIND(INC(L));
DO I=1 TO N;
IF I=BLOCK THEN DO;
D2(I),CTT(I)=CTT(BLOCK);
D1(I),TT(I)=CTT(BLOCK)-(SDENS(I,1)/RO(Q))*SIND(INC(L));
IF I=BLOCK & TT(I)<100 THEN TT(I),D1(I)=105;
IF TT(I)>CTT(BLOCK)-1 THEN D1(I),TT(I)=CTT(BLOCK)-1;
END; END;
CALL SUBR2(N,D1,D2,ZT,ZB,XX1,XX,Z);
DO I=2 TO N+1;
TXX(I)=XX(I);
END;
TXX(1)=XX(1); TXX(N+2)=XX(N+2);
CALL SUBR3(ZT,ZB,XX,POS,AC,RO(Q),N,M,FI,FA,ANG(L),TXX,INC(L));
DO I=1 TO M;
MAO(I,1)=AD(I)-AC(I);
END;
L1:DO AA=1 TO ITERATION;
LSIDE(BLOCK)=LSIDE(I);
RSIDE(BLOCK)=RSIDE(I);
DO I=1 TO N;
```

```

IF I=BLOCK THEN DO;
D1(I)=TT(I)-100;
D2(I)=TT(I);
END;
ELSE DO;
D1(I)=CTT(I);
D2(I)=(TT(I)+100);
END; END;
CALL SUBR1 (I,M,MAO,KK,POS,LSIDE,RSIDE,SDENS,D1,D2,FINISH,AA,
ANG(L),INC(L),FI,FA);
D1(BLOCK)=CTT(BLOCK);
CTT(BLOCK),D2(BLOCK)=CTT(BLOCK)+(SDENS(BLOCK,1)/RO(Q))*
SIND(INC(L));
DO I=1 TO N;
IF I=BLOCK THEN DO;
TT(I),D1(I)=TT(I)-(SDENS(I,1)/RO(Q))*SIND(INC(L));
CTT(I)=CTT(BLOCK);
END;
IF TT(I)>CTT(BLOCK)-1 THEN TT(I),D1(I)=CTT(BLOCK)-1;
IF I=BLOCK & TT(I)<100 THEN TT(I),D1(I)=100;
D2(I)=CTT(BLOCK);
END;
D1(BLOCK)=US(TTT);
LSIDE(BLOCK)=RSIDE(BLOCK-1);
RSIDE(BLOCK)=LSIDE(BLOCK+1);
CALL SUBR2 (I,D1,D2,ZT,ZB,XX1,XX,Z);
DO J=2 TO N+1;
TXX(J)=TXX(1);
END;
CALL SUBR3 (ZT,ZB,XX,POS,AC,RO(Q),I,M,FI,FA,ANG(L),TXX,INC(L));
DO I=1 TO M;
MAO(I,1)=AO(I)-AC(I);
END;
IF AA=ITERATIC THEN DO;
PUT LIST (MODELNAME) PAGE;
PUT EDIT ('MODEL',COUNT,'_',Q,'_',RR)(A,F(2),A,F(1),A,
F(1)) SKIP(2); PUT EDIT ('ESTIMATE',AA,'MAGNETISATION=',
RO(Q),'BODY-ANGL= ',ANG(L),'BODY INCLINATION=',INC(L),
'FIELD-ANGLE=',FA,'FIELD-INCLINATION=',F1)(A,F(3),X(3),A,
F(6,5),X(2),A,F(2),X(2),A,F(3),X(2),A,F(3),X(2),A,F(3))
SKIP(2); PUT EDIT ('SIDE','XTOP','XBOT','DTOP','DBOT')
(A,X(3),A,X(5),A,X(6),A,X(5),A) SKIP(2);
DO I=1 TO N+2; PUT EDIT (I,TXX(1),XX(1),ZT(I),ZB(I))
(F(3),4 F(9,0)) SKIP(1); END; PUT LIST
('LOCATION OBSERVED CALCULATED RESID')
SKIP(4); DO I=1 TO M;
PUT EDIT (POS(I),AC(I),AC(I),MAO(I,1)) (F(7,0),F(10,1),
F(13,1),F(11,1)) SKIP(1); END LI;
FINISH: PUT EDIT ('END OF MODEL',COUNT,'_',Q,'_',RR)
(A,F(3),A,F(1),A,F(1)) SKIP(3); END LOOP1;
PUT LIST ('END OF DATA') SKIP(3); STOP;
SUBR1:PROC(A,R,I,KK,LOC,LS,RS,S,DD,CDD,LL,TIMEX,ANG,INC,
FI,FA);
DCL ((B,C)(K,I),(LS,RS,DD,CDD)(A),G(A,I),(FH,KK)(A,R),

```

```

      LCC(R) FLOAT BIN, (A,R) FIXED BIN (3);
(1,J,TIME X) FIXED BIN,
      (I,IER) FIXED BIN (3); IPIV(A) FIXED BIN (31);
      AUX(*A,1) FLOAT BIN, (X,ANG,INC,FI,FA) FLOAT BIN, LL
      LABEL;
      CALL SUBR4(KK,LCC,DD,CDD,A,R,ANG,INC,FI,FA,LS,RS);
      HH=KK; C=B; I1=1; A1=0.0001;
      CALL LLSQ(HH(1,1),C(1,1),R,A,I1,C(1,1),IPIV(1),A1,IER,
      AUX(1,1));
      IF IER=0 THEN DO; PUT EDIT('PROC UNSUCCESSFUL',IER)
      (A,F(3)) SKIP(2); GO TO LL; END; END SUBR1;
      SUBR2:PROC(N,T,CT,ZT,ZB,LS,XX,V);
DCL (N) FIXED BIN (31);
      DCL (LS(N+1),(T,CT)(N),(XX,ZT,ZB)(N+2)) FLOAT BIN,
      V(N) FLOAT BIN;
      DO I=2 TO N+1;
      XX(I)=LS(I-1)+V(I-1)/2;
      ZT(I)=T(I-1); ZB=CT(I-1); END; XX(1)=LS(1)-V(1)/2;
      XX(N+2)=LS(N+1)+V(N)/2; ZB(1)=CT(1); ZB(N+2)=CT(N);
      ZT(1)=ZB(1)-1; ZT(N+2)=ZB(N+2)-1;
      END SUBR2;
      SUBR3:PROC(ZT,ZB,XS,LCC,ACS,RO,N,H,FI,FA,ANG,XT,INC);
DCL (H,H) FIXED BIN (31);
      DCL((ZT,ZB,XS)(N+2),(EA,EB,LCC,ACS)(N),(X,Z,C,S)(2*N+5),
      (ANG,INC,FI,FA,RO)) FLOAT BIN; ACS=0;
      DCL XT(N+2) FLOAT BIN;
      PX=COSD(INC)*SIND(ANG); PZ=SIND(INC); PXE=COSD(FI);
      PZE=SIND(FI); E=SINC(FA);
      DO I=1 TO N+2; Z(I)=ZB(I); X(I)=XS(I); END;
      DO I=N+2 BY -1 TO 1; Z(2*N+5-I)=ZT(I);
      X(2*N+5-I)=XT(I); END; Z(2*N+5)=Z(1); X(2*N+5)=X(1);
      DO J=1 TO H; EA(J)=C; EB(J)=0; DO I=1 TO 2*N+4;
      H=SQRT((X(I)-X(I+1))**2+(Z(I+1)-Z(I))**2);
      S(I)=(Z(I+1)-Z(I))/H; C(I)=(X(I)-X(I+1))/H;
      X1=X(I)-LCC(J); X2=X(I+1)-LCC(J); Z1=Z(I); Z2=Z(I+1);
      B=X1/Z1; D=X2/Z2; H=B-D; B=1+B*D; A=ATAN(H,B);
      H=0.5*LCC((X2**2+Z2**2)/(X1**2+Z1**2));
      EA(J)=EA(J)+RO*20000*S(I)*(A*S(I)-H*C(I));
      EB(J)=EB(J)+RO*20000*S(I)*(H*S(I)+A*C(I)); END;
      DH=(PX*EA(J)+PZ*EB(J))*E; DZ=PX*EB(J)-PZ*EA(J);
      ACS(J)=PXE*DH+PZE*DZ; END; END SUBR3;
      SUBR4:PROC(KK,XS,DD,CDD,N,H,ANG,INC,FI,FA,LS,RS);
DCL (H,M) FIXED BIN (31);
      DCL((C,S,X,Z)(5),(LS,RS)(N),(ANG,INC,FI,FA),
      (EA,EB,XS)(M),(DD,CDD)(H),KK(N,M)) FLOAT BIN;
      PX=COSD(INC)*SIND(ANG); PZ=SIND(INC); PXE=COSD(FI);
      PZE=SIND(FI); E=SINC(FA);
      DO I=1 TO H;
      X(1),X(2),X(5)=LS(I);
      X(3),X(4)=RS(I);
      Z(1),Z(4),Z(5)=DD(I);
      Z(2),Z(3)=CDD(I);
      DO J=1 TO M; EA(J)=C; EB(J)=0; DO K=1 TO 4;
      X1=X(K)-XS(J); X2=X(K+1)-XS(J); Z1=Z(K); Z2=Z(K+1);

```



MAGGIT4:PROC OPTIONS (MAIN); /\*GESS LAVING 1970 \*/

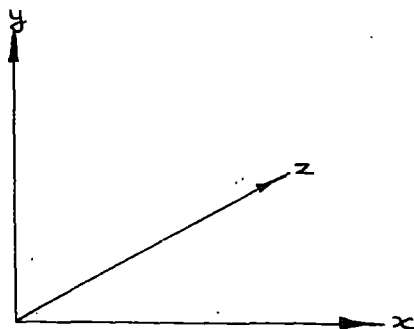
```
H=SQRT((X(K)-X(K+1))**2+(Z(K+1)-Z(K))**2);
S(K)=(Z(K+1)-Z(K))/H; C(K)=(X(K)-X(K+1))/H;
B=X1/Z1; D=X2/Z2; H=B-D; B=1+B*D; A=ATAN(H,B);
H=0.5*LOG((X2**2+Z2**2)/(X1**2+Z1**2));
EA(J)=EA(J)+20000*S(K)*(A*S(K)-H*C(K))*0.01;
EB(J)=EB(J)+20000*S(K)*(H*S(K)+A*C(K))*0.01; END;
DH=(PX*EA(J)+PZ*EB(J))*E;
DZ=PX*EB(J)-PZ*EA(J);
KK(1,J)=PXE*DH+PZE*DZ; END; END; END SUBR4;
END MAGGIT4;
```

3 MAR 1972  
LIBRARY

APPENDIX 2

PROOF OF MAGNETIC MOMENT THEOREM (R.A. Smith).

Notice that it is sufficient to prove the theorem for a body consisting of a single linear dipole. This can then be extended at once to a collection of dipoles by superposition.



A unit line charge passing through the point  $(a, -b, 0)$  and extended parallel to the  $z$ -axis produces a potential  $P$  at the point  $(x, y, z)$  given by:

$$P(x, y) = -\log ((x-a)^2 + (y+b)^2) \text{ ----- (A2-1)}$$

A linear dipole passing through  $(a, -b, 0)$  and having magnetic moment per unit length  $\underline{J} = (U, V, C)$  produces a potential  $Q = \underline{J} \cdot \underline{\nabla} P$

The resolved part  $A$  parallel to  $\underline{s} = (l, m, 0)$  of the field produced by this dipole at the point  $(x, y, z)$  is:

$$\begin{aligned} A &= -(\underline{s} \cdot \underline{\nabla}) Q \\ &= -(\underline{s} \cdot \underline{\nabla}) (\underline{J} \cdot \underline{\nabla}) P \\ &= -lU \frac{d^2 P}{dx^2} - (lV + mU) \frac{d^2 P}{dx dy} - mV \frac{d^2 P}{dy^2} \\ &= (mV - lU) \frac{d^2 P}{dx^2} - (lV + mU) \frac{d^2 P}{dx dy} \end{aligned} \quad \text{(A2-2)}$$

since  $\frac{d^2P}{dx^2} + \frac{d^2P}{dy^2} = 0$

if we define

$$F(x) = \int_{-\infty}^x A(t) \cdot dt. \tag{A2-3}$$

we have:

$$A(x) = \frac{\lambda(b^2 - (x-a)^2) - 2\mu b(x-a)}{(b^2 + (x-a)^2)^2} \tag{A2-4}$$

and:

$$F(x) = \frac{\lambda(x-a) + \mu \cdot b}{b^2 + (x-a)^2} \tag{A2-5}$$

where  $\lambda = 2(mV - IU)$ ,  $\mu = -2(IV + mU)$  (A2-6)

we note from (A2-5) that  $F(x) \rightarrow 0$  as  $x \rightarrow \infty$  proving that the area under the magnetic anomaly curve is equal to zero.

That is:

$$\int_{-\infty}^{\infty} A(x) \cdot dx = 0 \tag{A2-7}$$

also from (A2-5) we get:

$$\int_0^R (F(x) + F(-x)) \cdot dx = \frac{\lambda}{2} \log \left\{ \frac{(R-a)^2 + b^2}{(R+a)^2 + b^2} \right\} + \mu \left\{ \tan^{-1} \frac{(R-a)}{b} + \tan^{-1} \frac{(R+a)}{b} \right\} \tag{A2-8}$$

where the coordinate origin is situated roughly above the middle of the body and where  $A(x)$  has been measured experimentally over the range  $-\infty < x < \infty$ . Assume  $b > 0$  and make  $R \rightarrow \infty$  in this. It gives  $J_1 = \mu$

where  $J_1 = \frac{1}{\pi} \int_0^{\infty} x (A(x) - A(-x)) dx$  (A2-9)

If  $x$  is large compared with  $a$  and  $b$ , (A2-4) and (A2-5) give the asymptotic formulae:

$$A(x) = \frac{\lambda}{x^2} - 2 \frac{(\lambda a + \mu b)}{x^3} + O\left(\frac{1}{x^4}\right), \text{ ----(A2-10)}$$

$$F(x) = \frac{\lambda}{x} + \frac{(\lambda a + \mu b)}{x^2} + O\left(\frac{1}{x^3}\right), \text{ ----(A2-11)}$$

$$\frac{1}{2} x^2 (A(x) + A(-x)) = -\lambda + O\left(\frac{1}{x^2}\right) \text{ (A2-12)}$$

∴ if  $J_2 = -\lambda$  we get

$$J_2 = \lim_{x \rightarrow \infty} \frac{1}{2} x^2 (A(x) + A(-x)) \text{ (A2-13)}$$

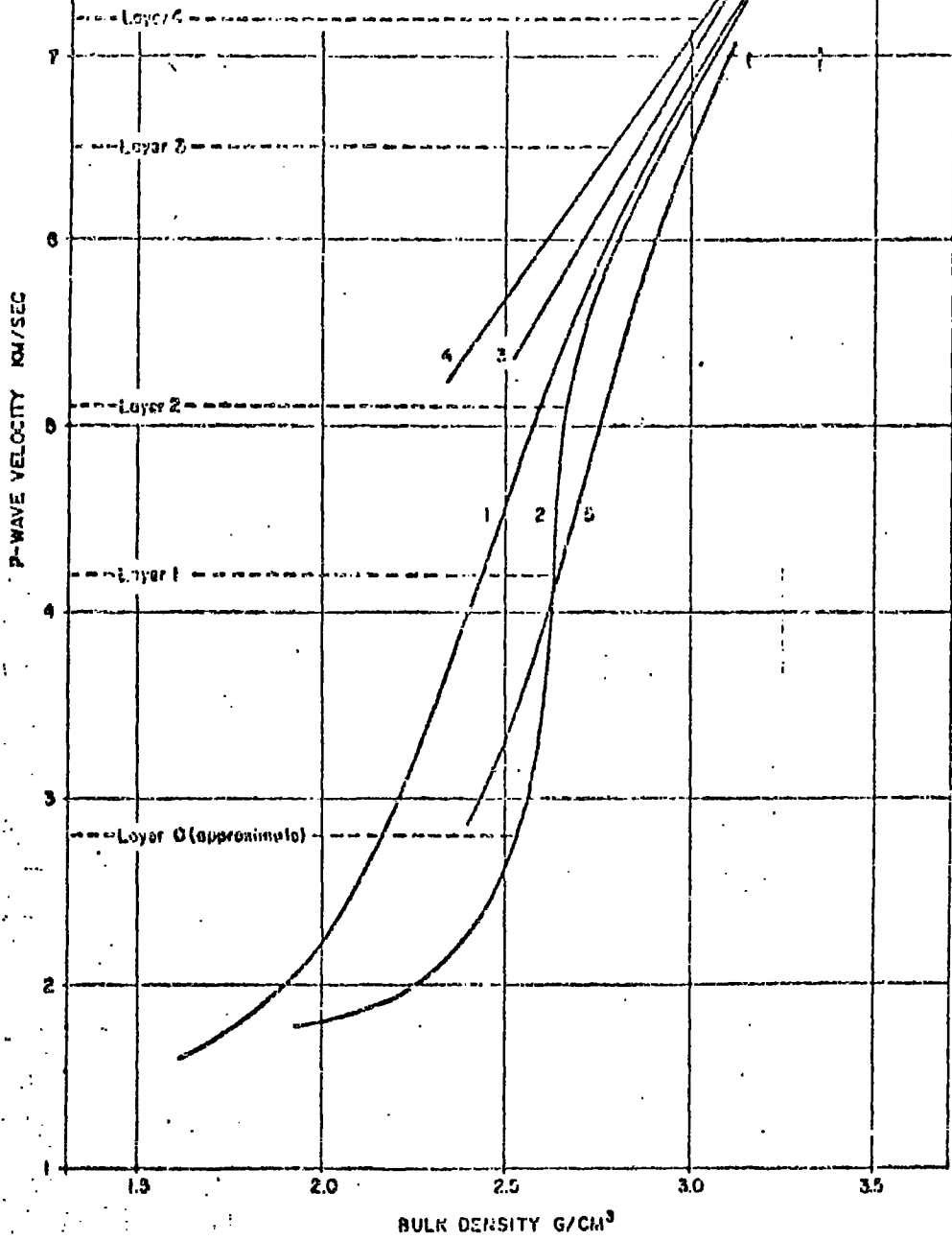
Substituting  $\mu = J_1$  and  $\lambda = -J_2$  in (A2-6) we obtain:

$$U = -(1J_2 + m J_1) / 2 (1^2 + m^2) \text{ (A2-14)}$$

$$V = (m J_2 - 1 J_1) / 2 (1^2 + m^2) \text{ (A2-15)}$$

# P-WAVE VELOCITY VS DENSITY FOR CRUSTAL ROCKS

- 1 Hata-Drake curve ; Toksoni et al., 1959
- 2 Woollard, 1959
- 3 Woollard, 1962
- 4 Konanoni and Mizutani, 1965
- 5 Mung'handi and Woollard, 1968 (Hawaiian Basalts)



REFERENCES

- Al-Shalabi, M., 1970. The application of non linear optimisation techniques in geophysics. Ph.D. thesis, University of Durham.
- Allen, P.M., 1968. The stratigraphy of a geosynclinal succession in western Sierra Leone, West Africa. Geol. Mag., 105, No. 1, 62-73.
- Anderson, D.L., 1967. Latest information from seismic observations, in The Earth's Mantle, edited by T.F. Gaskell, 355-420, Academic Press, New York.
- Anderssen, R.S., 1969. On the solution of certain over-determined systems of linear equations that arise in geophysics. J. geophys. Res. 74, 1045-1051.
- Andrew, E.M., Masson Smith, D. and Robson, G.R., 1970. Gravity anomalies in the Lesser Antilles. Geophysical Paper No. 5. London, Her Majesty's Stationery Office.
- Andrew-Jones, D.A., 1968. Petrogenesis and geochemistry of the rocks of the Kenema district, Sierra Leone. 12th Ann. Rep. Res. Inst. African Geol., Univ. Leeds, 20.
- Aymō, J.M., 1965. The Senegal salt basin. 83-90, in Salt Basins around Africa. London, Institute of Petroleum.
- Baker, C.C. and Bott, M.H.P., 1961. A gravity survey over the Freetown basic complex of Sierra Leone. Overseas Geol. Miner. Resour., No. 3, 269-278.

- Baranov, V., 1957. A new method for interpretation of aeromagnetic maps: pseudo-gravimetric anomalies. Geophysics, 22, 359-383.
- Bassinger, B.G., Harbison, R.N. and Weeks, L.A., 1971. Marine geophysical study northeast of Trinidad - Tobago. Bull. Am. Ass. Petrol. Geol., in press.
- Ball, M.M., Harrison, G.C.A. and Supko, P.R., 1969. Atlantic opening and the origin of the Caribbean. Nature, London, 223, 167-168.
- Ball, M.M., Harrison, G.C.A., Supko, P.R., Bock, W. and Maloney, N.J., 1971. Marine geophysical measurements on the southern boundary of the Caribbean sea, contribution to the Univ. of Miami Institute of Marine and Atmospheric Sciences.
- Bhattacharyya, B.K., 1964. Magnetic anomalies due to prism shaped bodies with arbitrary polarisation. Geophysics, 29, No. 4, 517-531.
- Bhattacharyya, B.K., 1966. A method for computing the total magnetisation vector and the dimensions of a rectangular block-shaped body from magnetic anomalies. Geophysics, 31, 74-96.
- Birch, F., 1969. Density and composition of the upper mantle: first approximation as an Olivine layer, in the Earth's Crust and Upper Mantle, edited by P.J. Hart, 18-36, Geophysical Monograph No.13, American Geophysical Union.

- Bott, M.H.P., 1960. The use of rapid digital computing methods for direct gravity interpretation of sedimentary basins. Geophys. J.R. astr. Soc., 3, 63-67.
- Bott, M.H.P., 1965. The deep structure of the northern Irish Sea. A problem of crustal dynamics. Colston Papers, 17, 179-204. Butterworth, London.
- Bott, M.H.P., 1967. Solution of the linear inverse problem in magnetic interpretation with application to oceanic magnetic anomalies. Geophys. J.R. astr. Soc., 13, 313-323.
- Bott, M.J.P., 1969. GRAVN. Durham geophysical computer program specification No. 1.
- Bott, M.H.P., 1969. MAGN. Durham geophysical computer program specification No. 2.
- Bott, M.H.P. and Hutton, M.A., 1970. Limitations on the resolution possible in the direct interpretation of magnetic anomalies. Earth. Planet. Sci. Letters, 8, 317-319.
- Bott, M.H.P., Smith, R.A. and Stacey, R.A., 1966. Estimation of the direction of magnetisation of a body causing a magnetic anomaly using a pseudo-gravity transformation. Geophysics, 31, 803-811.
- Bruckshaw, J.M. and Kunaratnam, K., 1963. The interpretation of magnetic anomalies due to dykes. Geophys. Prospect, 11, 509-522.



- Bunce, E.T., Phillips, J.D., Chase, R.L. and Bowin, C.C.  
1970. The Lesser Antilles arc and the eastern margin of the Caribbean Sea. Woods Hole Oceanographic Institution, Contribution No. 2288.
- Bush, S.A., and Bush, P.A., 1969. Isostatic gravity map of the eastern Caribbean region. Gulf Coast Assoc. Geol. Soc. Trans., 19, 281-285.
- Chase, R.L. and Bunce, E.T., 1969. Underthrusting of the eastern margin of the Antilles by the floor of the western north Atlantic Ocean, and origin of the Barbados Ridge. J. Geophys. Res., 74, No. 6, 1413-1420.
- Clifford, T.N., 1966. Tectono metallogenic units and metallogenic provinces of Africa. Earth Planet. Sci. Letters, 1, 421.
- Clifford, T.N. 1970. The structural framework of Africa, in African Magmatism and Tectonics, edited by T.N. Clifford and I.G. Gass, 1-23, Oliver and Boyd, Edinburgh.
- Cordell, L. and Henderson, R.G. 1968. Iterative three dimensional solution of gravity anomaly data using a digital computer. Geophysics, 33, 596-601.
- Deitz, R.S., 1961. Continent and ocean basin evolution by spreading of the sea floor. Nature, London, 190, 354-357.



- Dewey, J.F. and Bird, J.M., 1970. Mountain belts and the new global tectonics. J. geophys. Res., 75, No. 14, 2625-2647.
- Dixey, F., 1922. The norite of Sierra Leone, British West Africa. Q.J. geol. Soc. Lond., 78, 299-347.
- Emilia, D.A. and Bodvarsson, G., 1970. Numerical methods in the direct interpretation of marine magnetic anomalies. Earth Planet. Sci. Letters, 7, 194-200.
- Ewing, M., 1937. Gravity measurements on the U.S.S. Baracuda. Trans. Am. geophys. Un. 18, 66-69.
- Ewing, J.I., Officer, C.B., Johnson, H.R. and Edwards, R.S., 1957. Geophysical investigations in the Caribbean: Trinidad Shelf, Tobago Trough, Barbados Ridge, Atlantic Ocean. Bull. geol. Soc. Am., 68, 897-912.
- Ewing, J.I., Antoine, J. and Ewing, M., 1960. Geophysical measurements in the western Caribbean sea and in the Gulf of Mexico. J. geophys. Res., 65, 4087-4126.
- Funnel, B.M. and Smith, A.G. 1968 Opening of the Atlantic ocean. Nature, London, 219, 1328-1333.
- Gay, S.P., 1963. Standard curves for the interpretation of magnetic anomalies over long tabular bodies. Geophysics, 28, 161-200.

- Graf, A., and Schulze, R., 1961. Improvements on the sea gravimeter. Gss 2. J. geophys. Res., 66, 1813-1821.
- Haaz, I.B., 1953. Relations between the potentials of the attraction of the mass concentrated in a finite rectangular prism and its first and second derivatives. Geofizikai "Kozlemanyek, II, No. 7.
- Harrison, J.C., 1960. The measurement of gravity at sea, in Methods and Techniques of Modern Geophysics edited by S.C. Runcorn, Interscience Publishers, New York.
- Hartman, R.R., Teskey, D.J. and Friedberg, J.L., 1961. A system for rapid digital aeromagnetic interpretation. Aero Service - unpublished manuscript.
- Haughton, S.H., 1963. The stratigraphic history of Africa south of the Sahara, 365 pp. (New York: Hafner Pub. Co.).
- Henderson, R.G. and Eeitz, I., 1949. The upward continuation of anomalies in total <sup>magnetic</sup> intensity fields. Geophysics, 14, 517-534.
- Hess, H.H., 1958. Gravity anomalies and island arc structure with particular reference to the West Indies. Proc. Amer. phil. Soc., 79, 71-96.
- Hess, H.H., 1960. The evolution of ocean basins, unpublished manuscript, (report submitted to office of naval research).

- Hess, H.H., 1962. History of the ocean basins, in Petro-  
logical Studies: A Volume in Honour of  
A.F. Buddington, edited by A.E.J. Engle  
et al.
- Hess, H.H. and Maxwell, J.C., 1953. Caribbean research  
project. Bull. geol. Soc. Amer., 64, 1-6.
- Hsu, H.P., 1967. Outline of Fourier analysis., published  
by Associated Educational Services Corp.,  
New York.
- Hutchinson, R.D., 1958. Magnetic analysis by logarithmic  
curves. Geophysics, 23, 749-769.
- Hutton, M.A., 1970. Interpretation of oceanic magnetic  
anomalies using a linear inverse technique.  
Ph.D. thesis, Univ. of Durham.
- Isacks, B., Oliver, J. and Sykes, L.R., 1968. Seismology  
and the new global tectonics. J. geophys.  
Res., 73, 5855-5899.
- Junner, N.R., 1930. Geology and mineral resources of  
Sierra Leone. Mineralog. Mag., 42, No. 2,  
73-82.
- Kellogg, O.D., 1929. Foundations of Potential Theory.  
New York, Fredrick Ungar Publishing Company.
- Krause, D.C., 1963. Seaward extension and origin of the  
Freetown layered basic complex of Sierra  
Leone. Nature, London, 200, 1280-1281.

- Kuno, H., 1965. Lateral variation of basalt magma across continental margins and island arcs. Can. Geol. Survey Paper 66-15, 317.
- LaCoste, L.J.B., 1967. Measurement of gravity at sea and in the air. Review of Geophysics., 5, No.4, 477-526.
- Lagaay, R.A., 1969. Geophysical investigations of the Netherlands Leeward Antilles, published by N.V. North Holland Publishing Co., Amsterdam.
- LaPorte, M., 1963. Calcul de la forme d'une structure homogene a partir de son champ gravimetrique. Geophys. Prospect., 11, 276-291.
- Lattimore, R.K., Weeks, L.A. and Mordock, L.W., 1971. Marine geophysical reconnaissance of the continental margin north of Paria peninsula, Venezuela. Bull. Am. Ass. Petrol. Geol., in press.
- Läuchli, P., 1961. Jordan elimination und Ausgleichung nach Kleinsten Quadraten. Num. Math., 3 226.
- Lehman, H.-J., 1970. A control of two dimensional magnetic interpretation by three dimensional model body anomalies. Geophys. Prospect. 29, 133-155.
- Liddle, R.A., 1946. The geology of Venezuela and Trinidad Paleontological Research Institution. Ithaca, New York.

- Magrath, P.H. and Hood, P.J., 1970. The dipping dyke case. A computer curve matching method of magnetic interpretation. Geophysics, 35, No. 5, 831-848.
- Molnar, P. and Sykes, L.R., 1969. Tectonics of the Caribbean and middle America regions from focal mechanisms and seismicity. Bull. geol. Soc. Am., 80, 1639-1684.
- Martin-Kaye, P.H.A., 1969. A summary of the geology of the Lesser Antilles. Overseas Geol. and Miner Resour., 10, No. 2, 172-206.
- Masson-Smith, D.J. and Andrew, F.M., 1965. Gravity and magnetic measurements in the Lesser Antilles, preliminary report. Overseas Geol. Survey, London.
- Maxwell, J.C., 1948 Geology of Tobago, B.W.I. Bull. geol. Soc. Am., 59, 801-854.
- McMaster, R.L., De Boer, J. and Ashraf, A., 1970. Magnetic and seismic reflection studies on the continental shelf off Portuguese Guinea, Guinea and Sierra Leone, West Africa. Bull. Am. Ass. Petrol. Geol., 54, No. 1, 158-167.
- McMaster, R.L., Lachance, T.P., Ashraf, A. and De Boer, J., 1971. Geomorphology, structure and sediments of the continental shelf and upper slope off Portuguese Guinea, Guinea and Sierra Leone. in Geology of the East Atlantic Continental Margin, No. 4, Africa, edited by F.M. Delany. H.K.S.C. London.

- Metz, H.L. 1964. Geology of the El-Pilar Fault Zone, State of Sucre, Venezuela. Ph.D. thesis. Princeton Univ.
- Miner, J.W. and Toksoz, M.N. 1970. Thermal regime of a downgoing slab and new global tectonics. J. geophys. Res., 75, No. 8, 1397-1419.
- Nafe, J.E. and Drake, C.L. 1963. Physical properties of marine sediments, in the Sea, vol. 3. Interscience, New York, 794-815.
- Nagle, F. 1970. Caribbean Geology. Contribution to the University of Miami, Rosenstill School of Marine and Atmospheric Sciences.
- Nagy, D. 1966. The gravitational attraction of a right rectangular prism. Geophysics, 31, No. 2, 362-371.
- Naudy, H. 1970. Automatic interpretation of aeromagnetic anomalies, presented at Society of Exploration Geophysicists Meeting, New Orleans.
- Nettleton, L.L. 1940. Geophysical Prospecting for Oil. McGraw-Hill, New York.
- Officer, C.B., Ewing, J.I., Edwards, R.S., Johnson, H.R., 1957. Geophysical investigations in the Caribbean. Bull. geol. Soc. Amer., 68, 359-378.
- Officer, C.B., Ewing, J.I., Hennion, J.F., Harkrider, D.G. and Miller, D.E. 1959. Geophysical investigations in the eastern Caribbean - Summary of the 1955 and 1956 cruises, in Physics and Chemistry of the Earth, 3, Pergamon Press, London, 17-109.



- Oliver, J. and Isaacs, B. 1967. Deep earthquake zones, anomalous structures in the upper mantle and lithosphere. J. geophys. Res., 72, 4259-4275.
- Coxburgh, E.R. and Turcotte, 1968. Problems of high heat flow and volcanism associated with zones of descending mantle convective flow. Nature, London, 218, 1041.
- Peter, G., Weeks, L.A. and Burns, R.E. 1966. A reconnaissance geophysical survey in the Andaman Sea and across the Andaman-Nicobar Island Arc. J. geophys. Res., 71, No. 2, 495-509.
- Peters, L.J. 1949. The direct approach to magnetic field interpretation and its practical application. Geophysics, 14, 290-320.
- Pirson, S.J. 1940. Polar charts for interpreting magnetic anomalies: A.I.M.E. Trans., 8, 173-192.
- Pollett, J.D. 1951. The geology and mineral resources of Sierra Leone. Colon. Geol. Miner. Resour., 2, No. 1, 3-23.
- Rod, R. 1956. Strike-slip faults of northern Venezuela. Amer. Ass. Pet. Geol. Bull., 40, 457-476.
- Roy, A. 1962. Ambiguity in geophysical interpretation. Geophysics, 27, No. 1, 90-99.
- Ringwood, A.E. 1969. Composition and evolution of the upper mantle, in the Earth's Crust and Upper Mantle, Monogr. 15. edited by P.J. Hart. 1-17. American Geophysical Union Washington, D.C.

- Senn, A. 1940. Paleogene of Barbados and its bearing on history and structure of the Antillean - Caribbean region. Bull. Am. Ass. Petrol. Geol., 24, No. 9, 1548-1610.
- Sheridan, R.E., Houtz, R.E., Drake, C.L. and Ewing, M. 1969. Structure of continental margin off Sierra Leone, West Africa. J. geophys. Res., 74, No. 10, 2512-2530.
- Shurbet, G.L. and Ewing, M. 1956. Gravity reconnaissance survey of Puerto Rico. Bull. geol. Soc. Am., 67, 511-534.
- Shurbet, G.L., Worzel, J.L. and Ewing, M. 1956. Gravity measurements in the Virgin Islands. Bull. geol. Soc. Am., 67, 1529-1536.
- Skeels, D.C. 1947. Ambiguity in gravity interpretation. Geophysics, 12, 43-56.
- Sougy, J. 1962. West African fold belt. Bull. geol. Soc. Amer., 73, No. 7, 871-876.
- Sykes, L.R. and Ewing, M. 1965. The seismicity of the Caribbean region. J. geophys. Res., 70, No. 20, 5065-5074.
- Talwani, M. and Ewing, M. 1960. Rapid computation of gravitational attraction of three dimensional bodies of arbitrary shape. Geophysics, 25, 203-225.

- Talwani, I. 1936. Some recent developments in gravity measurements aboard surface ships, in Gravity Anomalies: Unsurveyed Areas, edited by H. Cralin. Am. geophys. Union Monograph No. 9.
- Talwani, M. and Heirtzler, J.L. 1964. Computation of magnetic anomalies caused by two-dimensional structures of arbitrary shape. In Computers in the Mineral Industry, edited by G.A. Parks. The School of Earth Sciences, Stanford Univ.
- Talwani, M., Sutton, G.H. and Worzel, J.L. 1959. A crustal section across the Puerto Rico Trench. J. geophys. Res., 64, 1545-1555.
- Takeuchi, H. and Uyeda, S. 1965. A possibility of present day regional metamorphism. Tectonophysics, 2, 59.
- Tanner, J.G. 1967. An automated method of gravity interpretation. Geophys. J.R. astr. Soc., 13, 339-347.
- Tenaille, H., Nicod, M.A. and de Spangler, A. 1960. Petroleum exploration in Senegal-Mauritania and Ivory Coast coastal basins (West Africa), Paper presented at the 45th annual meeting of the American Association of Petroleum Geologists, Atlantic City, N.J.
- Thomsen, L. 1967. On the distributions of density and temperature in the low velocity zone. J. geophys. Res., 72, No. 23, 5649-5653:



- Trenchmann, C.T. 1933. The uplift of Barbados. Geol. Mag., 70, 19-46.
- Vaquier, V., Steenland, N.C., Henderson, R.G., and Zeitz, I. 1951. Interpretation of Aeromagnetic maps. Mem. geol. Soc. Amer. Memoir 47.
- Vening Meinesz, F.A. 1934. Gravity expeditions at sea 1923-1932, II, Pub. Neth. Geod. Comm., Waltman, Delft.
- Vening Meinesz, F.A. 1948. Gravity expeditions at sea 1925-1938, 4, Pub. Neth. Geod. Comm., Waltman, Delft.
- Weeks, L.A., Harbison, R.N., Peter, G. 1967. Island arc system in Andaman Sea. Bull. Am. Ass. Petrol. Geol., 51, No. 9, 1803-1815.
- Weeks, L.A., Lattimore, R.K., Harbison, R.N., Bassinger, B.G. and Merrill, G.F. 1971. Structural relationships between Lesser Antilles, Venezuela and Trinidad-Tobago. Bull. Am. Ass. Petrol. Geol., in press.
- Wells, M.K. 1962. Structure and petrology of the Freetown layered basic complex of Sierra Leone. Overseas Geol. Miner. Resour. Bull. Supplement No. 4 H.M.S.O. - London.
- Wells, M.K. and Baker, C.C. 1956. The anorthosites of the colony complex near Freetown, Sierra Leone. Colon. Geol. Miner. Resour., 6, No. 2, 137-158.
- Woollard, G.P. and Strange, W.E. 1961. Gravity anomalies and the crust of the earth in the Pacific basin. Am. geophys. Union Monograph No. 6, 60-80

Woollard, G.P., Harding, N.C., Muckenfuss, C., Bonini, W.A., and Black, W.A. 1952. World-wide gravity measurements conducted during the period June, 1949 - January, 1952. (Wood's Hole, Mass., U.S.A.: Oceanographic Institution).

Heiland, C.A., 1940. Geophysical Exploration, Prentice-Hall, New York.

Talwani, M., Worzel, J.L. and Landisman, M., 1959. Rapid gravity computations for two-dimensional bodies with application to Mendocino submarine fracture zone. J. geophys. Res., 64, 49-59.

Worzel, J.L. and Ewing, M., 1948. Explosion sounds in shallow water, in Propagation of sound in the oceans. Geol. Soc. Amer., Memoir 27.

